Deciphering the functional and molecular differences between MTM1 and MTMR2 to better understand two neuromuscular diseases

Matthieu Raess

UNIVERSITÉ DE STRASBOURG

ÉCOLE DOCTORALE DES SCIENCES DE LA VIE ET DE LA SANTE (ED 414)

Génétique Moléculaire, Génomique, Microbiologie (GMGM) – UMR 7156

&

Institut de Génétique et de Biologie Moléculaire et Cellulaire (IGBMC)

UMR 7104 – INSERM U 964

THÈSE présentée par :

Matthieu RAESS

soutenue le : **13 octobre 2017**

pour obtenir le grade de : **Docteur de l'université de Strasbourg**

Discipline/ Spécialité : Aspects moléculaires et cellulaires de la biologie

Deciphering the functional and molecular differences between MTM1 and MTMR2 to better understand two neuromuscular diseases.

THÈSE dirigée par :

Mme FRIANT Sylvie	Directrice de recherche, Université de Strasbourg
& Mme COWLING Belinda	Chargée de recherche, Université de Strasbourg

RAPPORTEURS :

Mme BOLINO Alessandra	Directrice de recherche, Institut San Raffaele de Milan
M. BITOUN Marc	Chargé de recherche, Institut de Myologie

AUTRES MEMBRES DU JURY :

M. ECHARD Arnaud	Directeur de recherche, Institut Pasteur
M. VITALE Nicolas	Directeur de recherche, Université de Strasbourg

Acknowledgements

It is my pleasure to acknowledge the roles of many people who made this PhD research possible.

I will start by respectfully thanking the members of the jury Dr. Alessandra Bolino, Dr. Marc Bitoun, Dr. Arnaud Echard and Dr. Nicolas Vitale for accepting to read and evaluate my PhD work.

I would like to sincerely thank Dr. Sylvie Friant and Dr. Jocelyn Laporte for welcoming me in their respective teams. Both of you have been a constant and powerful source of advice and motivation. Of course many thanks to Dr. Belinda Cowling for accepting to be my co-director (and my official Aurora specialist) for the last two years, your help and your enthusiasm have been a great support to me.

I would like to express my appreciation to the Association Française contre les Myopathies (AFM Téléthon) for financially supporting my thesis project during 3 years.

When it comes to my team(s) members, it is difficult to individually express all my gratitude. I will simply thank all of you for your precious help, your fruitful discussions and most importantly your kindness and positive atmosphere. It has always been a pleasure and a privilege to share your scientific and social life. Special thanks go to Bruno Rinaldi, Christine Kretz, Pascal Kessler (except Pascal's jokes), Hichem Tasfaout and Raphael Schneider for their significant technical assistance.

I would also like to thank our collaborators for this work: Dr. Bernard Payrastre and Jean-Marie Xuereb for the yeast lipid dosage and Dr. Norma Romero for sharing precious patient biopsies. I am also grateful to Alessandra Bolino and Marta Guerrero for sharing their mouse tissues.

This work would not have been possible without our technical platforms. I especially thank Nadia Messaddeq, Josiane Hergueux and Coralie Spiegelhalter for their help in electron

microscopy; Philippe Hammann, Lauriane Kuhn and Johana Chicher (IBMC) for all the work on mass spectrometry; Pascale Koebel and Paola Rossolillo (IGBMC) for virus production; and finally the IGBMC animal facility, cell culture facility and antibody facility.

I gratefully thank all members and organizers of the OpenLAB operation. Going in all these high schools through Alsace was an exciting opportunity to practice scientific vulgarization and really confirmed my project of becoming a teacher in biology.

Special thanks go to my loving partner Florine, who is a constant support and source of happiness in my life.

I would like to finish my acknowledgements by thanking my parents, my brothers Vincent, Christophe and Sébastien, and my sister Anne. They supported me during all my life and made all this possible for me.

Table of contents

List of tables

List of figures

Essential abbreviations

Aa, amino acids

ANOVA, analysis of variance

AAV, adeno-associated virus

BIN1, amphiphysin 2

CMT, Charcot-Marie-Tooth

CNM, centronuclear myopathy

DNM2, dynamin 2

FYVE, Fab1-YOTB-Vac1-EEA1

GFP, green fluorescent protein

HE, hematoxylin-eosin

KD, knockdown

KI, knockin

KO, knockout

MTM, myotubularin

MTMR, myotubularin-related

PH-GRAM, Pleckstrin Homology, Glucosyltransferase, Rab-like GTPase Activator and Myotubularin

PPIn, phosphoinositides

PtdIns, phosphatidylinositol

PtdIns3*P*, phosphatidylinositol 3-phosphate

PtdIns5*P*, phosphatidylinositol 5-phosphate

PtdIns(3,5)P_2, phosphatidylinositol 3,5-bisphosphate

TA, tibialis anterior

WT, wild type

Ymr1, Yeast myotubularin-related protein 1

Part One - Introduction

I. Setting the scene

Myotubularins (MTMs) are active or dead phosphoinositide phosphatases defining a large protein family conserved through evolution, from yeast to human, and involved in different neuromuscular diseases. Mutations in the myotubularin *MTM1* gene cause the severe congenital myopathy called myotubular myopathy (or X-linked centronuclear myopathy) affecting the myocytes, while mutations in the myotubularin-related *MTMR2* gene cause the recessive Charcot-Marie-Tooth peripheral neuropathy CMT4B1 affecting the Schwann cells. This tissue-specificity is quite intriguing, since MTM1 and MTMR2 are ubiquitously expressed and are two similar proteins: they have comparable sequences homologies, share domain organizations and catalytic functions, and dephosphorylate the same lipid substrates, phosphatidylinositol-3-monophosphate (PtdIns3*P*) and phosphatidylinositol-3,5-bisphosphate (PtdIns(3,5)P_2).

Before presenting my project, I would like to give an overview of three main aspects: first the neuromuscular diseases associated with myotubularins, then the large myotubularin family itself, and finally the phosphoinositide substrates of these phosphatases.

II. Myotubularin-related diseases

A. The X-linked centronuclear myopathy

1. The causative gene

The X-linked centronuclear myopathy (XLCNM, OMIM # 310400) or X-linked recessive myotubular myopathy (XLMTM; OMIM # 310400) is a congenital muscle disorder first described in 1969 by Van Wijngaarden *et al.* (Van Wijngaarden, G.K. et al., 1969). XLCNM belongs to a group of rare congenital myopathies named centronuclear myopathies (CNM). This group was initially composed of 3 forms: the X-linked form, the autosomal dominant form (due to mutations in *DNM2*) and the autosomal recessive form (due to mutations in *BIN1*) (Bitoun et al., 2005; Nicot et al., 2007) but more recently, other genes

such as *RYR1*, *TTN* or *SPEG* have been related to CNM and make the classification more difficult (Agrawal et al., 2014; Ceyhan-Birsoy et al., 2013; Wilmshurst et al., 2010).

The MTM1 gene

The causative gene of XLCNM was localized on the Xq28 chromosome (Thomas et al., 1990) and then isolated by positional cloning and identified for the first time by a consortium of 3 groups in 1996 (Laporte et al., 1996). Named *MTM1*, this gene contains 15 exons forming a 3.9 kb transcript that is ubiquitously expressed. A second transcript of 2.4 kb was specifically detected in muscle and testis, due to an alternative polyadenylation signal resulting in a shorter transcript. However, no muscle-specific exon that could explain the muscle-specificity of the associated disease has been identified yet (Laporte et al., 1996).

The *MTM1* gene codes for a 603 amino acids protein with a specific phosphoinositide (PPIn) 3-phosphatase activity. MTM1 was the first described protein of the large myotubularin family that currently contains 14 identified members. This family deserves a full presentation and will be more thoroughly characterized in chapter III.

MTM1 mutations

Up to now and according to the Human Gene Mutation Database (http://www.hgmd.cf.ac.uk), 245 mutations on the *MTM1* gene have been identified and associated with the myotubular myopathy. XLCNM patients have been found in all ethnical groups including European (de Gouyon et al., 1997; Tanner et al., 1999b), Japanese (Nishino et al., 1998; Tsai et al., 2005) South American (Zanoteli et al., 1998) and North American populations (Herman et al., 2002).

These mutations mainly affect the PH-GRAM (Pleckstrin Homology - Glucosyltransferase, Rab-like GTPase Activator and Myotubularins) domain (lipid binding domain) and the phosphatase domain of MTM1, with no real hotspot (Figure 1) (Biancalana et al., 2003; McEntagart et al., 2002). Most of them are nonsense or frameshift mutations that induce a truncated and non-functional protein and seem correlated with severe muscular phenotypes (McEntagart et al., 2002). The others (77 up to now) are missense mutations

which often lead to milder phenotypes (McEntagart et al., 2002), and affect amino acids that are highly conserved in the MTM1 proteins through evolution. This suggests their important role in protein structure, interaction or catalytic activity. However, the genotype-phenotype correlation can be surprising and the same mutation (such as the E404K mutation) can induce various degrees of XLCNM severity from one patient to another (Hoffjan et al., 2006; McEntagart et al., 2002), indicating some aggravation of compensation factors.

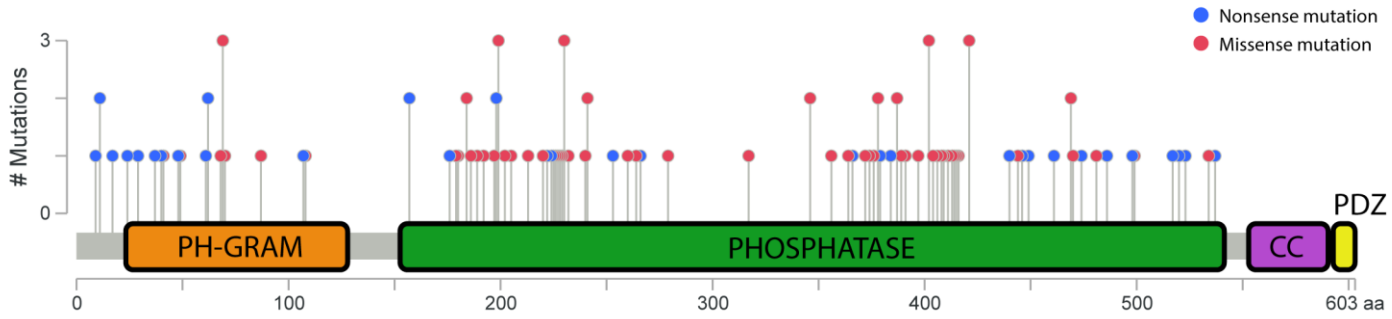

Figure 1: Position of XLCNM-linked nonsense and missense mutations on human MTM1 protein. Each dot represents a nonsense (blue) or missense (red) mutation listed in the Human Gene Mutation Database (http://www.hgmd.cf.ac.uk) for MTM1. In total, 35 nonsense and 77 missense mutations were linked to XLCNM in human MTM1. The number of different mutations found for the same amino acid is indicated by the scale on the left. The mapping was done using the mutation mapper of cBioPortal (http://www.cbioportal.org/mutation_mapper.jsp). PH-GRAM (Pleckstrin Homology - Glucosyltransferase, Rab-like GTPase Activator and Myotubularins) domain, phosphatase domain, CC (coiled-coil) domain and PDZ domain are represented.

MTM1 cellular functions

In vitro studies show that MTM1 (and active myotubularins in general) is a specific phosphoinositide (PPIn) 3-phosphatase that dephosphorylates the phosphatidylinositol-3-monophosphate (PtdIns3*P*) and PtdIns(3,5)P_2 into PtdIns and PtdIns5*P*, respectively (Blondeau et al., 2000; Taylor et al., 2000; Tronchere et al., 2004; Walker et al., 2001).

MTM1 cellular functions are not fully understood, and the specific role of MTM1 in muscle remains under investigation. The majority of *MTM1* mutations result in the loss of MTM1 protein that is presumably the cause of the disease. But we do not precisely know why

MTM1 mutations specifically affect the muscle. Data show that MTM1 interacts with desmin, a muscle-specific intermediate filament (Hnia et al., 2011). Moreover, MTM1 or desmin defects lead to abnormal mitochondrial dynamic and positioning in muscle, where mitochondrial production of energy is crucial for muscle contraction (Hnia et al., 2011). MTM1 has also been shown to interact with the amphiphysin BIN1 that is implicated in the autosomal recessive form of CNM (Royer et al., 2013). MTM1 enhances BIN1 activity (membrane tubulation) in skeletal muscle, and BIN1 patient mutations alter its binding and regulation by MTM1 (Royer et al., 2013). Studies in cell cultures suggest that MTM1 is able to dephosphorylate endosomal pools of PtdIns3*P* (and thus to decrease its levels) (Kim et al., 2002), and is implicated in late endosome formation and functions through interactions with PtdIns(3,5)P_2 (Tsujita et al., 2004). In addition to this, surface delivery of endosomal cargo requires PtdIns3*P* hydrolysis by MTM1 (Ketel et al., 2016).

Finally, a study in mice lacking MTM1 shows aberrant mTORC1 signaling and impaired autophagy, suggesting that myotubularin is implicated in these pathways (Fetalvero et al., 2013).

2. Clinical and histological features

The XLCNM affects about 1/50 000 newborn males, and is generally characterized by hypotonia at birth, a very severe and generalized muscle weakness, external ophthalmoplegia and respiratory distress (Jungbluth et al., 2008; Laporte et al., 1996). To date, no specific therapeutic treatment is available. In 1999, Herman *et al.* classified XLCNM-affected patients in 3 categories, according to their phenotype severity: he described a severe (and classical), moderate and mild XLCNM (Herman et al., 1999).

The most severe form is characterized by prenatal polyhydramnios and reduced fetal movements, chronic ventilator dependence (with risk of respiratory infection), highly delayed motor milestones and absence of independent ambulation (Das et al., 1993; Herman et al., 1999). This severe form often results in neonatal death due to respiratory failure (mostly because of diaphragm weakness). Many surviving infants need a 24 hours/day ventilatory support and rarely reach 3 years old. Note that the newborn cases are often similar between XLCNM and myotonic dystrophy, but can be distinguished by examination of the mother

who shows mild facial weakness and clinical or electrical myotonia in case of myotonic dystrophy (Heckmatt et al., 1985).

Moderate and mild forms of XLCNM have been described by several groups (Barth and Dubowitz, 1998; Biancalana et al., 2003; Hoffjan et al., 2006; Yu et al., 2003). Affected patients are less dependent on ventilatory support and present less severely delayed motor milestones with some independent ambulation. Only a few patients with pathogenic variants in *MTM1* were described to reach adulthood (Herman et al., 1999), and only two reached their sixties (Biancalana et al., 2003; Hoffjan et al., 2006). Also, a rare adult-onset form was reported, with apparently no clinical symptoms at birth and a progressive development of the myopathy during adulthood (Biancalana et al., 2003; Hoffjan et al., 2006; Yu et al., 2003).

Due to the X-linked recessive inheritance, the myotubular myopathy almost exclusively affects newborn males, and the mutation is usually transmitted by the asymptomatic mother (Herman et al., 2002). The short life expectancy and the severe muscle weakness of XLCNM patients prevent a transmission by the father. However, some rare heterozygote female carriers manifest XLCNM phenotypes similar to affected male phenotypes, with a high variability (Biancalana et al., 2017; Hammans et al., 2000; Jungbluth et al., 2003; Penisson-Besnier et al., 2007; Schara et al., 2003; Sutton et al., 2001; Tanner et al., 1999a; Tanner et al., 1999b). The inactivation of the other X chromosome (not carrying the *MTM1* mutations) could explain these female cases (Kristiansen et al., 2003). Moreover, the degree and tissue-specificity of the X chromosome inactivation seems to determine the phenotype severity (Grogan et al., 2005; Jungbluth et al., 2003; Tanner et al., 1999a). Compared to males, manifesting female carriers present less severe phenotypes, with childhood or adolescent onset and a progressive muscle weakness with no impact on the lifespan (Grogan et al., 2005; Hammans et al., 2000; Penisson-Besnier et al., 2007; Tanner et al., 1999a). As these milder phenotypes present as adult-onset limb-girdle myopathy, and as several of the affected females carry large heterozygous MTM1 deletions not detectable by Sanger sequencing, the prevalence of affected female carriers is likely to be greatly underestimated (Biancalana et al., 2017).

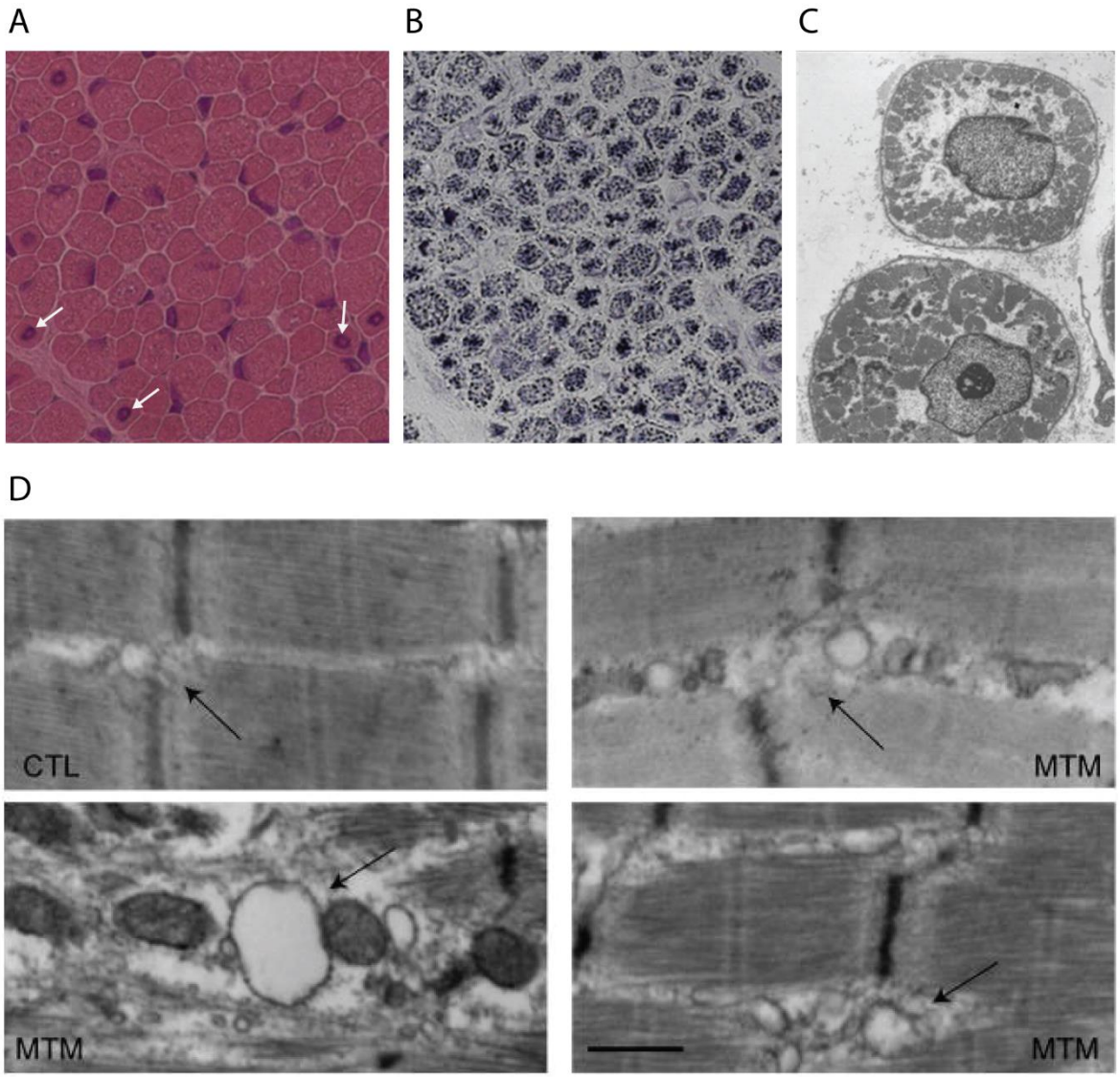

Figure 2: Muscle histology and ultrastructure of XLCNM patients. (A) H&E staining of a transverse muscle section, showing small round fibers and centralized nuclei (white arrows). **(B)** NADH-TR staining of a transverse muscle section, showing abnormal central accumulation of peripheral aggregates (necklace) of mitochondria **(C)** Electron microscopy of a transverse muscle section, showing two centralized nuclei and abnormal myofibers. **(A)**, **(B)** and **(C)** were adapted from Romero *et al.*, 2010. **(D)** Electron microscopy of longitudinal muscle sections, showing ultrastructural changes in triads (black arrows) of 3 different XLCNM patients (MTM) compared to control (CTL). Triads from XLCNM patients are dilated and disorganized. Scale bar 500nm. Adapted from Dowling *et al*. 2009.

Concerning histology, skeletal muscle biopsies of XLCNM patients reveal similar structural abnormalities independent of the phenotype severity. Myofibers show characteristics of fetal myotubes, hence the name "myotubular myopathy". Compared to normal myofibers, XLCNM myofibers are smaller and rounder (Silver et al., 1986), present centralized nuclei instead of being at the periphery (Ambler et al., 1984; Gayathri et al., 2000; Helliwell et al., 1998) and possess a perinuclear halo ("necklace") lacking contractile

elements and containing mitochondria aggregates and glycogen granules (Figure 2A, B and C) (Romero, 2010; Sarnat et al., 1981). The characteristic centralized nuclei visible after Hematoxylin & Eosin (H&E) staining are present in all skeletal muscles and may affect up to 90% of fibers (Romero, 2010), hence the name “centronuclear myopathy”. For now, this abnormal nuclei positioning is not explained, but some data suggest that desmin intermediate filaments (that interact with MTM1) are implicated in the actin-driven positioning of the nucleus in skeletal muscle (Dupin et al., 2011; Ralston et al., 2006). A recessive desmin-null form of myopathy has also been described, with centralized nuclei in the myofibers (Henderson et al., 2013). Finally, a predominance of type I fibers (slow contraction, high oxidative capacity) in XLCNM patients muscles can be seen after succinate dehydrogenase (SDH) staining or NADH-tetrazolium reductase (NADH-TR) staining (Figure 2B) (Ambler et al., 1984; Helliwell et al., 1998; Romero, 2010).

Skeletal muscle ultrastructure shows a profound disorganization of myofibrils, sarcomeres and triads (Figure 2C and D) (Ambler et al., 1984; Dowling et al., 2009; Silver et al., 1986). Furthermore, the neuromuscular junctions are smaller and the N-CAM protein essential for a proper neuromuscular junction adhesion is abnormally expressed (Coers et al., 1976; Fidzianska et al., 1994). Since all these elements are essential for Excitation-Contraction (E-C) coupling, it partially explains the muscle weakness of the XLCNM patients.

Noteworthy, truncating mutations leading to an absence of MTM1 protein are usually related to the presence of very small myofibers and to a severe myopathy phenotype, while missense mutations are linked to larger myofibers (but still small compared to a normal muscle) and higher life expectancy (Pierson et al., 2007). Thus, measuring the fiber size could be an easy way to evaluate the vital prognostic of XLCNM patients.

3. Animal models

To better understand the pathophysiological mechanisms of myotubular myopathy and the cellular and molecular functions of MTM1, several vertebrate models of XLCNM have been generated (Lawlor et al., 2016).

Zebrafish model

A zebrafish (*Danio rerio*) model of myotubular myopathy was generated by *Mtm1* knockdown (KD) using morpholino antisense technology (Dowling et al., 2009). Reduced levels of MTM1 induce impaired motor functions, myofiber atrophy, central and abnormally rounded nuclei, organelles mislocalization, sarcomere and triad disorganization, and abnormal neuromuscular junctions (Figure 3B) (Dowling et al., 2009). These phenotypes are similar to that seen in XLCNM patients. Dowling *et al.* also observed increased PtdIns3*P* levels in zebrafish muscles. Morphological changes can already been observed at the embryonic stage, with abnormal dorsal curvature and a diminution of spontaneous muscle contractions.

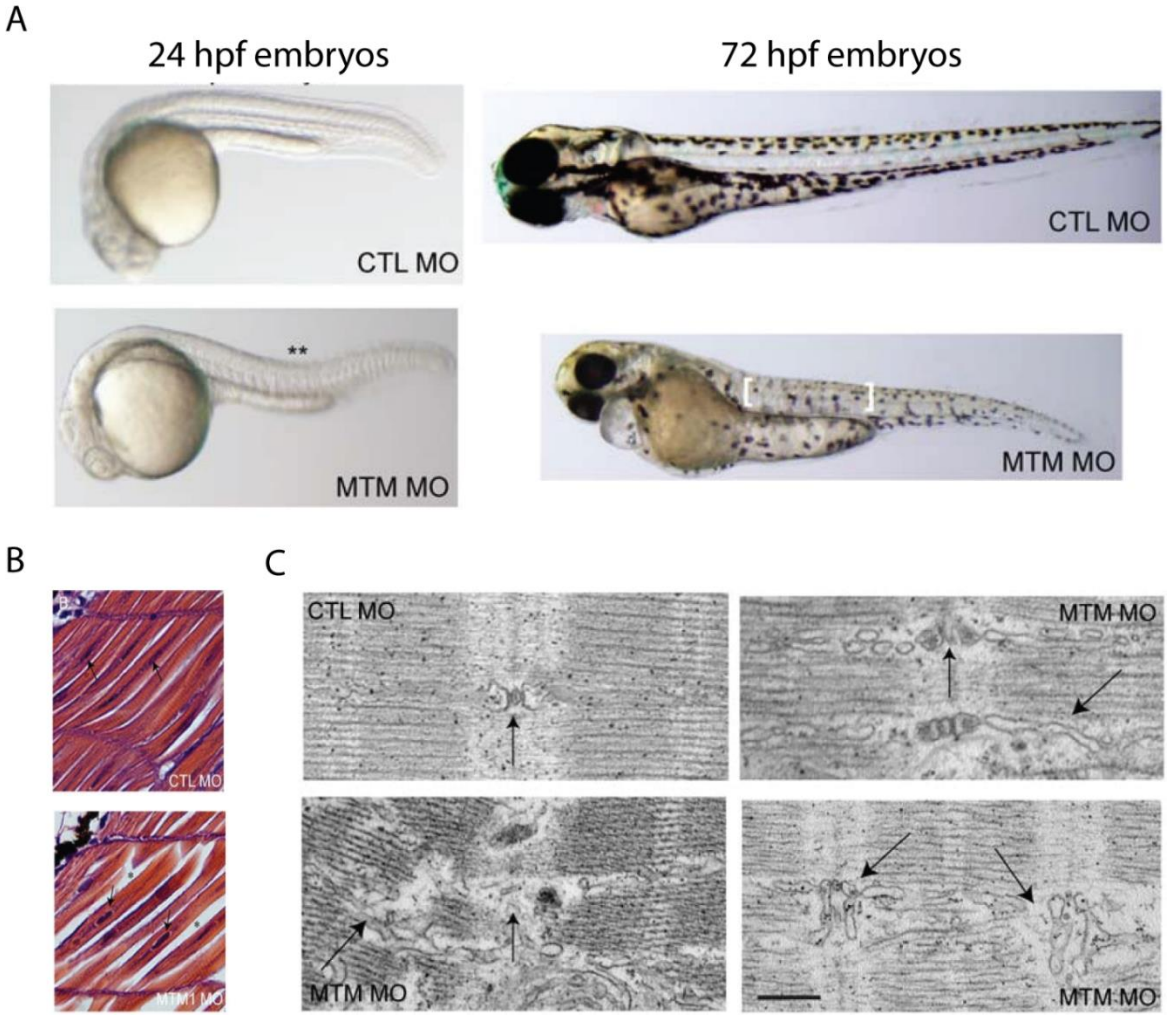

Figure 3: Morphological and histological phenotypes of the XLCNM zebrafish model. Adapted from Dowling *et al*. 2009. **(A)** Live embryos at 24 and 72 hours post fertilization (hpf) injected with either control (CTL) or myotubularin (MTM) morpholinos. Abnormal dorsal curvature in MTM morphant at 24 hpf is indicated by a double star (**). MTM morphants at 72 hpf show a tail shortening and a selective thinning of the muscle compartment (brackets). **(B)** H&E staining of longitudinal muscle sections from control (CTL) and myotubularin (MTM) morphants at 72 hpf. MTM morphants show abnormally rounded nuclei (arrows) and an increased space between the myofibers. **(C)** Electron microscopy of longitudinal muscle sections from control (CTL) and myotubularin (MTM) morphants. MTM morphants display dilated and dysmorphic triads (arrows). Scale bar represents 500nm.

Mouse models

Buj-Bello *et al.* generated constitutive *Mtm1* knockout (KO) mice by homologous recombination (Buj-Bello et al., 2002b). These mice are viable but develop a progressive centronuclear myopathy starting at around 3-4 weeks of age, leading to death at 5 to 8 weeks of age.

The myopathy reproduces the majority of clinical phenotypes of the XLCNM patients, as a respiratory distress, an amyotrophy and a severe progressive muscle weakness (Figure 4A-B). Histologically, skeletal muscles fibers show smaller and rounder myofibers with a progressive accumulation of central or paracentral nuclei, and a mitochondrial accumulation in the center or the periphery of the fiber ("necklace" phenotype characteristic of human XLCNM) (Figure 4C-D). Highly disorganized sarcomeres and triads, with an accumulation of abnormal longitudinal T-tubules can be seen by electron microscopy (Figure 4E) (Al-Qusairi et al., 2009; Buj-Bello et al., 2002b; Lawlor et al., 2013). While the XLCNM was proposed to result from an arrest in myogenesis, as the myofibers exhibit fetal myotube characteristics (Spiro et al., 1966; van Wijngaarden, G. K. et al., 1969), this *Mtm1* KO mouse model revealed that the cause of the pathology is likely a muscle maintenance defect (Buj-Bello et al., 2002b).

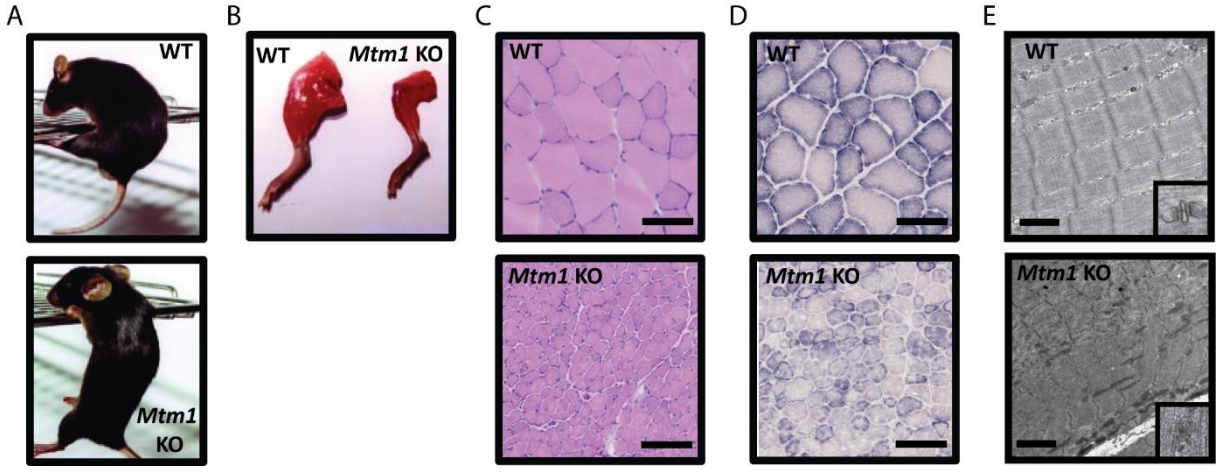

Figure 4: Clinical and histological phenotypes of the XLCNM mouse model. (A) Grid climbing test of wild type (WT) and *Mtm1* KO mice. *Mtm1* KO mice are unable to climb. **(B)** Dissected hind limbs of WT and *Mtm1* KO mice, illustrating the major muscle mass reduction in *Mtm1* KO mice. **(A)** and **(B)** were adapted from Buj-Bello *et al*. 2002b. **(C)**, **(D)** and **(E)** represent personal data of tibialis anterior (TA) sections of 7 week-old WT and *Mtm1* KO mice, adapted from my article Raess *et al.* 2017. **(C)** H&E staining of transversal tibialis anterior (TA) sections. Scale bar 100 µm. **(D)** Succinate dehydrogenase (SDH) staining of transverse TA sections. Scale bar 100 µm. **(E)** Electron microscopy of longitudinal TA sections displaying sarcomere, mitochondria and triad organization. Scale bar 1 µm. Representative triads are displayed in the zoom square.

This model is also frequently used for preclinical development of treatments, with various strategies to compensate the loss of MTM1 and rescue the myopathic phenotypes. Gene therapy by systemic injection of adeno-associated virus serotype 8 (AAV8) expressing MTM1 improves motor activity, contractile force and prolonged survival (Childers et al., 2014).

Another potential therapeutic strategy is to decrease PtdIns3*P* levels that are increased in *Mtm1* KO mice: inhibition or muscle-specific depletion of the class II PtdIns 3-kinase also improved motor functions, calcium release and lifespan (Kutchukian et al., 2016; Sabha et al., 2016). These results highlight the importance of MTM1 phosphatase activity for muscle maintenance and function. However, the same disease model can also be partially rescued by expressing a phosphatase inactive MTM1 protein (Amoasii et al., 2012), supporting the concept that PPIn-unrelated functions of myotubularin are also implicated in this pathology.

A third approach based on targeting DNM2 has been investigated, as increased levels of DNM2 dynamin have been detected in XLCNM patients and in *Mtm1* KO mice, and mutations in DNM2 lead to the autosomal dominant form of centronuclear myopathy (Bitoun et al., 2005; Cowling et al., 2014). Based on this, the downregulation of *DNM2* expression by genetic cross (generating heterozygote mice KO for *DNM2*) or by antisense oligonucleotide-mediated knockdown also improved the muscular phenotypes and the survival of *Mtm1* KO mice (Cowling et al., 2014; Tasfaout et al., 2017).

An *Mtm1* p.R69C mouse line has been generated based on the patient mutation, to mimic milder forms of XLCNM. These knockin (KI) mice carry a splice site mutation leading to the expression of only a low level of functional MTM1 protein (Pierson et al., 2012). However, this low level is sufficient to ameliorate the myopathic phenotypes compared to *Mtm1* KO mice, with an increased muscular strength and a lifespan often exceeding one year. This model has also been used to test therapeutic approaches for XLCNM, with variable degrees of success (Dowling et al., 2012; Lawlor et al., 2014; Lim et al., 2015).

Canine model

Contrary to other vertebrate models of centronuclear myopathy, the canine model was not generated but was discovered as a naturally occurring mutation in several related litters of Labrador Retriever puppies (Beggs et al., 2010). The causative N155K mutation in *MTM1* induces a general muscle weakness and atrophy starting at 8 weeks of age and leading to premature death at 15 to 26 weeks of age (Figure 5A). Expression of this mutant in COS-1 cells shows a sequestration of MTM1-N155K in proteasomes, where it is presumably degraded. Affected dogs exhibit histological phenotypes similar to mouse models, including myofiber hypotrophy, centralized nuclei, organelles mislocalization and sarcotubular system disorganization (Figure 5B-C) (Beggs et al., 2010; Childers et al., 2014). It also presents specific histological patterns of mislocalized organelles and mitochondria that are absent from both murine and human XLCNM (Beggs et al., 2010; Childers et al., 2014). Note that another canine XLCNM (p.Q384P caused by a missense mutation in exon 11 of *MTM1*) was recently reported in Rottweiler dogs, presenting similar clinical and histological phenotypes than Labrador Retriever dogs (Shelton et al., 2015).

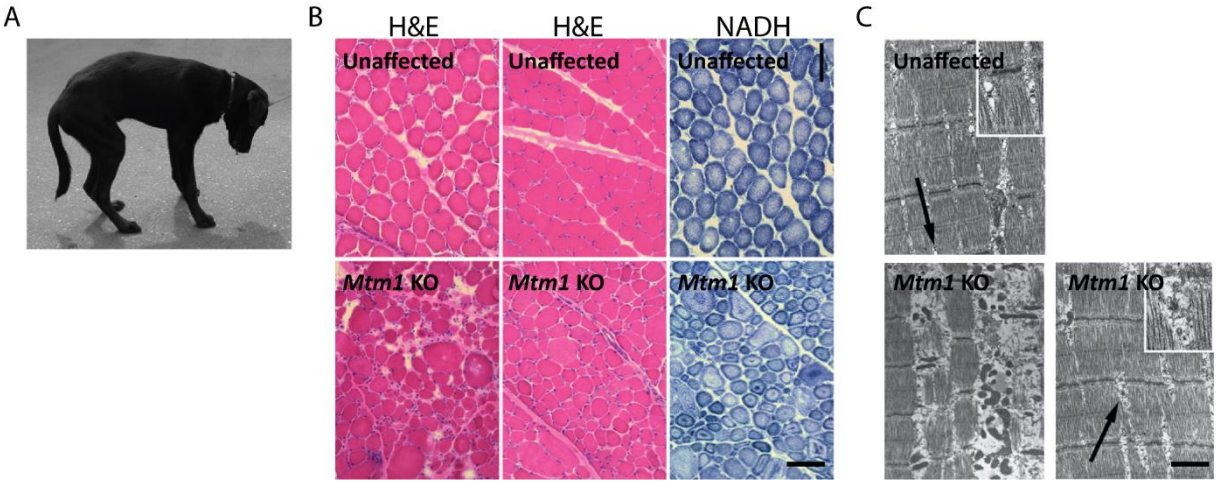

Figure 5: Clinical and histological phenotypes of the XLCNM canine model. Adapted from Beggs *et al*. 2010. **(A)** Picture of a 4 month-old male Labrador Retriever affected with XLCNM, illustrating the generalized muscle atrophy and characteristic kyphosis. **(B)** H&E and NADH staining of transverse muscle sections from unaffected female carrier (Unaffected) and *Mtm1* KO dogs. Scale bar 100 µm. **(C)** Electron microscopy of longitudinal muscle sections from unaffected female carrier (Unaffected) and *Mtm1* KO dogs. Scale bar 2 µm. Representative triads are showed by an arrow and displayed in the zoom square.

The Labrador Retriever canine model has been used to test gene therapy for XLCNM: systemic intravenous injection of serotype 8 adeno-associated virus (AAV8) expressing MTM1 improves muscle strength, histology and dog survival (Childers et al., 2014; Mack et al., 2017). Combined with the results obtained in the *Mtm1* KO mouse model, this paves the way for clinical trial and the use of gene therapy to treat XLCNM patients.

B. The Charcot-Marie-Tooth neuropathy Type 4B1

1. The causative gene

The Charcot-Marie-Tooth neuropathy Type 4B1 (CMT4B1, OMIM # 601382) is one of the various forms of inherited neuropathies grouped under the name of Charcot-Marie-Tooth (CMT) syndrome, also called hereditary motor and sensory neuropathy (HMSN). CMT has been named after the 3 investigators who described them in 1886, and gather neurological diseases affecting the peripheral nervous system.

This pathology affects 1/2500 newborn and is the most common inherited neurological disorder (Saporta et al., 2011). Even if mutations in more than 30 different genes have been implicated in CMT, most affected patients share clinical similarities, with onset in the first two decades of life, a progressive distal weakness and atrophy associated with sensory loss, *pes cavus* foot deformity, and absent ankle reflexes (Saporta et al., 2011).

CMT has been divided into 9 subgroups based on clinical features, gene localization (autosomal or allosomal) and mode of transmission (dominant or recessive). Thus, CMT4 define axonal and demyelinating neuropathies transmitted by autosomal recessive inheritance. To date mutations in 11 genes have been identified: *GDAP1* (CMT4A), *MTMR2* (CMT4B1), *MTMR13/SBF2* (CMT4B2), *MTMR5/SBF1* (CMT4B3), *SH3TC2* (CMT4C), *NDRG1* (CMT4D), *EGR2* (CMT4E), *PRX* (CMT4F), *HK1* (CMT4G), *FGD4* (CMT4H), *FIG4* (CMT4J) and *SURF1* (CMT4K).

MTMR2 gene

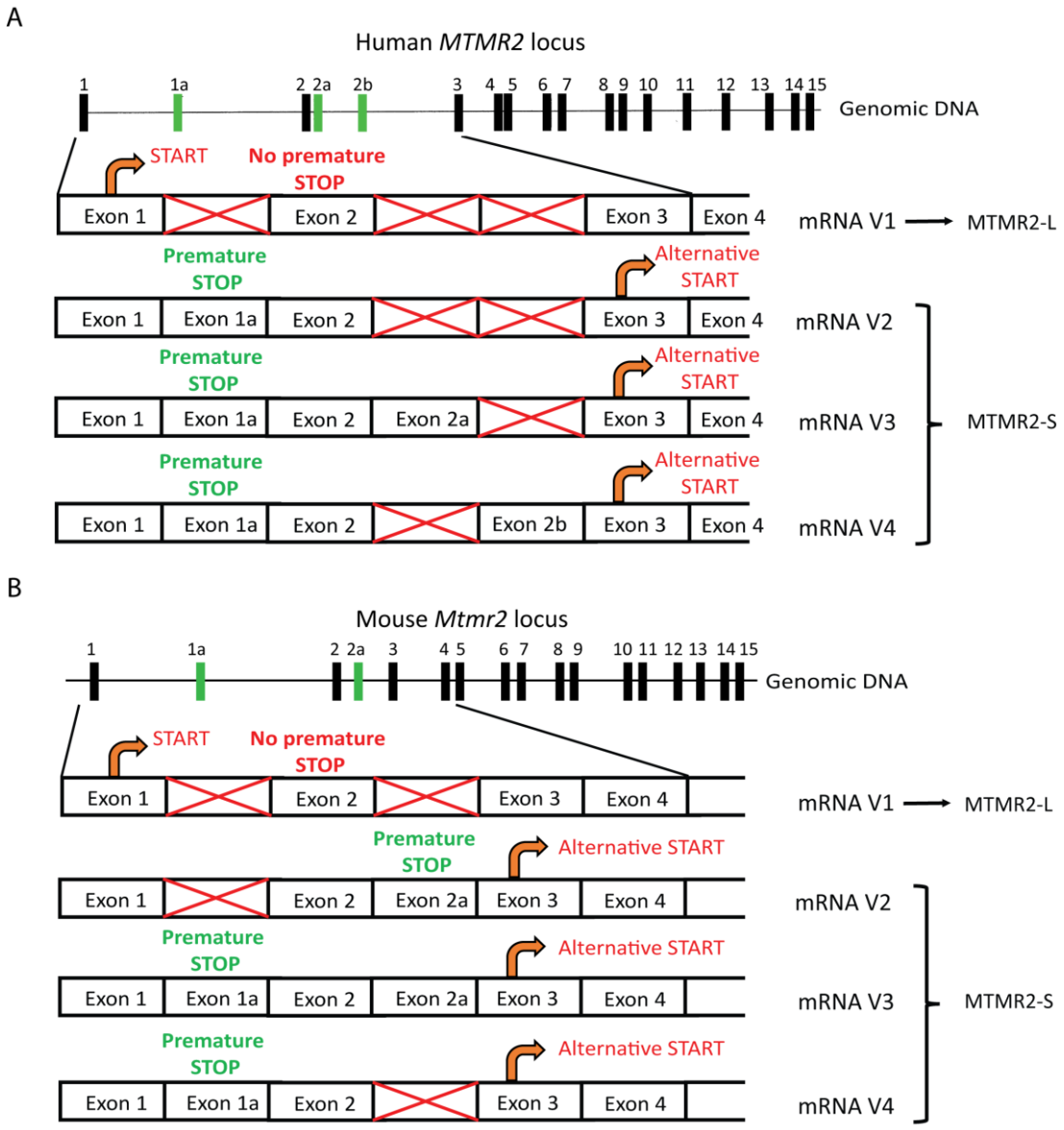

Figure 6: Genomic structure and mRNA isoforms of MTMR2 in humans (A) and mice (B). Inclusion of any shown combination of the alternative exons 1a, 2a or 2b (2b being only present in humans) brings a premature stop codon and unmasks an alternative start site in exon 3. In humans and mice, MTMR2 V1 encodes for MTMR2-L while isoforms V2 to V4 encode for MTMR2-S.

MTMR2 localized on chromosome 11q21 is the causative gene of CMT4B1 (Bolino et al., 2000; Houlden et al., 2001; Laporte et al., 1998). 15 exons were initially identified, but Bolino *et al.* described 3 additional exons named 1a, 2a and 2b and their inclusion by alternative splicing allows the expression of 4 different transcripts variants (V1 to V4) that are ubiquitously expressed (Figure 6A) (Bolino et al., 2002; Bolino et al., 2000). Transcript

variant V1 does not contain any additional exons and leads to the translation from exon 1 encoding for a 643 amino acids (aa) protein isoform, while V2 to V4 include exon 1a, leading to a premature STOP codon and to the translation from an alternative start codon in exon 3. Thus, V2 to V4 are used for the translation of a shorter MTMR2 protein isoform of 571 aa. This translational start site multiplicity is present in other genes and allowed by a mechanism of leaky ribosomal scanning (Calkhoven et al., 1994; Kozak, 1995). In this manuscript I named MTMR2-L (long) the most studied 643 aa isoform and MTMR2-S (short) the less known 571 aa isoform.

In mice, a similar alternative splicing system has been found (containing only two additional exons compared to three in human) and also leads to the translation of MTMR2-L and MTMR2-S (Figure 6B) (Bolino et al., 2002). To date, the specific functions of these MTMR2 isoforms are not known, and this constitutes one of the main questions addressed in this thesis.

Finally, a recent paper identified an alternative SOX10-responsive promoter at *MTMR2* that displays strong regulatory activity in immortalized rat Schwann cells. This promoter directs transcription of a new MTMR2 transcript that is predicted to encode the short MTMR2-S isoform.

MTMR2 mutations

According to the Human Gene Mutation Database (http://www.hgmd.cf.ac.uk), 23 mutations in *MTMR2* have been linked to CMT4B1. As for *MTM1*, most of the mutations found in *MTMR2* are nonsense or frameshift mutations leading to a premature STOP codon and the production of a truncated dysfunctional protein (Bolino et al., 2000). Some missense mutations highlight amino acids that are important for MTMR2 structure and function (Figure 7).

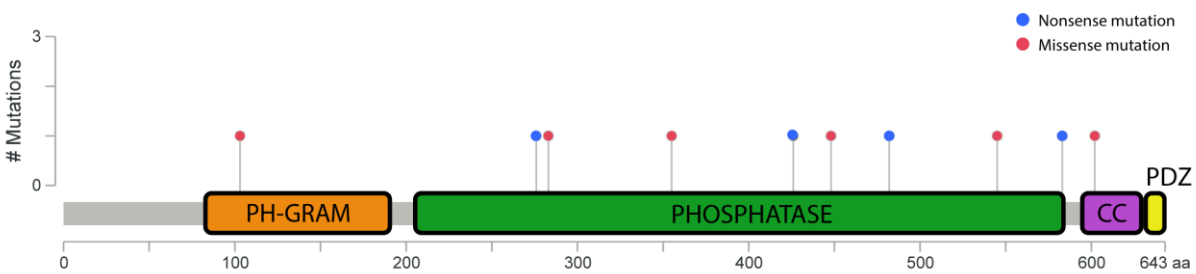

Figure 7: Position of CMT4B1-linked nonsense and missense mutations on human MTMR2 protein. Each dot represents a nonsense (blue) or missense (red) mutation listed in the Human Gene Mutation Database (http://www.hgmd.cf.ac.uk) for MTMR2. In total, 4 nonsense and 6 missense mutations were linked to CMT4B1 in human MTMR2. The mapping was done using the mutation mapper of cBioPortal (http://www.cbioportal.org/mutation_mapper.jsp). PH-GRAM (Pleckstrin Homology - Glucosyltransferase, Rab-like GTPase Activator and Myotubularins) domain, phosphatase domain, CC (coiled-coil) domain and PDZ domain are represented.

MTMR2 cellular functions

In vitro studies show that MTMR2, as MTM1, is a specific phosphoinositide (PPIn) 3-phosphatase that dephosphorylate the PtdIns3*P* and PtdIns(3,5)P_2 into PtdIns and PtdIns5*P*, respectively (Berger et al., 2002; Tronchere et al., 2004). MTMR2 showed high efficiency and peak activity at neutral pH, suggesting an in vivo function in the cytosol or in non-acidic vesicles (Berger et al., 2002). However, MTMR2 cellular functions are not fully understood.

In vivo, the ability of MTMR2 to dephosphorylate its substrates is still under debate. Lorenzo *et al.* show that MTMR2 (as MTM1) is able to dephosphorylate an endosomal pool of PtdIns3*P* when overexpressed in HeLa cells (Lorenzo et al., 2006), while Kim *et al.* state that overexpression of MTMR2 in COS-1 cells does not change the PtdIns3*P* level (Kim et al., 2002). A third study shows that MTMR2 is able to dephosphorylate a late endosomal pool of PtdIns3*P* and affects late endosome trafficking (Cao et al., 2008). Finally, Vaccari et al. suggest that PtdIns(3,5)P_2 is the physiological substrate of MTMR2 in the nerve (Vaccari et al., 2011) These experimental differences could be due to post-transcriptional modifications of MTMR2. Indeed, Franklin *et al*. described two phosphorylation sites (S58 and S631) that regulate the targeting of MTMR2 to different endosomal compartments, to regulate different pools of PtdIns3*P* (Franklin et al., 2013; Franklin et al., 2011). Phosphomimetic MTMR2-S58E mutant remains in the cytoplasm when overexpressed in HeLa cells, while unphosphorylable MTMR2-S58A mutant colocalizes with early endosomes. The S631 phosphorylation site regulates the shift of MTMR2 between Rab5-positive and APPL1-positive endosomes. Through this mechanism, MTMR2 seems to be implicated in endosome maturation, endosome signaling, and potentially in endocytosis (Franklin et al., 2013; Xhabija et al., 2011).

Other myotubularins implicated in CMT4

Two other myotubularins, MTMR5/SBF1 and MTMR13/SBF2, have been found to be mutated in CMT4B3 (OMIM # 615284) and CMT4B2 (OMIM # 604563), respectively (Alazami et al., 2014; Azzedine et al., 2003; Nakhro et al., 2013; Senderek et al., 2003). MTMR5 and MTMR13 are two dead (catalytically inactive) members of the myotubularin family that interact with active MTMR2 to form heterodimers and regulate MTMR2 function and phosphatase activity (Kim et al., 2003; Robinson and Dixon, 2005). Thus, mutations in

these two genes induce CMT4 through MTMR2 dysregulation, which may explain why CMT4B1, 2 and 3 are clinically indistinguishable.

2. Clinical and histological features

CMT4B1, as most of the CMT, is clinically characterized by distal motor and sensory impairment, pronounced muscular atrophy, and a foot deformity named *pes cavus* (fixed plantar flexion) (Figure 8A) (Quattrone et al., 1996). Patients often develop a *pes equinovarus* (or "clubfoot") with internally rotated feet, and facial muscle weakness. Compared to XLCNM, CMT4B1 is a much less severe disease, with a mean age of onset at 3-5 years old and a progressive distal and proximal muscle weakness of lower limbs. Patients have no cognitive defects and a life expectancy of 40-50 years old. Since no therapeutic treatment is available at this point, CMT patients are only treated for the associated symptoms. Orthopedic care helps for autonomous ambulation and to prevent falls.

Contrary to *MTM1* mutations that specifically affect muscle cells, *MTMR2* mutations affect the peripheral nervous system, and more specifically the Schwann cells. These specialized cells wrap around axons of motor and sensory neurons to form the myelin sheath, an essential component that isolates the axon and accelerates the action potential. The main histopathological features of CMT4B1 are the demyelination and the presence of focally folded (outfoldings) myelin sheaths around peripheral nerves, inducing a reduced nerve velocity (Figure 8B-C) (Quattrone et al., 1996).

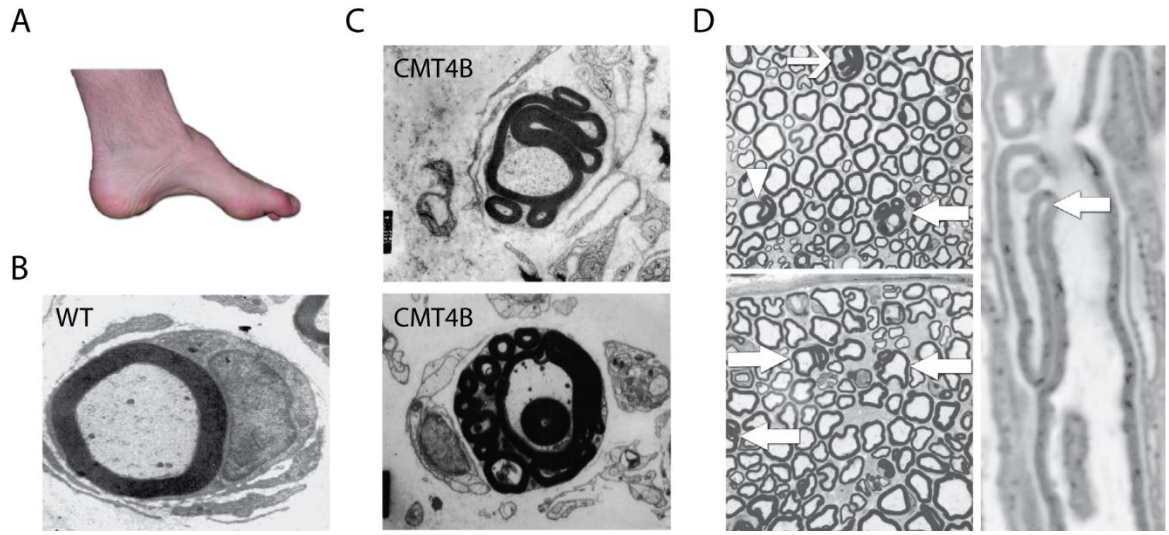

Figure 8: Clinical and histological phenotypes of CMT4B1 patients and associated mouse model. **(A)** Characteristic *pes cavus* phenotype. **(B)** Electron microscopy of a transverse section of peripheral nerves from unaffected human. Adapted from Kumar *et al.* 2003. **(C)** Electron microscopy of transverse sections of peripheral nerves from two CMT4B1 patients, illustrating the characteristic myelin sheath outfoldings. Adapted from Quattrone *et al.* 1996 and Gambardella *et al.* 1998. (D) Tranverse (left) and longitudinal (right) sections of sciatic nerves from 7 week-old *Mtmr2* KO mice. Myelin outfoldings are indicated by white arrows. Adapted from Bolino *et al.* 2004.

3. Animal models

To better understand the pathophysiological mechanisms of CMT4B1 and the cellular and molecular functions of MTMR2, several mouse models of have been generated.

Bolino *et al.* generated *Mtmr2* KO mice by excision of exon 4 that induces a frameshift and the production of a dysfunctional protein (Bolino et al., 2004; Houlden et al., 2001). These mice present a CMT4B1-like neuropathy with myelin outfoldings (as in CMT4B1 patients) and impaired spermatogenesis (Figure 8D). Histology of the brain, spinal cord and muscle (including ATPase isotype staining) was normal at 2 months of age (Bolino et al., 2004). Two other mouse models were generated, with specific depletion of *MTMR2* in either Schwann cells or motor neurons (Bolino et al., 2004; Bolis et al., 2005). Disruption of *MTMR2* in Schwann cells reproduces the same phenotypes as observed in *MTMR2*-null mice, while the disruption of *MTMR2* in motor neurons has no visible incidence on the peripheral nervous system. This corroborates a Schwann cells-specific function of MTMR2, which negatively regulates the membrane/vesicle trafficking and delivery to the plasma membrane, that is essential during myelination (Bolis et al., 2005; Bolis et al., 2009).

Another team generated a CMT4B1 mouse model that mimics a patient mutation, by introducing an E276X mutation (G to T mutation in exon 9 of *MTMR2*) and deleting the 3' terminal region immediately after the stop codon of *MTMR2* (Bolino et al., 2000; Bonneick et al., 2005). The histology shows complex myelin infoldings and outfolding in peripheral nerves, and especially in distal nerves. However contrary to CMT4B1 patients, no electrophysiological change was observed, suggesting that the nerve velocity is not necessarily linked to the myelin sheath morphology (Bonneick et al., 2005).

III. The myotubularin family

To better understand MTM1 and MTMR2 specific functions, it is essential to understand the protein family they belong to. Here I focus on gene expression, protein interactions and protein structure in the myotubularin family. This chapter is mainly based on the review "**WANTED - Dead or alive: Myotubularins, a large disease-associated protein family**" that we published recently (Raess et al., 2017) (Appendix 1). Several points have been discussed in more detail here to develop key points relevant to my project.

A. Introduction

Myotubularins constitute a large disease-associated family highly conserved through evolution with similarities to phosphatases. In humans there are 14 clear paralogs of myotubularins: the first identified was MTM1 followed by 13 myotubularin-related proteins MTMR1 to MTMR13 (Laporte et al., 2003; Laporte et al., 1996; Robinson and Dixon, 2006). Among them, 8 proteins are active phosphatases while 6 are catalytically dead, with a functional cooperation between members of these two classes (Kim et al., 2003; Nandurkar et al., 2003). In addition MTMR14 protein (also named hJUMPY) has been described (Tosch et al., 2006), however phylogenetic studies and protein domain composition suggested it defines a close but distinct protein family, and therefore this protein will not be discussed further in this chapter. Additional pseudogenes related to myotubularins also exist (Alonso et al., 2004).

Although active myotubularins have been tentatively classified as Protein Tyrosine Phosphatases (PTP) based on the presence of a $C(X)_5R$ motif, they are specific phosphoinositide (PPIn) 3-phosphatases that dephosphorylate the phosphatidylinositol-3-monophosphate (PtdIns3*P*) and PtdIns(3,5)P_2 into PtdIns and PtdIns5*P*, respectively (Blondeau et al., 2000; Taylor et al., 2000; Tronchere et al., 2004; Walker et al., 2001). Conversely, dead myotubularins share a similar organization in domains but lack the phosphatase activity (Cui et al., 1998; Nandurkar et al., 2001).

PPIn are lipid second messengers implicated in a wide range of cellular processes from cell growth and survival to cytoskeleton dynamics (Di Paolo and De Camilli, 2006;

Staiano et al., 2015). More specifically, PtdIns3*P* and PtdIns(3,5)P_2 regulate membrane trafficking at the endosomal level and autophagy, which are the most studied and characterized functions of myotubularins (Nicot and Laporte, 2008; Robinson and Dixon, 2006). PtdIns5*P* is implicated in several cellular processes including oxidative stress signaling, growth factor signaling and transcriptional regulation (Bulley et al., 2015; Giudici et al., 2016; Gozani et al., 2003a; Keune et al., 2013; Ramel et al., 2011).

Myotubularins have been found in almost all eukaryotes from yeast to mammals, with few exceptions as *Plasmodium falciparum* (Lecompte et al., 2008). Orthologs for the 14 human myotubularins are found in chordates except in rodents where MTMR8 is absent at least in mice and rats. A co-evolution has been observed between active and dead myotubularins, as well as between active myotubularins and antagonist kinases (Lecompte et al., 2008). For example MTM1 with the class-III PtdIns 3-kinase VPS34 (PIK3C3) and its regulator VPS15 (PIK3R4).

In yeast, there is only one myotubularin homolog, named *YMR1* for Yeast Myotubularin Related 1. *YMR1* deletion leads to a 2-fold increase of the myotubularin substrates PtdIns3*P* and PtdIns(3,5)P_2, leading to a fragmented vacuole phenotype (Parrish, W.R. et al., 2004; Taylor et al., 2000). The absence of major phenotype despite the depletion of the unique active myotubularin can be explained by the existence of two close phosphatases, the synaptojanin-like proteins Sjl2 and Sjl3. These proteins non-specifically dephosphorylate the D3, D4 or D5 phosphate of phosphoinositides, while Ymr1 (and other myotubularins) mainly dephosphorylate the D3 phosphate (Guo et al., 1999). Contrary to *ymr1Δ*, the triple deletion *ymr1Δsjl2Δsjl3Δ* is lethal (Parrish, W.R. et al., 2004).

Why have so many myotubularins been duplicated and conserved? Indeed, the presence of 14 similar proteins in humans could lead to functional redundancy, however this high evolutionary pressure suggests that each myotubularin has one or several specific function(s). This specificity could be related to tissue expression or splice isoforms, or particular protein-protein interactions. This specific point will be developed in this chapter.

To date, mutations were found in 4 myotubularin genes in monogenic human diseases. *MTM1* is mutated in X-linked centronuclear myopathy (XLCNM, OMIM # 310400)

(Jungbluth et al., 2008; Laporte et al., 1996). Three other myotubularins, *MTMR2* (encoding active phosphatase), *MTMR5/SBF1* and *MTMR13/SBF2* (both dead phosphatases), are mutated in Charcot-Marie-Tooth neuropathy type 4B1 (CMT4B1, OMIM # 601382), 4B3 (CMT4B3, OMIM # 615284) and 4B2 (CMT4B2, OMIM # 604563), respectively (Alazami et al., 2014; Azzedine et al., 2003; Bolino et al., 2000; Nakhro et al., 2013; Senderek et al., 2003). In addition, several myotubularins are linked to multifactorial diseases as colorectal, gastric and lung cancers (MTMR3 and 7) (Hu et al., 2011; Song et al., 2010; Weidner et al., 2016), obesity (MTMR9) (Hotta et al., 2011) and Creutzfeldt–Jakob disease (MTMR7) (Sanchez-Juan et al., 2012). The fact that ubiquitously expressed myotubularins are implicated in different tissue-specific diseases again indicates that the apparent biochemical redundancy is in fact hiding tissue-specific functions.

B. Myotubularins: protein domains and interactions

Myotubularins are multidomain proteins that share the same central core composed of the PH-GRAM (Pleckstrin Homology - Glucosyltransferase, Rab-like GTPase Activator and Myotubularins) domain and the phosphatase-like domain (Figure 9A) (Begley et al., 2003; Choudhury et al., 2006; Doerks et al., 2000; Tsujita et al., 2004). In the 8 active myotubularins (MTM1, MTMR1-4 and 6-8), the catalytic domain contains the consensus $C(X)_5R$ signature motif (Alonso et al., 2004; Zhang et al., 1994). In the 6 phosphatase-dead myotubularins (MTMR9-12, MTMR5/Sbf1 and MTMR13/Sbf2), the absence of enzymatic activity is due to the substitution of catalytically essential residues such as the cysteine in the consensus motif (Cui et al., 1998; Nandurkar et al., 2003).

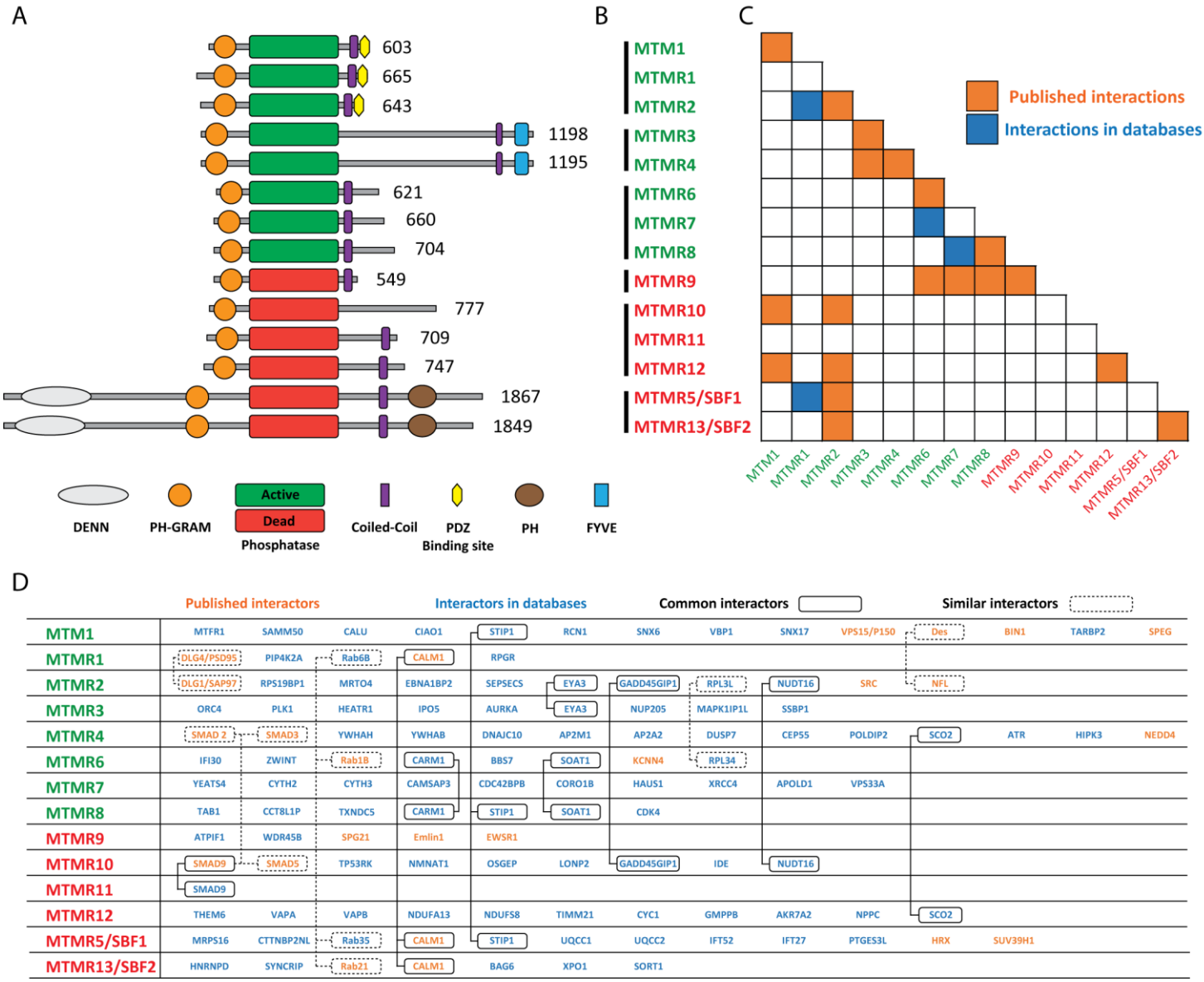

Figure 9: Human myotubularins: domain organization and interactome. (A) Scaled representation of the protein domains of human myotubularins. All myotubularins share the PH-GRAM and phosphatase (active or dead) domains. For each myotubularin, amino acid length of the most described protein isoform is indicated. **(B)** Classification of myotubularins into 6 subgroups based on protein organization and phylogenetics (indicated by the vertical bars on the left). Active myotubularins are represented in green and dead myotubularins in red. (**C)** Known protein interactions within the myotubularin family. Published interactions are in orange while interactions found in databases (Biogrid - thebiogrid.org) are in blue. (**D)** List of known interactors for each myotubularin. Published interactors are represented in orange while interactors found in databases with a minimum MUSEscore of 0,95 (Biogrid and Li *et al.*, 2016) are in blue. Common interactors and interactors of the same protein family are surrounded and related together by a continuous and stippled line, respectively. Similar interactors found for a specific myotubularin are not surrounded.

Myotubularins can have several other functional domains: the PDZ binding site (MTM1, MTMR1 and 2) mediates protein-protein interactions, the PH (Pleckstrin homology) (MTMR5 and 13) and FYVE (Fab1-YOTB-Vac1-EEA1) (MTMR3 and 4) domains can bind PPIn (Itoh and Takenawa, 2002), and the DENN domain (MTMR5 and 13) is involved in small GTPase Rab regulation (Fabre et al., 2000; Jean et al., 2012; Yoshimura et al., 2010),. By combining domain organization and phylogenetics, 6 different subgroups are highlighted, each containing exclusively active or dead members (Figure 9B). In addition, all myotubularins except MTMR10 contain a coiled-coil (CC) domain that is critical for their homodimerization and/or heterodimerization (Berger et al., 2006; Lorenzo et al., 2006). Dimerization also appears to depend on the PH-GRAM domain (Berger et al., 2006).

Indeed, all myotubularins except MTMR11 have been shown to interact either with themselves or with other myotubularins (Figure 9C) (Berger et al., 2006; Gupta et al., 2013; Kim et al., 2003; Lorenzo et al., 2006; Mochizuki and Majerus, 2003; Nandurkar et al., 2003; Schaletzky et al., 2003; Zou et al., 2009). Within the 14 members, 9 have been reported to form homodimers; this could enhance the membrane targeting by coupling two PH-GRAM domains (Berger et al., 2003). At least for MTM1, homo-oligomerization controls its allosteric activity, and *in vitro* MTM1 incubated with its substrate PtdIns3*P* forms a heptamer in the presence of PtdIns5*P* (Schaletzky et al., 2003).

Myotubularins also form heterodimers, and one of the most notable characteristics of this family is that most heterodimers are formed by a coupling between active/dead phosphatases. For example, MTMR2 forms heterodimers with its dead homologs MTMR5/Sbf1, MTMR10, MTMR12 and MTMR13/Sbf2. The fact that mutations in MTMR5 and MTMR13 lead to a similar neuropathy (CMT4B) as defects in MTMR2 confirms the physiological importance of dead phosphatases. MTMR9 interacts with 3 different active myotubularins of the same phylogenic subgroup (MTMR6, 7 and 8) and increases their enzymatic activity (Mochizuki and Majerus, 2003). In the same way, MTMR5 increases the enzymatic activity of MTMR2 and both are related to male infertility due to impaired spermatogenesis (Bolino et al., 2004; Firestein et al., 2002; Kim et al., 2003). In some heterodimers, such as MTM1-MTMR12, MTMR2-MTMR5 and MTMR2-MTMR13, the dead myotubularin may regulate the cellular localization of the active member (Gupta et al., 2013; Kim et al., 2003; Nandurkar et al., 2003). Dead myotubularins appear early in evolution

and are conserved in many species (Laporte et al., 2003; Lecompte et al., 2008). Altogether, this suggests (1) a co-evolution between active and dead myotubularins and (2) that myotubularins rely on oligomerization for their function since very early in the evolution. Heterodimers can also be formed between two active members of the same phylogenic subgroup, as for MTMR1-MTMR2, MTMR3-MTMR4, MTMR6-MTMR7 and MTMR7-MTMR8 (Figure 9C).

Numerous interactors have been identified for each myotubularin (Figure 9D) (Biogrid - thebiogrid.org and Intact - http://www.ebi.ac.uk/intact/) (Agrawal et al., 2014; Berggard et al., 2006; Cao et al., 2007; Cui et al., 1998; Fabre et al., 2000; Firestein et al., 2000; Jean et al., 2012; Li et al., 2016; Plant et al., 2009; Royer et al., 2013; Rual et al., 2005; Srivastava et al., 2005; Yu et al., 2013; Zhang et al., 2005). Some myotubularins share common interactors or interactors from the same protein family. For example, MTMR6 and MTMR8 both interact with SOAT1, a protein localized in the endoplasmic reticulum, which is also the presumed localization of these myotubularins. MTM1 interacts with desmin and MTMR2 with neurofilament light chain (NFL), that are two intermediate filament proteins specifically found in muscles and neurons, respectively (Hnia et al., 2011; Previtali et al., 2003). This is consistent with mutations in MTM1 and desmin leading to myopathies and mutations in MTMR2 and NFL leading to CMT neuropathies (Goldfarb et al., 1998; Mersiyanova et al., 2000). Another well-represented group of interactors is the Rab family: MTMR1-RAB6B, MTMR6-RAB1B, MTMR5-RAB35 and MTMR13-RAB21 (Jean et al., 2012; Mochizuki et al., 2013). Rabs constitute a very large GTPase family regulating many steps of membrane trafficking, one of the main cellular functions in which myotubularins are implicated (Barr, 2013). Of note, myotubularins implicated in 3 heterodimers share common or similar interactors: MTMR1-MTMR2, MTMR1-MTMR5 and MTMR2-MTMR10. For example, MTMR1 and MTMR5 heterodimerize and interact with similar Rab GTPases (Figure 9D).

C. Myotubularins: tissue expression

To investigate how myotubularin genes are expressed in human tissues, we mined the Genotype-Tissue Expression (GTEx) database, which has been built by systematic RNA-sequencing using samples of 51 different tissues coming from hundreds of donors and 2 transformed cell types in culture.

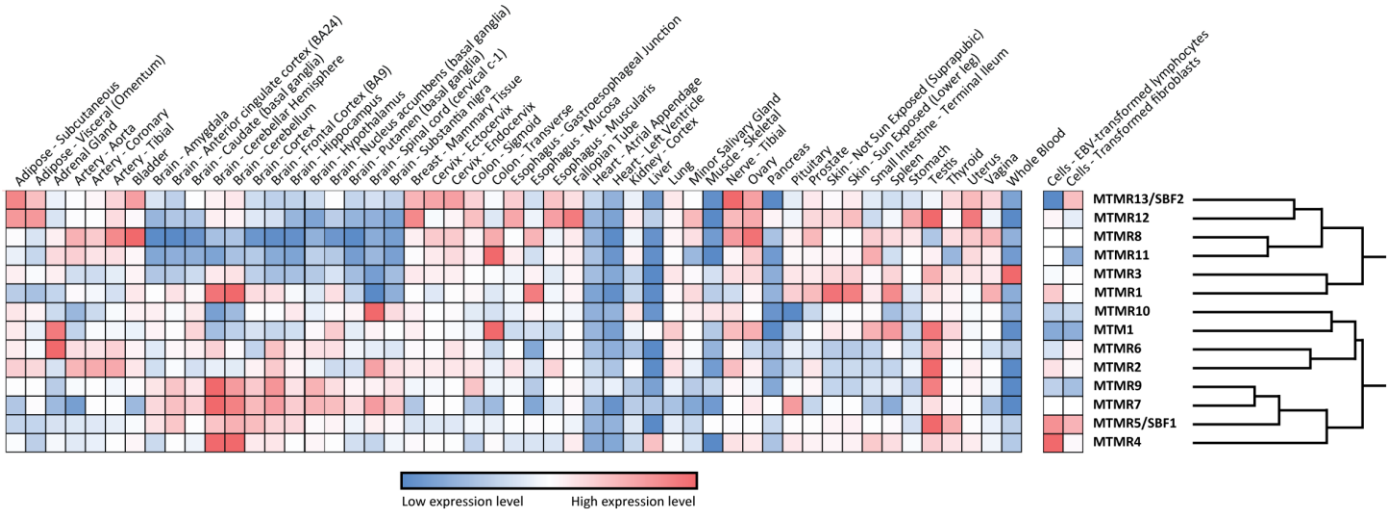

Figure 10: Myotubularins tissue expression. Heat map of myotubularin genes relative expression within 51 different tissues and 2 cell types, underlining in which tissue a specific myotubularin is the most/less expressed (left panel). Expression levels have been obtained by mining the GTEx database (www.gtexportal.org/home/). Dendrogram highlighting the hierarchical clustering of myotubularins (right panel), using the Pearson correlation coefficient and average linkage.

Figure 10 shows for each gene the relative expression in all tested tissues, and highlights in which tissue a specific myotubularin is the most/less expressed. This is not absolute expression, therefore we should keep in mind that each gene cannot be directly compared to another for the same tissue. A dendrogram was generated using the Pearson correlation coefficient to highlight hierarchical clustering of myotubularins sharing similar profiles of expression. Whilst this is one of many possible dendrograms and thus it has to be interpreted cautiously, two main groups of myotubularins can be distinguished based on expression profiles: MTMR1-3-8-11-12-13 (upper branch, Figure 10), and the others (lower branch). Discriminant tissues between the two groups are brain (almost all regions), skin, vagina and prostate. This does not seem to be directly related to phylogenetic classification, to active/dead and active/active heterodimers or to myotubularins sharing common interactors. However, some links can be made. For example, MTMR7 and MTMR9 that form an

active/dead heterodimer have the closest expression profiles and are both strongly expressed in brain tissues. A similar link applies to MTM1, MTMR2 and MTMR10, which have correlated expression patterns: they form two active/dead heterodimers MTM1/MTMR10 and MTMR2/MTMR10, and MTMR2 and MTMR10 have common interactors (Figure 9C and D) (Lorenzo et al., 2006).

Concerning myotubularins related to monogenic diseases, while MTM1 has a low expression level in striated muscles compared to other tissues such as nerves, colon or testis, mutations in the *MTM1* gene lead to a severe myopathy. Thus, the MTM1 tissue-specific function could be explained by interactions with partners that are only expressed in muscle, such as desmin (Hnia et al., 2011). On the contrary, MTMR2 and MTMR13 are highly expressed in nerves, which is consistent with the neuropathies observed due to mutations in these genes. In addition, MTMR2 binds the neuronal intermediate filament NFL (Previtali et al., 2003), highlighting a potential molecular basis common to different CMT neuropathy forms. A link can be observed between MTMR2 and MTMR5, known to form heterodimers; they both have a high relative expression level in testis, and defects of these genes lead to male infertility by impaired spermatogenesis (Bolino et al., 2004; Firestein et al., 2002), therefore adding weight to the physiological significance of these data.

Myotubularins expression levels have also been measured in two cell types, lymphocytes and fibroblasts that could be easily derived from human biopsies. These cells could allow diagnosis at the protein level or be dedifferentiated into induced pluripotent stem (IPS) cells that could be reprogrammed into specific cell types, allowing study of the pathocellular mechanisms. This time, absolute expression levels of all myotubularins are compared (Figure 10). Some myotubularins, such as MTMR5 or MTMR2, are well expressed in both lymphocytes and fibroblasts. Whereas for other myotubularins such as MTMR13, their expression level is higher in fibroblasts than in lymphocytes, suggesting that their study in these cell types might be more adapted. Therefore, interpreting these data can be useful in deciding which cell lines should be used for research and diagnostic purposes.

D. Myotubularin: mRNA isoforms

The study of gene expression does not take splicing events into account. Indeed, a specific gene is often spliced into several mRNA isoforms that could be translated into different protein isoforms. In this review, we use the term “isoform” to define a variant of the same protein or mRNA, and “homologs” for different genes. Figure 11 summarizes the myotubularin mRNA isoforms expression within all tissues present in the GTEx database. Only significantly expressed mRNA isoforms have been represented, and color-coded based on their predicted protein product: the main protein isoform from the literature, longer/shorter protein isoforms, or non-coding mRNA isoforms. For each mRNA isoform, the expression level is indicated as a percentage of total gene expression.

Interestingly, the main mRNA isoform studied in the literature is not always the most expressed (MTM1, MTMR3, MTMR10, MTMR11 and MTMR12). For MTMR10, the most expressed isoform encodes only the PH-GRAM; it raises the possibility that this protein isoform exerts a dominant negative effect on oligomerization of myotubularins or on cellular functions. MTMR2 has 4 well expressed mRNA isoforms: one translated into the main 643 amino acids (aa) protein isoform and the three others translated into a 571 aa protein isoform lacking the N-terminal extremity before the PH-GRAM (Bolino et al., 2001). The latter is present in all tissues except brain, and may have a specific function. In addition, some isoforms are tissue-specific, as for MTM1 with 2 isoforms only expressed in skeletal muscle. Corresponding peptides lack a part of the PH-GRAM domain and could support a muscle-specific function altered in the MTM1-related myopathy.

In total, 10 myotubularins express mRNA isoforms leading to shorter proteins and MTMR1 displays an isoform predicted to encode a longer protein. These differences can affect various protein domains as the FYVE domain for MTMR3 and MTMR4 or the DENN domain for MTMR5, and thus could highly impact on protein conformation or protein-protein/protein-lipid interactions.

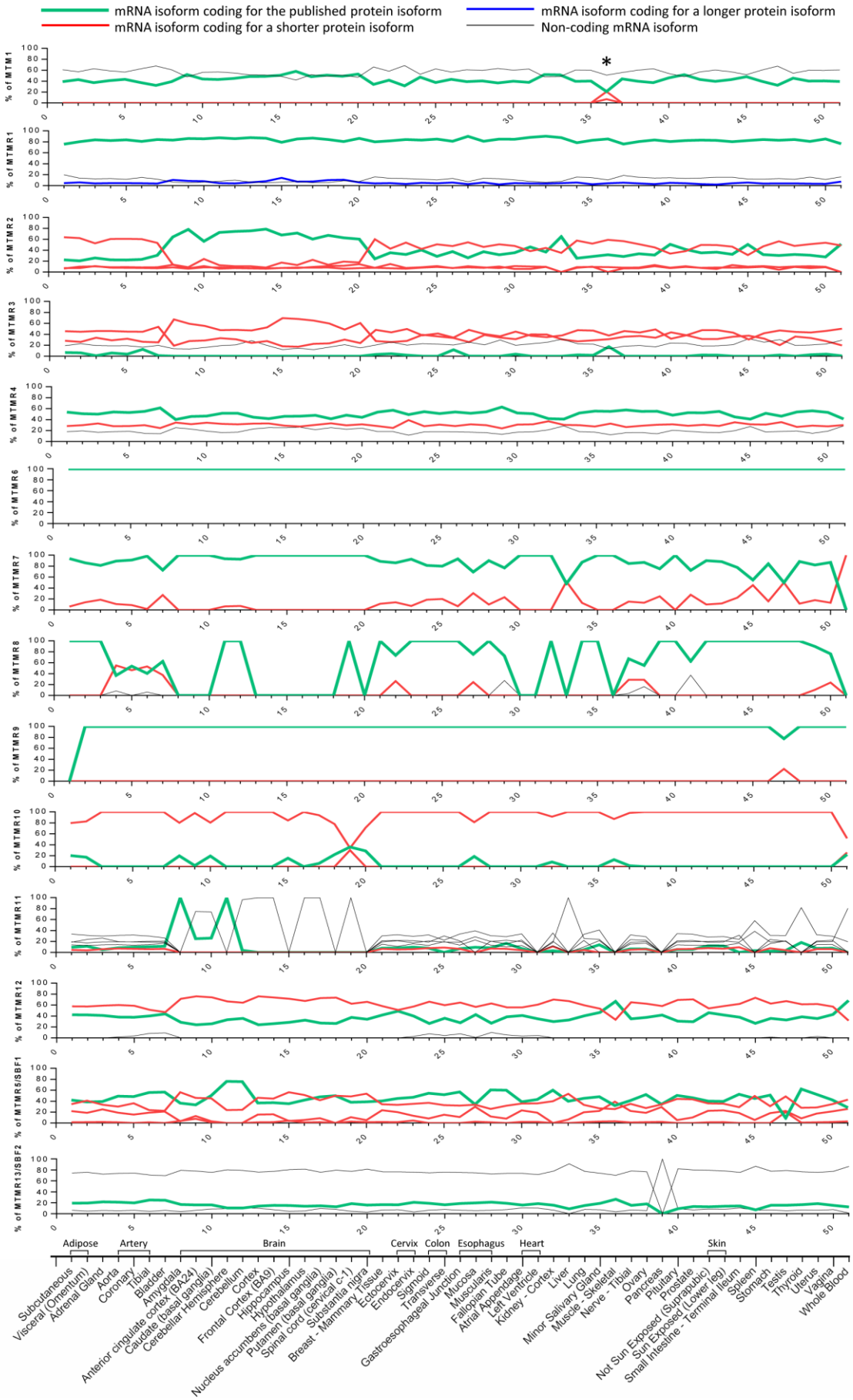

Figure 11: Myotubularin mRNA isoforms. For each myotubularin indicated on the left, the most expressed isoforms present in the GTEx database are represented as a percentage of total gene expression. Only the most expressed isoforms are shown. The mRNA isoforms coding for the main published protein isoforms are indicated in green, shorter isoforms in red and longer isoforms in blue. Several non-coding isoforms indicated in black have been found well expressed, for which no corresponding peptides have been described yet. The star indicates specific MTM1 mRNA isoforms in skeletal muscle, the tissue affected in MTM1-related myopathy. For several myotubularins as MTMR3, MTMR10 and MTMR12, and to a less extend MTMR2, the main expressed isoforms are different than the published isoforms used for functional characterization of the related proteins; for MTMR11 and MTMR13 the main expressed isoforms are predicted non-coding.

For MTM1, MTMR11 and MTMR13, the prevailing mRNA isoforms are non-coding, or the corresponding peptides have not been identified yet, questioning the function of such isoforms. Finally, some isoforms described in the literature are not represented here because they were absent in the GTEx database. This is the case for various MTMR1 mRNA isoforms that are known to be expressed in some tissues (Buj-Bello et al., 2002a).

In the future, it would be important to characterize the cellular activity of these tissue-specific isoforms, in order to get insight into their physiological relevance.

E. Myotubularins: protein structure.

Between 2003 and 2016, the crystal structures of 4 active myotubularins have been determined: MTMR1 (PDB: 5C16), MTMR2 (1LW3, 1ZVR, 1M7R and 1ZSQ), MTMR6 (2YFO) and MTMR8 (4YZI) (Begley et al., 2006; Begley et al., 2003; Bong et al., 2016). A crystal structure of mouse MTMR5 has also been solved, but only contains the C-terminal PH domain (1V5U). No major differences have been described between the 4 structures, except for the orientation of the MTMR6 PH-GRAM domain; this could impact MTMR6 oligomerization properties (Bong et al., 2016).

From a tridimensional point of view, myotubularins are globular proteins with two main parts: the PH-GRAM domain and the catalytic domain, connected by a linker (Figure 4A) (Begley et al., 2003). N-terminal extremities, coiled-coil domains and PDZ binding sites are absent of these structures, presumably because they are too flexible or cleaved by proteolysis. In addition, the cysteine residue of the catalytic $C(X)_5R$ motif has been mutated into a serine for crystallization, except for MTMR6.

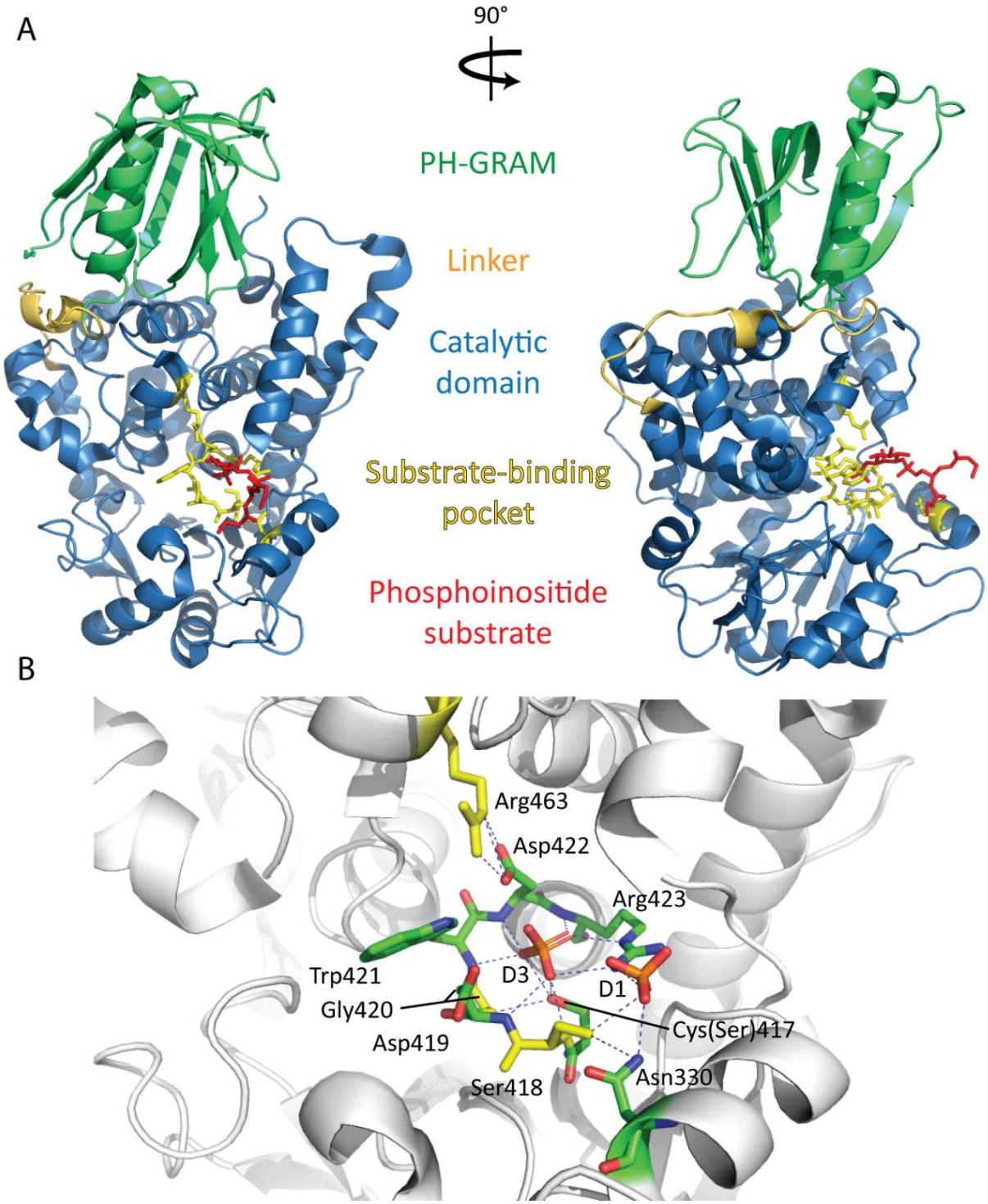

Figure 12: The myotubularins protein structure. (A) Overall view of the myotubularin structure. The crystal structure of MTMR2 (PDB:1ZSQ) is used as a model, with a front view and a view rotated at 90°. Domain names and the phosphoinositide substrate (here PtdIns3*P*) are indicated on the the two representations. (**B)** Zoom on the substrate-binding pocket. Residues forming the $C(X)_5R$ loop and other important residues are represented using stick models. Residues affected by missense mutations in MTM1-linked centronuclear myopathy are colored in yellow. No missense mutations have been found in *MTMR2* or *MTMR13* genes in the catalytic pocket. The cysteine residue of the $C(X)_5R$ motif is mutated to serine in the structure for crystallization purposes. Hydrogen bonds between the two phosphate groups in position D1 and D3 of PtdIns3*P*/PtdIns(3,5)P_2 and surrounding residues of the active site are represented by stippled lines.

The PH domain consists in 2 β-strands and 1 α-helix, combined with the 5 β-strands of the GRAM domain. The main characteristic of the catalytic domain is the substrate binding pocket that is significantly deeper and wider than that of classical tyrosine phosphatases, explaining the unique specificity of myotubularins for membrane-embedded PPIn substrates (Figure 4A) (Begley et al., 2003). Indeed, active myotubularins specifically hydrolyze the D-3 position of PtdIns3*P* and PtdIns(3,5)P_2, two PPIn with large phosphorylated inositol headgroups that perfectly fit in the catalytic pocket. The D-3 phosphate is then trapped by its interaction with the main chain of 6 residues from the $C(X)_5R$ motif loop (on MTMR2 sequence: Cys417, Ser418, Gly420, Trp421, Asp422 and Arg423) (Figure 4B). Concerning the catalytic activity, the nucleophile Cys417 residue attacks the phosphorous atom in position D-3 of the PPIn substrate, forming a phosphoenzyme intermediate, then the aspartic acid (Asp422 in MTMR2) donates a proton to the released dephosphorylated substrate, before hydrolysis yielding free enzyme and inorganic phosphate (Begley and Dixon, 2005; Begley et al., 2006; Nandurkar and Huysmans, 2002). Myotubularins are different from classical PTPs because the catalytic aspartate residue lies directly in the catalytic $C(X)_5R$ loop and not in a WPD-loop. The D-1 phosphate of the PPIn interacts with the side chain of two residues from the $C(X)_5R$ motif (on MTMR2 sequence: Ser418 and Arg423), but also with Asn330, which is conserved in all active myotubularins suggesting an important role in PPIn substrate binding. Some other residues help to maintain the three-dimensional structure of this catalytic pocket, like Arg463 (on MTMR2) that is also conserved in all myotubularins. However, a phosphate in position D-4 would generate a steric clash with several residues of the catalytic pocket, excluding PtdIns(3,4)P_2 and PtdIns(3,4,5)P_3 from potential substrates.

Another consideration for myotubularin substrate specificity is that active myotubularins are electrostatically polarized proteins, with one strongly electropositive side containing the catalytic site (Begley et al., 2006). This would create electrostatic interactions between the positively charged face of myotubularins and the negatively charged membranes containing PPIn, contributing to substrate-binding affinity. This electropositive patch around the pocket seems to be specific for active myotubularins, while several dead myotubularins have an electronegative surface, suggesting a poor affinity toward lipid membranes. Furthermore, active myotubularins could bind either membranes or dead-phosphatase homologs through the same interface.

The tridimensional structure is also very useful to understand the effect of disease-associated mutations and thereby to evaluate the importance of mutated residues for the function or the stability of the protein. The majority of MTM1, MTMR2 and MTMR13 missense mutations affect residues in the hydrophobic core structure of the PH-GRAM and catalytic domains, and replace native amino acids by bulkier residues, or decrease van der Waals contacts or alter internal hydrogen bonds, consequently disrupting the protein core structure. In addition, two clusters of solvent-accessible missense mutation at the surface of the MTM1 protein can be observed: the Pro179-Asn180-Arg184 cluster and the Asp431-Asp433 cluster (numbered in MTM1 sequence) that could be potential binding sites for interactors (Begley et al., 2003). In the active site, the Ser376, Gly378 and Arg421 (numbered Ser418, Gly420 and Arg463 in MTMR2 structure in Figure 4B) are frequent sites of mutations found in MTM1: the Ser376 and Gly378 directly bind the D-3 phosphate of the PPIn and the Arg421 is a key factor to maintain the position of the catalytic loop. Thus, mutations of these residues would directly prevent any catalytic activity.

F. Conclusion

Myotubularins define a large and highly conserved family of proteins with some noteworthy characteristics. They are classified in the Protein Tyrosine Phosphatases (PTP) family but have a specific phosphatase activity against phosphoinositides. One other feature is the presence of catalytically active and dead phosphatases, where dead myotubularins regulate their active homologs. Although they are ubiquitously expressed, four myotubularin genes – *MTM1*, *MTMR2*, *MTMR5* and *MTMR13* – are mutated in tissue-specific neuromuscular diseases, suggesting tissue-specific splice isoforms or specific protein-protein or protein-lipid interactions.

Future experiments will be needed to address this tissue specificity. While the function of myotubularins and PPIn substrates and products was well studied in cell systems, their physiological role *in vivo* is still barely understood. Another key issue is the pathological mechanism(s) associated with myotubularin-related diseases. Preliminary data showed that MTM1-related myopathy can be rescued in mice by inhibition or muscle-specific ablation of the class II PtdIns 3-kinase (Sabha et al., 2016; Velichkova et al., 2010). However, the same

disease model can also be rescued by expressing a phosphatase inactive MTM1 protein, supporting that PPIn-unrelated functions of myotubularin are implicated in this pathology (Amoasii et al., 2012). Due to the importance of myotubularins and PPIn pathways in metabolism and cellular integrity, it would not be surprising that their dysregulation will be highlighted in other diseases in the future.

IV. Phosphoinositides: key lipids in intracellular trafficking

It was inconceivable to me to talk about myotubularins without presenting their lipid substrates: the phosphoinositides. This chapter is based on the review of Dimitri Bertazzi *et al.* in which I participated, entitled "**Les phosphoinositides, des lipides acteurs essentiels du trafic intracellulaire.**" (Translation: Phosphoinositides, essential lipidic actors in the intracellular traffic) (Bertazzi et al., 2015) (Appendix 2). As was already mentioned in previous chapters, myotubularins are specific PPIn 3-phosphatases that dephosphorylate the PtdIns3*P* and PtdIns(3,5)P_2 into PtdIns and PtdIns5*P*, respectively (Blondeau et al., 2000; Taylor et al., 2000; Tronchere et al., 2004; Walker et al., 2001). Therefore I will mainly focus on these 4 phosphoinositides. The review was published in French in 2015, so I translated and updated it. The Figure 13 and Figure 14 come from De Craene *et al.*, another review about PPIn in which I did not take part (De Craene et al., 2017).

A. The metabolism of membrane phosphoinositides

1. Lipids are the main membrane constituents

Membranes are essential cell components with a highly dynamic structure, and allowed the emergence of life through their physicochemical properties. Indeed, the broader environment is characterized by variations in temperature, humidity, pH, sun exposure, osmotic pressure or energy. Thus, each living organism has to adapt to these factors and to organize itself in order to preserve its internal balance and stability. The plasma membrane is

the first barrier of the cell that separates the cytoplasm from the external environment. It acts as a very selective filter that mechanically protects the cell and allows a fine control of the exchanges between the outside and inside environments.

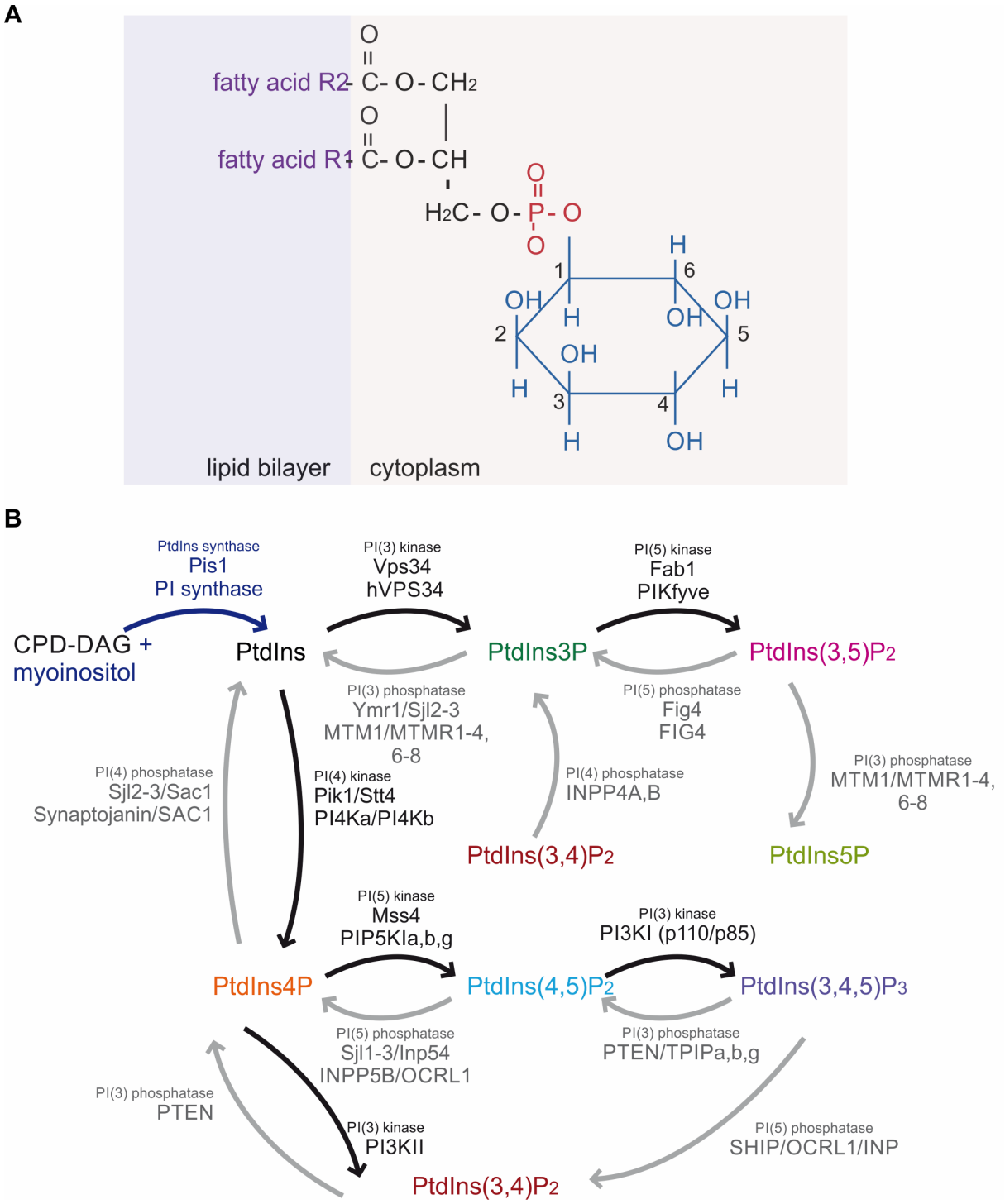

Figure 13: Phosphoinositide metabolism in yeast and human cells. Adapted from De Craene *et al.* 2017. **(A)** The chemical structure of phosphatidylinositol (PtdIns); **(B)** Phosphoinositides synthesized in yeast and in human cells with the enzymes involved. Phosphorylation reactions are represented with black arrows and dephosphorylation reactions by grey arrows. The name of the yeast enzyme (when relevant) is written on top of its human homolog.

The plasma membrane is composed of a phospholipid bilayer encompassing proteins, sterols and glycolipids. Phospholipids are amphiphilic molecules with a hydrophilic head linked to a hydrophobic tail (Figure 13A). Hydrophobic groups face each other, generating a hydrophobic space between the two phospholipid layers. This property is required for the membrane embedding of lipids (as sterols or ceramides), transmembrane proteins or proteins with a lipid anchor. The lipid composition of the membrane depends on the organism (eukaryote or prokaryote), the cellular type (within the tissues of a multicellular organism), the membrane type (plasma membrane, endoplasmic reticulum, endosomes, Golgi apparatus, mitochondria and other intracellular compartments) and even on the state of the cell (resting state or under stimulus/stress) (Spector and Yorek, 1985; Zinser et al., 1991).

Membranes are mainly composed of 5 phospholipids: phosphatidylcholine (PC), phosphatidylethanolamine (PE), phosphatidylserine (PS), phosphatidylinositol (PtdIns) and sphingomyelin (SM). For note, sterols are also present in the membranes but their function is primarily to control the membrane fluidity, an essential factor for the lateral diffusion of molecules in the bilayer. This bilayer also presents an asymmetrical distribution of the phospholipids between the external and the internal layers, due to the vertical diffusion between these two layers by the flip-flop mechanism and the activity of membrane proteins called flippases (Kornberg and McConnell, 1971; Nakano et al., 2009a; Nakano et al., 2009b).

Lipids play an essential role as selective barrier via the plasma membrane, but they are also the major constituents of eukaryotic intracellular membranes such as compartments, organelles and transport vesicles. Membrane organization and composition differ depending on the cellular compartment. On one hand, the endoplasmic reticulum, the Golgi apparatus, the lysosome (named vacuole in yeast cells), the endosomes and transport vesicles are surrounded by a single lipid bilayer. The inner space of these intracellular compartments is called the lumen. On the other hand, the nucleus, mitochondria, chloroplasts of chlorophyll containing plants, and autophagic vesicles are surrounded by a double lipid bilayer. Each of these intracellular compartments has specific functions that are essential to cell life (Spector and Yorek, 1985), and all of them are interconnected by a fine-tuned vesicular transport of proteins. Thus, it is crucial for the cell to properly discriminate between intracellular compartments. To this end, each organelle has its own identity defined by molecules in the cytoplasmic layer of the membranes, allowing for a distinction even between the “cis” and the

"trans" faces of the Golgi network. Among these molecules, lipids, and specifically phosphoinositides, play a major role in the spatiotemporal regulation of cellular processes as the cytoskeleton dynamic, membrane trafficking, proliferation and cell survival.

2. Phosphoinositides are lipid signaling molecules

Phosphoinositides (PPIn) refer to a group of 7 different types of phosphorylated phosphatidylinositol (PtdIns). If we exclude the PtdIns, PPIn are minor membrane constituents in terms of their abundance, as they only represent 1% of total cellular phospholipids (Payrastre et al., 2001). PtdIns itself only represents less than 10% of total phospholipids. PPIns are composed of a glycerol esterified on SN1 and SN2 positions by two fatty acid chains and its SN3 position is linked to an inositol ring via a phosphate group (Figure 13A) (Payrastre et al., 2001). In humans, the most common fatty acids in PtdIns are stearic acid (lipid number 18:0, 18 defining the number of carbons and 0 the number of double bonds) on SN1 position and arachidonic acid (20:4) on SN2 position (Marcus et al., 1969). In yeast *Saccharomyces cerevisiae*, commonly used fatty acids are oleic acid (18:1), palmitoleic acid (16:1) and palmitic acid (16:0) (Trevelyan, 1966). Since all PPIns derive from the non-phosphorylated PtdIns, it is assumed that they have the same composition in fatty acids as the PtdIns.

The PPIn inositol ring is a polyol cyclohexane of which positions D3, D4 and D5 can be phosphorylated, potentially generating 7 different PPIns (Figure 13B): phosphatidylinositol 3-phosphate (PtdIns3*P*), PtdIns4*P*, PtdIns5*P*, PtdIns 3,4-bisphosphate (PtdIns(3,4)P_2), PtdIns(3,5)P_2, PtdIns(4,5)P_2 and PtdIns 3,4,5-trisphosphate (PtdIns(3,4,5)P_3). Despite their low concentrations in lipid membranes, PPIns play an essential role in the recruitment and/or activation of effector proteins. Moreover, their levels in membranes are regulated by membrane-specific lipid kinases and phosphatases, allowing for the spatiotemporal regulation of diverse cell events as budding, fusion or membrane dynamic (Payrastre et al., 2001).

3. Phosphatidylinositol is the precursor of phosphoinositides

Phosphatidylinositol (PtdIns) is a ubiquitous phospholipid in eukaryote cells and the starting point of PPIns metabolism. Indeed, all PPIns are directly or sequentially synthetized

from PtdIns (Figure 13B). In yeast, the PtdIns is synthetized by the PtdIns synthase 1 (Pis1) in the cytoplasmic layer of the endoplasmic reticulum, Golgi, mitochondria and microsomes membranes (Nikawa and Yamashita, 1984). In human, PtdIns is synthetized by the Pis1 protein homolog, the PtdIns Synthase which has a similar distribution to Pis1 in yeast (Antonsson, 1994).

PtdIns is also recycled from PtdIns3*P*, PtdIns4*P* and PtdIns5*P* thanks to lipid phosphatases (Figure 13B). In humans, active myotubularins (MTM1, MTMR1-4, 6, 7 and 8) are 3-phosphatases dephosphorylating specifically the PtdIns3*P* into PtdIns (Laporte et al., 2003). The other PPIns phosphatases are less specific, such as SAC1 which is able to dephosphorylate the PtdIns3*P* into PtdIns, but also to dephosphorylate the PtdIns4*P* (and probably the PtdIns5*P*) into PtdIns (Liu and Bankaitis, 2010). In yeast, there is only one myotubularin named Ymr1, which also shows a phosphatase activity specific to the D3 position. This activity on the PtdIns3*P* is shared with the less specific phosphatases Sjl2, Sjl3 and Sac1, which are also able to convert PtdIns4*P* into PtdIns (Parrish, W. R. et al., 2004).

B. The PtdIns3*P* is essential for endosomal trafficking

1. PtdIns3*P* synthesis

In yeast, PtdIns3*P* represents 30% of all the PPIns and is as abundant as PtdIns4*P*. In human cells, it accounts for 15% of all the monophosphorylated PPIns and is in minority compared to PtdIns4*P* (Payrastre et al., 2001). PtdIns3*P* is produced by the phosphorylation of PtdIns at the D3 phosphate of the inositol ring, or by PtdIns(3,4)P_2 or PtdIns(3,5)P_2 dephosphorylation (Figure 13B).

In yeast, only the lipid kinase Vps34 (Vacuolar Protein Sorting 34) specifically catalyzes the phosphorylation of PtdIns into PtdIns3*P* (Herman and Emr, 1990; Schu et al., 1993). Vps34 activity is regulated by the protein kinase Vps15, and is essential for endosomal trafficking and autophagy (Kihara et al., 2001). Noteworthy, it has been shown that the positive regulation of Vps34 by Vps15 is stimulated by the direct interaction between the 7 WD (Trp-Asp) repetitions in the C-terminal region of Vps15 and the Gα subunit of Gpa1.

Thus, the C-terminal domain of Vps15 could acts as the γ subunit of the yeast G protein. This would result in a coupling between the G protein signaling at the plasma membrane and the receptor sorting at the endosomes. Furthermore, the interaction between the Vps34-Vps15 complex and Gpa1 stimulates the PtdIns3*P* production at the endosomes (Slessareva et al., 2006).

The human genome encodes for 8 lipid kinases able to produce PtdIns3*P*. These kinases are classified in 3 classes, depending on their substrate specificity and their homology (Vanhaesebroeck et al., 2010; Vanhaesebroeck et al., 2001):

- 4 members of the class I phosphoinositide 3-kinases (PIK3C) which phosphorylate predominantly PtdIns(4,5)P_2 to generate PtdIns(3,4,5)P_3
- 3 members of the class II phosphoinositide 3-kinases (PIK3C2) which phosphorylate predominantly PtdIns4*P* to generate PtdIns(3,4)P_2
- Only 1 member of the class III phosphoinositide 3-kinase (PIK3C3) which is homologous to the yeast protein Vps34. As the latter, the human VPS34 is specific for PtdIns and thus probably generates most of the cellular PtdIns3*P*. Its activity is regulated by p150 (also termed PIK3R4/VPS15), the human homolog of the yeast Vps15 (Panaretou et al., 1997). A phylogenetic study brought to light a coevolution between the unique PIK3C3 and its regulatory subunit Vps15 in most eukaryotes, from yeast to human through amoeba and parasites (Lecompte et al., 2008).

In yeast, PtdIns3*P* is also synthetized by lipid phosphatases Fig4 (Factor Induced Gene 4, also named Sac3), Sjl2, Sjl3 and Sac1. These proteins all contain a SAC catalytic domain allowing to dephosphorylate different PPIns, such as the PtdIns(3,5)P_2 into PtdIns3*P* (Liu and Bankaitis, 2010). Fig4 is the only PtdIns 5-phosphatase specific for PtdIns(3,5)P_2 (Gary et al., 2002), and the human homolog FIG4 has similar functions. Interestingly, mutations in human *FIG4* gene are responsible for CMT4J, which is highly similar to the MTMR2-linked CMT4B (Liu and Bankaitis, 2010). Thus, FIG4 is - with MTM1 and MTMR2 – the third active phosphatase implicated in both PPIn regulation and a neuromuscular disease (Nicot and Laporte, 2008).

2. PtdIns3*P* physiological role

In yeast and mammalian cells, PtdIns3*P* is enriched at membranes of early endosomes and membranes of intraluminal vesicles at the late endosome also termed multivesicular body (MVB) (Figure 14) (Gillooly et al., 2000). In early endosomes, PtdIns3*P* plays a central role in recruiting effector proteins as yeast Vps27 or its human homolog Hrs (Hepatocyte growth factor-Regulated tyrosine kinase Substrate). These two proteins belong to the ESCRT-0 (Endosomal Sorting Complex Required for Transport) complex and are implicated in endosomal protein sorting and MVB formation (Henne et al., 2011). They both contain a FYVE (Fab1, YGL023, Vps27, and EEA1) domain able to bind the endosomal PtdIns3*P*, and a specific motif to recruit the ESCRT-1 complex (Gruenberg and Stenmark, 2004). The latter allows ESCRT-2 and 3 recruitment and their combined action induces the internalization of membrane proteins into the intraluminal vesicles of the MVB (Henne et al., 2011). This internalization is necessary to stop the signaling cascades mediated by transmembrane proteins and to address membrane proteins to the lumen of the vacuole/lysosome.

The human adaptor EEA1 (Early Endosomal Antigen 1) binds with a high affinity to PtdIns3*P* via its FYVE domain, and regulates the membrane fusion process between endosomes, by recruiting the Rab5 GTPase to the endosomes (Gruenberg and Stenmark, 2004).

Similarly, the PtdIns3*P* 5-kinase Fab1 (yeast)/PIKfyve (human) - that phosphorylate the PtdIns3*P* into PtdIns(3,5)P_2 - is able to bind the PtdIns3*P* through its FYVE domain (Payrastre et al., 2001). Thus, one of PtdIns3*P* physiological roles is to be a precursor for PtdIns(3,5)P_2 synthesis.

In yeast, the *VPS34* deletion is not lethal but induces a strong growth phenotype and a decreased resistance to many factors (temperature, pH, hyperosmotic stress, or presence of ethanol, hygromycin B, caffeine or rapamycin). The *vps34Δ* yeast cells also present important defects in membrane trafficking, such as an abnormal vacuolar morphology and defective vacuolar transport with abnormal excretion of vacuolar carboxypeptidase Y (CPY) and alteration in autophagy (Kihara et al., 2001). Indeed, yeast Vps34 is responsible for the proper

sorting of proteins to the vacuole via the production of PtdIns3*P*, which allows the recruitment of endosomal effector proteins (Henne et al., 2011).

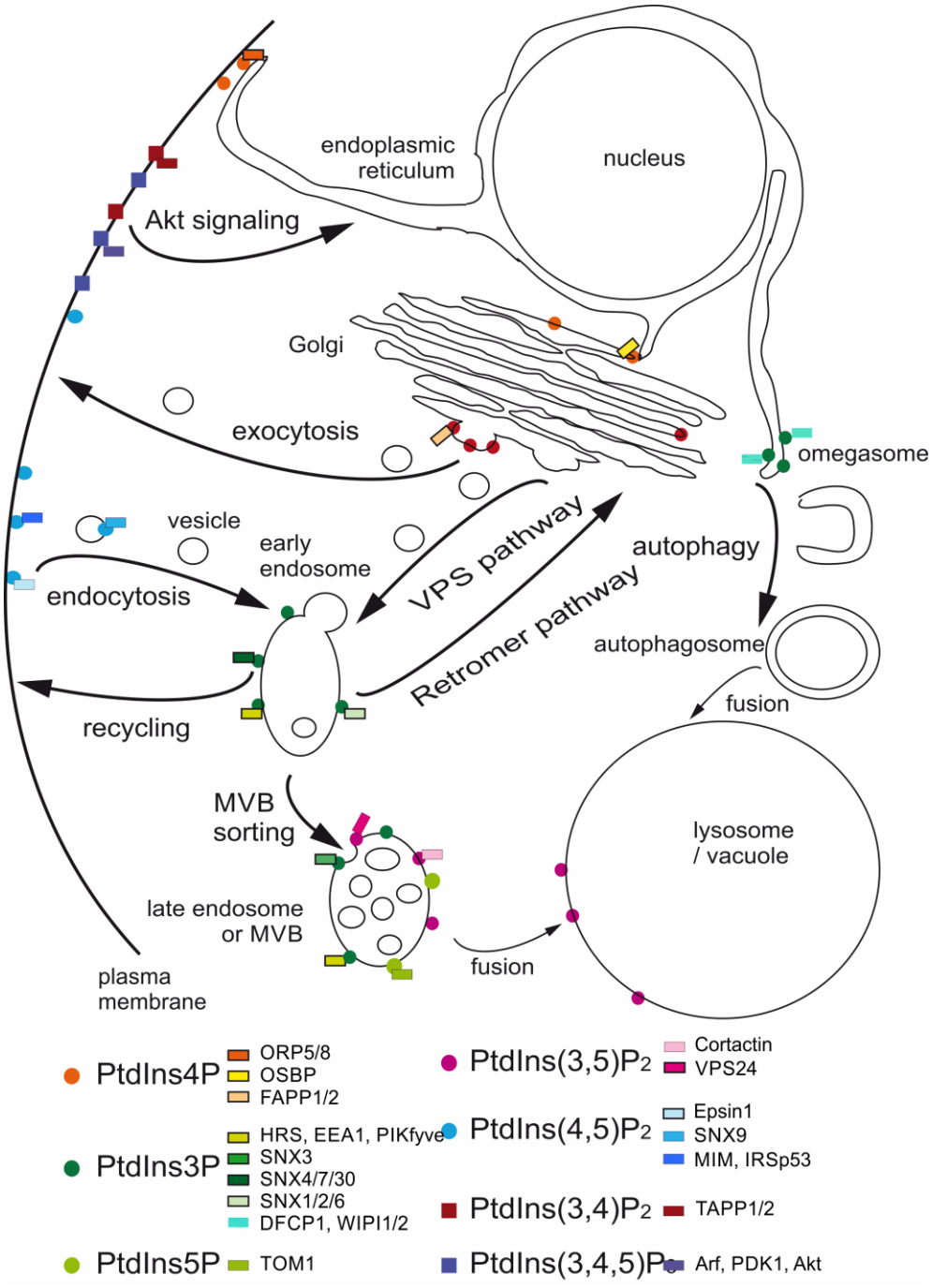

Figure 14: intracellular localization of the different phosphoinositides and the membrane trafficking pathways. The different phosphoinositides (PPIn) are represented by symbols: circles for PPIn involved in intracellular trafficking with the corresponding steps they regulate; squares for PPIn involved in cell signaling, the latter being absent from yeast. The human proteins interacting with the different PPIn are represented by a rectangle. The MVB stands for multivesicular body and the VPS for vacuolar protein sorting. Adapted from De Craene *et al*. 2017.

C. PtdIns(3,5)P_2 is a regulator of endosomal-lysosomal trafficking

1. PtdIns(3,5)P_2 synthesis

PtdIns(3,5)P_2 is a poorly abundant PPIn that represents less than 5% of all the PPIns in human cells and in *S. cerevisiae*. PtdIns(3,5)P_2 is enriched in membranes of the late endosomes, MVB and lysosome/vacuole (Figure 14) (Di Paolo and De Camilli, 2006).

In yeast, PtdIns(3,5)P_2 is sequentially produced, first from the phosphorylation of PtdIns into PtdIns3*P* by the PtdIns 3-kinase Vps34, and then from the phosphorylation of PtdIns3*P* into PtdIns(3,5)P_2 by the PtdIns3*P* 5-kinase Fab1 (Figure 13B). A hyperosmotic stress induces a 20-fold increase in PtdIns(3,5)P_2 intracellular levels (Dove et al., 1997). PtdIns(3,5)P_2 is regulated by the membrane vacuole proteins Vac7 and Vac14 (Bonangelino et al., 2002). Indeed, PtdIns(3,5)P_2 is not detected in yeast cells where *FAB1*, *VAC7* or *VAC14* genes are deleted, and this is independent of osmotic conditions (Bonangelino et al., 2002). However, Vac7 and Vac14 do not interact with each other: Vac7 is the major activator of Fab1 in a hyperosmotic stress, whereas Vac14 acts with the lipid phosphatase Fig4 to regulate PtdIns(3,5)P_2 renewal (Duex et al., 2006b). This is quite intriguing, since the stimulation of PtdIns(3,5)P_2 synthesis by an osmotic stress depends on two antagonist processes, PtdIns3*P* phosphorylation into PtdIns(3,5)P_2, as well as PtdIns(3,5)P_2 dephosphorylation into PtdIns3*P*, creating a futile loop (Duex et al., 2006a). Thus, there is an essential interdependence between the lipid kinase Fab1 and the antagonist phosphatase Fig4 to regulate PtdIns(3,5)P_2 levels, but also to activate PtdIns(3,5)P_2 synthesis after a stimulus.

In human, PtdIns(3,5)P_2 synthesis pathway is similar to the one described in yeast, and PtdIns(3,5)P_2 synthesis is ensured by PIKfyve, the unique Fab1 homolog, which phosphorylates the PtdIns3*P* on its 5-position (Figure 14) (Shisheva, 2008). PtdIns3*P* seems to be the unique source of PtdIns(3,5)P_2, since as of now, no PPIn 4-phosphatase hydrolyzing the PtdIns(3,4,5)P_3 has been identified. Moreover, the regulation of PtdIns(3,5)P_2 synthesis is conserved in humans, and PIKfyve interacts with multiple partners playing a role in PtdIns(3,5)P_2 homeostasis (Shisheva, 2008). For example, PIKfyve interacts with its antagonist enzyme FIG4 (also named SAC3) that specifically dephosphorylates the

PtdIns(3,5)P_2 into PtdIns3P. This interaction is mediated by the adaptive protein ArPIKfyve/Vac14 which stabilizes the PIKfyve/FIG4 complex and stimulates PIKfyve activity (Ikonomov et al., 2010).

A recent study clearly showed the homology between PtdIns(3,5)P_2 synthesis pathways in yeast and mammals (Jin et al., 2008). Indeed, in yeast as well as in mice, Vac14 acts as a protein platform for PtdIns(3,5)P_2 synthesis regulation. Vac14 interacts with Fab1/PIKfyve, Fig4/Sac3 and Vac7, and allows the regulation of the activity of the kinase and phosphatase (Ikonomov et al., 2010; Jin et al., 2008).

The link between all these PPIn-regulating kinases and phosphatases becomes clearer with time. Noteworthy, autosomal recessive mutations in *FIG4* and *MTMR2* are both linked to CMT4 neuropathy, and *Mtmr2* KO mice display elevated PtdIns(3,5)P_2 levels (Bolino et al., 2000; Chow et al., 2007; Vaccari et al., 2011). There is also a genetic interaction between *FIG4* and *MTMR2*, since reduction of *FIG4* expression rescues the myelin outfoldings phenotype of the *Mtmr2* KO mice (Vaccari et al., 2011). In addition, autosomal dominant mutations in *FIG4* induce lateral sclerosis (Chow et al., 2009), and bi-allelic mutations in *VAC14* are responsible for a pediatric-onset neurological disorder (Lenk et al., 2016).

2. Physiological role of PtdIns(3,5)P_2

Several studies showed a physiological role for PtdIns(3,5)P_2 in the trafficking regulation between endosomes and the vacuole/lysosome (Figure 14).

In yeast *S. cerevisiae*, *fab1Δ* cells have growth defects at 23°C, are not viable at 37°C and show defaults in vacuole acidification and an enlarged vacuole that occupies up to 80% of total cell volume (Yamamoto et al., 1995). The abnormal vacuolar size can induce an incorrect segregation of chromosomes during cell division. Vac7 and Vac14 regulate PtdIns(3,5)P_2 synthesis via Fab1, and thus are necessary for a normal vacuolar morphology and for a proper vacuole transmission from mother to daughter cell (Bonangelino et al., 2002).

PtdIns(3,5)P_2 has an essential function in membrane protein sorting at the late endosomes/MVB (Odorizzi et al., 1998). Membrane proteins addressed to the vacuole are

ubiquitinated in endosomes. These ubiquitinated cargos are successively recognized by ESCRT-0 to 2 complexes for their internalization into the intraluminal vesicles of the MVB (Gruenberg and Stenmark, 2004). The MVB then fuses with a vacuole, releasing the vesicles into the lumen of the vacuole. At endosomes, yeast epsins Ent3 and Ent5 interact with PtdIns(3,5)P_2 through their ENTH domain, and are necessary for the sorting of ubiquitinated cargos to the MVB (Eugster et al., 2004; Friant et al., 2003).

To date, the protein having the highest affinity toward PtdIns(3,5)P_2 *in vitro* is the yeast Svp1/Atg18, which has a role in yeast autophagy. Interestingly, Svp1/Atg18 also regulated Fab1 activity, by interacting with Vac7 (that is recruited by Vac14 platform). Thus, Svp1/Atg18 acts as a sensor for PtdIns(3,5)P_2 and regulates its synthesis via a Vac7-Vac14 feedback (Efe et al., 2007).

PIKfyve$^{-/-}$ KO mice do not survive after the embryonic stage (Ikonomov et al., 2011), highlighting the fundamental role of PtdIns(3,5)P_2 in development and cellular processes. Yeast Fab1 and human PIKfyve both have a FYVE domain able to specifically bind the PtdIns3*P*. This interaction with PtdIns3*P* induces their recruitment to endosomes where PtdIns3*P* is enriched, and allows PtdIns(3,5)P_2 synthesis (Figure 14) (Sbrissa et al., 2002). Finally, PIKfyve has a role in diverse processes as endosomal protein sorting, vacuolar/lysosomal homeostasis or signaling pathway regulation (Payrastre et al., 2001; Shisheva, 2008). In particular, inhibition or depletion of PIKfyve in mammalian cells induces an endosomal and lysosomal enlargement similar to the enlarged vacuole observed in yeast (Shisheva, 2008).

D. PtdIns5*P* is an underappreciated phosphoinositide

1. PtdIns5*P* synthesis

PtdIns5*P* is the most recently identified PPIn monophosphate (Rameh et al., 1997). This is due to its low basal concentration in mammalian cells (less than 10% of all monophosphate PPIns) (Payrastre et al., 2001), but also to technical issues rendering it difficult to study since it co-fractionates with PtdIns4*P*.

In humans, PtdIns5*P* can be produced directly from PtdIns by the lipid kinase PIKfyve (Figure 14). The *in vivo* overexpression of PIKfyve induces an increased level of PtdIns5*P*, while PIKfyve$^{+/-}$ heterozygote mice are viable and show a reduction in PtdIns5*P* levels compared to control mice (Ikonomov et al., 2011).

However, the major source of PtdIns5*P* in human cells comes from the 3-phosphatase activity of the myotubularin family (8 active members) on PtdIns(3,5)P_2 (Figure 14) (Laporte et al., 2003). This has been demonstrated in particular for MTM1 in cell cultures and in myotubes (Tronchere et al., 2004) and for MTMR3 in *Drosophila* fibroblasts after activation of cell migration using FGF-1 (fibroblast growth factor) (Oppelt et al., 2013).

Finally, a third possible (and unusual) source of PtdIns5*P* in human cells comes from the 4-phosphatase activity of the bacterial IpgD upon infection by *Shigella flexneri* which is responsible for dysentery (Niebuhr et al., 2002).

2. PtdIns5*P* physiological role

The physiological role of PtdIns5*P* in mammalian cells is still poorly understood. A fraction of the pool of PtdIns5*P* has been detected in the nucleus and could be implicated in stress response, notably by modulating the activity of the transcriptional regulator ING2. The latter is the first protein with an identified PtdIns5*P*-specific binding domain, which is a zinc finger domain named PHD (Plant HomeoDomain finger) (Gozani et al., 2003b). The Dok protein (downstream of tyrosine kinase) also shows strong binding properties toward PtdIns5*P* through its PH domain, and this binding activates the T cell signaling (Guittard et al., 2009). Moreover, PtdIns5*P* has been found to be implicated in autophagy since its addition to cells promotes the autophagosome biogenesis and compensates PtdIns3*P* depletion in *Vps34* cells (Vicinanza et al., 2015). PtdIns5*P* also regulates actin cytoskeleton remodeling at the plasma membrane, by binding to the guanine nucleotide exchange factor (GEF) Tiam1, thus activating the Rho GTPase Rac1 (Viaud et al., 2014). Finally, PtdIns5*P* is a regulator of endosomal protein sorting via its interaction with the endosomal adapter TOM1 (Boal et al., 2015).

E. A word about the other phosphoinositides

Other phosphoinositides also exist in eukaryote cells. For example PtdIns4*P* is mainly generated by 4-phosphorylation of PtdIns by PI 4-kinases (De Matteis et al., 2002), and is a key effector of the Golgi trafficking (Audhya et al., 2000; Lemmon, 2003; Mizuno-Yamasaki et al., 2010). PtdIns(4,5)P_2 is the most abundant bis-phosphorylated PPIn, and is implicated in endocytosis. Finally, PtdIns(3,4)P_2 and PtdIns(3,4,5)P_3 have not been detected in yeast, and are essentially localized at the plasma membrane in humans (Figure 14), where they could act as second messengers (for PtdIns(3,4)P_2) and kinase regulators (for PtdIns(3,4,5)P_3) in the PI3K/Akt pathway. However for the remainder of this manuscript I will focus on the phosphoinositides linked directly to myotubularin function.

V. Objectives of this thesis

As previously established in this introduction, MTM1 and MTMR2 are two very similar ubiquitously expressed proteins which are surprisingly associated with two different neuromuscular disorders, a centronuclear myopathy affecting muscles, and a CMT neuropathy affecting nerves, respectively. The molecular bases of this specificity are still unknown.

The first aim of my thesis was to investigate the molecular and functional specificities of MTM1 and MTMR2. I thus studied their differences in terms of sequence, regulation, *in vivo* activity and localization, by using different cellular models. The impact of these differences was assessed by different MTMR2 constructs carrying truncating or point mutations.

The second aim was to evaluate MTM1 and MTMR2 ability to compensate for each other in a pathological context. Since our team is focusing on myopathies, I tested here the ability of MTMR2 to compensate for MTM1 loss in XLCNM, using the *Mtm1* KO mouse model.

Part Two – Results

I. Differences in sequence and regulation between MTM1 and MTMR2

In order to investigate to functional differences between MTM1 and MTMR2, I started by comparing their sequence, structure and regulation.

Most of the data presented for the remainder of this manuscript in relation to MTMR2-L and MTMR2-S were published in the article "**Expression of the neuropathy-associated MTMR2 gene rescues MTM1-associated myopathy**" in Human Molecular Genetics (Raess et al., 2017) (Appendix 3).

A. MTM1 comparison to MTMR2-L and MTMR2-S

I first evaluated if MTM1 and MTMR2 functional differences could be linked to differences in their primary sequences or their domain organization. I started by comparing MTM1 to the main described MTMR2 protein isoform, MTMR2-L. The sequence alignment shows that human MTM1 and MTMR2-L present a good overall identity of 64.5% (with a similarity of 76%) and share the 4 same domains (Figure 15A):

- the **PH-GRAM** domain that can bind to PPIn or proteins
- the **active phosphatase** domain that specifically dephosphorylates the PtdIns3*P* and PtdIns(3,5)P_2.
- the **coiled-coil (CC)** domain that is essential for their homodimerization and/or heterodimerization
- finally, the **PDZ** binding site that mediates protein-protein interactions.

The most conserved domain is the phosphatase domain, which presents 73% of identity, and more than 80% in its central part around the catalytic site. In comparison, the PH-GRAM and the C-terminal part (CC and PDZ domains) are much less conserved between the two proteins, with 55% and 38% of identity, respectively (Figure 15A). Since these domains interact with lipids and other proteins, and thus impact on the localization and specificity of MTM1 and MTMR2, this lower conservation could be a first explanation for the functional differences between the two proteins.

As detailed in the introduction, expression of the *MTMR2* gene leads (by an alternative splicing mechanism described in humans and mice) to **two MTMR2 isoforms that we named MTMR2-L (long) and MTMR2-S (short)** (Figure 6) (Bolino et al., 2002). The two protein isoforms differ only in their translation start sites; MTMR2-S starts right before the PH-GRAM domain while the MTMR2-L has an **extended N-terminal sequence of 72 amino acids** without known homology to any protein domain and that was not resolved in the crystal structure (Figure 15B) (Begley et al., 2006; Begley et al., 2003). **This N-terminal extension specific to MTMR2-L is mostly absent in MTM1, with the two proteins sharing only a few amino acids in their N-terminal region (Figure 15).**

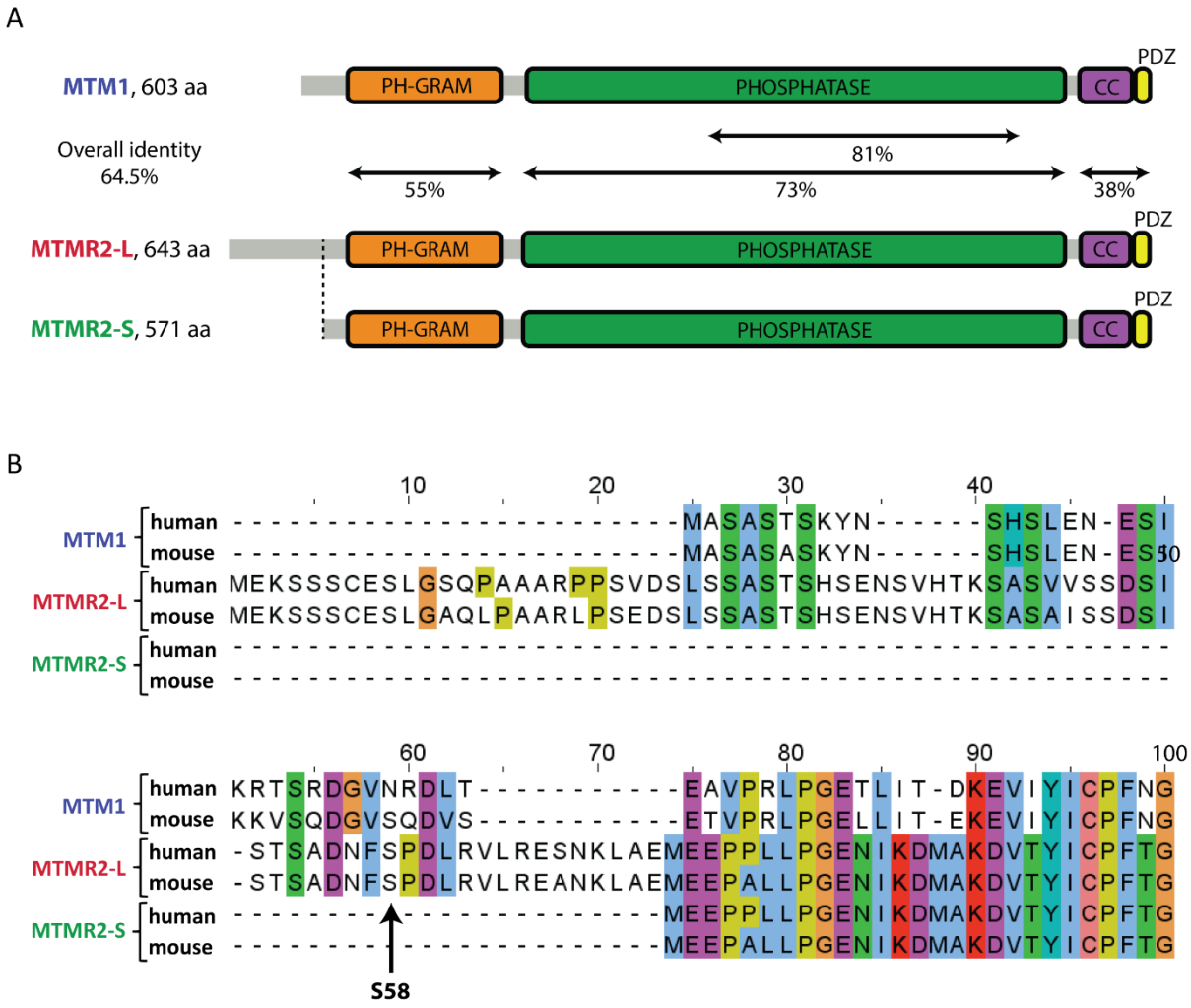

Figure 15: MTMR2-L has an N-terminal extension compared to MTM1 and MTMR2-S (A) Comparison between MTM1, MTMR2-L and MTMR2-S domain organization. Percentage of identity between MTM1 and MTMR2-L are indicated for each domain, except the coiled-coil (CC) and PDZ domains that are grouped. **(B)** Protein alignment of the first 100 amino acids of human and mouse MTM1, MTMR2-L and MTMR2-S. The serine S58 of MTMR2-L is indicated by the arrow.

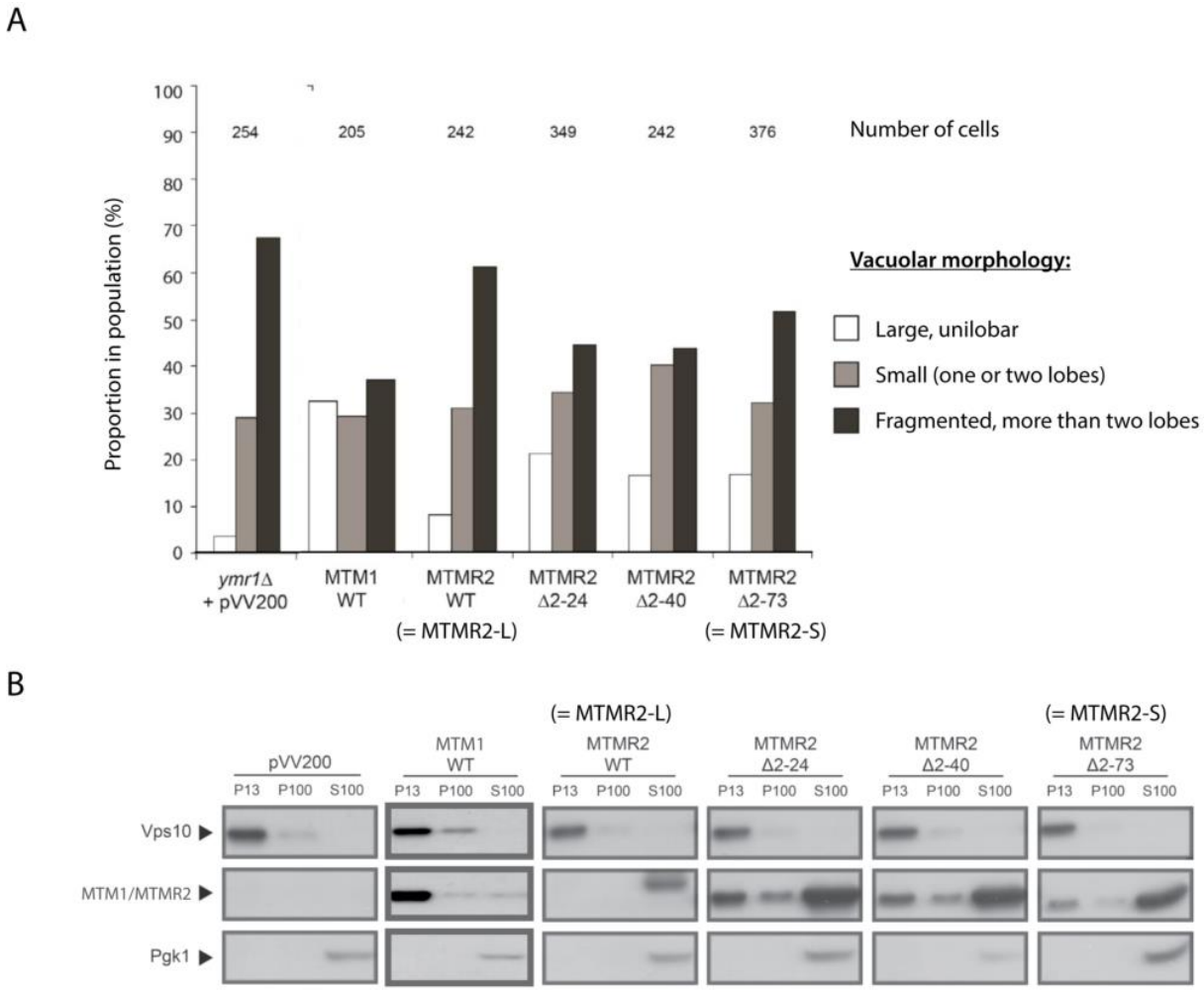

Figure 16: Truncated forms of MTMR2-L induce an MTM1-like phenotype. Adapted from Dimitri Bertazzi thesis manuscript **(A)** Quantification of the vacuolar phenotypes observed in *ymr1Δ* yeast cells with empty vector or overexpressing MTM1, MTMR2-L or truncated forms of MTMR2-L. The number of cells counted per clone is indicated above. **(B)** Subcellular distribution of overexpressed myotubularins in yeast. Protein extracts of *ymr1Δ* yeast cells with empty vector or overexpressing MTM1, MTMR2-L or truncated forms of MTMR2-L, were subjected to subcellular fractionation. MTM1 is mainly in the P13 membrane fraction, while MTMR2-L is mainly in the S100 cytoplasmic fraction. Truncated forms of MTMR2-L display an intermediary phenotype and are also present in P13 and P100 membrane fractions. Vps10 (membrane protein) and Pgk1 (cytoplasmic) are used as controls for the subcellular fractionation.

The study of this N-terminal extension of MTMR2-L was initiated by Dimitri Bertazzi, a previous PhD student in Sylvie Friant's laboratory, in collaboration with Jocelyn Laporte laboratory. Dimitri used, among others, an MTMR2-Δ2-73 construct in which amino acids 2 to 73 are absent. This MTMR2-Δ2-73 exactly corresponds to the MTMR2-S isoform. To compare the cellular functions of MTM1, MTMR2-L and MTMR2-S proteins *in vivo*, Dimitri used the heterologous expression of human myotubularins in *ymr1Δ* yeast cells. This

system will be more deeply explained in chapter III. To summarize, data show that MTMR2-L and MTM1 overexpression induce different vacuolar phenotypes, due to different subcellular localizations (Figure 16). The vacuole morphology is regulated by the PtdIns(3,5)P_2 level, and thus reflects the myotubularin phosphatase activity. Interestingly, MTMR2-S induces intermediary phenotypes compared to MTM1 and MTMR2-L. **Altogether, this suggests that MTMR2-S is closer to MTM1 and that the N-terminal extension of MTMR2-L is important for its specific functions.**

B. The MTMR2-Δ2-24 truncated construct

In his thesis, Dimitri Bertazzi started to investigate the N-terminal sequence of MTMR2-L. Indeed, MTMR2-L is 40 aa longer than MTM1, and this difference is mainly due to 3 additional sequences (amino acids 1-24, 35-40 and 63-73) in MTMR2-L (Figure 15B). The truncated constructs MTMR2-Δ2-24, MTMR2-Δ2-40 and MTMR2-Δ2-73 induce the same phenotypes when overexpressed in *ymr1Δ* yeast cells (Figure 16). Thus, deleting the first 24 amino acids of MTMR2-L is sufficient to induce an MTM1-like phenotype in yeast. **This suggests that the functional specificity of MTMR2-L compared to MTMR2-S and MTM1 is mainly due to the 24 first amino acids of its N-terminal extension.**

C. MTMR2-L function is regulated by the S58 phosphorylation on its N-terminal extension

As mentioned in the introduction, Franklin *et al*. described two phosphorylation sites (S58 and S631) that regulate the targeting of MTMR2 to different endosomal compartments in mammalian cells, to regulated different pools of PtdIns3*P* (Franklin et al., 2013; Franklin et al., 2011). Indeed, the MTMR2-S58A phosphorylation-defective mutant localizes to endosomes and is active toward PtdIns3*P*, contrary to the phosphomimetic mutant MTMR2-S58E that remains cytoplasmic (Figure 17). The S58 phosphorylation is mediated by Erk1/2 kinase and the endosomal targeting of MTMR2 is regulated through an Erk1/2 negative feedback mechanism (Franklin et al., 2013; Franklin et al., 2011). The S631 phosphorylation site regulates the shift of MTMR2 between Rab5-positive and APPL1-positive endosomes. Through this mechanism, MTMR2 seems to be implicated in endosome maturation,

endosome signaling, and potentially in endocytosis (Franklin et al., 2013; Xhabija et al., 2011).

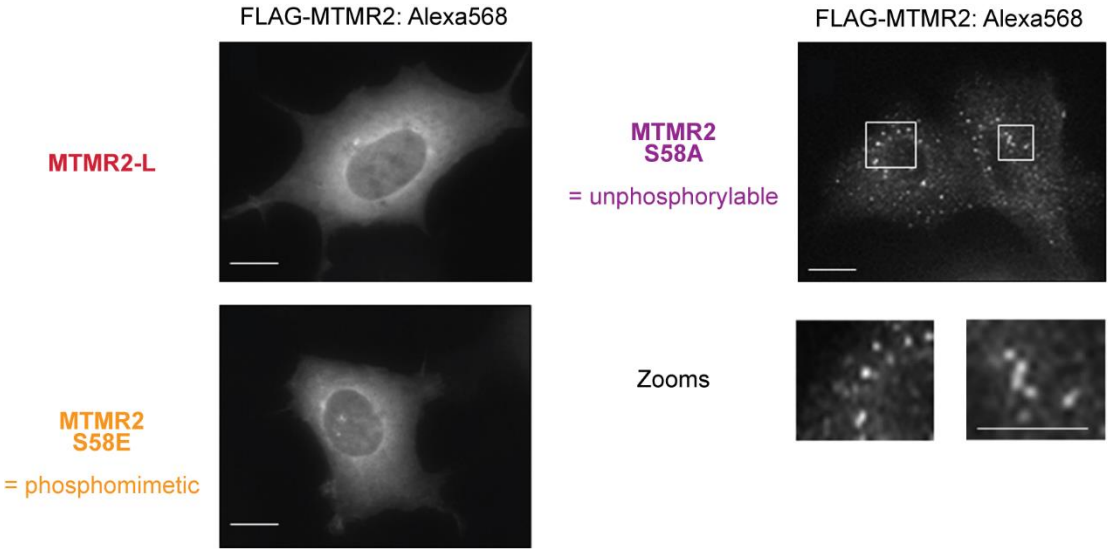

Figure 17: MTMR2 localization in mammalian cells is regulated by its S58 phosphorylation site. Adapted from Franklin *et al.* 2011. HeLa cells were transfected with MTMR2-L or phosphorylation mutants carrying an N-terminal FLAG. After fixation, cells were immunostained with anti-FLAG monoclonal antibody. Scale bar 15 µm.

This S58 phosphorylation site is in the N-terminal extension of MTMR2-L, and is absent in MTMR2-S and in human MTM1 (Figure 15B). **This suggests that the regulation of MTMR2-L by its specific S58 phosphorylation site could be implicated in functional differences between MTM1 and MTMR2.** Note that this phosphorylation site is conserved in mouse MTM1 (S28 in mouse MTM1 sequence, Figure 15B), and thus could potentially be phosphorylated to regulate MTM1 localization and function in mice but not in human.

D. MTMR2 constructs used for this study

Based on preliminary data investigating MTMR2 molecular specificities, I selected several MTMR2 constructs for this study:

- **MTMR2-L and MTMR2-S:** to compare the two physiological isoforms and evaluate the molecular impact of MTMR2-L N-terminal extension (1-72).
- **MTMR2-Δ2-24:** as an intermediary truncated form between MTMR2-L and MTMR2-S, to see if deleting only the 2-24 extremity is sufficient to change MTMR2 localization and function.
- Mutations targeting phosphorylation of MTMR2: the non-phosphorylable **MTMR2-S58A**, and the two phosphomimetics **MTMR2-S58E** and **MTMR2-S58D**. MTMR2-

S58D was not studied by Franklin *et al.* but also mimics a phosphorylated S58 and was chosen here to confirm MTMR2-S58E results.

To assess the impact of these modifications on MTMR2 function, I overexpressed these different constructs in several cellular and animal models, using MTM1 and MTMR2-L as controls. If the modification induces an MTM1-like phenotype, it suggests that the modified site is implicated in the molecular specificities observed between MTM1 and MTMR2.

II. Detection of MTMR2 proteins

Before analyzing the effect of myotubularin overexpression in cells and tissues, it is crucial to determine if they are indeed expressed. Our team previously tested several commercial antibodies directed against MTMR2. The results were not optimal, especially for detection in tissues and mammal cells extracts. **Thus, we decided to produce new anti-MTMR2 antibodies.**

First, I induced the production of recombinant MTMR2-L protein fused to GST in *E. coli* bacteria cells by growth in presence of IPTG. Then I extracted total proteins by sonication and successive centrifugations, and GST-MTMR2-L was affinity purified by using glutathione-sepharose beads. The first 5 eluted fractions have been separated by SDS-PAGE, proteins were stained by Coomassie blue, and the proteins corresponding to the expected size of GST-MTMR2-L were analyzed by mass-spectrometry (Figure 18A). Finally E2, E3 and E4 fractions that contained GST-MTMR2-L (as stated by mass spectrometry) were pooled and given to the antibody facility of IGBMC (Illkirch), were the recombinant protein was then used to immunize mice and produce mouse monoclonal anti-MTMR2 antibodies. I used the full length MTMR2-L instead of a peptide, to directly obtain several antibodies against multiple conformational epitopes from throughout the sequence, and thus maximize the chances to recognize the native protein.

In total, 8 different mouse monoclonal antibodies were produced and tested against protein extracts from COS cells and yeast cells overexpressing MTMR2-L (Figure 18B).

Among them, only the anti-MTMR2 4G3 (number 7 in Figure 18B) detected properly MTMR2 at the expected size (73 kDa) in both COS and yeast cells. In comparison, the commercial antibody gave a very weak signal for the same samples. Since this homemade antibody has been raised against the full-length MTMR2-L and not a specific peptide, we do not know its MTMR2 epitope. However, it is able to recognize MTMR2-S, so the epitope is not in the N-terminal extension of MTMR2-L (Figure 18C). **In conclusion, this 4G3 antibody detects both MTMR2-L and -S isoforms. Therefore this antibody was used for the remainder of the studies presented here, allowing a detection of all overexpressed MTMR2 constructs in all tested cellular and animal models, by western blot and immunofluorescence (Figure 18C and D).**

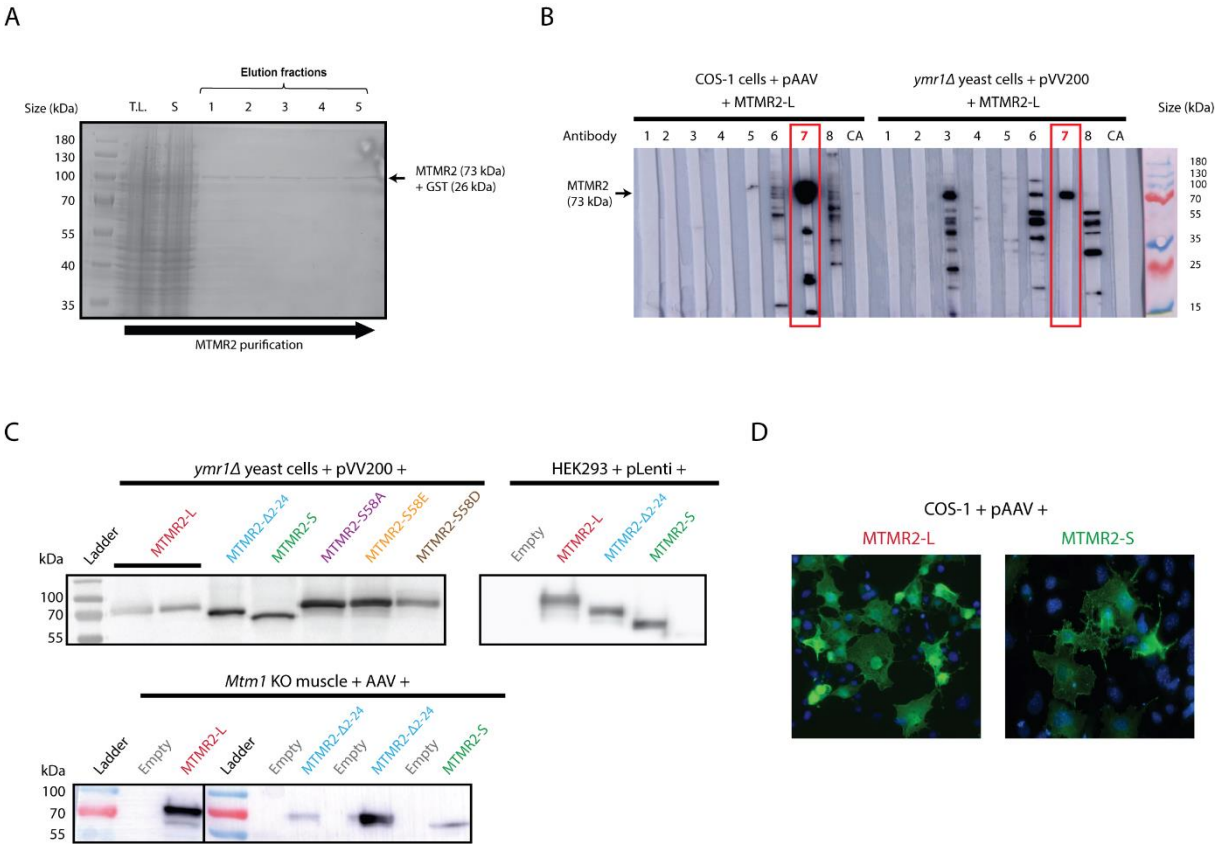

Figure 18: Production and characterization of a new anti-MTMR2 antibody. (A) Purification of MTMR2-L fused to GST. Coomassie staining of SDS-polyacrylamide gel with the 5 elution fractions of GST-MTMR2-L purification. Total lysate (T.L.) and supernatant after centrifugation (S) were also tested to control the affinity-purification step. **(B)** Testing the 8 potential anti-MTMR2 antibodies by western blot on protein extracts from COS-1 and yeast overexpressing MTMR2-L. The commercial anti-MTMR2 antibody (CA) from Abnova was used as control. Expected size for MTMR2-L is indicated by an arrow on the left. The 4G3 antibody (number 7 in the figure) is the only one able to detect MTMR2-L at the expected size in both COS and yeast extracts. **(C)** Testing the anti-MTMR2 4G3 antibody by western blot on yeast, HEK293 or TA muscle protein extracts for all MTMR2 constructs. Stainfree has been used as a loading control (no shown). **(D)** Testing the anti-MTMR2 4G3 antibody by immunofluorescence on COS-1 cells transfected by a pAAV overexpressing MTMR2-L or MTMR2-S (green signal). Nuclei have been stained by Hoechst (blue signal).

III. MTM1 and MTMR2 display different phosphatase activities *in vivo*

MTM1 and MTMR2 are two active myotubularins sharing a specific 3-phosphatase activity toward PtdIns3*P* and PtdIns(3,5)P_2. *In vitro* studies show that MTMR2, like MTM1, dephosphorylates its substrates with high efficiency and peak activity at neutral pH (Berger et al., 2002; Tronchere et al., 2004). However, when I started my thesis, it was unclear whether MTMR2 could dephosphorylate its substrates *in vivo*: one reports that MTMR2 (as MTM1) is able to dephosphorylate an endosomal pool of PtdIns3*P* when overexpressed in HeLa cells (Lorenzo et al., 2006), while another states that overexpression of MTMR2 in COS-1 cells does not change the PtdIns3*P* level (Kim et al., 2002). **I thus decided to compare MTM1 and MTMR2 phosphatase activities and cellular functions in a unicellular eukaryote model, the yeast *Saccharomyces cerevisiae*.**

Yeast is a powerful eukaryotic model to study human myotubularins, as its intracellular organization, membrane trafficking and phosphoinositides substrates metabolism are well characterized and conserved from yeast to human (Introduction and (Katzmann et al., 2003)). Ymr1 is the unique yeast myotubularin and the heterologous expression of human MTM1 myotubularin in *ymr1Δ* yeast cells rescued the vacuolar fragmentation phenotype defect, decreased the intracellular levels of PtdIns3*P* and increased the production of PtdIns5*P* (Amoasii et al., 2012)). This *ymr1Δ* yeast strain also allows the study of the human myotubularin proteins activity without any competition from another myotubularin. Moreover, yeast is as very useful model to study proteins from other eukaryotic organisms in general, with low culture costs and easy gene manipulation compared to mammalian systems (Byrne et al., 2005; Holz et al., 2003; Joubert et al., 2010). A study investigating the systematic humanization of hundreds of yeast genes showed that 43% of them could be replaced by their human ortholog, and most of them coded for metabolic enzymes involved in conserved pathways, like myotubularins (Kachroo et al., 2015).

To better understand MTM1 and MTMR2 specificities concerning their basic cellular functions and activities, I transformed the *ymr1Δ* yeast strain with 2µ plasmids (high copy number, overexpression) or CEN plasmids (low copy number, expression)

containing the cDNA of human MTM1 and all MTMR2 variants, fused or not with GFP (green fluorescent protein) at the C-terminal of the protein. Then I analyzed the expression, localization and phosphatase activity of expressed myotubularins.

A. MTMR2 expression is regulated in yeast

I started by testing protein expression of human myotubularins transfected in yeast, by SDS-page and western blot analysis. All human myotubularins were well detected at the expected molecular weights, with 2µ or CEN plasmids (Figure 19).

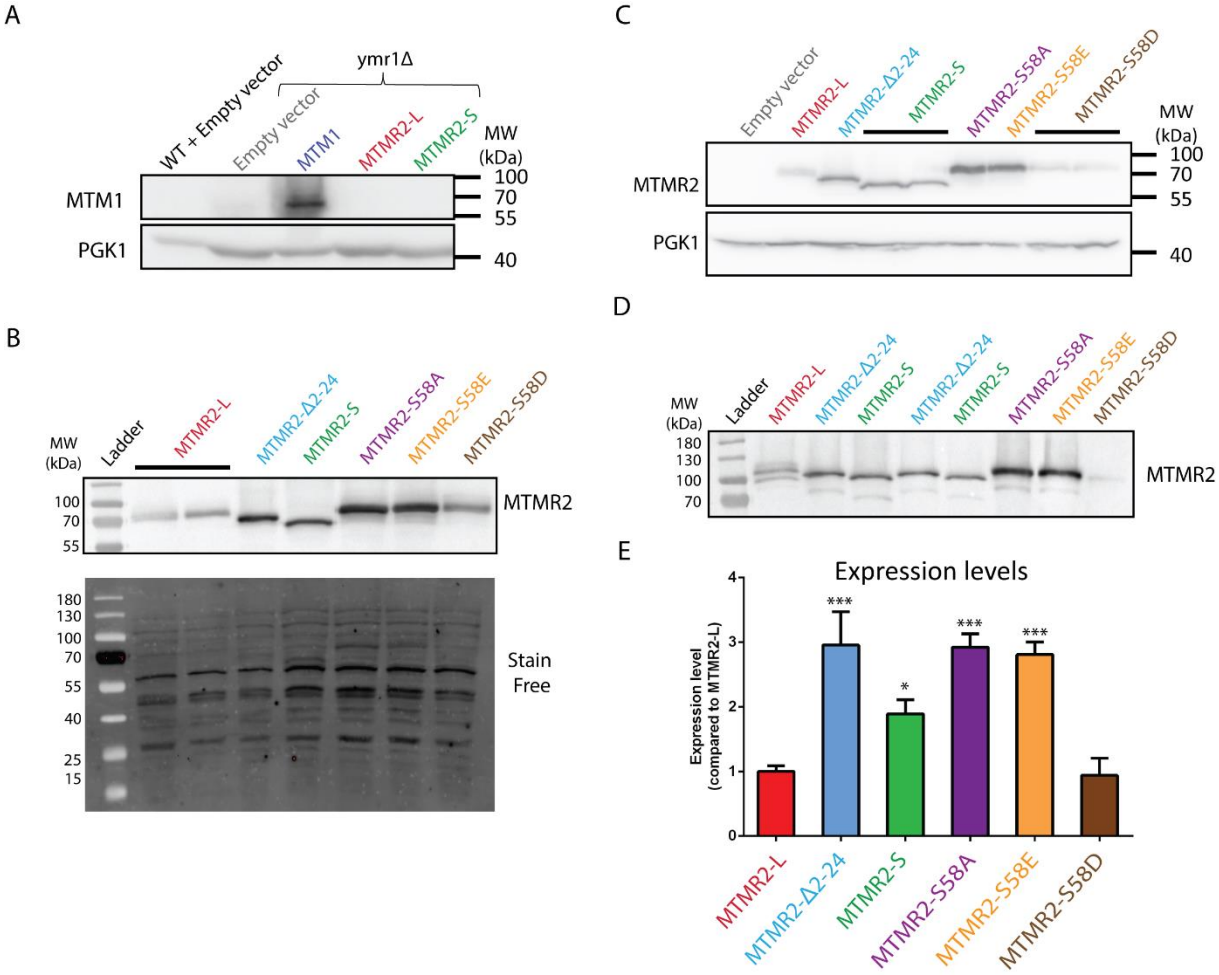

Figure 19: MTMR2 expression is regulated in yeast. (A) Detection of overexpressed (2µ plasmids) MTM1 in *ymr1Δ* yeast cells, by western blot using polyclonal anti-MTM1 antibodies that does not recognize MTMR2. Wild-type (WT) and *ymr1Δ* yeast strains with empty vectors are used as controls. Pgk1p is used as a loading control. **(B)** Detection of overexpressed (2µ plasmids) MTMR2 constructs in *ymr1Δ* yeast cells, by western blot using the homemade monoclonal anti-MTMR2 antibody. The stain free signal on the membrane is used as loading control. **(C)** Detection of expressed (CEN plasmids, low copy number) MTMR2 constructs in *ymr1Δ* yeast cells, by western blot using the homemade monoclonal anti-MTMR2 antibody. Pgk1p is used as a loading control. **(D)** Detection of overexpressed (2µ plasmids) GFP-tagged MTMR2 constructs in *ymr1Δ* yeast cells, by western blot using the homemade monoclonal anti-MTMR2 antibody. **(E)** Quantification of MTMR2 variants expression levels compared to MTMR2-L. Three different clones and western blots per construct. The stain free blots were used to normalize protein levels. Data represent means ± s.e.m. *p<0.05 ***p<0.001 compared to MTMR2-L (ANOVA test).

Surprisingly, the expression level of MTMR2 was different depending on the construct: all variants of MTMR2 displayed a 2 to 3 fold higher expression level compared to the wild-type MTMR2-L, except MTMR2-S58D which was expressed at the same level as MTMR2-L (Figure 19B and E). **Therefore, there is a specific regulation of the protein level for MTMR2 and its variants in yeast cells.** I could not compare this result with MTM1 protein expression, as MTM1 and MTMR2 are not detected by the same antibody.

GFP-tagged myotubularins were also detected at the expected sizes, but a second lower band was also detected for each construct (Figure 19D). This second band was not detected for untagged myotubularins and was always at the same distance from the upper band, suggesting some protein degradation induced by the C-terminal GFP-tag.

B. MTM1 and MTMR2 display different intracellular localizations in yeast

Then I analyzed the intracellular localization of overexpressed GFP-tagged myotubularins in *ymr1Δ* cells. MTM1 exhibited a punctate signal adjacent to the vacuole (also positive for the FM4-64 lipid dye, and probably corresponding to the MVB), whereas MTMR2-L signal was mainly cytoplasmic (Figure 20A). Interestingly, MTMR2-S isoform presented a signal in the cytoplasm and some intense dots at the vacuolar membrane, as observed for MTM1. It was also the case for MTMR2-Δ2-24, MTMR2-S58A and MTMR2-S58E. The only exception was MTMR2-S58D that presented a cytoplasmic localization similar to MTMR2-L. **This suggests that MTMR2 localization in yeast depends on its N-terminal extension.**

I wanted to complete and quantify this localization study by a subcellular fractionation. I performed differential centrifugations on protein extracts of *ymr1Δ* yeast cells overexpressing MTMR2 variants. I tested several techniques and protocol adjustments to finally find the suitable conditions for yeast cell lysis to maintain the different compartments and have the proper fractionation of the endogenous yeast proteins used as controls. The fractionation results were in accordance with the microscopy: MTM1 was mainly detected in the P13 membrane fraction, whereas MTMR2-L was mainly in the S100 cytoplasmic fraction (Figure 20B). All other variants of MTMR2 were detected in the S100 fraction as MTMR2-L,

but they were also detected in the P13 and P100 membrane fractions as MTM1. This time, no difference was detected for MTMR2-S58D compared to other phosphorylation mutants.

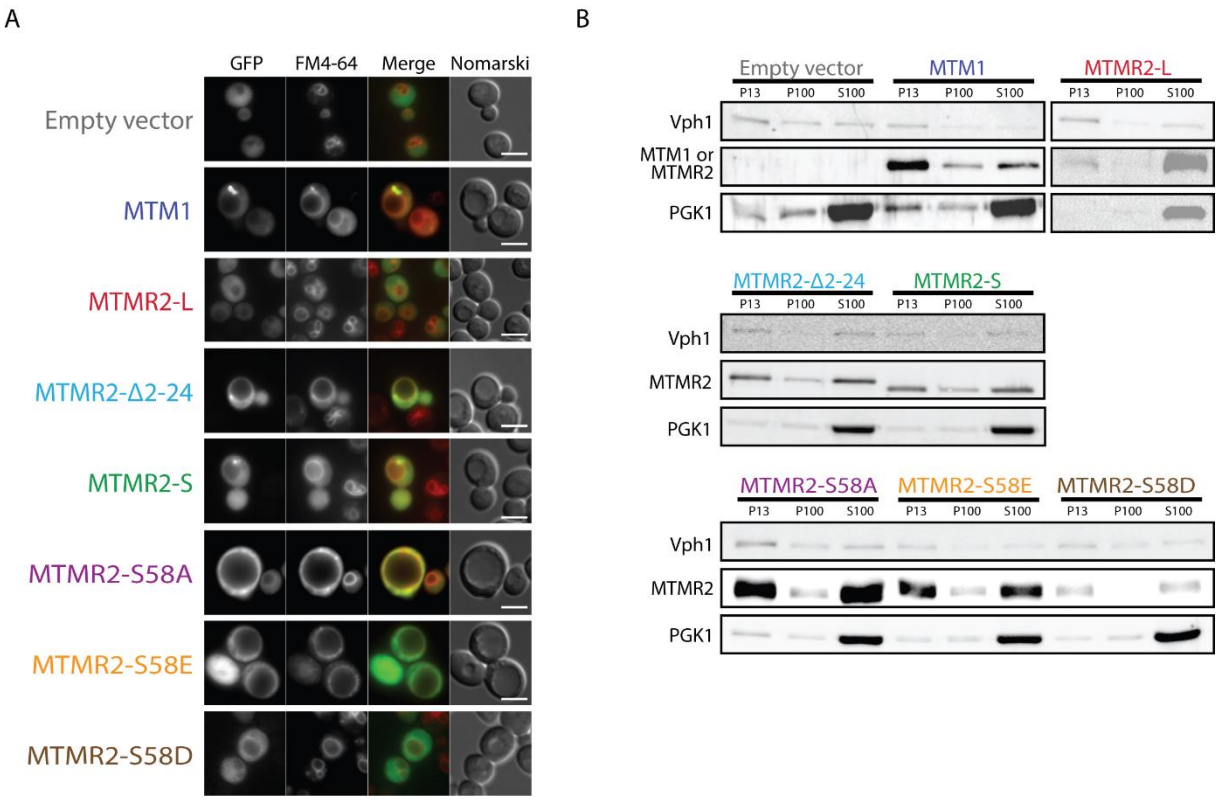

Figure 20: MTM1 and MTMR2 display different intracellular localizations in yeast. (A) Localization of GFP-tagged human myotubularins in *ymr1Δ* yeast cells. Vacuole morphology is assessed by the lipophilic dye FM4-64 and Nomarski differential contrast. Scale bar 5 µm. **(B)** Subcellular distribution of the untagged constructs overexpressed in *ymr1Δ* yeast cells. Subcellular fractionation by differential centrifugations: P13 and P100 are membrane fractions, S100 is the cytoplasmic fraction. Vph1 (membrane) and PGK1 (cytoplasm) are used as controls.

In conclusion, MTM1 and the most described MTMR2-L isoform localize differently in yeast. Interestingly, the MTMR2-S isoform which lacks the N-terminal extension localizes similarly to MTM1. Deleting the first 24 amino acids of MTMR2-L or modifying the S58 phosphorylation site also seems to induce an MTM1-like localization. **Thus, MTMR2 localization seems to depend on its N-terminal part.**

C. MTM1 and MTMR2 display different phosphatase activities in yeast

The different human MTM1 and MTMR2 constructs display different localizations within the yeast cell. A membrane localization could suggest a better access to the lipid substrates compared to a cytoplasmic localization, and thus have an impact on the enzymatic activity. I therefor studied MTM1 and MTMR2 enzymatic activity in yeast.

In yeast cells, vacuole volume, morphology, acidity and membrane potential are controlled by PtdIns(3,5)P_2 that is produced through the phosphorylation of PtdIns3*P* by the Fab1 kinase. In *fab1Δ* mutant cells, the vacuole is very large and unilobed due to low levels of PtdIns(3,5)P_2 (Amoasii et al., 2012; Cooke et al., 1998; Dove et al., 1997). On the contrary, *ymr1Δ* cells lacking the unique yeast myotubularin have fragmented vacuoles due to excess of PtdIns(3,5)P_2 and/or PtdIns3*P* (Parrish, W.R. et al., 2004), and this phenotype is complemented by the expression of the human MTM1 that induces a large vacuole phenotype (Amoasii et al., 2012) (Figure 20A and Figure 21A). **Thus, the vacuolar morphology reflects the PtdIns(3,5)P_2 level, and consequently the myotubularin phosphatase activity.**

I assessed the vacuolar morphology upon overexpression (2µ plasmids) or expression (CEN plasmids) of untagged human myotubularins in *ymr1Δ* cells by staining the vacuolar membrane with the lipophilic dye FM4-64. Vacuoles were significantly enlarged upon overexpression of MTM1 while they remained mainly fragmented with MTMR2-L (Figure 21A). Again, the overexpression of MTMR2-S induced an MTM1-like phenotype with large vacuoles. It was also the case for MTMR2-Δ2-24, MTMR2-S58A and MTMR2-S58E. Again, the exception was MTMR2-S58D that showed a lower percentage of large vacuoles compared to other variants and seemed closer to MTMR2-L. This correlates with the protein localization, as the enlargement of the vacuole is dependent on the phosphatase activity of myotubularins, and on their localization at the vacuolar membrane to have access to their lipid substrate (Figure 20 and Figure 21A and Table 1). Of note, these myotubularins did not induce a wild-type vacuolar morphology but a large vacuolar morphology mimicking a *fab1Δ* phenotype, due to their high expression levels (overexpression plasmid). **These results show that only the membrane localized myotubularin constructs (MTM1, MTMR2-S,**

MTMR2-Δ2-24, MTMR2-S58A and MTMR2-S58E) rescued the vacuole morphology defects of *ymr1Δ* cells.

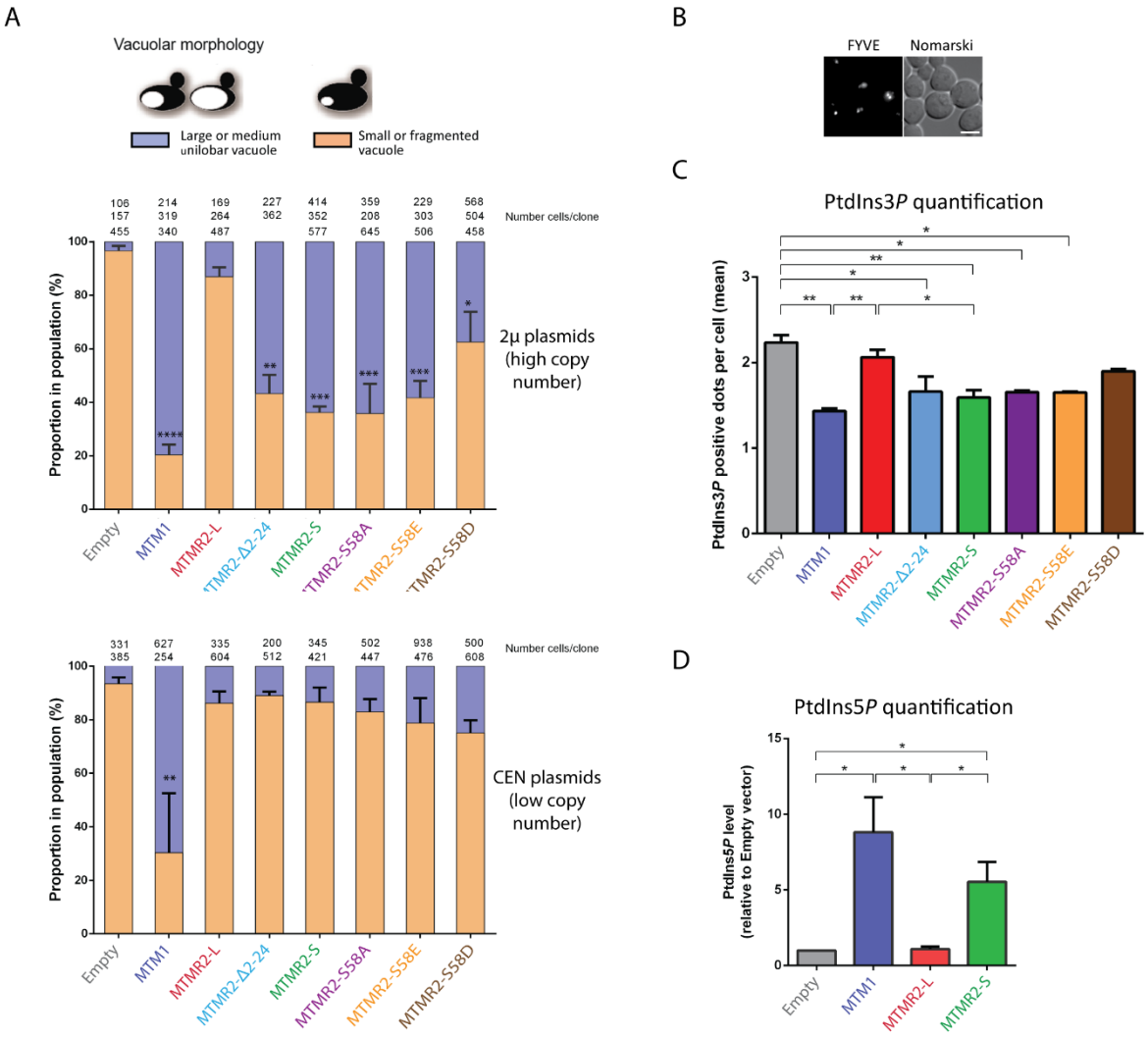

Figure 21: MTM1 and MTMR2 display different phosphatase activities in yeast. (A) Quantification of vacuolar morphology in yeast cells over-expressing (2µ plasmids, top) or expressing (CEN plasmids, bottom) untagged myotubularins. Two to three clones analyzed per constructs; the number of cells counted per clone is indicated above. Data represent means ± s.e.m. . *p<0.05, **p<0.01, ***p<0.001, ****p<0.0001 compared to empty vector (ANOVA test). **(B)** Example of FYVE punctuated localization in yeast clones expressing untagged myotubularins and DsRED-tagged FYVE domain that specifically binds PtdIns3*P*. Scale bar 5 µm. **(C)** PtdIns3*P* quantification by counting the number of FYVE-positive dots per cell, as represented in (B). Data represent means ± s.e.m. *p<0.05, **p<0.01 (ANOVA test). **(D)** PtdIns5*P* quantification by mass assay on total lipid extract from yeast cells over-expressing untagged myotubularins. Three clones analyzed per constructs. Data represent means ± s.e.m. *p<0.05 (ANOVA test).

The differences observed for MTMR2-L and MTMR2-S58D could also be explained by their lower levels of expression compared to other MTMR2 variants (Figure 19B and E). Indeed, using CEN plasmids (low copy number), only MTM1 was able to induce a large vacuole phenotype, whereas the vacuole remains mainly fragmented with all MTMR2 variants (Figure 21A). **This indicates that the level of expression is also important for MTMR2 phosphatase activity.** However, the expression level alone is not responsible for the differences observed, as MTMR2-S was less expressed than MTMR2-Δ2-24, MTMR2-S58A and MTMR2-S58E but had the same phosphatase activity.

Whilst the vacuolar morphology reflects the PtdIns(3,5)P_2 level, this lipid is not abundant enough to be detected in normal growth conditions (Dove et al., 1997). That is why we focused on PtdIns5*P* and quantified its *in vivo* level by mass assay, in collaboration with Jean-Marie Xuereb (Bernard Payrastre laboratory, Toulouse). Sylvie Friant and I extracted the total lipids from *ymr1Δ* cells overexpressing untagged MTM1, MTMR2-L and MTMR2-S, and Jean-Marie Xuereb performed the PtdIns5*P* mass assay. **As expected by vacuolar morphology, PtdIns5*P* level was increased by MTM1 and MTMR2-S overexpression in *ymr1Δ* cells, while MTMR2-L had no effect (Figure 21D).**

I also quantified the PtdIns3*P* myotubularin substrate level, by counting the punctate structures that were positive for DsRED-FYVE, a reporter for PtdIns3*P*-enriched membranes (Katzmann et al., 2003) (Figure 21B and C). Overexpression of MTM1 significantly reduced PtdIns3*P* level while MTMR2-L had no effect. As for the other tested phenotypes, MTMR2-S, MTMR2-Δ2-24, MTMR2-S58A and MTMR2-S58E significantly reduce PtdIns3*P* level similarly to MTM1. MTMR2-S58D behaves differently and induces an intermediary PtdIns3*P* level.

In conclusion, data in yeast cells show that **MTM1 and MTMR2 have different phosphatase activities *in vivo*, depending on the protein localization**: myotubularins localized to membranes (such as MTM1 and MTMR2-S) are able to dephosphorylate their lipid substrates, contrary to cytoplasmic myotubularins (such as MTMR2-L). These results are summarized in **Table 1**.

MTMR2 activity and localization seems dependent to its N-terminal extension: MTMR2-L long isoform remains in the cytoplasm where it is unable to dephosphorylate its lipid substrates, while MTMR2-S lacking the N-terminal extension displays MTM1-like phenotypes with a membrane localization and low PPIn substrate levels. Deleting only the first 24 amino acids of MTMR2-L seems enough to induce an MTM1-like phenotype in yeast. **Thus, this N-terminal extension could be the key to understand MTM1 and MTMR2 molecular differences *in vivo*.**

Finally, the S58 phosphorylation site regulates MTMR2 localization and activity in yeast. Surprisingly, the two phosphomimetics MTMR2-S58E and MTMR2-S58D induce different phenotypes, and only MTMR2-S58D remains in the cytoplasm and has a low phosphatase activity, as it was expected based on Franklin *et al.* results (Franklin et al., 2011). Conversely, MTMR2-S58E phosphomimetic mutant induces the same MTM1-like phenotypes than the unphosphorylable MTMR2-S58A. This indicates that in yeast cells, the MTMR2-S58D variant could be the real phosphomimetic, and not MTMR2-S58E. **This S58 phosphorylation site is in the N-terminal extension of MTMR2-L, highlighting the importance of this extension for MTMR2 cellular function.**

	Empty vector	MTM1	MTMR2-L	MTMR2-Δ2-24	MTMR2-S	MTMR2-S58A	MTMR2-S58E	MTMR2-S58D
Expression	-		+	+++	++	+++	+++	+
Punctate localization	-	✓	✗	✓	✓	✓	✓	✗
Phophatase activity	-	++++	+/-	+++	+++	+++	+++	++

Table 1: Correlation between expression, localization and phosphatase activity of myotubularins expressed in *ymr1Δ* yeast cells. "+,++,+++,++++": increasing expression or activity of myotubularins. "-": negative control phenotype. ✓ positive and ✗ negative.

IV. Study of MTM1 and MTMR2 localization and functions in mammalian cells

The yeast model was very useful to study MTM1 and MTMR2 cellular activity on their PPIns substrates. It also provided novel data on a link between their intracellular localization and phosphatase activity. In yeast cells, MTM1 preferentially localizes to membranes where it dephosphorylates its lipid substrates, while the most studied MTMR2 long isoform (MTMR2-L) remains in the cytoplasm. MTMR2-S short isoform lacking the N-terminal extension of MTMR2-L exhibited a similar membrane localization and phosphatase activity to MTM1. **I thus decided to study MTM1 and MTMR2 localization in mammalian cells.**

In the following experiments in mammalian cells (and further in mice), **I focused on the function of MTMR2-L and -S isoforms to compare with MTM1, as the function of MTMR2 in skeletal muscle is not known.** Indeed, MTMR2-L and MTMR2-S are endogenously expressed in mice and human and could have specific physiological roles. MTMR2-Δ2-24 is also used in some experiments to compare the truncation of the first 24 amino acids of MTMR2-L to the total deletion of the N-terminal extension (corresponding to MTMR2-S).

A. MTMR2 localization depends on its N-terminal extension

I first cloned human MTM1 and human MTMR2 long and short isoforms into pAAV plasmids, and then transfected these constructs into COS-1 cells to test for expression. To avoid any potential bias induced by an N-terminal or C-terminal tag, I decided to use untagged proteins and then detect them by western blot (Figure 23A) and immunofluorescence (Figure 22). This also allowed me to test the ability of the homemade anti-MTMR2 antibody to detect overexpressed MTMR2 constructs by immunostaining on fixed cells.

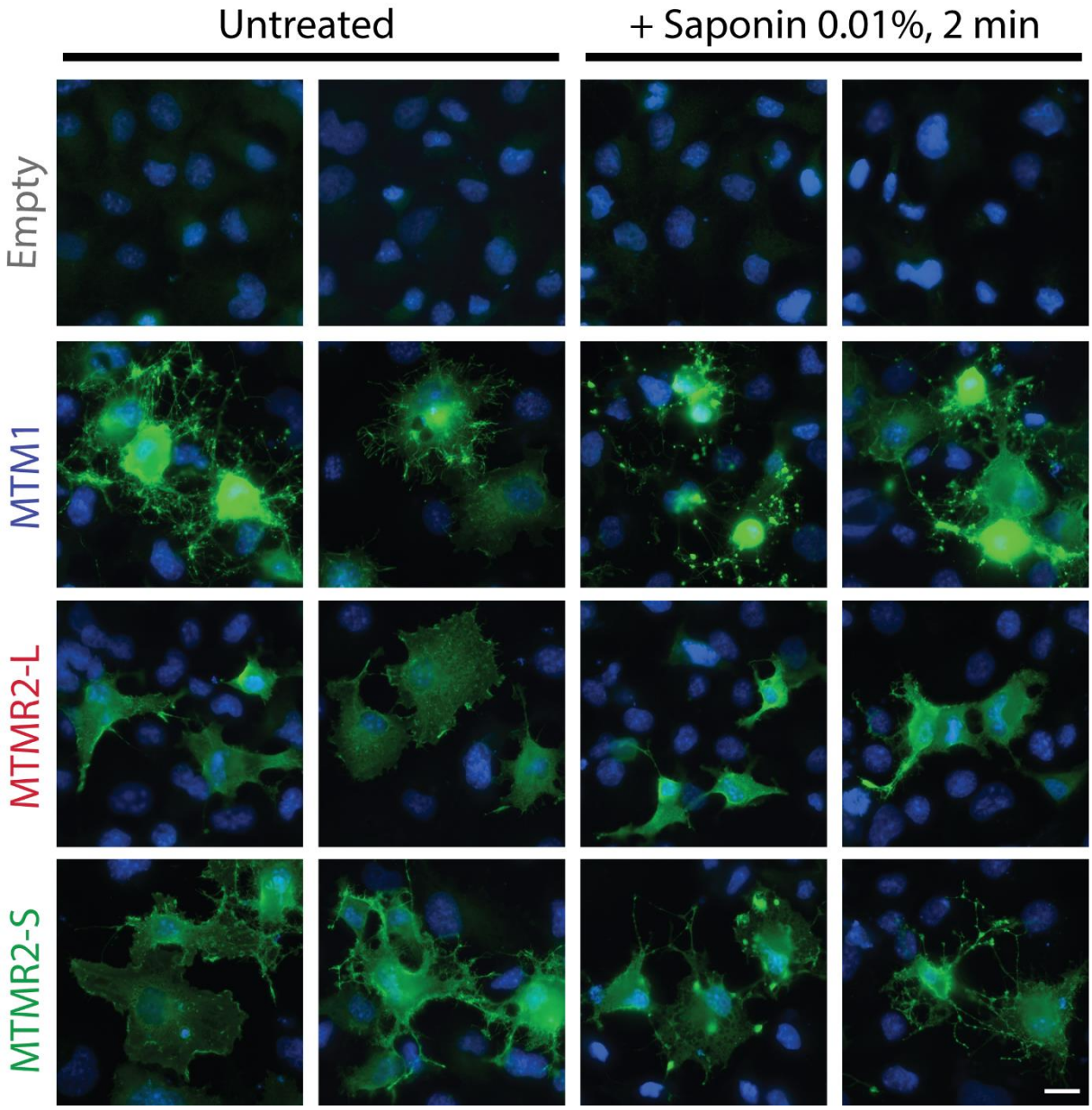

Figure 22: MTM1 and MTMR2-S localize to specific punctuate structures in COS cells membrane projections. COS-1 cells have been transfected with empty pAAV or pAAV overexpressing MTM1, MTMR2-L or MTMR2-S. Following fixation, the cells were immunostained with anti-MTM1 or anti-MTMR2 primary antibodies. Saponin treatment (right panels) was used to enhance detection of membrane-localized proteins via depletion of cytosolic contents. Scale bar 20 µm.

MTM1 and MTMR2-L both exhibited a cytosolic staining pattern in COS cells, with highest intensities in the perinuclear region (Figure 22). However, in most transfected cells MTM1 also presented a specific localization with a needle-like pattern in large membrane projections. These patterns have already been reported in the literature, and could result from oligomerization of MTM1 associated with membrane structures (Kim et al., 2002;

Spiegelhalter et al., 2014). This needle-like pattern is especially seen in hypo-osmotic conditions (Spiegelhalter et al., 2014), and was never observed here for MTMR2-L expression (Figure 22). The membrane projections are also specific to MTM1 expression.

The difference observed between MTM1 and MTMR2-L was exacerbated by 2 min treatment with 0.01% saponin (Figure 22). Saponin is a detergent that depletes the soluble cytoplasmic proteins and allows visualization of membrane-localized proteins (Lin et al., 1990). The MTMR2-L signal seemed to be restrained in the perinuclear region by the saponin treatment, while MTM1 localized around the nucleus and in numerous punctuate structures in membrane projections, strengthening the hypothesis that MTM1 is associated with membranes in the “needles”.

Interestingly, MTMR2-S was different from MTMR2-L and forms large membranes projections like MTM1. MTMR2-S presented mainly a cytosolic staining with highest intensities around the nucleus and close to the plasma membrane. In some cells, MTMR2-S also seemed to form needle-like structures, and the saponin treatment highlighted the same punctuate structures observed for MTM1. This confirms the MTM1-like localization observed for MTMR2-S in yeast cells.

In conclusion, in contrast with MTMR2-L, overexpressed MTM1 and MTMR2-S display a similar localization pattern in COS cells. Thus, MTMR2 localization in mammalian cells seems to depend on its N-terminal extension. This correlates with data in HeLa cells showing that the phosphorylation of MTMR2 on the S58 (that belongs to the N-terminal extension) regulates MTMR2 localization to punctate structures corresponding to endosomes (Franklin et al., 2011). This also supports the concept that the N-terminal extension of MTMR2 is mainly responsible for the functional differences between MTM1 and MTMR2.

B. MTMR2 N-terminal extension includes at least two phosphorylation sites

Since the N-terminal extension seems to regulate MTMR2 function, I then investigated if this 72 aa sequence could contain phosphorylation sites or binding sites for potential interacting partners. The protein extracts of COS cells overexpressing MTMR2-L, MTMR2-S or MTMR2-Δ2-24 were given to Philippe Hammann (mass spectrometry platform, Strasbourg) who immunoprecipitated the MTMR2 variants using our anti-MTMR2 monoclonal antibody (Figure 23A). After washing, the phosphorylation sites and interaction partners were identified by mass-spectrometry.

The analysis on human MTMR2 expression in COS cells allowed the identification of 3 phosphorylation sites, on serines S6, S58 and S631 (Figure 23B). S58 and S631 phosphorylations were already published for human MTMR2 (Franklin et al., 2013; Franklin et al., 2011), but the S6 was only reported for mouse MTMR2 (large scale analysis) (Villen et al., 2007) and we confirm here its conservation in human/primate cells. The S6 and S58 are both on the N-terminal extension of MTMR2-L, and S6 is logically deleted in the MTMR2-Δ2-24 construct. Thus, by analyzing MTMR2-L and MTMR2-Δ2-24, I also indirectly analyzed the function of S6 and S58 phosphorylation sites. A phosphorylation on the S9 has also been identified by a large scale analysis in mice liver, and could potentially be found in human cells (Huttlin et al., 2010). However, I did not detect this S9 phosphorylation in my assays on COS cells.

For note, the S58 phosphorylation was not identified in MTMR2-Δ2-24, while the concerned peptide (from S41 to R62) was present in both MTMR2-L and MTMR2-Δ2-24 construct. This raises the possibility of a S58 regulation by the first 24 amino acids of MTMR2-L, and more specifically by the S6 or S9 phosphorylation sites. Indeed, such a mechanism has already been brought to light in MTMR2 by Franklin *et al.* who showed that the S631 phosphorylation had an impact on MTMR2 localization (between early and late endosomes) only if the S58 was not phosphorylated (Franklin et al., 2013). However it cannot be excluded that the lack of detection could also be due to the lower level of MTMR2-Δ2-24 after immunoprecipitation compared to MTMR2-L (Figure 23A), rather than a difference in phosphorylation.

Finally, the differential interactome between the 3 MTMR2 variants is still under analysis and could provide novel information concerning the specific function and interactors of MTMR2-L N-terminal extension.

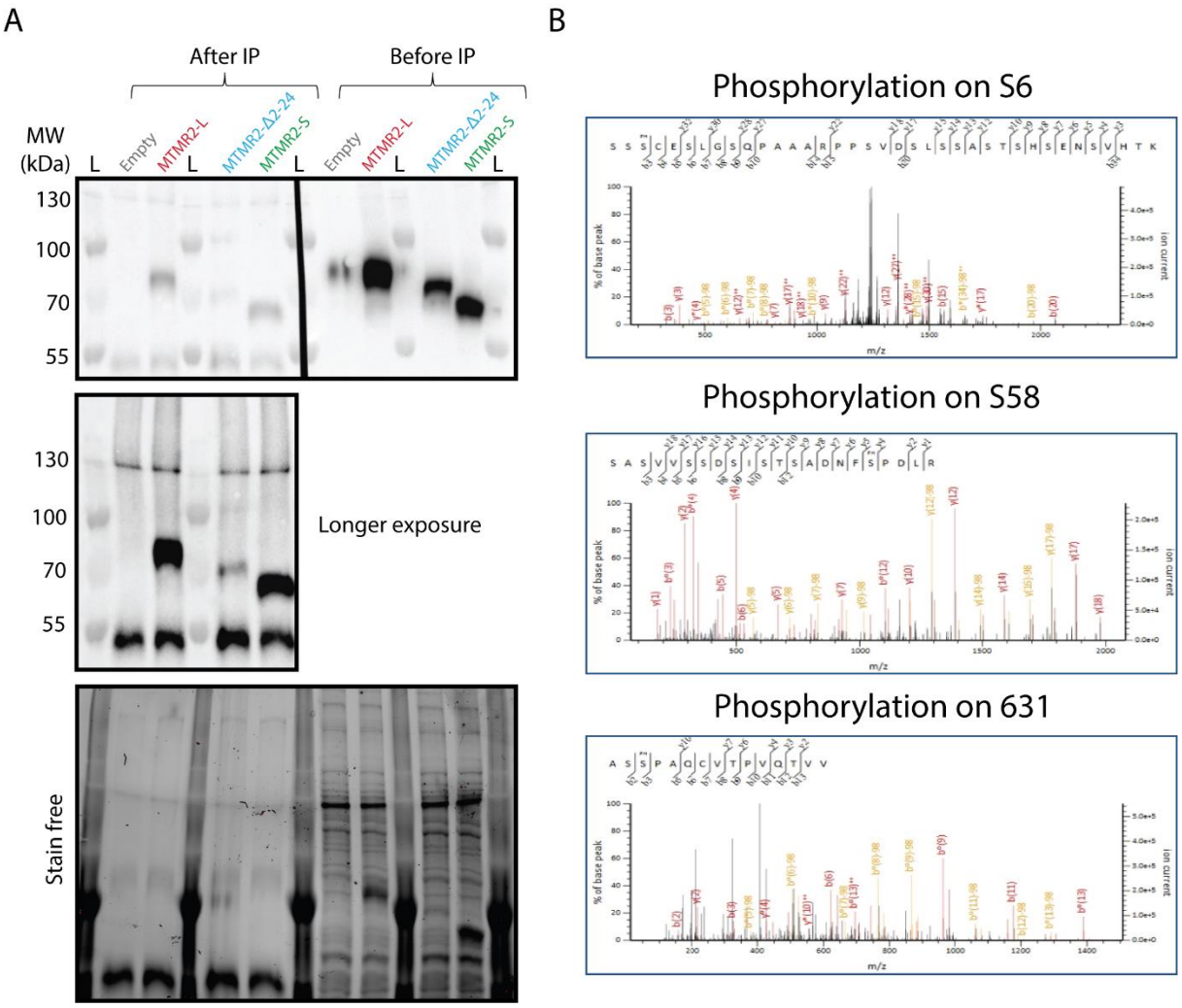

Figure 23: Detection of human MTMR2 phosphorylation sites by mass spectrometry. (A) Detection of MTMR2 constructs before and after immunoprecipitation (IP) using the homemade monoclonal anti-MTMR2 antibody. Immunoprecipitation of MTMR2-L, MTMR2-S and MTMR2-Δ2-24 was performed after overexpression in COS cells using pAAV vectors. L = Ladder. Stain free membrane shows the total proteins loaded in each well. The 55 kDa bands correspond to the anti-MTMR2 antibody. **(B)** Mapping of S6, S58 and S631 phosphorylation sites. MTMR2 tryptic peptides were fractionated and fragment ions are indicated on the m/z spectrum and peptide sequence. The fragment ions whose m/z value corresponds to *y* or *b* ions with the loss of a phosphate group (-98 m/z) are indicated on the spectrum.

C. Study of MTM1 and MTMR2 in C2C12 muscle cells

As previously mentioned, mutations in the ubiquitously expressed *MTM1* gene induce the muscle-specific XLCNM. Therefore, I next investigated MTM1 and MTMR2 cellular functions in a muscle cell context. **More precisely, I addressed whether MTMR2 could compensate for MTM1 loss in muscle cells.** To achieve this, I used the C2C12 cell line, an immortalized mouse myoblast cell line commonly used to study myoblast differentiation, myogenesis or muscle proteins/pathways.

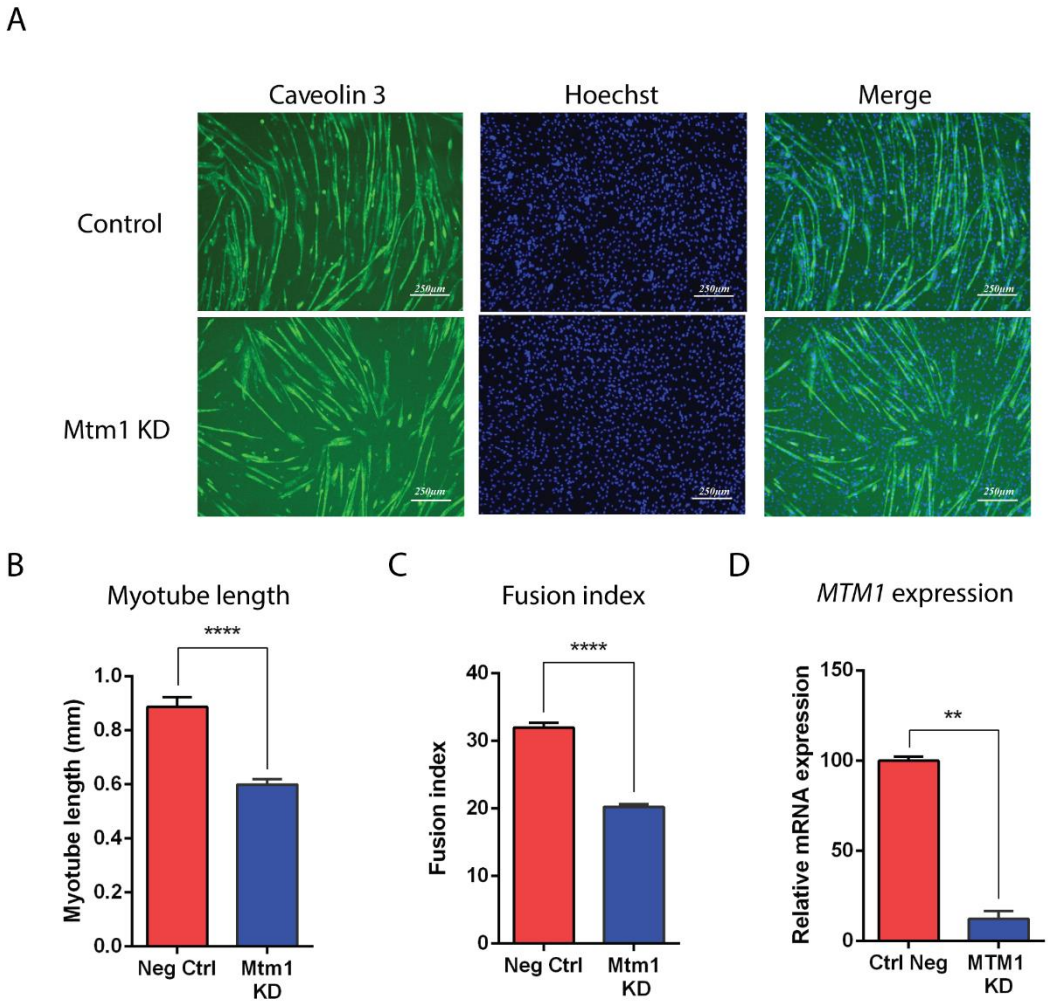

Figure 24: *Mtm1* knockdown C2C12 myotubes are shorter and have a lower fusion index. (A) Cellular morphology of C2C12 control and *Mtm1* knockdown (KD) myotubes after 9 days of differentiation. Caveolin 3 immunostaining and Hoechst staining were done to identify the myotubes and the nuclei, respectively. Scale bar 250 µm**. (B)** Quantification of the myotube length. n>300. ****p<0.0001 (Student's t test). **(C)** Quantification of the myotube fusion index. n>300. ****p<0.0001 (Student's t test). **(D)** Quantification of *MTM1* expression by RT-qPCR in *Mtm1* KD myotubes, compared to controls. N=2. **p<0.01 (Student's t test).

The first step was to identify a specific phenotype in muscle cells lacking MTM1. To this end, I differentiated control and *Mtm1* knockdown (KD) myoblasts into myotubes for 9 days, and then analyzed the myotube morphology (Figure 24). Compared to controls, *Mtm1* KD myotubes were approximately 60% shorter and displayed a lower fusion index (Figure 24B and C). The fusion index represents here the number of nuclei per myotube and reflects the ability of the myoblasts to fuse during their differentiation into myotubes. I also confirmed that the MTM1 expression level was significantly reduced in *Mtm1* KD myotubes after 9 days of differentiation (Figure 24D). **Thus, *Mtm1* KD C2C12 myotubes are shorter and have a lower fusion index.**

Then, I next wanted to determine if the expression of human myotubularins could compensate for the loss of MTM1 in *Mtm1* KD myotubes. Plasmid transfection has a very low efficiency in this cell line, and would not allow a stable and durable expression throughout differentiation. I thus decided to use lentiviral vectors which transduce C2C12 cells with a good efficiency and integrate into the mammalian cell genome. I transduced control and *Mtm1* KD myoblasts, then I re-plated them in several wells, and induced their differentiation into myotubes for 9 days. The lentiviral expression plasmid contained the human myotubularin (MTM1 or MTMR2) coding cDNA and the GFP coding cDNA (used as a control for transduction), under the control of two independent strong promoters. Indeed, preliminary immunofluorescence assays to detect overexpressed myotubularins using anti-MTM1 and anti-MTMR2 antibodies were not successful in C2C12 cells and I could not identify the transduced cells (data not shown). The independently expressed GFP (bicistronic) allows to identify the transduced myotubes while they are still living, and is not fused to the myotubularin to avoid any conformation defects due to the tag. So with this vector system, I could measure the length and fusion index of exclusively the transduced myotubes overexpressing the transduced myotubularin construct. Therefore, for the remainder of the experiments I used GFP as a marker for cell transfection (plasmid) or transduction (lentivirus).

These plasmids were first tested in HEK293 cells and induced a strong GFP expression detected by western blot and epifluorescence microscopy (Figure 25A).

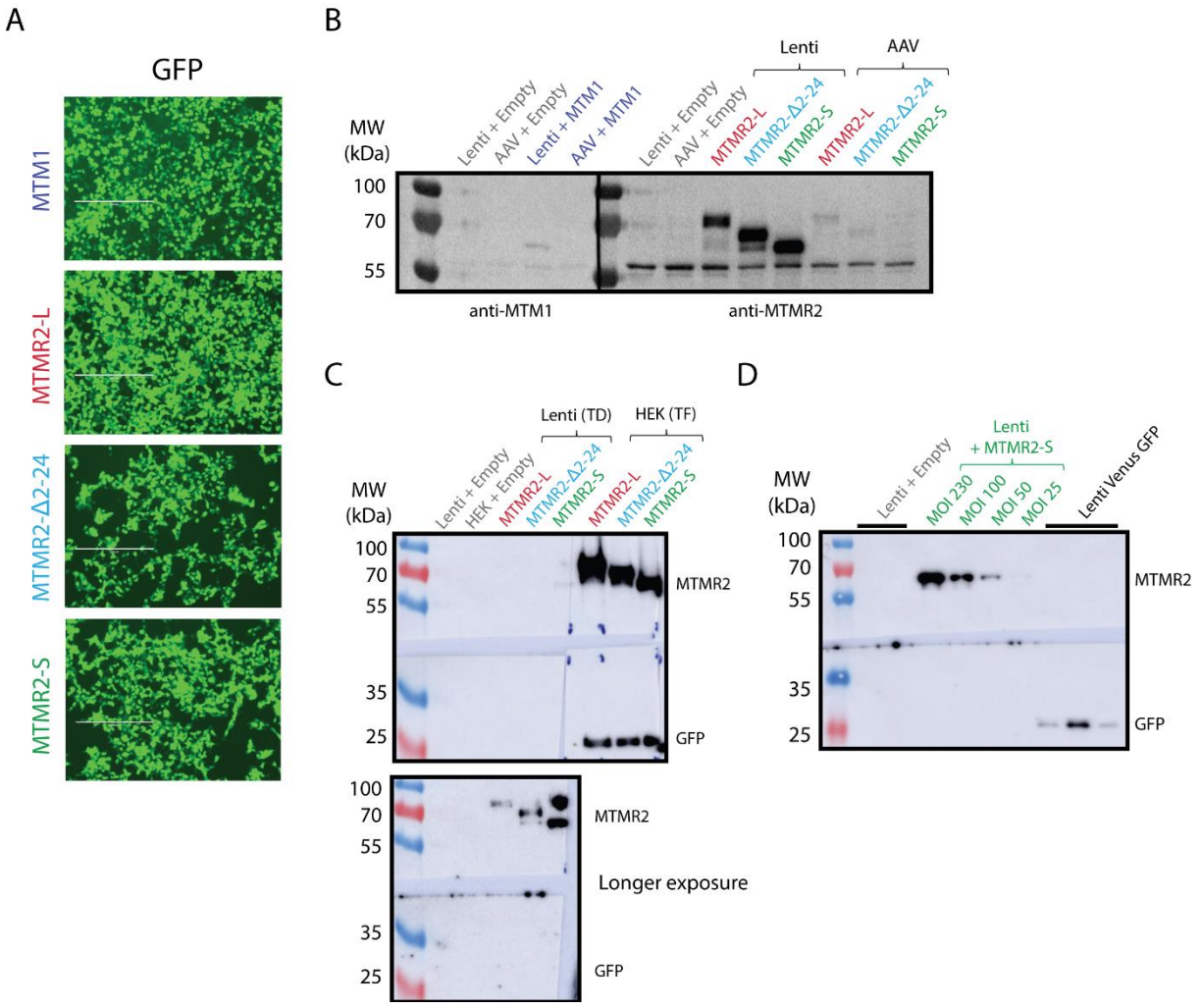

Figure 25: Independent expression of myotubularins and GFP in C2C12 using a unique lentiviral vector. (A) GFP expression in HEK293 cells transfected by the lentivirus plasmid overexpressing a myotubularin construct (indicated on the left) and the GFP by two independent strong promoters. **(B)** Detection of overexpressed myotubularins in C2C12 myotubes after 3 days of differentiation. Before differentiation, myoblasts have been transduced by a lentiviral (MOI 20) or AAV2 (MOI 20 000) vector overexpressing the myotubularin constructs. Empty vectors are used as negative controls. **(C)** Detection of overexpressed myotubularins and GFP in C2C12 myotubes after 3 days of differentiation using transduction (TD) of lentivirus, in comparison the same lentiviral plasmid transfected (TF) into HEK293 cells. GFP is only detected in HEK cells. **(D)** Detection of overexpressed MTMR2-S and GFP in C2C12 myotubes after 3 days of differentiation, with different MOI (multiplicity of infection). The GFP detection is compared to the Venus GFP lentiviral vector used to transduce the same C2C12 cells with the same protocol. GFP is only detected with the control Venus GFP lentivirus.

Transduction using lentiviral vectors of C2C12 cells also showed a good expression of MTM1 and MTMR2 constructs after 3 days of differentiation (Figure 25B). However, the GFP was not detected by western blot in these C2C12 cells, while I could easily detect it after HEK293 cells transfection with the same plasmids (Figure 25C). Next, I used a new control Venus GFP lentiviral vector that was transduced in C2C12 myoblasts and this time I could detect the GFP expression (Figure 25D). This suggests that with the first GFP vector, GFP is

not expressed in C2C12 cells. Even changing the promoter to control GFP expression (PGK to SV40) did not ameliorate the expression (data not shown), indicating that the plasmid background could be the problem.

This problem of GFP expression was also observed by fluorescence microscopy: transduced myoblasts show a weak GFP signal during the first days of differentiation, then this signal became hard to differentiate from the myotube auto-fluorescence (data not shown). A potential explanation could be that the cellular volume increases during differentiation due to myoblast fusion, and becomes too high compared to the GFP level of expression, inducing a dilution of the GFP signal in the cytoplasm.

Unfortunately, we could not draw conclusions from this experiment as I was not able to detect the GFP, and thus it was not possible to identify the transduced C2C12 myotubes overexpressing the different myotubularins. However, this system could have been (and could still be with a new vector) very useful to study the ability of MTMR2 to complement MTM1 loss in C2C12 myotubes.

Nevertheless, this experiment allowed me to compare lentiviral and AAV2 vectors ability to transduce C2C12 myoblasts. In a transduction experiment, the MOI (multiplicity of infection) represents the ratio between the number of viral vectors added to the cultured cells and the number of cells in the culture well. Even with a 1000x higher MOI, AAV2 vectors induced a very low myotubularin expression level compared to lentiviral vectors (Figure 25B). Moreover, for lentivirus the myotubularin expression level was proportional to the MOI (Figure 25D). These results could be useful for the setup of future experiments involving transduction of C2C12 cell lines.

The study of human MTM1 and MTMR2 in mammalian cells allowed me the better understand the cellular differences between the two proteins. In COS cells, expression of human MTM1 and MTMR2-S induces similar phenotypes, while MTMR2-L induced a significantly different phenotype. These results point to the novel concept that MTMR2 specific localization and function compared to MTM1 may be dependent on the N-terminal extension. The importance of this extension was confirmed by the identification of the two phosphorylation sites S6 and S58; S6 phosphorylation could potentially regulate S58 phosphorylation, and the S58 has been shown to regulate MTMR2 functions.

Furthermore I also showed that *Mtm1* KD C2C12 myotubes are shorter and have a lower fusion index compared to control myotubes. This is the first time this phenotype has been identified, and could therefore be used for future studies on MTM1, MTMR2 or other myotubularins in a muscle cell context, or to help understand the disease pathophysiology linked to loss of MTM1.

V. MTMR2 isoforms rescue the myopathic phenotypes of *Mtm1* KO mouse muscles

I have analyzed the structural and functional differences between MTM1 and MTMR2 isoforms in yeast and mammalian cells. I next wanted to analyze MTM1 in MTMR2 in skeletal muscles *in vivo* in ***Mtm1* KO mice**, to determine if the differences identified, notably different results relative to the N-terminal composition of MTMR2, are also observed in mice. Furthermore based on the functional similarities between MTM1 and MTMR2, I investigated if MTMR2 can compensate for the loss of MTM1 in mice.

For MTMR2, I focused my analyses on the two physiological isoforms resulting from alternative splicing: MTMR2-L and MTMR2-S (corresponding to MTMR2-Δ2-73). Moreover, I also added the MTMR2-Δ2-24 construct in some experiments to have a shorter N-terminal truncated form.

A. Is MTMR2 expressed in muscle?

Before studying MTM1 and MTMR2 specificities and trying to determine whether MTMR2 could be used to compensate for MTM1 loss in XLCNM, I wanted to determine whether MTMR2 could be detected in skeletal muscle. Indeed, the obvious absence of compensation in affected patients could be explained by an absence of MTMR2 in the affected tissues.

1. Expression of the MTMR2-S short isoform is reduced in *Mtm1* KO mice muscles.

I first analyzed the gene expression level, by analyzing MTMR2 mRNA variants in mice skeletal muscles. As described in the introduction, four *MTMR2* mRNA variants (V1 to V4) have been previously reported in peripheral nerves of mice, potentially coding for 2 protein isoforms (Bolino et al., 2002). Variants V2 to V4 differ from variant V1 by the inclusion of alternative exons 1a and/or 2a leading to a premature stop codon and unmasking

an alternative start site in exon 3 (Figure 26A and B). Variant V1 encodes the most described MTMR2-L (long) protein isoform (643 aa) while the other variants code for the MTMR2-S (short) isoform (571 aa) that was previously detected in various cell lines (Bolino et al., 2002).

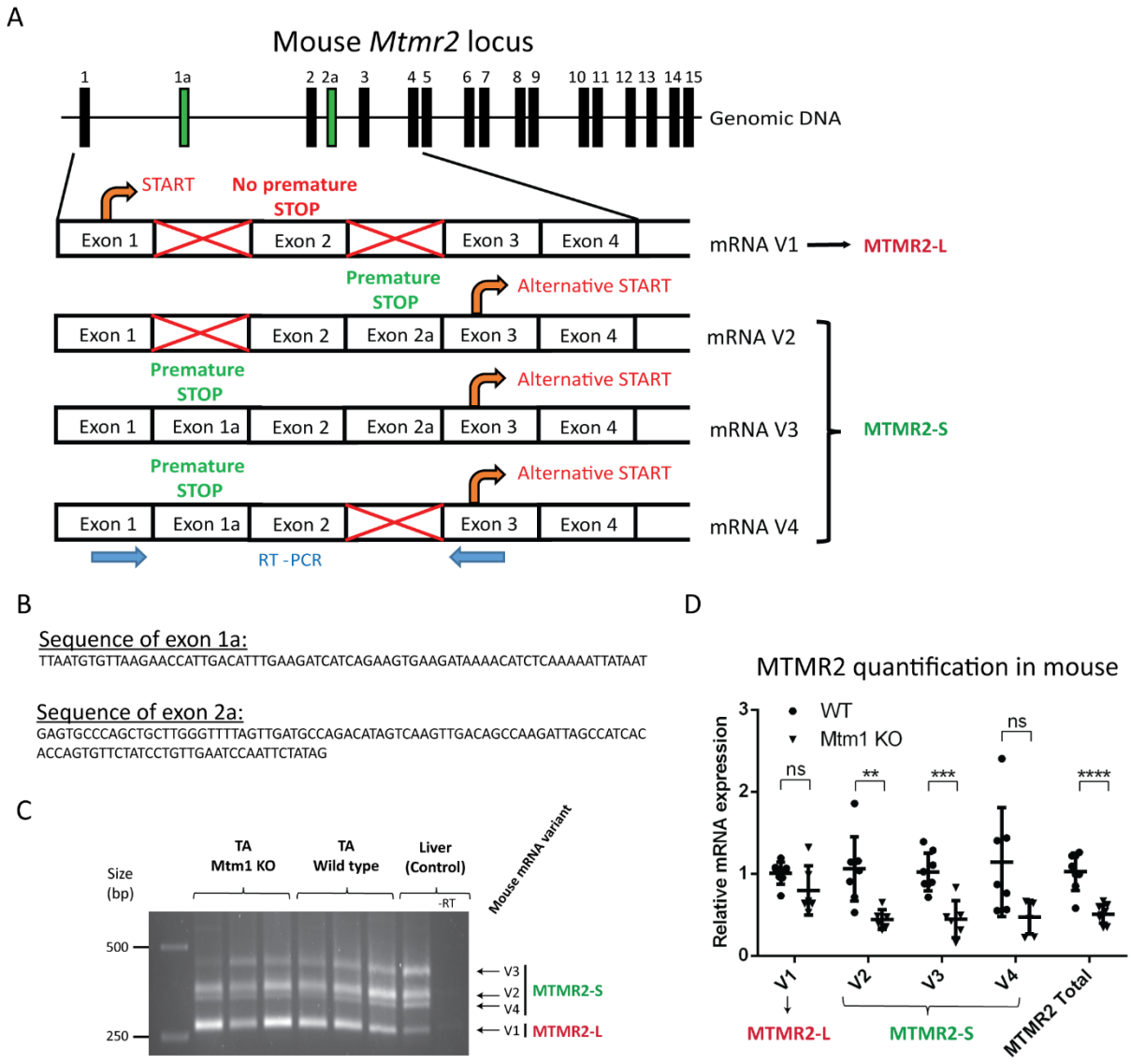

Figure 26: Detection and quantification of MTMR2 mRNA isoforms in mouse. (**A**) Genomic structure and mRNA isoforms of MTMR2 in mouse. Inclusion of any combination of the alternative exons 1a or 2a brings a premature stop codon and unmasks an alternative start site in exon 3. Murine MTMR2 V1 encodes for the MTMR2-L while isoforms V2 to V4 encode for MTMR2-S. (**B**) Sequence of mouse alternative exons 1a and 2a from Sanger sequencing of RT-PCR products from muscle. (**C**) PCR between exons 1 and 3 of MTMR2 on cDNA from TA muscles isolated from WT and *Mtm1* KO mice and from WT liver. The 4 mRNA variants are detected. **(D)** Quantification by RT-qPCR of MTMR2 isoforms (V1 to V4) in the TA muscle of *Mtm1* KO mice compared to WT mice. n>6. Each isoform is presented as an independent ratio, with a value of 1 set for expression in WT mice. Data represent means ± s.d. ***p*<0.01, ****p*<0.001, *****p*<0.0001, ns not significant (Student's t test).

I performed an RT-PCR on total mRNA from tibialis anterior (TA) skeletal muscle of wild type (WT) and *Mtm1* KO mice and from WT liver (as control) (Figure 26C). The PCR amplified a sequence between exons 1 and 3 of *MTMR2*, allowing to detect the additional exon 1a and 2a if they are included by alternative splicing. Four different bands were amplified in each sample, and I confirmed by cloning followed by Sanger sequencing that the 4 amplified sequences correspond to the 4 *MTMR2* mRNA variants (V1 to V4) (Figure 26B). **This shows that the four mRNA variants encoding for both MTMR2-L and MTMR2-S proteins are present in mouse skeletal muscle.**

Using specific sets of primers for each mRNA variant, I then quantified by RT-qPCR the mRNA levels of the different MTMR2 variants (V1 to V4) in TA muscles of *Mtm*1 KO compared to wild type (WT) mice (Figure 26D). The results show that MTMR2 mRNA total level was decreased in *Mtm1* KO muscles by 2 fold. This was mainly due to a strong decrease in the V2 and V3 transcripts encoding the MTMR2-S isoform, while the level of the V1 transcript coding for MTMR2-L remained statistically unchanged between *Mtm1* KO and WT mice. Note that these changes were not observed in Figure 26C since it presents a conventional RT-PCR that does not allow quantification. **These results show a decrease of MTMR2 expression in *Mtm1* KO mice, and more specifically of the V2 and V3 transcripts encoding the short MTMR2-S isoform.**

2. Expression of the MTMR2-S short isoform is also reduced in the XLCNM patient muscles

In human, a similar *MTMR2* alternative splicing has been described. 15 exons were initially identified, but Bolino *et al*. described 3 additional exons named 1a, 2a and 2b and their inclusion by alternative splicing allows the expression of 4 different transcripts variants (V1 to V4) that are ubiquitously expressed (Figure 6A) (Bolino et al., 2002; Bolino et al., 2000). Transcript variant V1 does not contain any additional exon and leads to the translation from exon 1 of MTMR2-L long protein isoform (643 aa), while V2 to V4 include at least exon 1a, leading to a premature STOP codon and to the translation from an alternative start codon in exon 3. Thus, as in mice, V2 to V4 are used for the translation of the shorter MTMR2-S protein isoform of 571 aa.

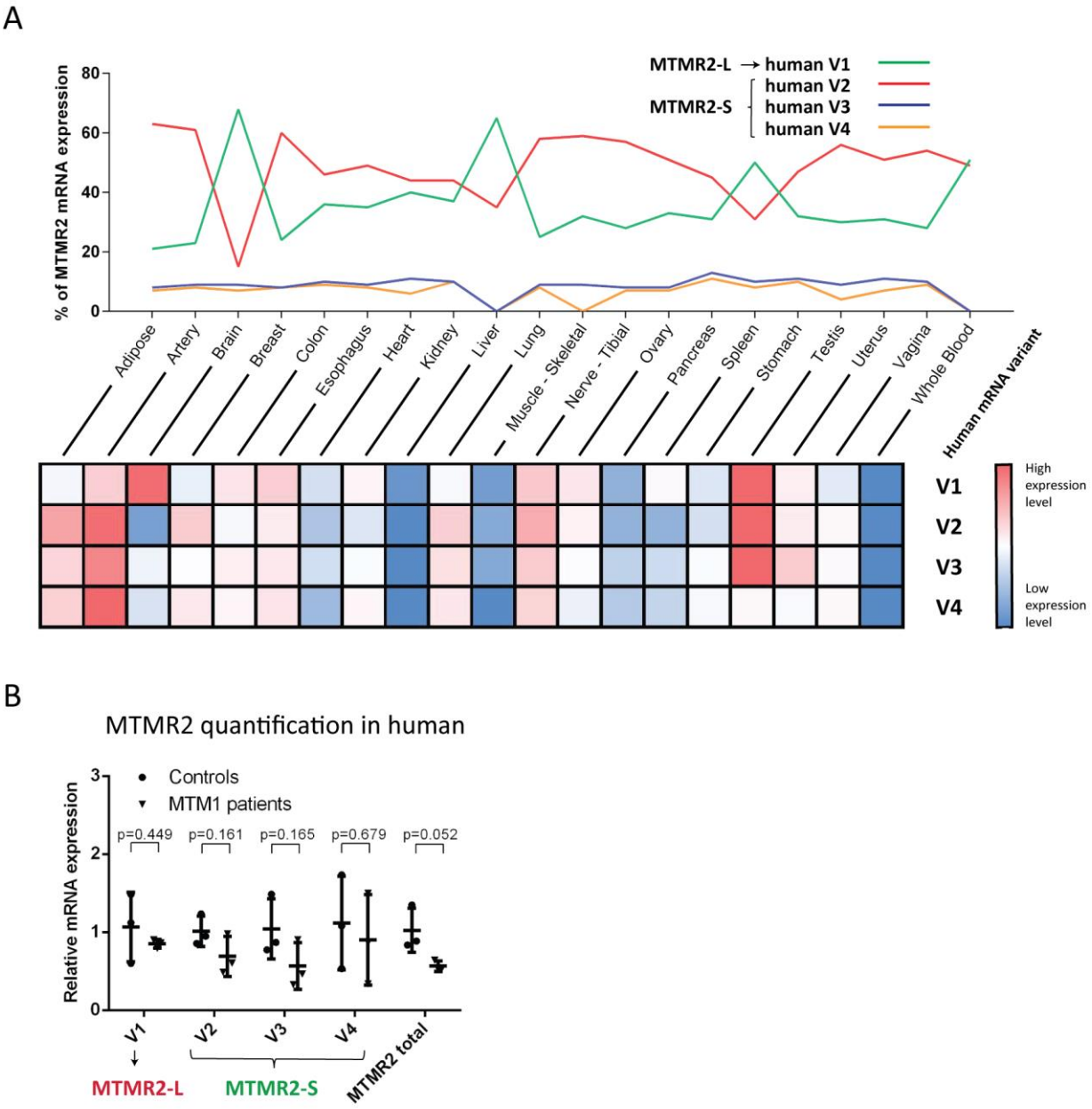

Figure 27: MTMR2-S expression is reduced in XLCNM patient muscles. (A) Comparative expression of MTMR2 mRNA isoforms V1 to V4 in 20 human tissues from GTEx database mining (top). Tissue expression of each isoform independently (bottom). **(B)** Quantification by RT-qPCR of MTMR2 isoforms (V1 to V4) in muscles of MTM1 patients compared to controls. N=3. Each isoform is presented as an independent ratio, with a value of 1 set for expression in control patients. Data represent means ± s.d. The *P* value is indicated for each isoform (Student's t test).

The expression level of these isoforms was first investigated in human through mining the GTEx expression database encompassing data on 51 human tissues (GTEx_consortium, 2015). Variant V1 is the major MTMR2 RNA in brain, liver and spleen while variant V2 is predominant in the other tissues (Figure 27A). Concerning their expression level, variant V1 was highest in brain, testis, esophagus, ovary, colon and spleen while V2 was predominant in

the other tissues including nerve, adipose and artery. **Interestingly the different variants of MTMR2 are poorly expressed in skeletal muscle.**

Using specific sets of primers for each human mRNA variants, I then quantified by RT-qPCR the mRNA levels of the different MTMR2 variants (V1 to V4) in muscles biopsies from 3 XLCNM patients compared to 3 unaffected muscles (Figure 27B). The low biopsies number did not allow to reach a statistical significance, but a clear tendency can be observed. **As observed in mice, human *MTMR2* total mRNA levels were reduced by 2 fold in XLCNM patient muscles compared to non-affected muscles. And as previously observed in mice muscles, this was mainly due to a strong decrease of V2 and V3 transcripts encoding the MTMR2-S isoform.**

These results show that MTMR2 expression level is low in healthy skeletal muscles compared to other tissues. Moreover, MTMR2 expression is reduced even further in both mice and human Mtm1 myopathic muscles. The short MTMR2-S isoform being the most affected by this decrease is intriguing, since overexpression of this isoform induced a strong phenotype similar to MTM1 overexpression in yeast and mammalian cells. **This suggests that the lack of compensation of MTM1 loss by endogenous MTMR2 could be due to two additive effects: the low expression level of MTMR2 in muscles and the even further decrease in MTMR2-S expression level in affected XLCNM skeletal muscles.**

3. Detection of MTMR2 protein isoforms in mice

As mRNA analysis indicated MTMR2 levels were reduced in *Mtm*1 KO mice, I next wanted to confirm this at the protein level. I tried to detect endogenous MTMR2 protein isoforms by western blot, using our homemade antibody. By increasing the anti-MTMR2 4G3 antibody concentration and the membrane exposure time, I could obtain several bands in brain and TA muscle from *Mtm1* KO and WT mice (Figure 28A). Some of them were at the expected size for MTMR2-L and –S. Unfortunately, all these bands were also detected in brain and TA control protein extracts from *Mtmr2* KO mice, and thus were non-specific bands. Thus, our homemade antibody did not allow to detect the mouse MTMR2 isoforms at the endogenous level.

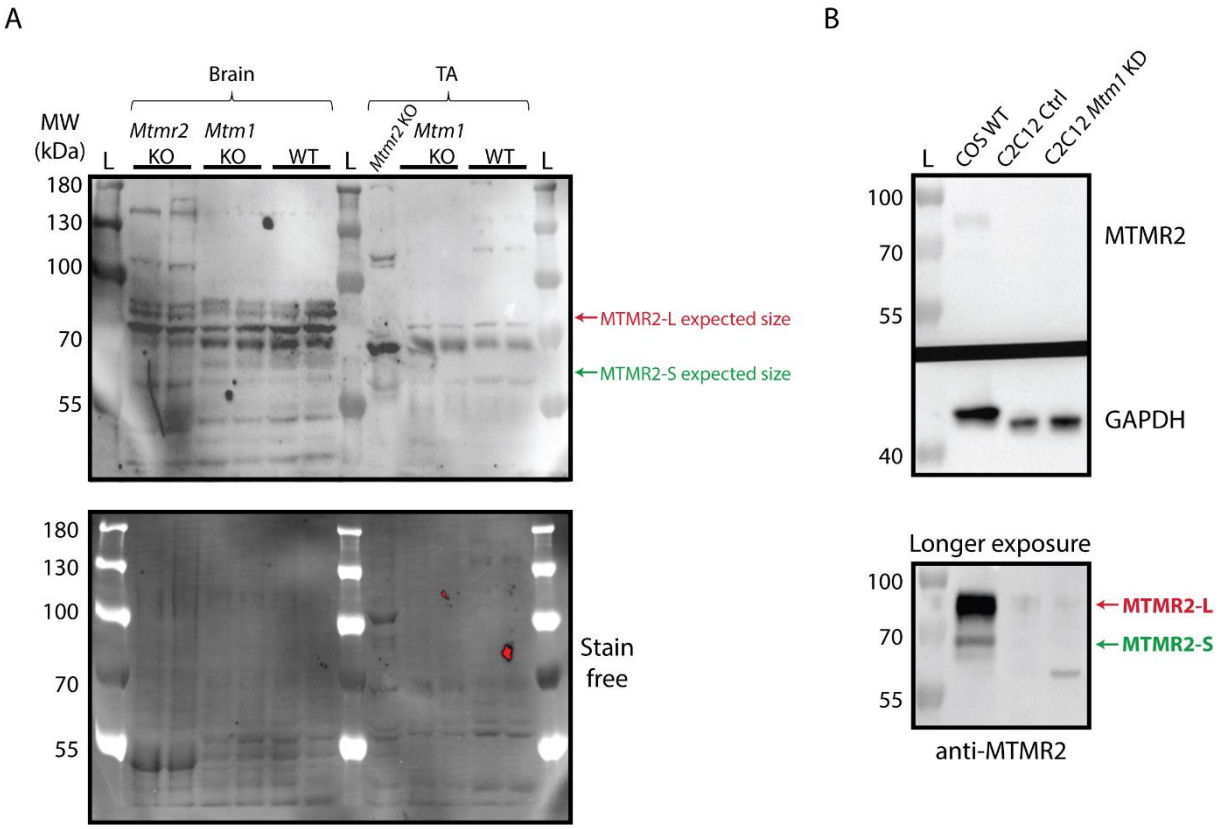

Figure 28: Detection of endogenous MTMR2 protein isoforms in mouse and cultured cells. (A) Western blot to detect endogenous MTMR2 in brain and TA from *Mtm1* KO and WT mice. Brain and TA protein extracts from *Mtmr2* KO mice were used as negative control, and showed that all detected bands are non-specific. Expected sizes for MTMR2-L and –S are indicated on the right. Stain free was used as loading control. L = Ladder. **(B)** Detection of endogenous MTMR2 isoforms in WT COS cells and in control and *Mtm1* KD C2C12 myotubes after 3 days of differentiation. GAPDH was used as loading control. A longer exposure for MTMR2 is presented below and expected sizes for MTMR2-L and –S are indicated on the right. L = Ladder.

However, I detected what could be the endogenous MTMR2 short and long isoforms in protein extracts from COS cells, showing that our anti-MTMR2 antibody could be able to detect the primate (and also probably the human) endogenous MTMR2 in western blots (Figure 28B). The MTMR2-L expression would then be higher than the MTMR2-S expression in COS cells. Without a negative control, it is of course possible that what I detected are non-specific bands, but they would be exactly at MTMR2-L and –S sizes.

Moreover, a faint band that could correspond to MTMR2-L was also detected in protein extracts from C2C12 control and *Mtm1* KD myotubes (Figure 28B). This could confirm the low expression level of MTMR2 in muscle cells. But since the signal was very low, it is also possible that this antibody - that was raised against the full length human

MTMR2 and whom we don't know the target epitope - does not recognize the mouse protein. The development of an MTMR2 antibody with a better specificity will be important for future investigations on MTMR2. However, the remainder of this thesis is focused on analyzing overexpressed MTMR2 in muscles, and the antibody works for this application.

B. Overexpression of MTM1 and MTMR2 in *Mtm1* KO mouse muscles using AAV vectors

To assess whether in an *in vivo* muscle context MTMR2-S is also functionally closer to MTM1 compared to MTMR2-L, I overexpressed MTM1, MTMR2-L and MTMR2-S in the TA muscles of the *Mtm1* KO mouse model and analyzed different myopathy-like phenotypes. MTMR2-Δ2-24 was also used in some experiments to have an intermediate truncated form of MTMR2.

The different myotubularins were expressed from Adeno-associated virus AAV2/1 under the control of the CMV promoter and the recombinant virions were injected into the TA muscles of 2-3 week old *Mtm1* KO mice. The *Mtm1* KO mice develop a progressive muscle atrophy and weakness starting at 2-3 weeks and leading to death by 8 weeks, the TA muscle being the most affected muscle detected in this model (Buj-Bello et al., 2002b; Cowling et al., 2014). Our team has previously shown that AAV-mediated expression of MTM1 for 4 weeks in the TA muscle, corrects the myopathy phenotype in *Mtm1* KO mice (Amoasii et al., 2012). Therefore to determine the impact of introducing MTMR2-L and MTMR2-S into *Mtm1* KO mice, I followed the previously described protocol for AAV injections (Amoasii et al., 2012), using MTM1 as a positive control for the rescue, and empty AAV2/1 as a disease control in the contralateral muscle. Wild type muscles injected with empty AAV2/1 were also used as positive control for healthy muscles.

The MTM1, MTMR2-L, MTMR2-S and MTMR2-Δ2-24 human myotubularins were detected in injected TA muscles four weeks after injection, as revealed by anti-MTM1 and anti-MTMR2 western-blot analyzes (Figure 29A and B). Endogenous MTMR2 proteins were not detected in muscles injected with empty AAV, most likely due to the low level of this protein, as previously described (Chapter V.A.).

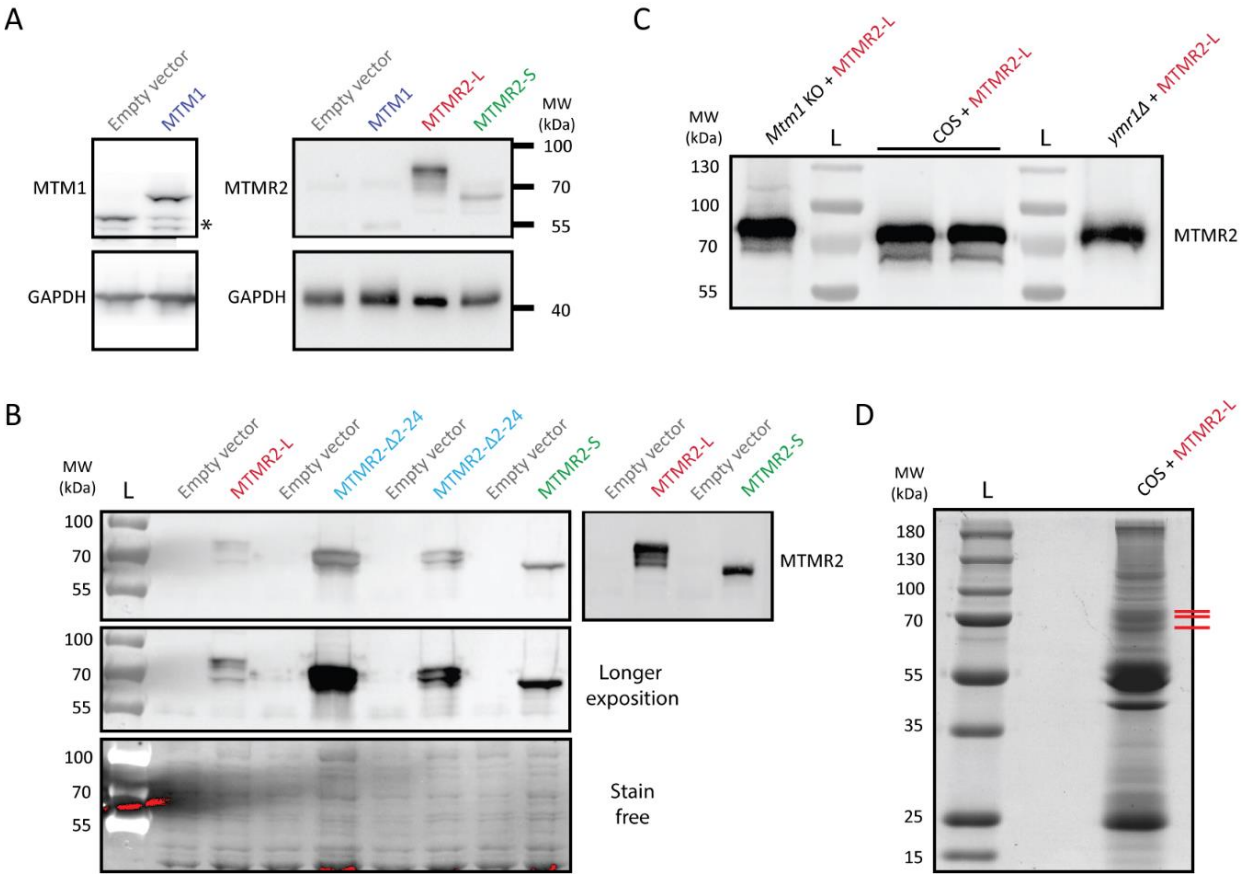

Figure 29: Detection of overexpressed myotubularins after intramuscular injections in mice. TA muscles from 2-3 week-old *Mtm1* KO mice were injected with AAV2/1 expressing myotubularins and analyzed 4 weeks later. **(A)** and **(B)** Detection of exogenously expressed human myotubularins by western blot using anti-MTM1 or anti-MTMR2 antibodies; GAPDH **(A)** or Stain free **(B)** are used as a loading control. L = Ladder **(C)** Detection of exogenously expressed human MTMR2-L in Mtm1 KO mouse TA, in COS-1 cells and in *ymr1Δ* yeast cells, by western blot. A lower supplementary band for MTMR2-L is detected in mice and COS cells but not in yeast. **(D)** Coomassie blue staining of SDS-Page gel with total protein extract from COS cells overexpressing MTMR2-L. The 3 indicated bands were given to mass spectrometry. L = Ladder.

Interestingly, detection of overexpressed MTMR2-L isoform by western blot revealed several bands: one at the expected MTMR2-L size, a second at the same size as MTMR2-S and sometimes a third band at the same size as MTMR2-Δ2-24 (Figure 29B). Moreover, MTMR2-Δ2-24 also displays a lower additional band at the same size as MTMR2-S (Figure 29B). On the contrary, no additional band was observed for MTMR2-S detection. This suggests some protein cleavage in the N-terminal extension of MTMR2-L and MTMR2-Δ2-24, more precisely around the 73rd amino acid of MTMR2-L, leading to the formation of MTMR2-S or a protein having a similar size. Another possibility is the use of the alternative start in exon 3 of the overexpressed mRNA, leading to the production of MTMR2-S, as it is

the case for endogenous mRNA when exons 1a or 2a are present. Post-transcriptional modifications might not explain these additional bands, since the distance between the upper and lower bands is different for MTMR2-L and MTMR2-Δ2-24.

The same 2-3 bands were detected for MTMR2-L when overexpressed in *Mtm1* KO TA muscle and in COS cells, but not in *ymr1Δ* yeast cells (Figure 29C). Thus, this potential cleavage or alternative start system seems specific of mammalian cells and may implicate some pathways or enzymes that are absent in yeast. I separated the 3 MTMR2-L bands for mass spectrometry analysis to determine whether the lower bands lacked the N-terminal extension, but unfortunately the results were not conclusive (Figure 29D and data not shown).

In conclusion, the different overexpressed myotubularins were detected in *Mtm1* KO mouse muscles after AVV-injection. However, we have to keep in mind for the later analysis of muscle phenotypes that MTMR2-L and MTMR2-Δ2-24 overexpression could potentially lead to the production of a shorter form of MTMR2 that might be similar to MTMR2-S.

C. Exogenous expression of MTMR2 short isoform in the *Mtm1* KO mice rescues muscle weight and force similarly to MTM1 expression

Next I analyzed the effect of overexpressed myotubularins on muscle weight and force. Four weeks after empty AAV control injection, the TA muscle weight of the *Mtm1* KO mice was decreased by 2.5 fold compared to WT mice (Figure 30A), as previously observed (Amoasii et al., 2012; Buj-Bello et al., 2002b). MTM1 or MTMR2-S expression in the TA muscle of *Mtm1* KO mice increased significantly the muscle mass compared to the empty AAV control (1.5 fold), contrary to MTMR2-L and MTMR2-Δ2-24. To address a potential hypertrophic effect of human MTM1 or MTMR2 constructs in wild type (WT) mice, TA muscle weight of injected WT mice was quantified (Figure 30B). No significant muscle mass increase was noted with any myotubularin indicating that **the amelioration observed in the *Mtm1* KO mice was not due to a hypertrophic effect but to a functional rescue.**

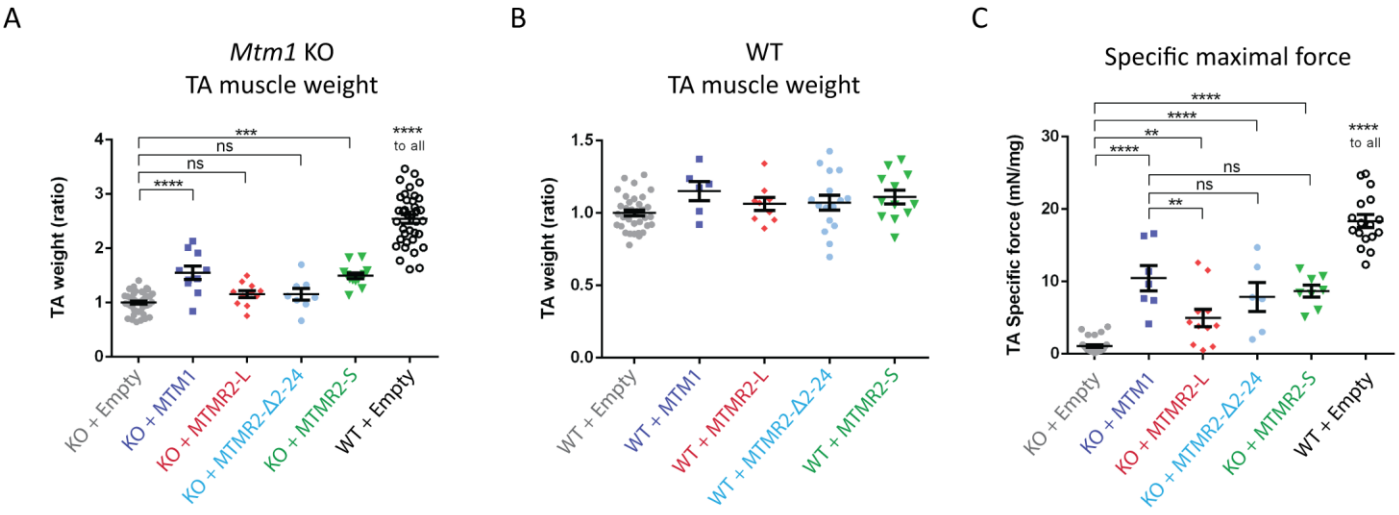

Figure 30: The MTMR2 short isoform rescues muscle weight and force similarly as MTM1 in the *Mtm1* KO myopathic mouse. TA muscles from 2-3 week-old *Mtm1* KO mice were injected with AAV2/1 expressing myotubularins and analyzed 4 weeks later. **(A)** Ratio of muscle weight of TA expressing human myotubularins compared to the contralateral leg injected with empty AAV. MTMR2-S improved muscle mass similarly as MTM1 while MTMR2-L and MTMR2Δ2-24 had no effect. A value of 1 was set for the *Mtm1* KO mice injected with empty AAV. n>9. Data represent means ± s.e.m. ****p<0.0001, ***p<0.001, ns not significant (ANOVA test). **(B)** Ratio of muscle weight of TA expressing human myotubularins compared to the contralateral leg injected with empty AAV. A value of 1 is set for the WT TA muscle weight. n>5. Data represent means ± s.e.m. No significant differences (ANOVA test). (**C**) Specific maximal force of TA muscle (absolute values). The 3 MTMR2 constructs improved muscle force. n>6. Data represent means ± s.e.m. **p<0.01, ****p<0.0001, ns not significant (ANOVA test).

The *Mtm1* KO mice displayed very weak muscle force compared to WT mice, and all myotubularin constructs including MTMR2-L improved the TA specific muscle force (Figure 30C). Noteworthy, a similar rescue was observed for MTM1 and MTMR2-S, significantly above that observed for MTMR2-L injected muscles. This time, MTMR2-Δ2-24 induced an intermediary force rescue between MTMR2-L and –S. **These results show that both MTMR2-L and MTMR2-S isoforms improve the muscle weakness due to loss of MTM1, but only MTMR2-S expression induces a rescue level similar to that observed for MTM1.**

D. The MTMR2 isoforms rescue the histopathological hallmarks of the *Mtm1* KO mouse

In the *Mtm1 KO* mice, TA injections of AAV2/1 carrying MTM1, MTMR2-L or MTMR2-S increased muscle mass (except for MTMR2-L) and force. To analyze the rescue at the histological level, fiber size and nuclei localization were determined four weeks after injection. HE (hematoxylin-eosin) staining revealed increased fiber size upon AAV-MTM1, AAV-MTMR2-S and AAV-MTMR2-Δ2-24 injection compared to *Mtm1* KO muscle treated with empty AAV or AAV-MTMR2-L (Figure 31). Morphometric analysis revealed that among the different myotubularins tested, MTM1 induced a clear shift toward larger fiber diameters compared to MTMR2 constructs and empty AAV (Figure 31A). This shift is clearer by analyzing the percentage of fibers superior to 800 µm^2 (Figure 31B).

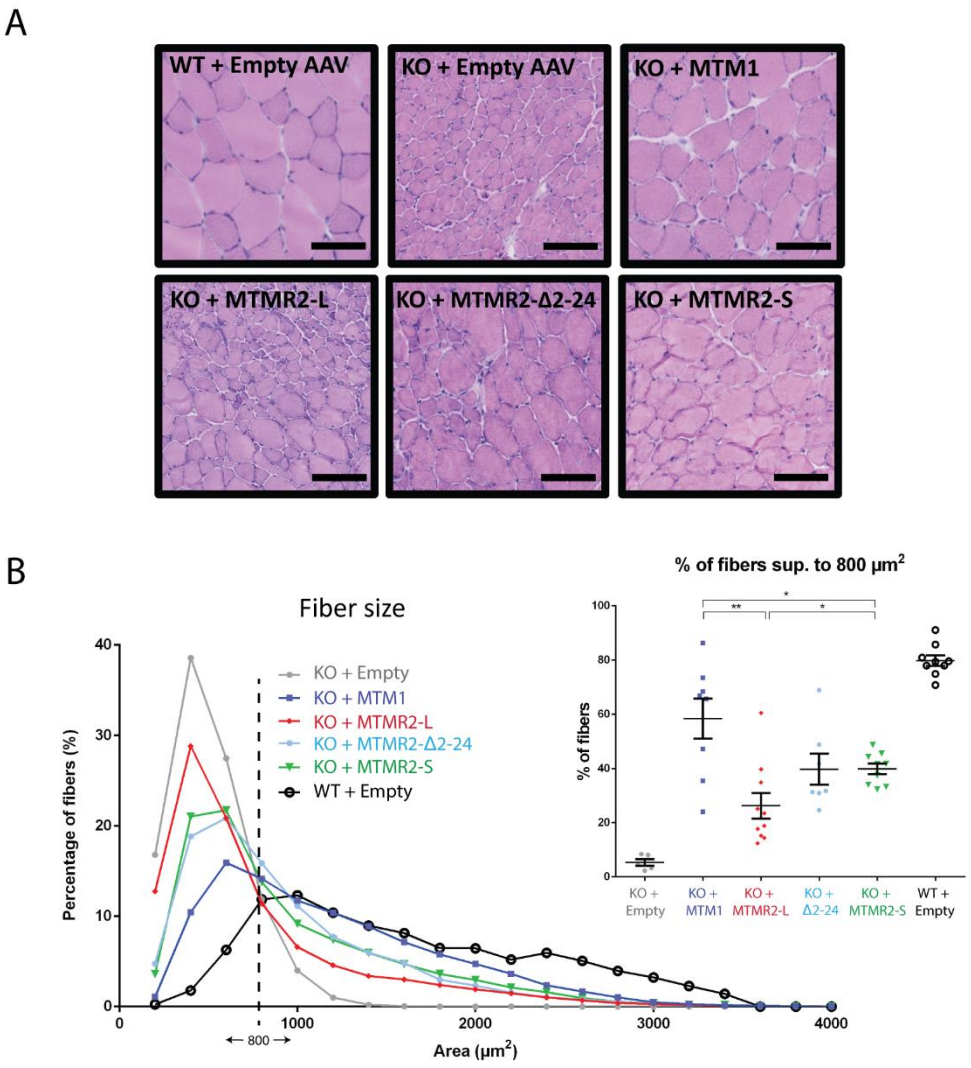

Figure 31: All MTMR2 constructs increase the myofiber size of *Mtm1* KO mice. TA muscles from *Mtm1* KO mice were injected with AAV2/1 expressing myotubularins and analyzed 4 weeks later. **(A)** Hematoxylin-eosin staining of TA muscle sections. Scale bar 100 µm. **(B)** Quantification of fiber area. Fiber size is grouped into 200 µm^2 intervals and represented as a percentage of total fibers in each group. n>1000 for 8 mice per construct. On the right is represented the percentage of fibers above 800 µm^2. n>8. Data represent means ± s.e.m. **p*<0.05, ***p*<0.01, (ANOVA test). The value for WT is statistically different from all *Mtm1* KO injected groups.

For all overexpressed myotubularin constructs, I observed spatial heterogeneity in the muscle, with some regions very well rescued and other regions still displaying smaller atrophic fibers characteristic of the XLCNM myopathy (Figure 32). This could be due to heterogeneity in the injections leading to low diffusion and transduction of the AAVs in some regions of the muscle.

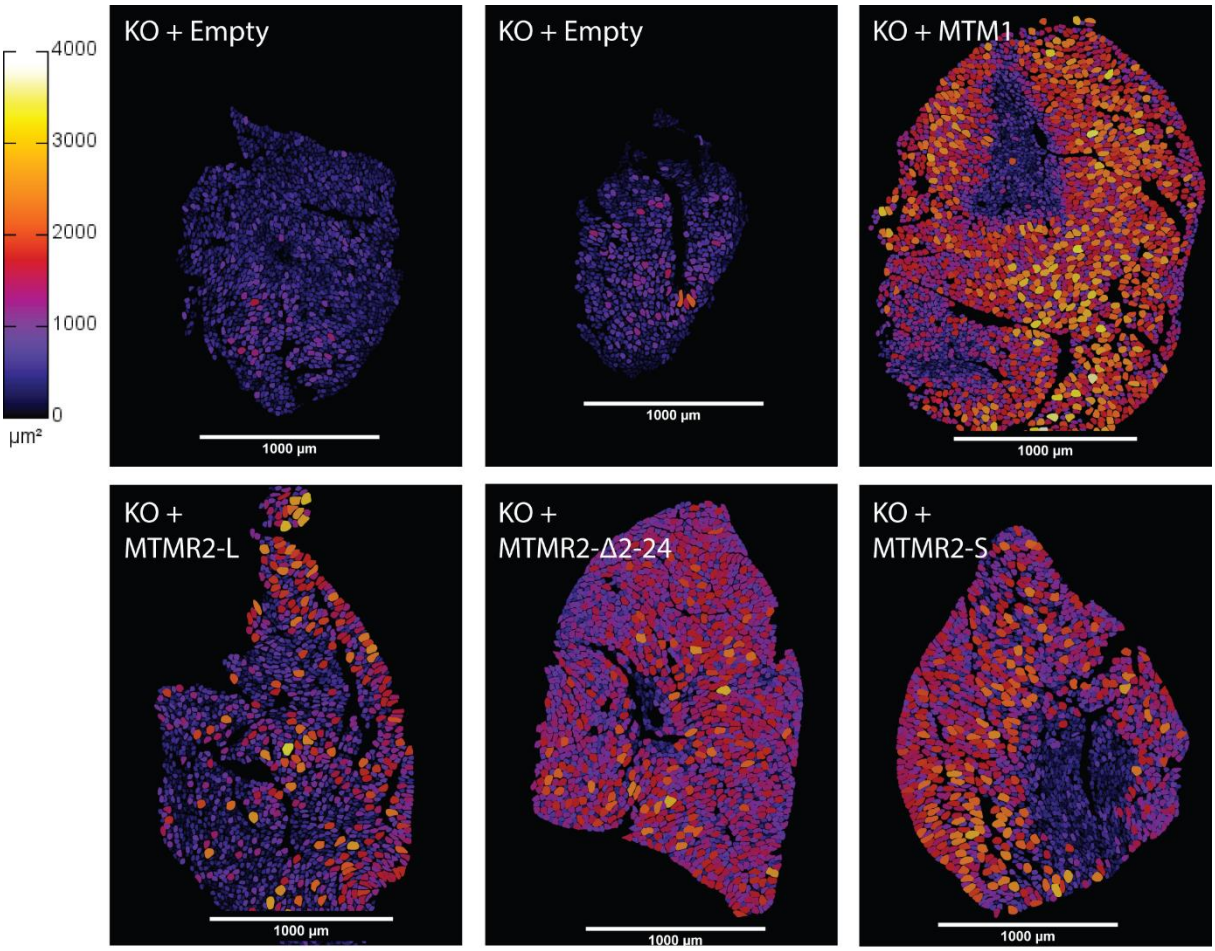

Figure 32: Fiber size heterogeneity in *Mtm1* KO rescued muscles. Hematoxylin-eosin staining of TA muscle sections were used to color code the myofibers depending on their area. The color coding is indicated on the left. Scale bar 1 mm.

Since nuclei are abnormally located within muscle fibers in *Mtm1* KO mice, I analyzed the distribution of nuclei. Injection of the different myotubularin constructs into the TA muscle of *Mtm1* KO increased significantly the percentage of nuclei positioned at the periphery compared with contralateral control muscles injected with empty AAV (Figure 33A). No significant differences have been observed between the different overexpressed myotubularins MTM1, MTMR2-S or MTMR2-L for this parameter. Interestingly, a correlation could be made between the nuclei positioning and the fiber size: for all overexpressed myotubularins, the percentage of well positioned peripheral nuclei increased

with the fiber size, the biggest fibers even reaching WT level (Figure 33B). This correlated with the spatial heterogeneity observed for the fiber size rescue, suggesting that the myotubularin constructs were not properly overexpressed in the small fibers. In contrast, the percentage of peripheral nuclei was independent from the fiber size in the TA muscles of *Mtm1* KO and WT mice. In patients, predominantly type 1 fibers are affected, which are the smallest fibers (Ambler et al., 1984; Oldfors et al., 1989; Silver et al., 1986). This may account for the more affected smaller fibers in this study.

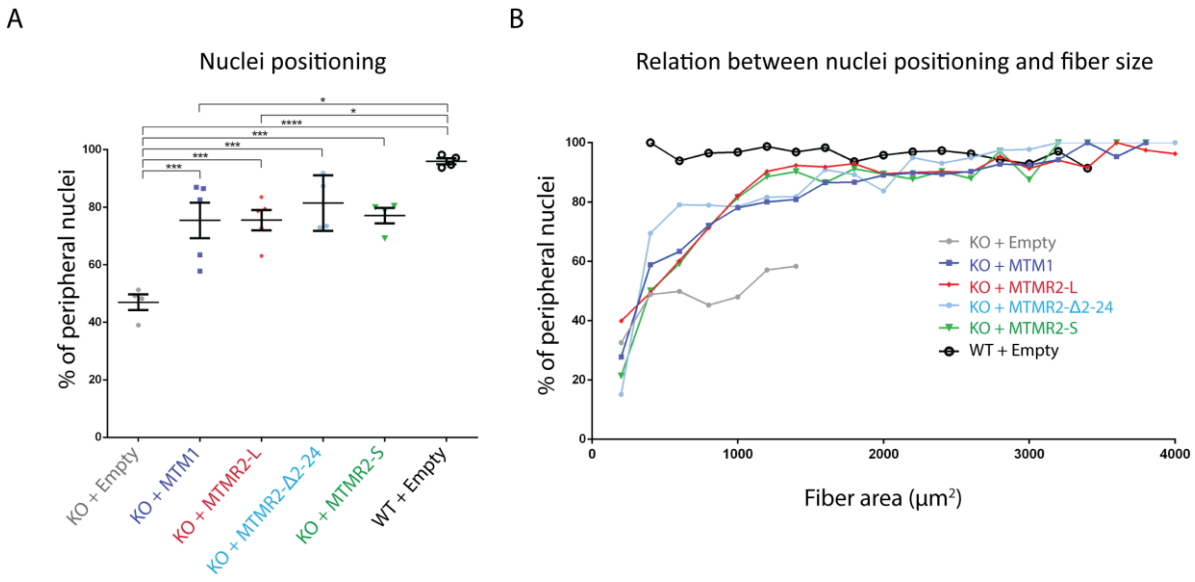

Figure 33: All MTMR2 constructs rescue the nuclei positioning in *Mtm1* KO mice. (A) Nuclei positioning in TA muscle. Percentage of well-positioned peripheral nuclei. n>6 animals. Data represent means ± s.e.m. **p*<0.05, ****p*<0.001, *****p*<0.0001 (ANOVA test). **(B)** Correlation between the nuclei positioning and the fiber size in TA muscles from Mtm1 KO mice overexpressing MTM1 and MTMR2 constructs.

The Mtm1 KO mouse muscle histology is also characterized by an abnormal distribution of the mitochondria. The succinate dehydrogenase (SDH) staining shows the oxidative fibers and abnormally accumulates at the periphery and center in the *Mtm1* KO fibers (Amoasii et al., 2012), while it is ameliorated with a more homogenous staining upon expression of the different myotubularin constructs (Figure 34).

Altogether, these results show that all MTMR2 isoforms were able to ameliorate the histopathological hallmarks of the MTM1 myopathy. Furthermore the truncated forms MTMR2-S and MTMR2-Δ2-24 provided a better rescue than the long MTMR2-L isoform, corroborating my previous results obtained in yeast (chapter III).

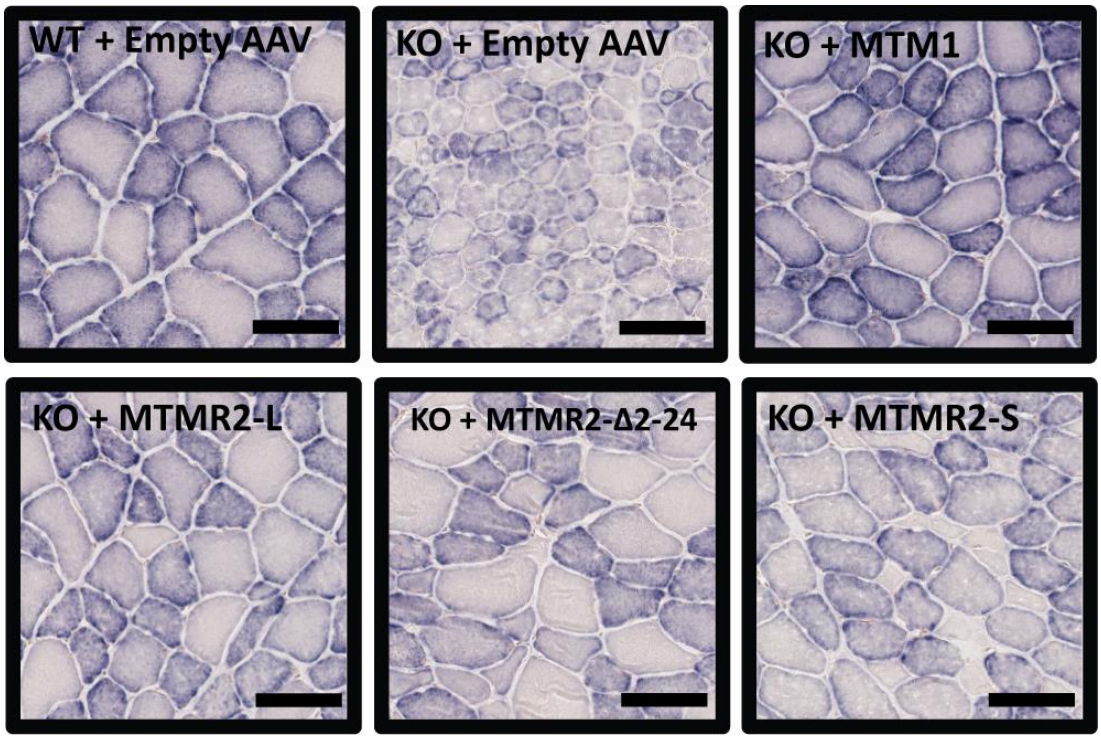

Figure 34: All MTMR2 constructs rescue the mitochondria organization in *Mtm1* KO mice. TA muscles from *Mtm1* KO mice were injected with AAV2/1 expressing myotubularins and analyzed 4 weeks later. Succinate dehydrogenase (SDH) staining of TA muscle sections. Scale bar 100 µm.

Finally, I did experiments to assess the protein localization of the overexpressed myotubularins in *Mtm1* KO myofibers (Figure 35). In contrast with localization experiments in cultured COS cells, immunofluorescence in mouse muscles was difficult to analyze. A good signal was obtained with polyclonal anti-MTM1 or our monoclonal anti-MTMR2 antibodies in some TA muscles samples overexpressing MTM1, MTMR2-S or MTMR2-L, compared to control muscles injected with empty AAV. However, most of the signal was not localized in the rescued fibers displaying a large fiber size. MTM1 and MTMR2-L signal was mostly at the plasma membrane and diffused in the cytoplasm. A pattern of aligned structures was observed for MTMR2-S but this could be an artefact due to the cutting of muscle sections, independent of MTMR2-S expression. **In conclusion, these localization experiments in injected TA muscles were not conclusive, even though they highlighted some protein overexpression inside the *Mtm1* KO myofibers upon AAV injection of MTM1, MTMR2-S or MTMR2-L construct.**

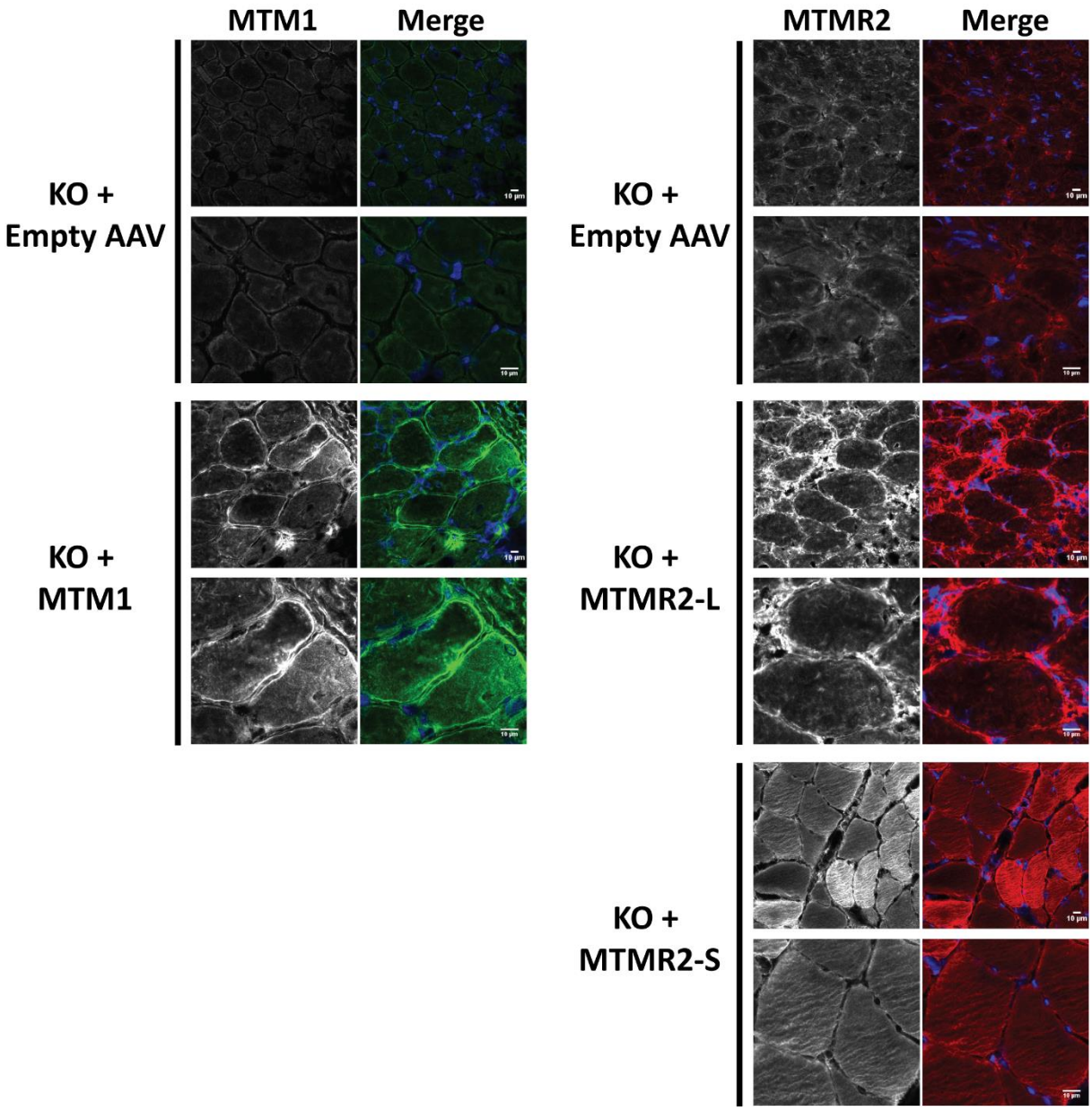

Figure 35: Localization in overexpressed myotubularins in Mtm1 KO muscles fibers. Detection of MTM1 (green) and both MTMR2 isoforms (red) by immunofluorescence on transverse sections of TA muscles from Mtm1 KO mice injected with empty AAV2/1 or AAV2/1 overexpressing the myotubularins. Nuclei stained with Hoechst appear in blue. For each construct, the lower montage is a zoom of the upper montage. Scale bar 10 µm.

E. MTMR2 isoforms rescue *Mtm1* KO muscle disorganization

In skeletal muscle, the excitation-contraction (EC) coupling machinery relates the muscle excitation to the calcium release from the sarcoplasmic reticulum. This system is formed by a highly specialized membrane structure, the triad that is formed by a central transverse (T)-tubule surrounded by two terminal cisternae from the sarcoplasmic reticulum (Figure 36A). T-tubule biogenesis and triad formation are complex and mostly unknown mechanisms, but have been linked to several proteins including MTM1 (Al-Qusairi and Laporte, 2011).

Indeed, patients with myotubular myopathy and the *Mtm1* KO mice display an intracellular disorganization of their muscle fibers at the ultrastructural level (Buj-Bello et al., 2002b; Spiro et al., 1966; Toussaint et al., 2011).

To determine the organization of the contractile apparatus and triads, the ultrastructure of the different injected TA muscles was assessed by electron microscopy (Figure 36B). As previously published, I observed Z-line and mitochondria misalignment, thinner sarcomeres and lack of well-organized triads in the *Mtm1* KO muscle injected with empty AAV (Figure 36B) (Amoasii et al., 2012). Expression of MTM1 and all MTMR2 isoforms improved these pathological phenotypes, with the observation of well-organized triads with two sarcoplasmic reticulum cisternae associated with a central transverse-tubule (T-tubule) in muscles injected with MTM1, MTMR2-L or MTMR2-S. Moreover, AAV-mediated expression of MTM1, MTMR2-L, MTMR2-Δ2-24 and MTMR2-S increased the number of triads per sarcomere back to almost WT levels, with a better effect for MTMR2-S compared to MTMR2-L (Figure 36C). MTMR2-Δ2-24 had again an intermediate phenotype between MTMR2 short and long isoforms.

Thus, similarly to MTM1, the overexpression of MTMR2 isoforms ameliorates the ultrastructure defects observed in Mtm1 KO muscle fibers. Furthermore, consistent with my previous results, the MTMR2-S isoform lacking the N-terminal extension displays better rescuing properties compared to the long MTMR2-L isoform.

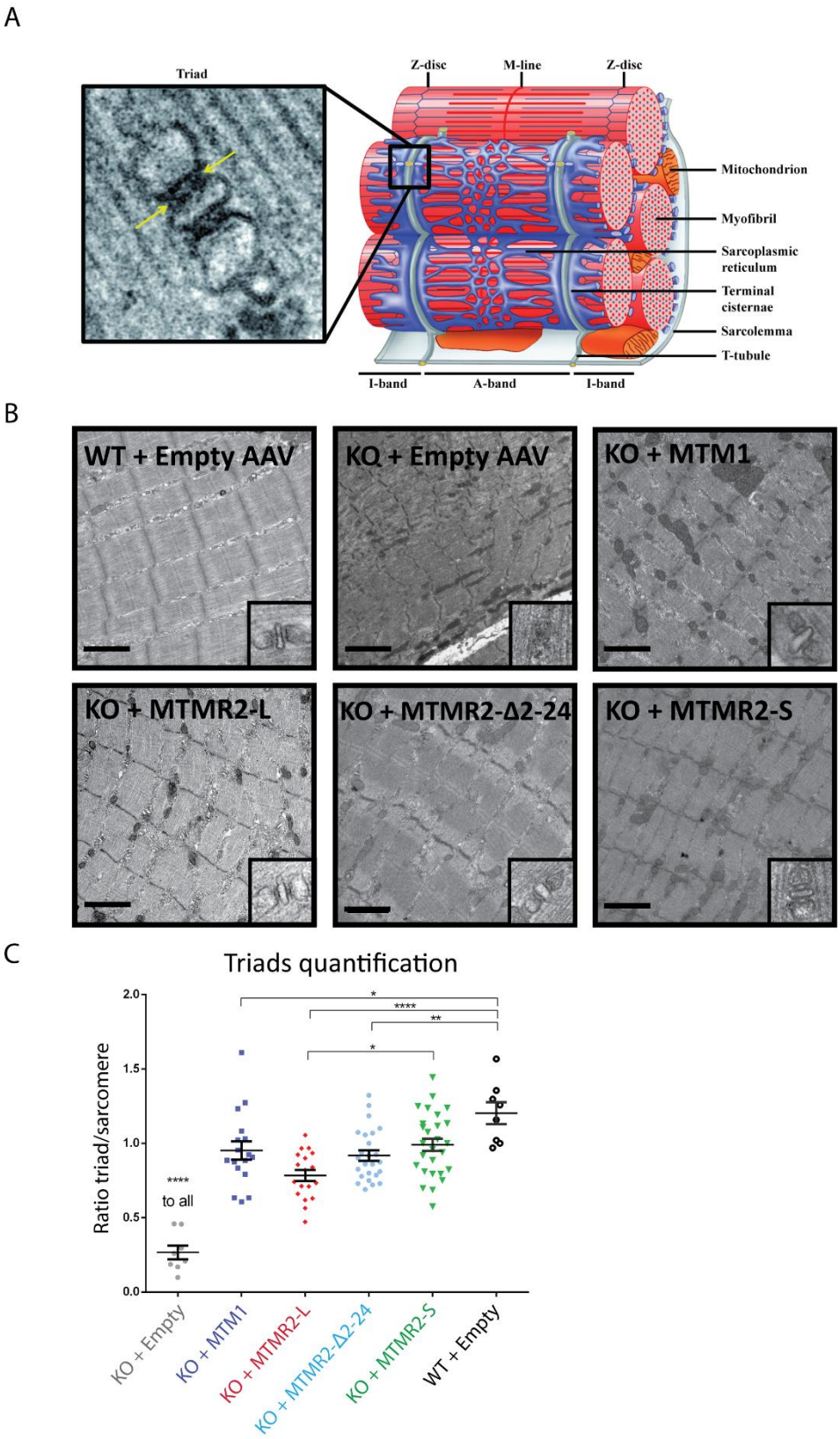

Figure 36: All MTMR2 isoforms ameliorate the muscle ultrastructure of *Mtm1* KO mice. (A) Triad organization in skeletal muscle. Adapted from Al Qusairi *et al.* 2011. **(B)** Electron microscopy pictures displaying sarcomere, mitochondria and triad organization or Mtm1 KO muscle fibers overexpressing myotubularins. Scale bar 1 µm. Representative triads are displayed in the zoom square. **(C)** Quantification of the number of well-organized triads per sarcomere. n>20 images for 2 mice each. All muscles expressing myotubularins quantify differently than the *Mtm1* KO. Data represent means ± s.e.m. **p*<0.05, **p<0.01, *****p*<0.0001 (ANOVA test).

F. Exploring the mechanistic of the rescue

To better understand how MTMR2 variants were able to rescue the XLCNM phenotypes of the *Mtm1* KO mice, I explored lipid and protein pathways known to be modified by MTM1 loss.

In yeast, only MTMR2-S but not MTMR2-L regulated the PtdIns3*P* myotubularin substrate level, as well as the one of PtdIns(3,5)P_2 as assessed by vacuolar morphology. To determine whether the rescuing capacity of MTMR2 in mice was linked to its enzymatic activity, I quantified the intracellular levels of PtdIns3*P* in the injected TA muscles of *Mtm1* KO mice (Figure 37A). PtdIns3*P* level was 2.3 fold higher in empty AAV injected *Mtm1* KO muscle than in WT muscle, reflecting the impact of the loss of MTM1 on its PtdIns3*P* lipid substrate. Upon expression of MTM1, the PtdIns3*P* level decreased to wild type levels, reflecting the *in vivo* phosphatase activity of MTM1. MTMR2-L, MTMR2-S and MTMR2-Δ2-24 induced a decrease in PtdIns3*P* level when expressed in the *Mtm1* KO mice, however only the short MTMR2-S isoform normalized PtdIns3*P* to wild type levels. **These results show that MTMR2 displays an *in vivo* enzymatic activity in muscle. Moreover, the MTMR2 catalytic activity correlates with the rescue observed in the muscle of *Mtm1* KO myopathic mice upon MTMR2 expression.**

Increased levels of DNM2 dynamin have been found in XLCNM patients and in *Mtm1* KO mice, and mutations in *DNM2* lead to the autosomal dominant form of centronuclear myopathy (Bitoun et al., 2005; Cowling et al., 2014). Moreover, the downregulation of *DNM2* expression by genetic cross (generating heterozygote mice for *DNM2*) or by antisense oligonucleotide-mediated knockdown also improved the muscular phenotypes and the survival of *Mtm1* KO mice (Cowling et al., 2014; Tasfaout et al., 2017). Based on this and other data, MTM1 and DNM2 are suspected to form with BIN1 amphiphysin the so-called M.A.D. pathway (Myotubularin Amphiphysin Dynamin) implicated in centronuclear myopathies. To determine if the rescuing capacity of human MTMR2 was linked to Dnm2 downregulation, I quantified Dnm2 protein levels in the injected TA muscles of *Mtm1* KO mice (Figure 37B). As expected, Dnm2 level was 2 fold higher in empty AAV injected *Mtm1* KO muscle than in WT muscle. All overexpressed myotubularins decreased Dnm2 level, to near WT level in some mice. The high heterogeneity in DNM quantification and the low

samples number did not allow to reach a statistical difference, but the tendency is clear for each myotubularin variant. **These results show that MTMR2, as MTM1, plays a role in the M.A.D. pathway and regulates DNM2 expression, allowing to compensate the MTM1-loss in the myopathy.**

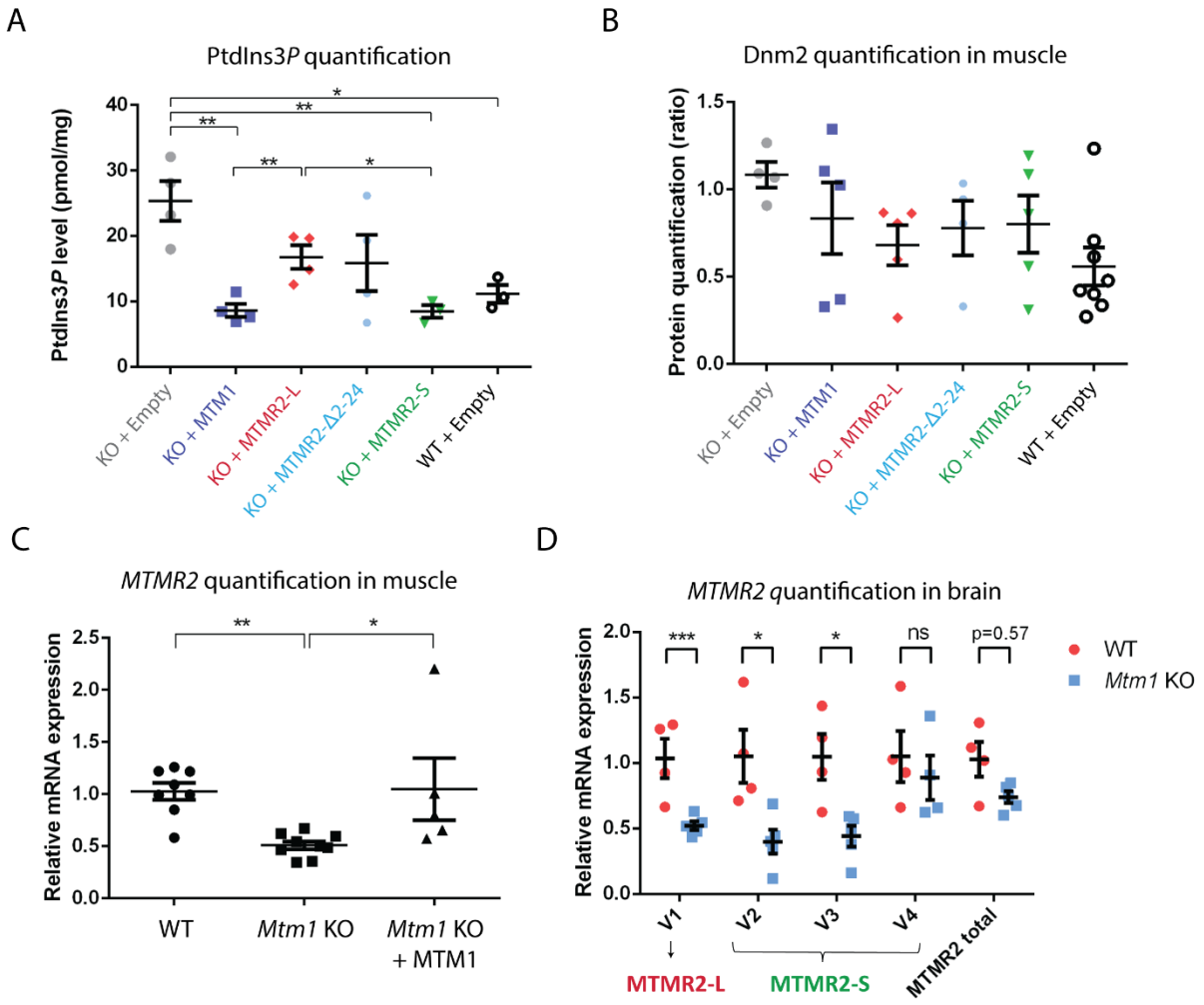

Figure 37: Mechanistic of *Mtm1* KO mouse muscle rescue by MTMR2. (A) Quantification of PtdIns3*P* level by competitive ELISA in TA muscles from *Mtm1* KO mice expressing different myotubularins and in WT muscles. n>3 mice. Data represent means ± s.e.m. **p*<0.05, ***p*<0.01 (ANOVA test). PtdIns3*P* levels in *Mtm1* KO muscles expressing the different myotubularins are not statistically different from the WT controls. **(B)** Quantification of mouse Dnm2 by western blot. Stain free was used for normalization. n>4. No statistical difference was detected by ANOVA test. **(C)** Quantification of total MTMR2 mRNA by RT-qPCR in WT muscles, Mtm1 KO muscles and Mtm1 KO muscles overexpressing human MTM1. n>4. *****p*<0.0001 (ANOVA test). **(D)** Quantification by RT-qPCR of MTMR2 isoforms (V1 to V4) in the brain of *Mtm1* KO mice compared to WT mice. n>3. Each isoform is presented as an independent ratio, with a value of 1 set for expression in WT mice. Data represent means ± s.d. ***p*<0.01, ****p*<0.001, a *P* value close to be significant is indicated, ns not significant (Student's t test).

I previously showed by RT-qPCR that total MTMR2 level was reduced by half in Mtm1 KO mouse muscles compared to WT muscles (Figure 26D). To better understand the link between MTM1 and MTMR2, I analyzed the effect on MTMR2 level of MTM1 overexpression by intramuscular injection of AAVs in Mtm1 KO mice. Interestingly, reintroduction of MTM1 induced an increase of *MTMR2* level back to normal level (Figure 37C). It would also be interesting to quantify MTMR2 mRNA variants (V1 to V4) levels under MTM1 overexpression in Mtm1 KO mice, to see if the upregulation is the same for all variants. To assess if MTMR2 upregulation was the same in other *Mtm1* KO tissues, I quantified its expression in brain where it is the most expressed (Figure 37D). As in muscles, MTMR2 total level was reduced almost by half, mainly caused by the downregulation of V2 and V3 mRNA variants responsible for translation of the short MTMR2-S protein isoform. However, in contrast with muscles, the V1 mRNA variant leading to MTMR2-L was also highly reduced, suggesting a different regulation of MTMR2 expression in brain compared to muscles. **Altogether, this confirms the genetic link between MTM1 and MTMR2.**

In conclusion, intramuscular injections of AAVs overexpressing MTMR2 long and short isoforms or the artificial MTMR2-Δ2-24 were able to rescue or ameliorate all hallmarks of the MTM1-linked myopathy: muscle mass and force, fiber size, nuclei positioning and muscle ultrastructure. For almost all parameters, MTMTR2-S performed better than MTMR2-L and similarly as MTM1. The artificial MTMR2-Δ2-24 seems to induce intermediary phenotypes. This highlights the importance of the N-terminal extension of MTMR2 for the regulation of MTMR2 *in vivo* functions and for the functional differences between MTM1 and MTMR2-L. **And more importantly, this shows that MTMR2 is able to compensate for the loss of MTM1 in the myopathy, suggesting novel therapeutic perspectives.** Finally, the rescuing properties of MTMR2 seem to implicate the PPIns and Dnm2 pathways that are affected in myopathic *Mtm1* KO mice.

	Mtm1 KO + empty AAV	*Mtm1* KO + MTM1	*Mtm1* KO + MTMR2-L	*Mtm1* KO + Δ2-24	*Mtm1* KO + MTMR2-S	WT + empty AAV
Muscle weight	-	++	-	-	++	++++
Muscle force	-	+++	+	++	+++	++++
Fiber size	-	+++	+	++	++	++++
Nuclei positioning	-	++	++	++	++	++++
Number of well-organized triads/sarcomere	-	+++	++	+++	+++	++++
PtdIns*3P* level	-	++++	++	++	++++	++++
Dnm2 level	-	++	++	++	++	++++

Table 2 : Rescuing effects of MTM1 and MTMR2 isoforms on several hallmarks of myotubular myopathy. "+,++,+++,++++": increasing rescuing ability of myotubularins, ranging from "-": no rescue to "++++": WT phenotype

VI. Both MTMR2 isoforms are able to improve the *Mtm1* KO mouse phenotypes

Intramuscular injections allowed to investigate the muscle-specific functions and rescuing capacities of MTM1 and MTMR2 in the *Mtm1* KO mouse model. **To complete this study and observe the effect of MTMR2 expression on the overall mouse, I performed systemic injections.** Here I present only a preliminary study with few mice per construct. The MTMR2-Δ2-24 truncated form was not tested this time, to only focus on endogenous MTMR2-L and MTMR2-S isoforms.

Mouse number	Genotype	AAV2/9 vector	Sacrificed at week	Dead at week
1	*Mtm1* KO	Empty	7	
2			7	
3	*Mtm1* KO	MTM1	7	
4			7	
5			7	
6			7	
7			7	
8	*Mtm1* KO	MTMR2-L	10	
9				8
10				8
11			9	
12			7	
13	*Mtm1* KO	MTMR2-S	10	
14				7
15			7	
16			7	
17	WT	Empty	7	
18			7	
19			7	
20			7	
21	WT	MTM1	7	
22			7	
23			7	
24			7	
25			7	
26			7	
27	WT	MTMR2-L	10	
28			10	
29			10	
30			9	
31			7	
32			7	
33	WT	MTMR2-S	10	
34			10	
35			10	
36			10	
37			9	
38			7	
39			7	
40			7	

Table 1: List of systemic injections. List of Mtm1 KO and WT mice systemically injected by empty AAV2/9 or AAV2/9 overexpressing MTM1, MTMR2-L or MTMR2-S. The week of sacrifice or natural death is indicated.

Wild type or *Mtm1* KO pups were intraperitoneally injected at birth or at Day 1 by $1.5x10^{12}$ units of empty AAV2/9 viral particles or AAV2/9 overexpressing human MTM1, MTMR2-L or MTMR2-S. The AAV2/9 serotype is supposed to transduce almost all organs by systemic injections. Then 3 weeks after injection I started to analyze weekly the body weight and the mice skeletal muscle strength by two different tests: the grip test and the hanging test. Initially, I was optimistic and planned to sacrifice the mice at 12 weeks of age to

compare MTM1 and MTMR2 rescuing capacities. However, around 7-8 weeks, 2 mice injected with MTMR2-L and 1 mouse injected with MTMR2-S died (Table 3). I then decided to sacrifice them before 12 weeks. For the last injections, I sacrificed the mice at 7 weeks when Mtm1 KO affected mice injected with empty AAV were still alive, allowing to compare the myotubularin overexpression to the empty vector.

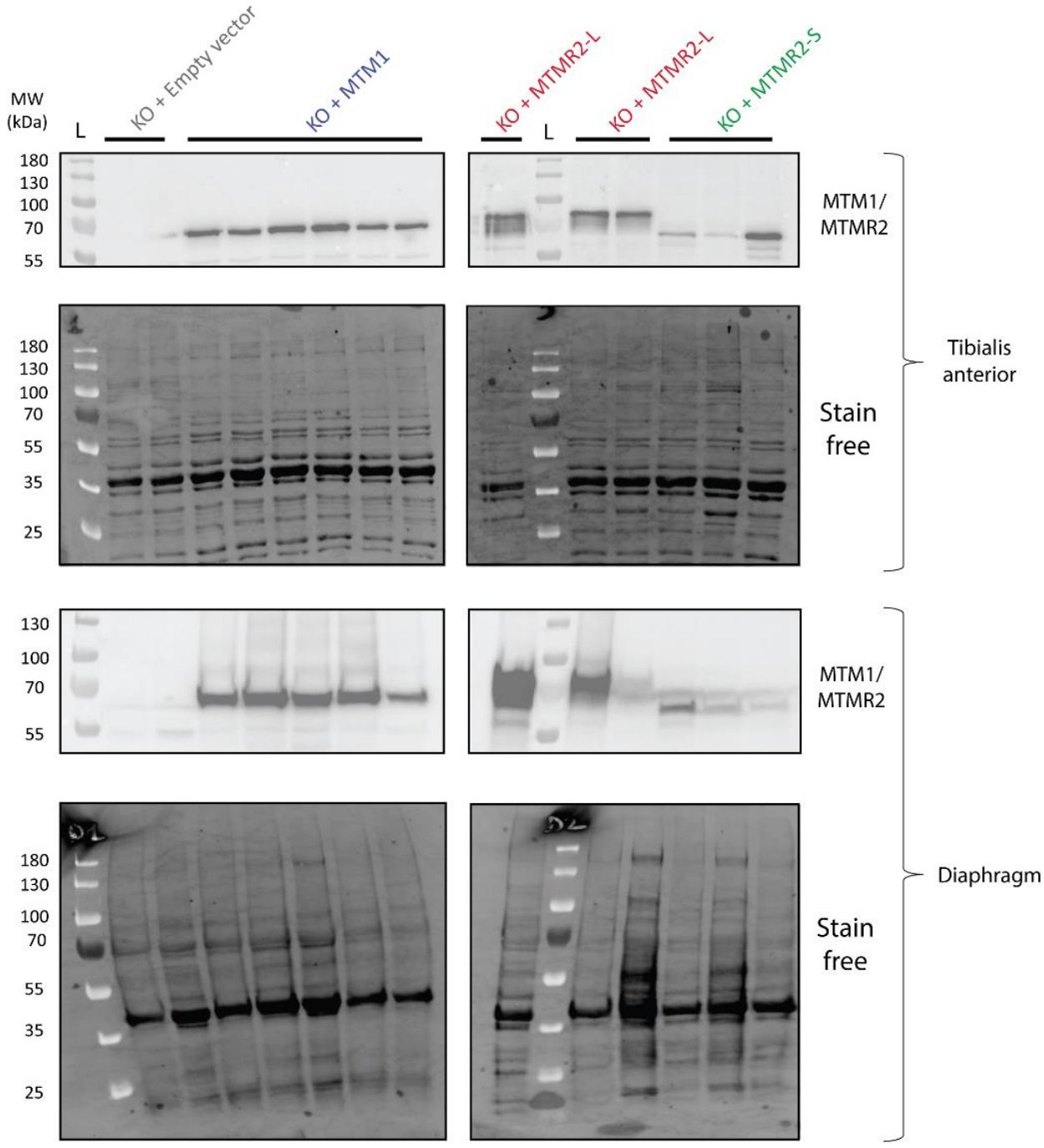

Figure 38: Detection of overexpressed myotubularins after systemic injections in mice. Detection of exogenously expressed human myotubularins in *Mtm1* KO TA and Diaphragms by western blot using anti-MTM1 or anti-MTMR2 antibodies. The Stain free membranes are used as a loading control. L = Ladder.

Overexpression of MTM1 and MTMR2 isoforms were assessed by western blot on tibialis anterior and diaphragm skeletal muscles (Figure 38). In both cases, myotubularins were well detected at the expected size, and additional lower bands were observed for MTMR2-L, as already seen for intramuscular injections. However, this time additional lower bands were surprisingly also observed for MTMR2-S, while it was never the case for intramuscular injections (n=13). This suggests either a curious differential regulation of the potential protein cleavage depending on the AAV serotype (AAV2/1 vs 2/9), or that the protein modification was very weak for MTMR2-S by intramuscular injections. **This confirmed that all myotubularins were well expressed in skeletal muscles after systemic delivery of AAV at day 1 postnatally in mice.**

A. Overexpression of both MTMR2 isoforms ameliorates the lifespan and body weight of Mtm1 KO mice

I started by analyzing the effect of systemic expression of the myotubularins on the lifespan and the body weight of the injected mice. The first major observation was that both MTMR2-L and MTMR2-S increased the lifespan of Mtm1 KO mice (Table 3). While the myopathic mice usually die around 5-7 weeks of age, the MTMR2 isoforms allowed two mice to reach 10 weeks-old (and potentially older, since at this point I sacrificed the mice for further analysis). MTM1 was already published to have a similar rescuing effect on the lifespan (Buj-Bello et al., 2008).

Major clinical phenotypes of myopathic *Mtm1* KO mice are the lower body weight since 2 to 3 weeks of age compared to WT mice, and the progressing loss of weight starting around 5 weeks of age (Buj-Bello et al., 2002b; Cowling et al., 2014). The latter is mainly due to a loss of muscle mass and in the final steps of the disease to difficulties to reach their food. In contrast, WT mice continue to progressively gain weight during the first 10-12 weeks of their life (Figure 39A). Mice overexpressing human MTM1 are initially bigger than *Mtm1* KO mice injected with empty AAV, and perfectly gain body weight at the same rate than WT mice. In comparison, mice overexpressing MTMR2-L and MTMR2-S also show a good rescue of the body weight from 3 weeks to 5 weeks old, but then start to lose weight and reach

the *Mtm1* KO level (Figure 39A). In correlation, the positive effects of MTMR2 expression were clinically clear (but not quantified) until 5 weeks of age, then the mice started to progressively gain the *Mtm1* KO typical phenotypes (loss of muscle weight and force, scoliosis, difficulties to breath and to walk).

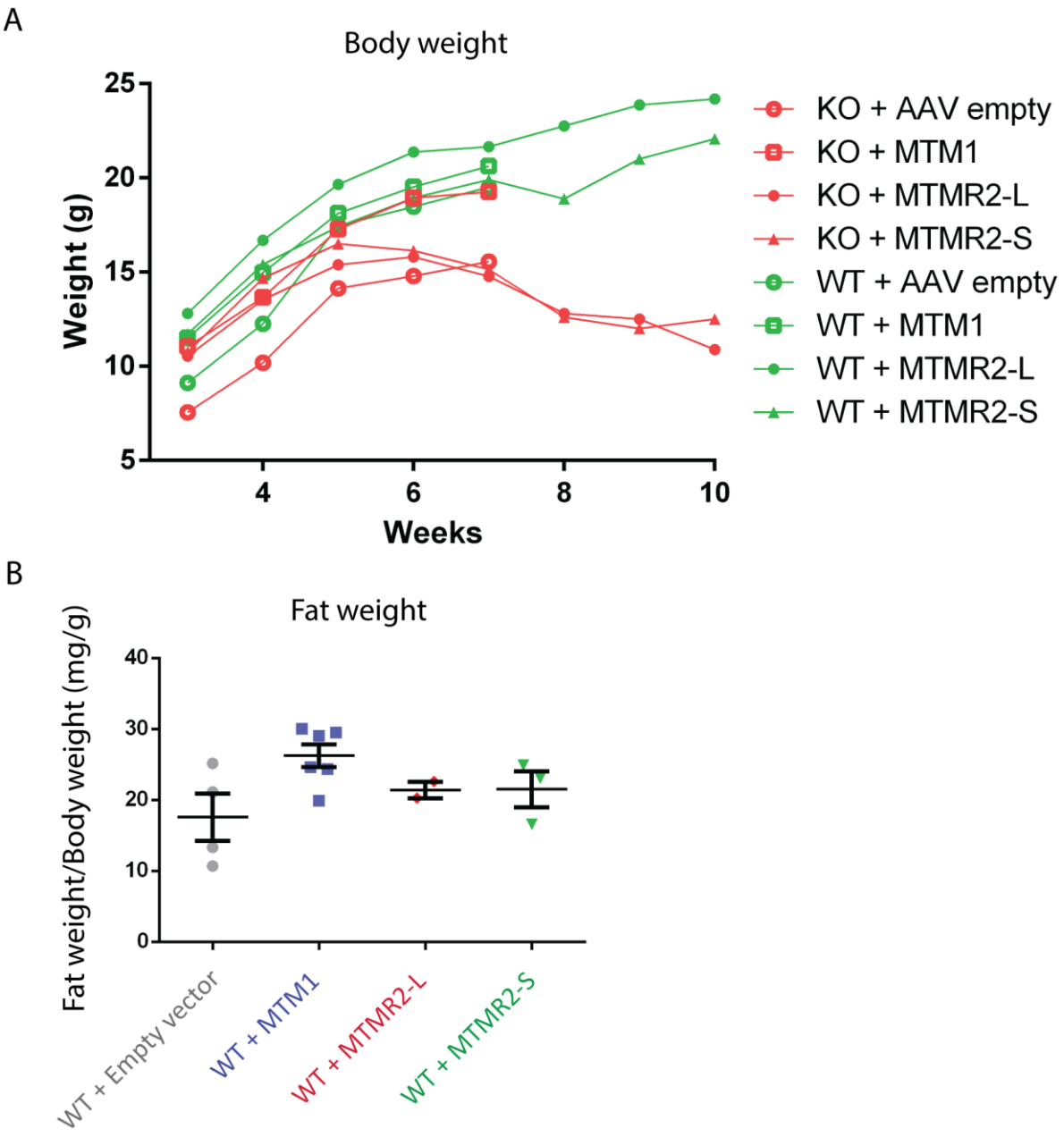

Figure 39: MTMR2 isoforms rescue the body weight of myopathic mice. (A) Measure of the body weight from 3 weeks to maximum 10 weeks of age of Mtm1 KO or WT mice overexpressing the different myotubularins. **(B)** Measure of the fat weight divided by the body weight for WT mice overexpressing the different myotubularins.

Overexpression of the myotubularin constructs in the WT mice seemed to increase the body weight compared to empty vector. I thus dissected and weighted their abdominal fat, and showed that WT mice overexpressing MTM1 had more fat than control WT mice (Figure 39B). This was not observed (or slightly) for mice overexpressing MTMR2 isoforms. A link can be made with MTMR9 that was associated with obesity (Hotta et al., 2011).

These results show that MTMR2 long and short isoform similarly improved the lifespan and body weight of *Mtm1* KO mice. However, this effect was temporary and lower than the rescue observed with MTM1 overexpression.

B. Overexpression of both MTMR2 isoforms rescues the muscle strength of Mtm1 KO mice

The other obvious clinical feature of myotubular myopathy is the severe muscle weakness that is reproduced in the *Mtm1* KO mouse model. The grip test showed that systemic expression of MTMR2-L and MTMR2-S increased similarly the muscle strength with an effect comparable to MTM1 and to WT mice (Figure 40A). The effect was even more impressive with the hanging test: **overexpression of MTMR2 isoforms allowed the Mtm1 KO mice to progressively hang longer and longer (starting at 30-40 seconds), until they reach the WT level and were able after 7 weeks to hang for 3 x 60 seconds (Figure 40B).** At the same age, half of the Mtm1 KO mice are usually dead, and the two mice that I tested were not able to hang more than few seconds after 5 weeks. MTM1 effect was even better and allowed the Mtm1 KO mice to perfectly hang for 60 seconds after 4 weeks. No negative effect was observed for any myotubularin on WT mice that were always able to hang for 60 seconds.

These results showed that MTMR2 isoforms similarly rescued the muscle strength of *Mtm1* KO mice. Notably these mice injected with MTMR2 isoforms that were sick in appearance (difficulties to breath, scoliosis) could hang for 60 seconds as well as WT mice.

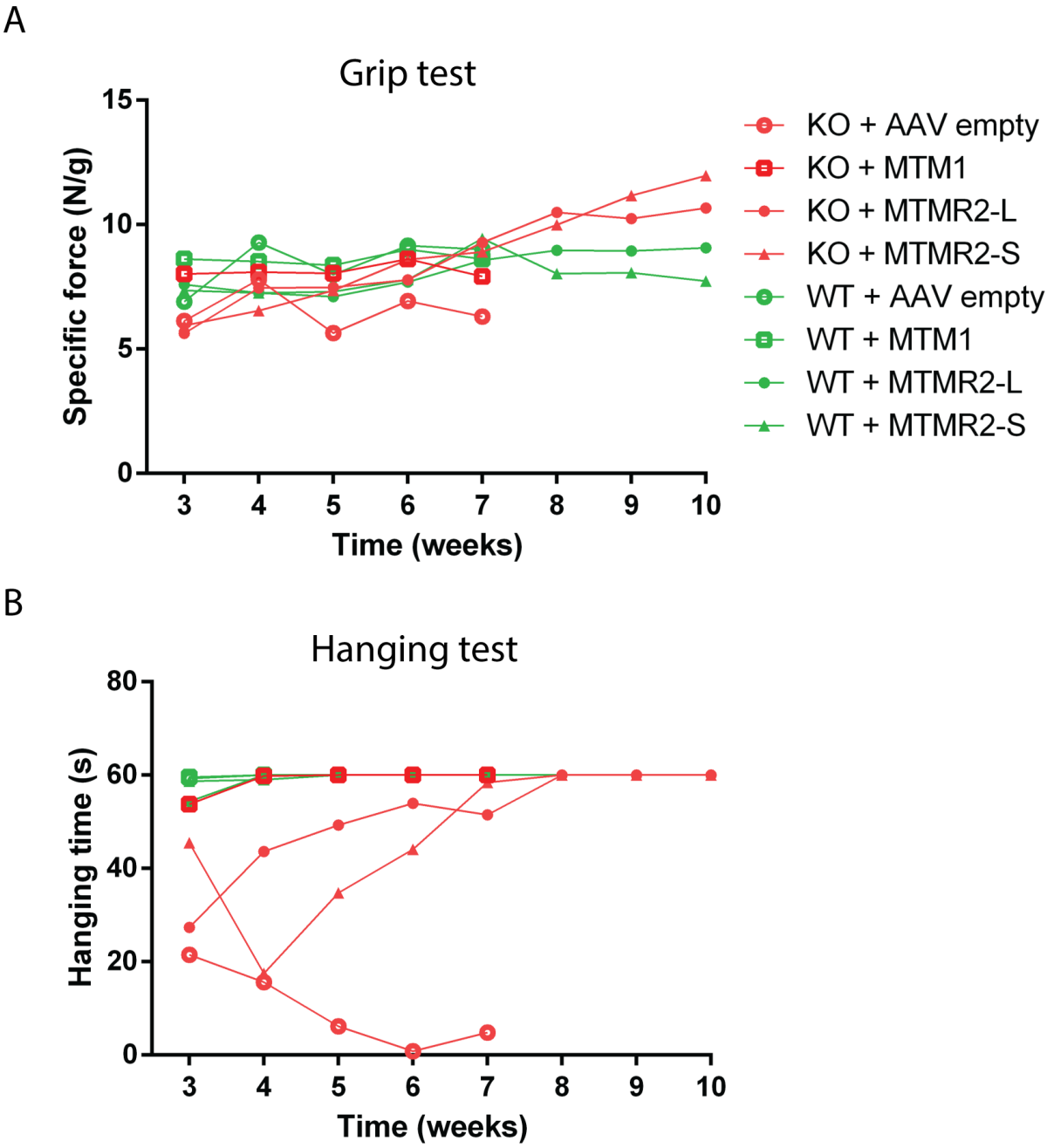

Figure 40: MTMR2 isoforms rescue the muscle force of *Mtm1* KO mice. The muscle strength of *Mtm1* KO or WT mice overexpressing the different myotubularins was assessed by grip test **(A)** or hanging test **(B)** each week from 3 to 10 weeks of age. The color and symbol coding is the same for both figures.

C. Overexpression of both MTMR2 isoforms rescues the histopathology of *Mtm1* KO limb muscles

Mice systemically overexpressing MTMR2 isoforms have improved lifespan, body weight and strong rescue of limb muscle force. However, these mice still died while MTM1 expression rescues completely the lifespan (Buj-Bello et al., 2008). This suggests that the rescue of the muscle weakness observed for limb muscles was maybe not present in other muscles or potentially affected organs.

To explore this hypothesis, I dissected the brain, lungs, heart, liver, diaphragm, testis, TA, gastrocnemius and sciatic nerves of injected mice, and gave the organs to the histology platform of the IGBMC. They are currently cutting and H&E staining them, and analyzing their histological features.

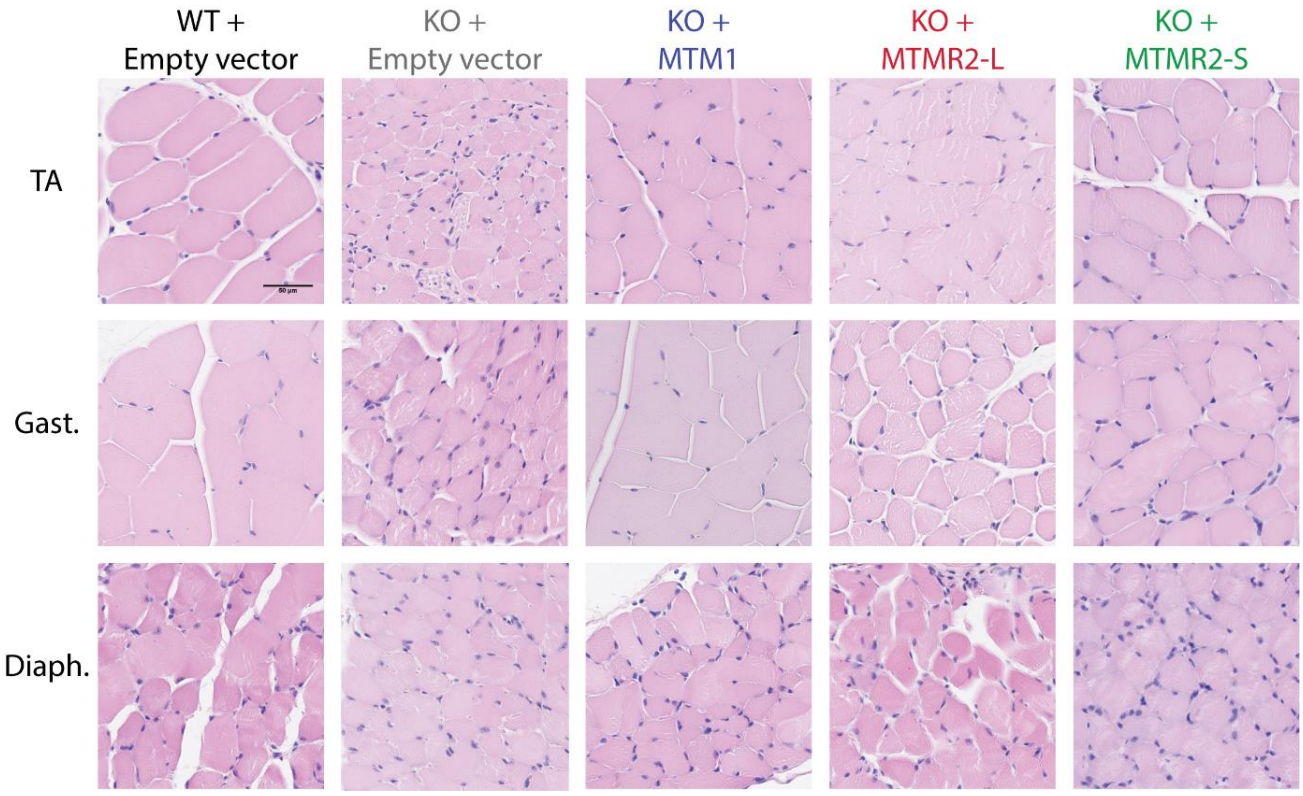

Figure 41: MTMR2 isoforms rescue the histology of limb muscles. Hematoxylin & Eosin (H&E) staining of tibialis anterior (TA), Gastrocnemius (Gast.) and Diaphragm (Diaph.) transverse sections from *Mtm1* KO mice overexpressing the different myotubularins, compared to *Mtm1* KO and WT mice injected with empty AAVs. Scale bar 50 µm.

They already analyzed the TA, gastrocnemius and diaphragm of injected *Mtm1* KO mice. H&E staining showed that all myotubularin constructs improve the muscle histology of Mtm1 KO TA and gastrocnemius, with bigger fibers and well positioned nuclei compared to empty vector (Figure 41). Interestingly, the results were less clear in diaphragm, suggesting that MTMR2-L and MTMR2-S could have a lower effect than MTM1 in this organ. A lack of muscle strength in diaphragm and other respiratory muscles (such as intercostal muscles) could explain why mice overexpressing MTMR2 isoforms have a low life expectancy compared to MTM1. The analysis of the other organs will provide further information about the rescuing capacities of MTMR2.

In conclusion, both MTMR2 isoforms allowed to delay the myopathic phenotype onset in *Mtm1* KO mice and significantly rescued their muscle force, at least in the limbs. In contrast to intramuscular injections, MTMR2-S effect was lower than MTM1 effect, and similar to MTMR2-L. Mice overexpressing MTMR2 isoforms were still affected but clearly more mobile than Mtm1 KO mice. A video analysis at each stage highlighted the differences in the ability of the mice to walk and move (data not shown).

Altogether, this systemic study shows exciting preliminary data, and warrants further investigation. A future complete study will be necessary to improve the significance of the results and better understand the functional specificities of MTM1, MTMR2-L and MTMR2-S in the full organism.

Part Three - Discussion and Perspectives (in French)

Etape par étape, depuis l'utilisation du simple (mais efficace) modèle de la levure jusqu'à l'analyse complexe de la souris et des patients, en passant par des études *in silico* et des cultures cellulaires, j'ai cherché à comprendre les spécificités moléculaires et les redondances de MTM1 et MTMR2. Bien que ces deux protéines appartiennent à la même famille des myotubularines, les mutations dans les gènes *MTM1* et *MTMR2* entraînent deux maladies différentes, respectivement une myopathie et une neuropathie, affectant des tissus différents.

En surexprimant ces myotubularines humaines dans les cellules de levure, les cellules de mammifère et dans le muscle squelettique de souris myopathiques *Mtm1* KO, j'ai caractérisé deux isoformes protéiques de MTMR2, nommés MTMR2-L (long) et MTMR2-S (short, court). Ces deux isoformes présentent des activités catalytiques différentes, liées à leur capacité respective d'accéder à leurs substrats lipidiques, les PPIn. De plus, j'ai démontré que la surexpression de MTMR2 permettait de sauver la myopathie causée par la perte de MTM1, et qu'en comparaison avec MTMR2-L, l'isoforme court MTMR2-S présentait une plus grande activité phosphatase dans les levures et les souris, en accord avec une meilleure correction des phénotypes des levures *ymr1Δ* et des souris *Mtm1* KO.

I. Les isoformes de MTMR2 et l'extension N-terminale

Il existe chez l'Homme et la souris quatre variants d'ARNm naturels pour MTMR2, encodant deux isoformes protéiques (MTMR2-L et –S), qui diffèrent par une extension N-terminale de 72 acides aminés. Mes travaux montrent que l'isoforme court MTMR2-S, ne contenant pas cette séquence N-terminale, est concentré dans les membranes lorsqu'il est surexprimé dans la levure (Figure 20) et présente une plus grande activité vis-à-vis de ses substrats lipidiques dans la levure (Figure 21) et dans les muscles de souris (Figure 37A), comparé à MTMR2-L.

Le site de phosphorylation S58 et l'extension N-terminale de MTMR2

Il a été montré que la phosphorylation de la serine 58, au sein de l'extension N-terminale, était importante pour la localisation de MTMR2 aux membranes des endosomes,

ainsi que pour sa fonction catalytique. En effet, dans les cellules mammifères, le mutant non-phosphorylable MTMR2-S58A était localisé au niveau de structures membranaires et était actif vis-à-vis du PtdIns3*P*, contrairement au mutant phosphomimétique MTMR2-S58E (Franklin et al., 2013; Franklin et al., 2011). J'ai confirmé cette différence dans la levure, en montrant que le mutant phosphomimétique MTMR2-S58D était localisé dans le cytoplasme et montrait une activité phosphatase plus faible que le mutant non-phosphorylable MTMR2-S58A présent aux membranes (Figures 20 et 21). Etonnamment, MTMR2-S58E (qui est censé être phosphomimétique) présentait la même localisation et activité que MTMR2-S58A. Cela suggère que les deux mutants phosphomimétiques MTMR2-S58E et -S58D adoptent dans la levure des conformations différentes, ou ont des interactions différentes, et que seul le mutant MTMR2-S58D permet d'imiter correctement la phosphorylation.

Ainsi, les résultats sur les formes tronquées et les mutants de phosphorylation de MTMR2 sont complémentaires et reflètent la même régulation protéique. Il existe deux formes de MTMR2, MTMR2-S qui est principalement localisé aux membranes et présente une forte activité phosphatase *in vivo*, et MTMR2-L dont la localisation membranaire dépend de sa phosphorylation sur le résidu S58. Ce site de phosphorylation S58 est donc une différence majeure entre MTMR2-L et –S, et la régulation de sa phosphorylation par la kinase humaine Erk2 pourrait expliquer les différences fonctionnelles observées entre ces deux isoformes. De plus, MTMR2-L se comporte dans la levure comme un phosphomimétique, suggérant que le S58 est principalement phosphorylé, et donc que la kinase de levure Mpk1 (homologue de Erk2) est capable de réguler la version humaine de MTMR2-L. Cela pourrait également signifier que MTMR2-L adopte dans la levure la même conformation que MTMR2-S58E dans les cellules humaines. De façon intéressante, dans le cerveau humain c'est majoritairement le transcrit MTMR2 V1 (codant pour MTMR2-L) qui est exprimé (Figure 27). De plus, l'expression de la kinase Erk2 est plus forte dans le cerveau que dans les autres tissus, et est donc corrélée avec l'expression de MTMR2-L (base de données GTEx).

Hypothèse pour la fonction et la régulation de l'extension N-terminale de MTMR2

L'extension N-terminale de MTMR2 n'a à ce jour pas pu être résolue dans la structure cristallographique de la protéine. On peut donc supposer que cette extension peut adopter différentes conformations, et pourrait ainsi réguler les fonctions de MTMR2 (Begley et al., 2006; Begley et al., 2003). Une hypothèse intéressante serait que la phosphorylation de la sérine 58 mette en place (ou révèle par changement de conformation) un site de liaison pour une ancre cytosolique, c'est-à-dire une protéine qui retiendrait MTMR2-L dans le cytoplasme (Figure 42). Lorsque S58 est déphosphorylé, le site de liaison disparaîtrait ou serait masqué par l'extension N-terminale, permettant à MTMR2-L de se détacher de l'ancre et d'atteindre ses substrats lipidiques au niveau des membranes. MTMR2-S ne possède pas l'extension N-terminale et la sérine 58, et donc ne serait pas retenu dans le cytoplasme.

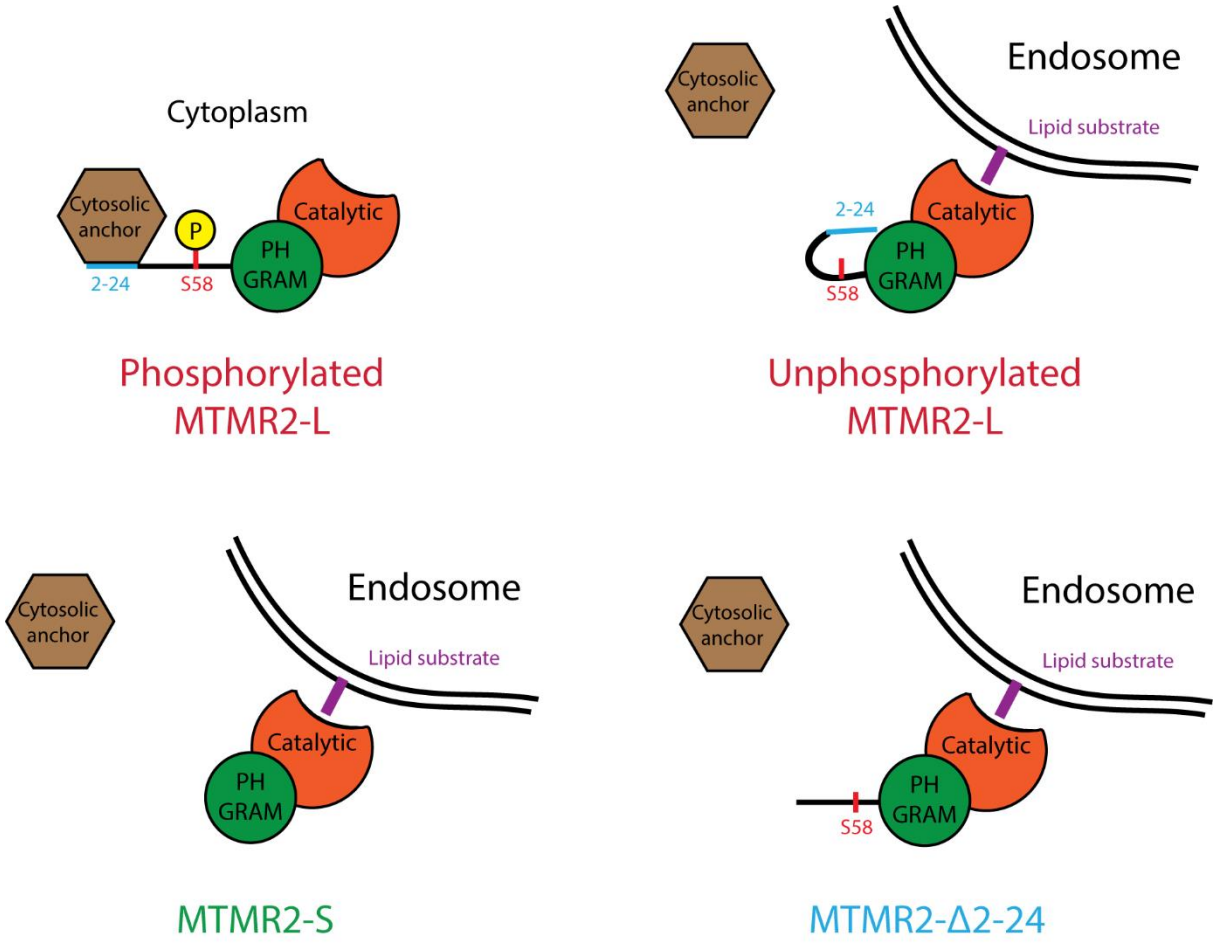

Figure 42: L'extension N-terminale de MTMR2 régule la localisation et l'activité de la protéine. Régulation hypothétique de la localisation de MTMR2 via son interaction avec une ancre cytosolique. L'ancre se lie à la séquence 2-24 de MTMR2-L lorsque le S58 est phosphorylé. Lorsque le S58 n'est pas phosphorylé, l'extension N-terminale adopte une conformation qui empêche toute interaction avec l'ancre cytosolique, permettant à MTMR2 d'atteindre les membranes endosomales et de déphosphoryler ses substrats lipidiques. MTMR2-S et MTMR2-Δ2-24 ne possèdent pas la séquence 2-24 et ne peuvent donc pas se lier à l'ancre cytosolique.

Cette hypothèse peut être complétée par l'analyse des résultats obtenus pour MTMR2-Δ2-24. En effet, cette construction est dépourvue des 24 premiers acides aminés de MTMR2-L, mais possède toujours le site de phosphorylation S58, et pourrait donc être régulé de la même façon que MTMR2-L. Cependant, MTMR2-Δ2-24 présente dans la levure une localisation membranaire et une activité phosphatase similaire à MTMR2-S, suggérant que la séquence 2-24 de MTMR2-L serait le site de fixation de l'hypothétique ancre cytosolique. La phosphorylation du S58 régulerait alors la conformation de l'extension N-terminale, et masquerait (forme non phosphorylée, localisation membranaire) ou révèlerait (forme phosphorylée, localisation cytoplasmique) la séquence 2-24 (Figure 42). Les constructions MTMR2-S et MTMR2-Δ2-24 ne possèdent pas cette séquence 2-24 et ne pourraient donc pas se lier à l'ancre cytosolique. L'analyse de l'interactome différentiel effectué sur les constructions de MTMR2 exprimées dans des cellules COS pourrait permettre d'identifier cette ancre cytosolique.

Une autre hypothèse pourrait également expliquer les résultats obtenus pour MTMR2-Δ2-24 : la phosphorylation du résidu S58 pourrait être régulée par le site de phosphorylation S6, de la même façon que la phosphorylation du résidu S631 dépend de la phosphorylation S58 (Franklin et al., 2013). Dans cette hypothèse, si le S6 n'est pas phosphorylé, ou s'il est manquant comme pour MTMR2-Δ2-24, alors le S58 ne pourrait pas non plus être phosphorylé, permettant une liaison à la membrane via le PH-GRAM. Dans la situation contraire, la phosphorylation du S6 permet celle du S58, induisant un changement de conformation qui empêche la liaison du PH-GRAM aux membranes. L'analyse par spectrométrie de masse semble aller dans le sens de cette hypothèse, puisque la phosphorylation du S58 n'a pas été détectée pour MTMR2-Δ2-24 (ne contenant pas le résidu S6) surexprimé dans les cellules COS, alors qu'elle a été détectée pour MTMR2-L.

Perspectives pour l'étude de l'extension N-terminale de MTMR2-L

Plusieurs points restent non élucidés concernant l'extension N-terminale de MTMR2. MTMR2-Δ2-24 présentait une localisation et activité similaires à MTMR2-S dans la levure. Cependant, une fois surexprimée dans les muscles de souris myopathiques *Mtm1* KO, MTMR2-Δ2-24 avait une activité plus faible que MTMR2-S (et plus forte que MTMR2-L) et corrigeait moins bien la myopathie que MTMR2-S (et mieux que MTMR2-L). Cette

différence mériterait d'être étudiée. Je n'ai pas non plus analysé l'impact de la phosphorylation du site S631 sur la fonction des constructions de MTMR2. En effet, Franklin *et al.* Ont montré que la phosphorylation du résidu S631 avait un impact sur la localisation de MTMR2-L (entre endosomes précoces et tardifs) uniquement si le résidu S58 n'était pas phosphorylé (Franklin et al., 2013). MTMR2-S ne possède pas le site S58 et se comporte comme le mutant non phosphorylé MTMR2-S58A, donc le site de phosphorylation S631 pourrait avoir un impact sur sa localisation et sa fonction. Ainsi, la régulation de la localisation membranaire de MTMR2-L semble très complexe, et des études plus approfondies (utilisant par exemple l'expression de double/triple mutants de phosphorylation de MTMR2 dans des cellules COS) seront nécessaires afin de mieux comprendre la régulation de l'extension N-terminale, et de façon plus générale la régulation de MTMR2.

Il serait également intéressant d'analyser l'impact de l'expression des mutants de phosphorylation S58 dans des souris *Mtm1* KO, et de comparer leur capacité à corriger les phénotypes myopathiques avec les autres constructions de MTMR2. Enfin, il serait très utile de produire un anticorps monoclonal reconnaissant spécifiquement l'extension N-terminale de MTMR2-L. Cet anticorps pourrait alors être utilisé pour détecter spécifiquement MTMR2-L par western blot ou immunofluorescence. On pourrait par exemple déterminer si la seconde bande détectée en western blot pour MTMR2-L est en effet due à un clivage de l'extension N-terminale. De façon plus générale, cet anticorps pourrait aider à étudier les spécificités de MTMR2-L et MTMR2-S et leur abondance dans différents tissus.

II. Les spécificités de MTM1 et MTMR2

Cette étude révèle que l'extension N-terminale en amont du domaine PH-GRAM constitue la base moléculaire de la différence fonctionnelle entre MTM1 et MTMR2. MTMR2-S ne possède pas cette extension et présent des fonctions *in vivo* similaires à MTM1 dans les levures et les souris. La suppression de cette extension N-terminale dans l'isoforme natif MTMR2-L convertit alors l'activité de MTMR2 en une activité similaire à MTM1.

Ces différences de fonction peuvent encore une fois être associées à des différences de localisation : contrairement à MTMR2-L et similairement à MTMR2-S, MTM1 est associé aux membranes et peut accéder à ses substrats lipidiques. De plus, MTM1 ne possède ni la

séquence 2-24 de MTMR2-L, ni le site de phosphorylation équivalent au S58 (Figure 15B). Ainsi, MTM1 ne serait pas retenu dans le cytoplasme par une hypothétique ancre cytosolique qui se lierait à l'extension N-terminale de MTMR2-L. La localisation membranaire de MTM1 (et potentiellement de MTMR2-S) pourrait également induire des interactions avec des protéines membranaires, lui conférant des fonctions cellulaires supplémentaires par rapport à MTMR2-L.

Les spécificités fonctionnelles entre MTM1 et MTMR2 pourraient également être expliquées par des changements d'acides aminés dans les domaines PH-GRAM, coil-coiled ou PDZ qui sont moins bien conservés que le domaine catalytique entre les deux protéines (Figure 15A), et qui permettent d'interagir avec des membranes ou des protéines. Par exemple, certaines protéines interagissant avec MTM1 ne pourraient pas interagir avec MTMR2 parce que le site de liaison a été perdu au cours de l'évolution. Encore une fois, ces interacteurs pourraient conférer une localisation ou fonction spécifique à MTM1 ou MTMR2. Cette question pourrait être examinée en clonant et en échangeant chacun de ces domaines entre les deux protéines, par exemple en échangeant les domaines PH-GRAM de MTMR2-L et MTM1. Si la construction PH-GRAM^{MTM1}-MTMR2-L se comporte comme MTM1, cela voudra dire que le PH-GRAM est fortement impliqué dans les différences entre MTM1 et MTMR2.

L'analyse de l'interactome différentiel entre MTM1 et MTMR2 pourrait également expliquer pourquoi ces protéines sont impliquées dans deux maladies neuromusculaires différentes, affectant deux tissus différents. En effet, MTM1 interagit avec la desmine et MTMR2 avec la chaine légère des neurofilaments (NFL), deux protéines de filaments intermédiaires qui sont également tissu-spécifiques et présentes respectivement dans les muscles et les neurones (Hnia et al., 2011; Previtali et al., 2003). Cela concorde avec les mutations dans les gènes *MTM1* et *desmine* qui sont liées à des myopathies, et les mutations dans les gènes *MTMR2* et *NFL* qui sont liées à des neuropathies (Goldfarb et al., 1998; Mersiyanova et al., 2000). MTMR2-L compense partiellement la perte de MTM1 dans les souris *Mtm1* KO, mais plus faiblement que MTM1 et MTMR2-S. Il serait donc possible que MTMR2-L ait (parmi d'autres fonctions) un rôle spécifique dans les cellules de Schwann qui impliquerait son extension N-terminale, tandis que MTMR2-S aurait une fonction plus générale/ubiquitaire similaire à MTM1. Enfin, il serait intéressant de chercher pourquoi les

mutations dans MTMR2 affectent les deux isoformes exprimés de façon ubiquitaire, et pourtant semblent avoir uniquement un impact dans les cellules de Schwann.

III. Mieux comprendre la correction de la myopathie

Compensation et régulation au sein de la famille des myotubularines

Il existe 14 myotubularines chez l'Homme, pour la plupart exprimées de façon ubiquitaire. Cependant, la perte de MTM1 est spécifiquement associée à une sévère myopathie. Cela implique que les homologues de *MTM1*, et notamment les plus proches tels que *MTMR1* et *MTMR2*, ne compensent pas la perte de MTM1 dans les muscles squelettiques, ou du moins pas par leur expression au niveau endogène. Il est possible que ces homologues compensent partiellement la perte de MTM1 dans d'autres tissus chez les patients XLCNM, évitant des phénotypes pathologiques plus sévères (tels qu'une létalité *in utero,* par exemple). Puisque la surexpression exogène de *MTMR2* dans les muscles de souris *Mtm1* KO permet d'améliorer les marqueurs phénotypiques de la myopathie, avec une amélioration comparable à MTM1 pour MTMR2-S, nous pouvons supposer que le niveau d'expression est l'un des points critiques de la capacité de compensation au sein de la famille des myotubularines.

De par ces travaux, j'ai montré que l'expression de MTMR2-S est diminuée dans les muscles squelettiques de souris *Mtm1* KO. De plus, en comparaison avec le cerveau ou d'autres tissus, l'expression des transcrits de MTMR2 est basse dans les muscles squelettiques. L'ensemble suggère que cette faible expression de MTMR2 dans le muscle, additionnée par la baisse d'expression dans les muscles de souris myopathiques et de patients XLCNM, est la cause du manque de compensation par MTMR2. En effet, l'isoforme MTMR2-S est celui qui améliore le plus les phénotypes fonctionnels et structuraux de la myopathie, et son niveau d'expression est davantage abaissé que celui de MTMR2-L dans les muscles myopathiques.

De plus, l'expression exogène de MTM1 humain dans les muscles de souris *Mtm1* KO permet de corriger l'expression d'ARNm total de MTMR2 jusqu'à son niveau normal, suggérant que MTM1 ou un de ses partenaires régule l'expression de *MTMR2* au niveau du gène ou du transcrit (Figure 37C). La prochaine étape serait de quantifier le niveau des 4 transcrit de MTMR2 dans des muscles myopathiques où MTM1 est surexprimé, afin de déterminer si cette correction impacte tous les transcrits de MTMR2 ou seulement certains d'entre eux. On pourrait également étudier la capacité de la surexpression de MTMR2-L ou MTMR2-S humain exogène à réguler le niveau d'expression endogène de MTMR2 dans le muscle, en utilisant des amorces spécifiques des séquences de souris pour la RT-qPCR. Si une correction similaire est observée, cela signifierait que la régulation fait intervenir la même voie de signalisation que pour MTM1, et donc potentiellement des interacteurs communs entre MTM et MTMR2-S et/ou MTMR2-L.

Comment se fait la compensation de la myopathie ?

Dans le cas d'autres maladies congénitales, la perte d'une protéine a déjà été compensée par la surexpression d'une protéine homologue. Par exemple, l'utrophine est un paralogue de la dystrophine avec laquelle elle partage 80% d'homologie ainsi que des fonctions communes (Love et al., 1989). L'expression de la version intégrale de l'utrophine a permis de d'empêcher le développement de la dystrophie musculaire causée par la perte de dystrophine fonctionnelle, dans les souris *mdx* (Tinsley 1998).

La capacité de MTMR2-S à corriger les phénotypes myopathiques des souris *Mtm1* KO après expression dans le muscle pourrait être expliquée par la normalisation des niveaux de PtdIns3*P*. Une étude précédente dans les mutants de drosophiles *mtm* (orthologue de MTM1) ont montré que la déficience de la PtdIns 3-kinase de classe II empêchait les phénotypes et la mort du mutant *mtm* (Velichkova et al., 2010). Plus récemment, deux études ont démontré une correction des phénotypes musculaires de souris *Mtm1* KO via 2 mécanismes : la baisse de l'expression de la PtdIns 3-kinase de classe II PIK3C2B, ou l'inhibition globale par la wortmannine de l'activité PtdIns 3-kinase et donc de la production de PtdIns3*P* (Kutchukian et al., 2016; Sabha et al., 2016).

D’autres preuves de concept thérapeutiques ont été publiées, ne visant pas la normalisation des niveaux de PPIn, mais la normalisation/régulation négative du niveau d’expression de *DNM2* (Cowling et al., 2014), l’expression d’une protéine MTM1-C375S sans activité catalytique (Amoasii et al., 2012) ou encore l’inhibition de l’autophagie (Fetalvero et al., 2013). Une hypothèse est que la dynamine DNM2 appartienne avec MTM1 et BIN1 à la voie MAD (Myotubularin Amphiphysin Dynamin). Les régulations au sein de cette voie de signalisation ne sont pas encore bien comprises, mais il est déjà admis que la dérégulation de DNM2 constitue le facteur clé induisant une myopathie centronucléaire. En effet, il y a une augmentation de l’activité de DNM2 (par gain de fonction ou perte de la régulation) dans les patients XLCNM et les souris *Mtm1* KO, et une régulation négative de l’expression de DNM2 dans ces souris permet de corriger les phénotypes myopathiques (Cowling et al., 2014; Tasfaout et al., 2017). D’où l’hypothèse que la fonction de MTM1 dans la voie MAD est de réguler négativement l’activité de DNM2, et de la maintenir ainsi à un niveau basal. Ainsi, puisque MTMR2 permet de compenser la perte de MTM1, cela suggère que la compensation par MTMR2 s’effectue également par régulation de DNM2. Une compensation par la voie MAD serait directement liée au trafic membranaire et à la tabulation. Il est donc possible que l’expression exogène de MTMR2-L ou MTMR2-S améliore le phénotype des souris *Mtm1* KO par un mécanisme indépendant des PPIn. Il est également intéressant de noter que le mutant MTM1-C375S sans activité catalytique ne permet pas d’améliorer la forme des triades, alors que celle-ci est très bien corrigée par l’expression de MTM1 ou MTMR2-S (actives), suggérant un rôle important des PPIn au niveau de la triade.

Les noyaux centraux (au lieu d’être à la périphérie cellulaire) sont l’un des phénotypes histologiques majeurs des muscles de patients XLCNM, et sont également observables dans les modèles animaux tels que les souris *Mtm1* KO. Des études récentes ont montré que le mouvement et le positionnement des noyaux à la périphérie de la fibre musculaire est un mécanisme régulé par la contraction de la fibre et par l’interaction du noyau avec le cytosquelette (dont l’actine et la desmine) (Janota et al., 2017; Roman et al., 2017). Ainsi, puisque la surexpression de MTMR2 (en particulier de MTMR2-S) permet de corriger la position du noyau dans les muscles de souris *Mtm1* KO, ce mécanisme pourrait impliquer l’interaction de MTMR2 (directe ou indirecte) avec le cytosquelette des fibres musculaires.

Les propriétés de compensation de MTMR2-L

Même si MTMR2-L ne présentes pas de capacités de compensation aussi bonnes que MTM1 et MTMR2-S, cet isoforme long est capable d'améliorer la plupart des phénotypes myopathiques observés chez les souris *Mtm1* KO (Table 2). Cela a déjà été observé dans des études précédentes utilisant des souris (Thèse de Thibaut Jamet, 2014, IGBMC et Institut de Myologie, laboratoire de Anna Buj-Bello) ainsi que des poissons zèbre (Dowling et al., 2009). Cela suggère que MTMR2-L agit sur les mêmes voies de signalisation que MTMR2-S (et potentiellement que MTM1), mais que MTMR2-L accède de façon moindre à ses substrats lipidiques ou présente une affinité plus faible pour ses interacteurs protéiques.

Bien que MTMR2-L ne présente pas de forte activité dans la levure, cet isoforme améliore partiellement les phénotypes des souris *Mtm1* KO. Ceci pourrait être expliqué par un manque de protéines régulatrices dans le système hétérologue de la levure. Le niveau d'expression de MTMR2-L pourrait également expliquer cette différence entre les résultats dans les levures et les souris : MTMR2-L et MTMR2-S sont exprimées au même niveau dans les muscles TA de souris, tandis que MTMR2-L est moins exprimé que MTMR2-S dans la levure (Figure 19), et j'ai justement montré que le niveau d'expression était important pour l'activité phosphatase de MTMR2 (Figure 21). Cependant, le niveau d'expression seul ne peut pas être responsable des différences observées, puisque dans la levure MTMR2-S était moins exprimée que MTMR2-Δ2-24, MTMR2-S58A et MTMR2-S58E, et pourtant présentait une activité phosphatase similaire à ces constructions (Figures 19 et 21).

L'analyse des constructions de MTMR2 par western blot suggère que les propriétés de compensation de MTMR2-L pourraient provenir non pas de ses propriétés intrinsèques, mais de sa modification en une protéine similaire à MTMR2-S. En effet, après surexpression de MTMR2-L et MTMR2-Δ2-24, j'ai pu détecter (en plus des bandes attendues) des bandes de taille inférieure, au même niveau que la bande MTMR2-S. Cela pourrait être expliqué par un clivage post-traductionnel de l'extension N-terminale de MTMR2-L, produisant une protéine plus courte, proche de MTMR2-S. Cela pourrait également être lié à la traduction, par l'utilisation du codon start alternatif dans l'exon 3 de l'ARNm de MTMR2-L, comme c'est le cas pour la traduction normale de MTMR2-S (Figure 26). Cette hypothèse pourrait être

étudiée en mutant le codon start alternatif, ce qui entrainerait alors la perte de la seconde bande sur le western blot.

La correction de la myopathie par injection systémique dans les souris Mtm1 KO

Des données prometteuses ont été apportées par l'analyse de la surexpression systémique de MTM1 et MTMR2 dans les souris *Mtm1* KO. Les deux isoformes de MTMR2 ont réussi à améliorer la force musculaire et la survie des souris injectées. Cependant, ces souris restaient malades et certaines d'entre elles sont mortes avant la fin de l'étude, suggérant que certains muscles ou autres organes étaient moins ou pas corrigés. L'histologie du diaphragme a montré des anomalies même après expression de MTMR2, ce qui pourrait induire des difficultés respiratoires. Si certains organes sont moins corrigés que d'autres, changer le sérotype de l'AAV pourrait changer la spécificité tissulaire et ainsi améliorer le phénotype.

Cette étude préliminaire a montré des tendances très encourageantes, qui demandent à être confirmées avec de plus larges cohortes et des investigations plus larges des phénotypes myopathiques, comme cela a été fait pour les injections intramusculaires d'AAV. En particulier, il serait intéressant de mesurer par Aurora la force musculaire spécifique des souris injectées, d'analyser l'ultrastructure de différents tissus (en particulier les muscles et le système nerveux), et de quantifier les niveaux de DNM2 et de PtdIns3*P* dans les tissus. L'utilisation d'un test « footprint » d'empreinte de pattes, d'un test « rotarod » ainsi qu'un détecteur de mouvements pourraient apporter des informations concernant la mobilité des souris *Mtm1* KO injectées en systémique. Enfin, cette étude pourrait être complétée en donnant un score de sévérité à différents marqueurs de la progression de la myopathie, tels que la scoliose. L'ensemble de ces procédés permettrait de déterminer la capacité de MTMR2 à compenser significativement la durée de vie et les phénotypes myopathiques des souris *Mtm1* KO, et également de confirmer si MTMR2-S a une capacité de compensation plus importante que MTMR2-L.

Le niveau d'expression de MTMR2 pourrait également être déterminé dans un maximum de tissus, puisque un niveau d'expression plus faible pourrait expliquer une correction plus faible de la myopathie dans certains organes. J'ai confirmé l'expression des

myotubularines dans le TA et le diaphragme, mais n'ai pas comparé ces tissus entre eux et n'ai pas testé d'autres organes. Une future étude pourrait tester différentes doses d'AAV afin de déterminer s'il existe une corrélation entre cette dose et le niveau/rapidité de la correction. Il est possible qu'une dose plus forte, et donc un niveau d'expression de MTMR2 plus élevé, puisse induire une survie et une correction aussi bonne et rapide que MTM1, et cela sans aucune toxicité.

IV. Stratégies thérapeutiques

Surexpression de MTMR2 dans les patients XLCNM

Cette étude apporte la preuve de concept que MTMR2 pourrait être utilisée comme cible thérapeutique. En effet, la surexpression de MTMR2 humain dans les muscles de souris *Mtm1* KO améliore grandement les phénotypes myopathiques, suggérant que que la correction des phénotypes est cellule-autonome dans le muscle. La compensation de la myopathie myotubulaire par une protéine MTM1 recombinante ou ré-exprimée grâce à l'injection d'AAV a déjà été proposée comme stratégie thérapeutique potentielle (Childers et al., 2014; Lawlor et al., 2013). L'expression de MTMR2 dans le muscle pourrait constituer une stratégie alternative, présentant l'avantage de ne pas induire de réponse immunitaire contre le transgène. En effet, la majorité des patients atteints de myopathie myotubulaire ont un niveau très faible voire nul de protéine MTM1, et leur système immunitaire pourrait donc considérer la protéine MTM1 exogène comme un antigène (Laporte et al., 2000; Laporte et al., 2001), tandis que MTMR2 est déjà exprimée de façon endogène dans les patients. Bien entendu, des études à long terme seraient essentielles afin de déterminer si la surexpression de MTMR2 n'est pas toxique ou n'induit pas de phénotype neuropathique de type CMT.

Le saut d'exon ou l'inclusion d'exon pour favoriser l'expression de MTMR2-S

Les données que j'ai obtenues montrent que l'isoforme MTMR2-S corrige davantage les phénotypes myopathiques que l'isoforme MTMR2-L qui était davantage décrit dans la littérature. L'isoforme court MTMR2-S est un variant naturel présent (si on se base sur les niveaux d'ARNm) dans tous les tissus, y compris dans les muscles. Puisque le niveau des transcrits de MTMR2-S est réduit dans les muscles de souris *Mtm1* KO et de patients

XLCNM, une stratégie serait d'augmenter l'expression de ces transcrits en modulant l'épissage alternatif de MTMR2, via saut d'exon ou inclusion d'exon. En effet, l'inclusion de l'exon 1a de *MTMR2* durant l'épissage produit le variant d'ARNm V2 chez l'homme (ou V4 dans la souris), qui est alors traduit en MTMR2-S (Figure 6). Ceci utiliserait donc le système existant d'épissage alternatif qui, nous le savons, est fonctionnel pour *MTMR2*. On pourrait également sauter l'exon 2 de *MTMR2*, induisant un décalage du cadre de lecture (l'exon 2 n'est pas en phase) et un codon STOP prématuré directement au début de l'exon 3, permettant la traduction de MTMR2-S à partir du codon start alternatif plus loin dans l'exon 3. Cette stratégie élégante éviterait l'apport de protéine exogène dans les patients, en changeant simplement la balance entre MTMR2-S et MTMR2-L et en favorisant l'expression de MTMR2-S qui est plus actif. Des stratégies similaires sont déjà employées en tests cliniques pour d'autres maladies congénitales, telles que la dystrophie de Duchenne : le saut d'exon est employé afin de supprimer des exons mutés et ré-établir un cadre normal de lecture dans le gène de la dystrophine, produisant ainsi une protéine plus courte et induisant une bien moins sévère dystrophie de Becker (Alter et al., 2006; Bremmer-Bout et al., 2004).

La limitation majeure de cette stratégie prometteuse de saut/inclusion d'exon est le faible niveau d'expression de MTMR2 dans les muscles, ce qui limite l'expression de MTMR2-S et donc ses capacités thérapeutiques. En effet, l'épissage alternatif change uniquement le ratio d'expression des isoformes d'ARNm, mais n'a pas d'impact sur le niveau d'expression total du gène. Or contrairement à MTM1, les protéines MTMR2 endogènes n'ont pas pu être détectées, alors que j'ai pu détecter MTMR2 surexprimée dans les mêmes conditions, confirmant que les isoformes endogènes sont très faiblement exprimées. Cependant, des études sur le modèle murin *Mtm1* p.R69C mimant une mutation de patient XLCNM ont montré qu'un niveau faible de MTM1 est suffisant pour améliorer les phénotypes myopathiques, avec une augmentation de la force musculaire et une espérance de vie excédant souvent 1 an (Pierson et al., 2012). Ainsi, même une faible augmentation du niveau de MTMR2-S pourrait améliorer les phénotypes myopathiques. Cette hypothèse doit cependant être modérée par mes résultats obtenus dans la levure, montrant que MTM1 est bien plus active que MTMR2-L ou –S à faible niveau d'expression (plasmide CEN) (Figure 21A).

Une solution pourrait être d'augmenter l'expression de *MTMR2* en régulant son promoteur. Cela a déjà été accompli pour d'autres gènes tels que l'utrophine, dont l'augmentation de l'expression est actuellement testée en phase 2 d'essais cliniques, afin de corriger la dystrophie musculaire (Tinsley et al., 2011). L'étude de la régulation du promoteur de *MTMR2* et de ses facteurs de transcriptions serait donc essentielle afin de construire une thérapie basée sur MTMR2 qui soit efficace pour la XLCNM.

Autres perspectives thérapeutiques

Durant ma thèse, je me suis focalisé sur les différences fonctionnelles entre MTM1 et MTMR2, qui sont impliquées dans deux maladies neuromusculaires différentes. Après des résultats dans la levure montrant une homologie fonctionnelle entre MTMR2-S et MTM1, j'ai comparé les capacités de MTMR2-L et MTMR2-S à corriger les phénotypes myopathiques de souris *Mtm1* KO. Cependant, si l'on se base sur les homologies de séquence protéique, MTMR1 pourrait également être un bon candidat pour un tel mécanisme de compensation. MTMR1 est en effet avec MTMR2 le plus proche homologue de MTM1, et montre la même spécificité de substrat. Six isoformes d'ARNm ont été décrit pour MTMR1, l'un d'entre eux étant spécifiquement exprimé dans le muscle (Buj-Bello et al., 2002a). Une étude dans le poisson zèbre montre même que MTMR1 est capable de compenser la perte de MTM1 (Dowling et al., 2009). Ainsi, MTMR1 constitue un nouveau candidat pour la correction de la myopathie myotubulaire. Un alignement de séquence montre que, comme MTMR2, MTMR1 possède une extension N-terminale comparé à MTM1, juste avant le PH-GRAM. Il est également intéressant de noter que le S58 de MTMR2 est conservé dans MTMR1 et pourrait réguler sa localisation et fonction. Il est donc possible que la perte de cette extension N-terminale confèrerait à MTMR1 des propriétés plus proches de MTM1, et augmenterait son activité enzymatique *in vivo*. Bien qu'aucun des 6 ARNm connus de MTMR1 ne présente de codon STOP dans les premiers exons, on notera que le codon start alternatif de l'exon 3 de MTMR2 est conservé dans la séquence de MTMR1. Un variant endogène non identifié d'ARNm de MTMR1 pourrait donc reproduire l'épissage alternatif montré pour *MTMR2*, avec l'inclusion d'un exon supplémentaire conduisant à un STOP prématuré et à la traduction à partir du codon start dans l'exon 3, produisant une protéine MTMR1 plus courte, sans extension N-terminale. Cela conduirait à une nouvelle thérapie potentielle, basée sur la surexpression de MTMR1 dans les muscles de patients myopathiques.

Enfin, puisque MTMR2 améliore la myopathie liée à la perte de MTM1, il serait intéressant de tester si l'expression de MTM1 pourrait être une option thérapeutique pour la neuropathie CMT4B causée par des mutations dans MTMR2.

V. Epilogue

Durant l'été 2017, l'identification de MTMR2-S comme cible thérapeutique potentielle pour la myopathie myotubulaire a été brevetée par la SATT-Connectus. Cela pourrait permettre la poursuite de l'étude de MTMR2-S et l'identification de cet isoforme comme candidat potentiel pour de futurs essais cliniques.

Materials and Methods

I. Plasmids and constructs

The human *MTM1* (1812 bp, 603 aa) and *MTMR2-L* (1932 bp, 643 aa) ORFs (with and without STOP codon) were cloned into the **pDONR207** plasmid (Invitrogen) to generate entry clones. The pDONR207-MTMR2-S (1716 bp, 571 aa) has been obtained by site-directed mutagenesis on the pDONR207-MTMR2-L vector, to delete the 216 first nucleotides of *MTMR2-L* corresponding to the 72 first amino acids. Three other site-directed mutagenesis on pDONR207-MTMR2-L were performed to obtain the S58A, S58E and S58D variants of MTMR2-L.

Gateway system (Invitrogen, Carlsbad, CA) was used to clone the different myotubularin constructs into the following destination expression vectors:

Plasmid	Insert	Selection in bacteria	Selection in yeast	Replication in yeast	Promoter	Origin
pVV200	ccdB	Amp	TRP1	2µ	PGK1	Euroscarf
pVV204	ccdB	Amp	TRP1	CEN	TetO	Euroscarf
pAG424GPD-ccdB-EGFP	ccdB	Amp	TRP1	2µ	GPD	S. Lindquist
pAAV-MCS	ccdB	Amp	-	-	CMV	

All plasmids in this study possess the *E. coli* replication origin (***ColE1***). For replication in yeast, pVV200 and pAG424GPD-ccdB-EGFP yeast plasmids contain a **2µ** episomal replication origin (high copy number) and pVV204 yeast plasmids contain a **CEN** centromeric replication origin (low copy number).

Lentiviral plasmids (pLenti) have been constructed by Paola Rossolillo (IGBMC, molecular biology facility). They contain a myotubularin construct (MTM1, MTMR2-L or MTMR2-S cloned by restriction enzymes BstBI/PstI) under the control of a CAG promoter (containing a CMV enhancer). The same plasmids also contain the *EGFP* ORF under the control of the PGK promoter.

The **pCS211 DsRED-FYVE** plasmid was previously described (Katzmann et al. 2003).

pGGWA GST plasmid (Amp, *ColE1 ori*) containing *MTMR2-L* ORF fused by its 5' extremity to *GST* (Glutathione-S-Transferase) ORF. This plasmid has been used for GST-MTMR2-L production in bacteria and purification (as described in Chapter VI).

II. *In vivo* models

A. Bacteria strains and culture conditions

Three different *E. coli* bacteria strains were used for this study:

- **DH5 alpha** was used for amplification of plasmids without the *ccdB* gene. Genotype: *fhuA2 lac(del)U169 phoA glnV44 Φ80' lacZ(del)M15 gyrA96 recA1 relA1 endA1 thi-1 hsdR17*

- **DB3.1** was used for amplification of plasmids containing the *ccdB* gene which is important for Gateway cloning. This strain is ccdB resistant. Genotype: *gyrA462 endA1 Δ(sr1-recA) mcrB mrr hsdS20 glnV44 (=supE44) ara14 galK2 lacY1 proA2 rpsL20 xyl5 leuB6 mtl1*.

- **Rosetta (pLysS)** was used for human protein production. Genotype: F^- *ompT* $hsdS_B(r_B^- m_B^-)$ *gal dcm* (DE3) pLysSRARE (Cam^R). Mutations in proteases induce proteolyse reduction. The pLysSRARE contains seven genes coding for tRNA specific for codons that are rare in *E. coli* but common in eukaryotes.

For liquid cultures, bacteria were grown at 37°C under agitation in LB (Lysogeny Broth, Yeast Extract 5 g/L ; Tryptone 10 g/L , NaCl 10 g/L) supplemented with the adapted antibiotic (Amp 1/1000 in general).

For culture in Petri dishes, agar-agar (20 g/L, Euromedex) was added to the LB medium, and bacteria were grown at 37°C.

B. Yeast strains and culture conditions

The S. cerevisiae *ymr1*Δ (MATa, ura3-52, leu2-3,112, his3-Δ200, trp1-Δ901, lys2-801, suc2-Δ9 ymr1::HIS3) (14) and WT (MATa, his3Δ1, leu2Δ0, lys2Δ0, ura3Δ0) strains were grown at 30°C in rich medium (YPD): 1% yeast extract, 2% peptone, 2% glucose or synthetic drop-out medium (SC): 0.67% yeast nitrogen base without amino acids, 2% glucose and the appropriate amino acids mixture to ensure plasmid maintenance. I did not use the *ymr1Δ* (MATa, his3Δ1, leu2Δ0, lys2Δ0, ura3Δ0, ymr1::KanMX) in the BY4742 background from the yeast systematic deletion collection, because it does not have the *ymr1*Δ phenotype described by Scott D Emr's laboratory (Parrish et al. 2004).

C. Mammalian cells and culture conditions

COS-1 and **HEK293** cells were grown at 37°C with 5% CO_2 in Dulbecco's Modified Eagle's Medium (DMEM) supplemented with 5% fetal calf serum (FCS).

Knockdown (KD) *Mtm1* and control C2C12 mouse myoblast cells were previously generated in triplicates in Jocelyn Laporte laboratory (Hnia et al. 2011). After selection by adding of 2 µg/ml puromycin to the culture medium, C2C12 myoblasts were maintained at 37°C in DMEM supplemented with 20% FCS for proliferation. Differentiation of confluent cells was induced by changing the medium into DMEM supplemented with 5% horse serum (HS). Cells were then left during 9 days (washing with PBS and medium change every 2 days) to differentiate into myotubes.

D. Mice and housing conditions

In this study I used **male wild-type (WT) and *Mtm1* KO 129 PAS mice**, generated by y crossing Mtm1 heterozygous females obtained by homologous recombination with WT males. The *Mtm1* KO mice are characterized by a progressive muscle atrophy and weakness starting at 2-3 weeks and leading to death by 8 weeks. Animals were housed in a temperature-controlled room (19–22°C) with a 12:12-h light/dark cycle and were given free access to standard food. DietGel were given after the first signs of myopathy and walking defaults, for better access to food. Mice were humanely killed by cervical dislocation after injection of pentobarbital, according to national and European legislations on animal experimentation. Protocols were approved by the institutional Ethics Committee.

***Mtmr2* KO mice tissues** were generously given by Alessandra Bolino team.

III. Antibodies

Following primary antibodies were used during this study.

Target protein	Animal used for production	Origin
MTM1	Rabbit	Homemade (R2827)
MTMR2	Mouse	Homemade (4G3)
DNM2	Rabbit	Homemade (R2680)
Pgk1 (yeast)	Mouse	Invitrogen
Vph1 (yeast)	Mouse	Molecular probes
GAPDH	Mouse	Chemicon
CAV3	Goat	Santa Cruz

Dilutions depend on the antibody and the technique used. Used secondary antibodies are specified for each technique.

IV. Biopsies from patients

Human sample collection was performed with written informed consent from the patients or parents according to the declaration of Helsinki. The 3 XLCNM patients had the following mutations in *MTM1*: [c.445-49_445-4 del], [c.523A>G in exon 7, p.Arg175Gly] and [c.145_161del17 in exon 4, p.Val49Phe fs*6].

V. Bacteria transformation and plasmid production

For **transformation**, chimiocompetent *E. coli* cells were unfrozen on ice then incubated on ice during 10 min with 1 µg of plasmid (1-5 µL). Cells were heat-chocked at 42°C for 45 sec and immediately replaced on ice for 2 min. 1 mL of LB was then added before incubation at 37°C for 30 min and streaking on LB agar + antibiotic.

For **plasmid purification**, transformed bacteria were cultured overnight at 37°C in 2-5 mL of LB + antibiotic. Pellets are obtained after centrifugation at 10 000 xg for 3 min. Plasmids are purified using the QIAprep Spin Miniprep Kit (Quiagen), according to the manufacturer protocol. Plasmid concentration was then measured using a Nanodrop spectrophotometer.

VI. Production of monoclonal anti-MTMR2 antibody

Recombinant MTMR2 protein fused to GST was produced using a 2L culture of *E.coli* bacteria cells transformed with a pGGWA-MTMR2 expression plasmid. The production of the fusion protein has been induced by IPTG addition and growth at 18°C overnight. Total proteins were extracted by sonication and successive centrifugations, and then GST-MTMR2 was affinity-purified using glutathione-sepharose beads. The first 5 eluted fractions have been analyzed by SDS-PAGE, proteins were stained by Coomassie blue. Finally E2, E3 and E4

fractions that contained GST-MTMR2 (controlled by mass spectrometry) were pooled and given to the antibody facility of IGBMC (Illkirch). The recombinant protein was then used to immunize mice and produce mouse monoclonal anti-MTMR2 antibodies.

VII. AAV production

rAAV2/1 and rAAV2/9 vectors were generated by a triple transfection of AAV-293 cell line with pAAV2-insert containing the insert under the control of the CMV promoter and flanked by serotype-2 inverted terminal repeats, pXR1 containing *rep* and *cap* genes of AAV serotype-1 or serotype-9, and pHelper encoding the adenovirus helper functions. Cell lysates were subjected to 3 rounds of freeze/thaw, then treated with 50U/mL Benzonase (Sigma) for 30 minutes at 37°C and clarified by centrifugation. Viral vectors were purified by Iodixanol gradient ultracentrifugation followed by dialysis and concentration against DPBS using centrifugal filters (Amicon Ultra-15 Centrifugal Filter Devices 30K). Physical particles were quantified by real time PCR using a plasmid standard pAAV-eGFP. Titers are expressed as viral genomes per ml (vg/ml) and rAAV titers used here were $5\text{-}7.10^{11}$ vg/ml for intramuscular injections (AAV2/1) and $3\text{-}6.10^{13}$ vg/ml for systemic injections (AAV2/9).

VIII. Lentiviral production

Lentiviral plasmids (pLenti) have been constructed by Paola Rossolillo (IGBMC, molecular biology facility). They contain a myotubularin construct (MTM1, MTMR2-L or MTMR2-S cloned by restriction enzymes BstBI/PstI) under the control of a CAG promoter (containing a CMV enhancer). The same plasmids also contain the *EGFP* ORF under the control of the PGK promoter.

Briefly, 293T cells were transfected with lentiviral plasmid and helper plasmids. Lentiviral supernatant was harvested 48-72 hours after transfection and concentrated by ultracentrifugation. Lentiviral tittering in 293T cells was performed with serially diluted lentivirus; after 3 days the 293T cell DNA was isolated for vector-specific quantitative PCR.

IX. Expression analysis

Total RNA was purified from tibialis anterior (TA) muscle, brain and liver of 7 week-old wild-type and *Mtm1* KO mice, from C2C12 cell pellets, or from muscle biopsies of XLCNM patients and controls, using TRIzol reagent (Invitrogen, Carlsbad, CA) according to the manufacturer's instructions. cDNAs were synthesized from 500 ng of total RNA using Superscript II reverse transcriptase (Invitrogen) and random hexamers.

PCR amplification of 1/10 diluted cDNA from TA muscle and liver was performed using a forward primer from the 5'-UTR of *MTMR2*: 5'-AGCGGCCTCCAGTTTCTCGCGC-3' and a reverse primer from exon 3: 5'-TCTCTCCTGGAAGCAGGGCTGGTTCC-3', for 35 cycles of amplification at 72°C (and 65°C as melting temperature) and 30 min of final extension at 72°C, as previously described (23). The products were analyzed on a 2% agarose gel, each band has been purified using Nucleospin Gel and PCR cleanup kit (Macherey-Nagel, Düren, Germany), then cloned into a pJet2.1 vector using the CloneJet PCR cloning kit (ThermoFisher Scientific, Waltham, MA), and sequenced by Sanger.

Quantitative PCR amplification (qPCR) of 1/10 diluted cDNAs from mouse TA muscles or brain or human muscle biopsies was performed on Light-Cycler 480 II instrument (Roche, Basel, Swiss) using 53°C as melting temperature.

Specific sets of primers were used for each **mouse *MTMR2* isoform**: forward 5'-GACTCACTGTCCAGTGCTTC-3' and reverse 5'-CCTCCCTCAGGACCCTCA-3' for mouse V1, forward 5'-GACTCACTGTCCAGTGCTTC-3' and reverse 5'-CAGCTGGGCACTCCCTCA-3' for mouse V2, forward 5'-AAGATAAAACATCTCAAAAATTATAATTGCTTC-3' and reverse 5'-CAGCTGGGCACTCCCTCA-3' for mouse V3, forward 5'-AAGATAAAACATCTCAAAAATTATAATTGCTTC-3' and reverse 5'-GACTCACTGTCCAGTGCTTC-3' for mouse V4.

Another set of primers (forward 5'-TCCTGTGTCTAATGGCTTGC-3' and reverse 5'-AACCAAGAGGGCAGGATATG-3') amplifying a sequence common to all mouse isoforms has been used to quantify **total mouse MTMR2** mRNA.

Other specific sets of primers were used for each **human *MTMR2* isoform**: forward 5'-ACTCCTTGTCCAGTGCCTC-3' and reverse 5'-GACTCCCTCAGGACCCTC-3' for human V1, forward 5'-AAGATAAAACATCTCAAAAATTATAATTGCCTC-3' and reverse 5'-GACTCCCTCAGGACCCTC-3' for human V2, forward 5'-AAGATAAAACATCTCAAAAATTATAATTGCCTC-3' and reverse 5'-GAGCGAGACTCCCTCCTC-3' for human V3, forward 5'-AAGATAAAACATCTCAAAAATTATAATTGCCTC-3' and reverse 5'-CTGGACTGCATGGGCCTC-3' for human V4.

Another set of primers (forward 5'-TTTCCTGTCTCTAATAACCTGCC-3' and reverse 5'-CCAGGAGGGCAGGGTATG-3') amplifying a sequence common to all human isoforms has been used to quantify **total human MTMR2** mRNA.

Finally, ***MTM1* was quantified in C2C12 cells** using the forward 5'-CATGCGTCACTTGGAACTGTGG-3' and reverse 5'- GCAATTCCTCGAGCCTCTTT-3' primers.

For all qPCR on cDNA from muscle samples and C2C12 myoblasts/myotubes samples, the ***HPRT*** gene expression was used as control because of the non-variation in its expression between control and myopathic muscles. For qPCR on cDNA from brain samples, the ***PGK1*** gene expression was used as control.

X. Protein extraction and Western blot

Total proteins were extracted from **yeast cells** (OD_{600nm}=0.5-0.9, minimum 3 clones per construct) by TCA precipitation and NaOH lysis. Total proteins were extracted from **mouse tissues and mammalian cells** by homogenization (using a tissue homogenizer (Omni TH) or the pipette) in RIPA buffer supplemented with PMSF 1 mM and complete mini

EDTA-free protease inhibitor cocktail (Roche Diagnostic). Protein concentrations were determined with the BIO-RAD Protein Assay Kit. Samples were denaturated at 95°C for 5 min in SBR 1x buffer (the 2x buffer being made of: TrisHCl pH6.8 120 mM, SDS 4%, β-mercaptoethanol 4%, Glycerol 20 %, bromophenol blue 0,004%)

Then an equal protein quantity (usually 20 µg) for each sample was loaded in buffer containing 50 mM Tris–HCl, 2% SDS, 10% glycerol, separated in 10% SDS– polyacrylamide gel electrophoresis electrophoretic gel and transferred on nitrocellulose membrane for 1.5 h at 200 mA. Membranes were blocked for 2 h in TBS containing 4% non-fat dry milk and 0.1% Tween20 before an incubation overnight at 4°C with the suitable primary antibodies (anti-MTM1 1/500, anti-MTMR2 1/1000, anti-DNM2 1/500, anti-Vph1 1/1000, anti-PGK1 1/1000 and anti-GAPDH 1/1000) followed by incubation 1.5 h at room temperature with the secondary antibody coupled to HRP, and extensive washing. Membranes were revealed by ECL chemiluminescent reaction kit (Supersignal west pico kit, ThermoFisher Scientific, Waltham, MA) and the signal was detected using a ChemiDoc (Bio-Rad).

For most of the western blots, 5% of trichloroethanol (TCE) were added to the acrylamide before gel preparation, allowing the detection of total protein in the gel and on the nitrocellulose membrane. This Stain free system was used for normalization and quantification using the Bio-Rad software.

XI. Mass spectrometry

For **differential interactome**, MTMR2 constructs were overexpressed in COS-1 cells after transfection of pAAV vectors, and total protein were extracted using a non-denaturing lysis buffer with a protease inhibitor cocktail, and lysis by manual grinding using mortar and pestle on ice. Immunoprecipitation was carried out with µMACS Protein A/G microbeads (Miltenyi Biotec) and MTMR2 4G3 antibody (homemade), according to the manufacturer's protocol. Each protein sample was split in half. The second halves were used as negative controls, omitting antibodies during the immunoprecipitations. Proteins complexes were eluted out of the magnetic stand with the SDS gel-loading buffer from the kit. Co-immunoprecipitation experiments were carried out in duplicates for all the samples.

The samples were prepared for mass spectrometry analyses as previously described (Chicher et al. 2015). Briefly, eluted proteins were precipitated with 0.1 M ammonium acetate in 100% methanol. After a reduction-alkylation step (dithiothreitol 5 mM–iodoacetamide 10 mM), proteins were digested overnight with 1/25 (W/W) of modified sequencing-grade trypsin (Promega, Madison, WI, USA) in 50 mM ammonium bicarbonate. Resulting peptides were vacuum-dried in a SpeedVac concentrator and re-suspended in water containing 0.1% FA (solvent A) before being injected on nanoLC-MS/MS (NanoLC-2DPlus system with nanoFlex ChiP module; Eksigent, ABSciex, Concord, Ontario, Canada, coupled to a TripleTOF 5600 mass spectrometer (ABSciex)). Peptides were eluted from the C-18 analytical column (75 µm ID × 15 cm ChromXP; Eksigent) with a 5–40% gradient of acetonitrile (solvent B) for 90 min.

XII. Bioinformatics analysis

Expression levels of *MTMR2* mRNA isoforms was obtained by mining the Genotype-Tissue Expression (GTEx, www.gtexportal.org/home/) database, which has been built by systematic RNA-sequencing using samples of 51 different tissues from hundreds of donors and two transformed cell types in culture. We then used this data to calculate the relative expression of *MTMR2* mRNA isoforms in the 20 most relevant tissues, and to create a heat map underlining in which tissue a specific isoform is the most/least expressed.

Alignment of the N-terminal part of MTM1, MTMR2-L and MTMR2-S was done using Jalview (www.jalview.org/) and aligning amino acids were identified by Clustalx color coding.

XIII. Protocols specific to yeast

A. Transformation of yeast cells

1 OD_{600nm} unit of overnight cultured yeast cells were pelleted by centrifugation at 4000 xg for 5 min. The pellet was washed with sterile water before adding of 5 µL of salmon sperm (10 mg/mL), 2µg of plasmid, and 500 µL of transformation buffer (Polyéthylène glycol

4000 40%, AcOLi 0,1M, TrisHCl pH7.5 10mM, EDTA 1mM). After mixing by vortexing, the tube is incubated at 42°C for 30-40 min. After 2 washings, the pellet is resuspended into 100 µL of sterile water and spread on solid SC medium lacking the suitable amino acid for plasmid selection.

B. Subcellular fractionation

Yeast cells were grown in 100 mL of suitable SC medium at 30°C to OD_{600} = 0.8-1. After wash using 10 mL of ice-cold lysis buffer (PBS 1X + 0.25 M Sorbitol + protease inhibitors), cell pellet was resuspended in 1 mL of lysis buffer + PMSF 1 mM final and transferred in 2 mL freezing tubes with 1 mL of glass beads. Cells were lysed by FASTprep (MP Biomedicals) at 6.5 M/S, 5 x 30 sec, 2 min in ice in between. The solution was then transferred into a 1.5 mL Eppendorf tube, and centrifuged at 500 xg for 5 min at 4°C to remove unbroken cells and massive cell wall debris. Supernatant S5 (900 µL) was transferred into a new tube for a 13 000 xg centrifugation during 10 min at 4°C. The obtained **P13 pellet** was resuspended in 200 µL of lysis buffer, while the S13 supernatant was transferred into a ultracentrifugation tube. The last centrifugation at 100 000 xg for 1h at 4°C separates the **P100 pellet** from the **S100 supernatant**. **P13**, **P100** and **S100** were set at equal volume and conserved in SBR 1x at -20°C for further western blot analysis.

C. Yeast phenotyping

For **vacuole staining**, 1 OD_{600nm} unit of cells was harvested by a 500 xg centrifugation for 1 min, incubated in 50 µl YPD medium with 2 µl FM4-64 (200 µM, Invitrogen) for 15 min at 30°C, prior washing with 900 µl YPD and chasing by incubation at 30°C for 10 min followed by a second wash in SC complete medium, the stained living yeast cells were observed by fluorescent microscopy. Between 100 and 600 cells per clone (three different clones per construct) were counted and classified into two categories: large or medium unilobar vacuole, and small or fragmented vacuole.

For **PtdIns*3P* quantification**, yeast cells were co-transformed by a pVV200 plasmid (empty or containing *MTM1*, *MTMR2-L* or *MTMR2-S* cDNA) and the pCS211 plasmid expressing the DsRED-FYVE reporter for PtdIns3*P*-enriched membrane structures

(Katzmann et al. 2003). After fluorescence microscopy, the number of dots per cell was quantified on minimum 100 cells per clone (2 different clones per construct).

For **PtdIns5*P* quantification**, yeast *ymr1*Δ cells producing the different MTM1 and MTMR2 constructs were grown to exponential phase. Lipid extraction was done as described in Hama *et al.* on 200 OD_{600nm} units of cells (Hama et al. 2000). Quantification of the PtdIns(5)P level was performed as described by Morris *et al.* (Morris et al. 2000) and the results were normalized based on the total lipid concentration.

All fluorescence microscopy observations were done with 100X/1.45 oil objective (Zeiss) on a fluorescence Axio Observer D1 microscope (Zeiss) using GPF or DsRED filter and DIC optics. Images were captured with a CoolSnap HQ2 photometrix camera (Roper Scientific) and treated by ImageJ (Rasband W.S., ImageJ, U. S. National Institutes of Health, Bethesda, Maryland, USA, http://imagej.nih.gov/ij/).

XIV. Protocols specific to mammalian cells

A. Cell transfection

All mammalian cell transfections were done using the lipofectamine 3000 reagent (Thermo Fisher Scientific) according to manufacturer instructions.

B. Cell transduction

Transduction of mammalian cells was performed by adding of viral vectors (AAV and Lentivirus) with polybrene (4µg/mL) to confluent cultured cells. After 24-48h of incubation at 37°C, cells were washed and observed 2-4 days later. In a transduction experiment, the MOI (multiplicity of infection) represents the ratio between the number of viral vectors added to the cultured cells and the number of cells in the culture well. Several MOI have been used depending on the viral vector and the experiment.

C. Immunofluorescence

Adherent mammalian cells were washed by PBS 1X prior fixation by paraformaldehyde (PFA) 4% 20 min, then neutralization by NH_4Cl 15 min and washing by PBS 1X 5 min. Cell permeabilization was performed with PBS-Triton 0.2% for 10 min before washing by PBS 1X 5 min and saturation by PBS-Triton 0.1% + 10% FCS for 1h. Cells were then incubated during 3-4h with the primary antibody diluted in PBS-Triton 0.1% + 3% FCS, and washed 3 times with PBS 1X before incubation 1h with the secondary antibody also diluted in PBS-Triton 0.1% + 3% FCS. After 4 washings with PBS1X, cell nuclei were stained by Hoechst (1/400 for 3-5 min), before a final washing with PBS 1X and mounting using FluorSave reagent (Merck Millipore). Observations were made using an upright motorized microscope (Leica DM 4000 B).

Primary antibodies were diluted at 1/200 for MTM1 and MTMR2 and 1/600 for CAV3 (caveolin 3). Secondary antibodies were goat anti-mouse Alexa 488 (for MTMR2), goat anti-rabbit Alexa 488 (for MTM1) and donkey anti-goat Alexa 488 (for CAV3).

For the figure 22, cells have been incubated with saponin 0.01% for 2 min prior fixation, to wash the cytoplasmic background.

D. C2C12 myotubes phenotyping

C2C12 myotube length was quantified using ImageJ by measuring the length of 10 random myotubes on 30 randomly taken images.

C2C12 myotube fusion index was quantified using the cell counter plugin of ImageJ, by counting the number of nuclei per myotube in 10 random myotubes on 30 randomly taken images. The fusion index was then calculated as the mean of the number of nuclei per myotube.

XV. Protocols specific to mice

A. AAV transduction in mice

For **intramuscular injections**, two- to 3-week-old wild-type or *Mtm1* KO male 129PAS mice were anesthetized by intraperitoneal injection of 5 µl/g of ketamine (20 mg/mL; Virbac) and xylazine (0.4%, Rompun). Tibialis anterior (TA) muscles were injected with 20 µl of AAV2/1 preparations (at 5-7.10^{11} vg/ml) or sterile AAV2/1 empty vector. Four weeks later, mice were anesthetized and the TA muscle was either functionally analyzed (as described below), or directly dissected and frozen in nitrogen-cooled isopentane for protein extraction and histology, or fixed for electron microscopy (as described below).

For systemic injections, wild type or *Mtm1* KO pups were intraperitoneally injected at birth or at Day 1 by 1.5x10^{12} units of empty AAV2/9 viral particles or AAV2/9 overexpressing human MTM1, MTMR2-L or MTMR2-S. The AAV2/9 serotype is supposed to transduce almost all organs by systemic injections. Then 3 weeks after injection I started to analyze weekly the body weight and the mice skeletal muscle strength by two different tests: the grip test and the hanging test (described below).

B. Clinical tests

Grip test: Mice were placed on the wire grid of the grip-strength apparatus which was connected to an isometric force transducer (dynamometer). They were lifted by the tail so that their all paws grasp the grid and they were gently pulled backward by the tail until they release the grid. The maximal force exerted by the mouse before losing grip was recorded. The mean of three measurements for each animal was calculated. Results are represented relative to whole body weight (specific force).

Hanging test: Mice were placed on a grid (cage lid) then turned upside down; the suspending animal should hold on to the grid to avoid falling. The latency to fall was measured three times for each mouse. The three trials were taken at ten minute intervals to allow a recovery period. The latency time measurements began from the point when the mouse was hanging free on the wire and ended with the animal falling to the cage underneath

the wire or grid. The maximum time measured was 60 s. The data were expressed as an average of three trials.

C. Dissection and sample preparation

Organs dissection was performed after the mice were anesthetized and sacrificed by cervical dislocation. Organs were weighed and then either frozen in isopentane by liquid nitrogen and stored at -80°C for future cryosection or protein/RNA extraction, or stored 24h in 4% PFA and then in 70% ethanol for future histological analysis. Abdominal fat depots of systemically injected mice were also dissected and weighed.

D. Functional analysis of the muscle

Muscle force measurements were evaluated by measuring *in situ* muscle contraction in response to nerve and muscle stimulation. Animals were anesthetized by intraperitoneal injection of pentobarbital sodium (50 mg per kg). The distal tendon of the TA was detached and tied with a silk ligature to an isometric transducer (Harvard Bioscience, Holliston, MA). The sciatic nerve was distally stimulated, response to tetanic stimulation (pulse frequency of 50 to 143 Hz) was recorded, and absolute maximal force was determined. After contractile measurements, the animals were sacrificed by cervical dislocation. To determine specific maximal force, TA muscles were dissected and weighed.

E. Histology

For intramuscular injections, transverse cryosections (9 µm) of mouse TA skeletal muscles were stained with hematoxylin and eosin (HE) or Succinate dehydrogenase (SDH) and viewed with a NanoZoomer 2.0HT slide scanner (Hamamatsu). Fiber area was analyzed on HE sections, using the RoiManager plugin of ImageJ image analysis software and a graphic tablet. The percentage of peripheral nuclei was counted using the cell counter plugin of ImageJ image analysis software. ImageJ plugins coded by Pascal Kessler were used to correlate the nuclei positioning to the fiber size, and for the color coding of the myofibers depending on the fiber size.

For systemic injections, 5 µm sections from paraffin-embedded organs were prepared, fixed and stained by Haematoxylin and Eosin (H&E). Sections were imaged with a NanoZoomer 2.0HT slide scanner (Hamamatsu).

F. Immunofluorescence on muscle sections

Transverse 9µ cryosections of TA muscles were washed on a slide by PBS 1X for 3 x 3 min. Permeabilization was done with PBS-Tween 0.2% for 10 min, followed by PBS 1X to rinse the muscle sections. Saturation was done with PBS-Tween 0.1% BSA 5% for 1.5 h, followed by PBS 1X to rinse. Muscle sections were then incubated overnight at 4°C with the primary antibody (1/50 for MTM1 and MTMR2), then washed 3 times with PBS 1X, and incubated 1h with the secondary antibody (1/100 for goat anti-rabbit Alexa 488 and goat anti-mouse Alexa 647). After washings and Hoechst staining, the muscle sections were mounted and observed with an inverted confocal microscope (SP8UV, Leica).

G. Electron microscopy

TA muscles of anesthetized mice were fixed with 4% PFA and 2.5% glutaraldehyde in 0.1 M phosphate buffer (pH 7.2) and processed as described (Cowling et al. 2011). Sections of 70 nm were examined by transmission electron microscopy (TEM) (Morgagni 268D, FEI). Ratio of triads/sarcomere was calculated by dividing number of triad structure identified by the total number of sarcomere present on the section (2 mice per genotype, minimum 10 fibers analyzed per mice, minimum 20 triads per fiber).

H. PtdIns3*P* quantification by ELISA in muscle extracts

PtdIns3*P* Mass ELISAs were performed on lipid extracts from whole tibialis anterior (TA) muscle preparations according to the manufacturer's recommendations and using the PtdIns3*P* Mass ELISA kit (Echelon Biosciences, Salt Lake City, UT). TA muscles from 7 week-old wild-type or *Mtm1* KO mice were weighed, grinded into a powder using a mortar and pestle under liquid nitrogen and then incubated in ice cold 5% TCA to extract lipids. Extracted lipids were resuspended in PBS-T with 3% protein stabilizer and then spotted on PtdIns3*P* Mass ELISA plates in duplicates. PtdIns3*P* levels were detected by measuring

absorbance at 450 nm on a plate reader. Specific amounts were determined by comparison of values to a standard curve generated with known amounts of PtdIns3*P*.

XVI. Statistical analysis

Data are mean ± s.e.m. or ± s.d. as noted in the figure legend. Statistical analysis was performed using 1-way ANOVA followed by Tukey's multiple comparisons test for all data except for expression analysis where an unpaired 2-tailed Student's *t* test was performed. A *P* value less than 0.05 was considered significant.

Bibliography

Bibliography

Agrawal, P.B., Pierson, C.R., Joshi, M., Liu, X., Ravenscroft, G., Moghadaszadeh, B., Talabere, T., Viola, M., Swanson, L.C., Haliloglu, G., Talim, B., Yau, K.S., Allcock, R.J., Laing, N.G., Perrella, M.A., Beggs, A.H., 2014. SPEG Interacts with Myotubularin, and Its Deficiency Causes Centronuclear Myopathy with Dilated Cardiomyopathy. Am. J. Hum. Genet. 95(2), 218-226.

Al-Qusairi, L., Laporte, J., 2011. T-tubule biogenesis and triad formation in skeletal muscle and implication in human diseases. Skeletal muscle 1(1), 26.

Al-Qusairi, L., Weiss, N., Toussaint, A., Berbey, C., Messaddeq, N., Kretz, C., Sanoudou, D., Beggs, A.H., Allard, B., Mandel, J.L., Laporte, J., Jacquemond, V., Buj-Bello, A., 2009. T-tubule disorganization and defective excitation-contraction coupling in muscle fibers lacking myotubularin lipid phosphatase. Proc. Natl. Acad. Sci. U. S. A. 106(44), 18763-18768.

Alazami, A.M., Alzahrani, F., Bohlega, S., Alkuraya, F.S., 2014. SET binding factor 1 (SBF1) mutation causes Charcot-Marie-tooth disease type 4B3. Neurology 82(18), 1665-1666.

Alonso, A., Sasin, J., Bottini, N., Friedberg, I., Friedberg, I., Osterman, A., Godzik, A., Hunter, T., Dixon, J.E., Mustelin, T., 2004. Protein tyrosine phosphatases in the human genome. Cell 117(6), 699-711.

Alter, J., Lou, F., Rabinowitz, A., Yin, H., Rosenfeld, J., Wilton, S.D., Partridge, T.A., Lu, Q.L., 2006. Systemic delivery of morpholino oligonucleotide restores dystrophin expression bodywide and improves dystrophic pathology. Nat. Med. 12(2), 175-177.

Ambler, M.W., Neave, C., Singer, D.B., 1984. X-linked recessive myotubular myopathy: II. Muscle morphology and human myogenesis. Hum.Pathol. 15, 1107-1120.

Amoasii, L., Bertazzi, D.L., Tronchere, H., Hnia, K., Chicanne, G., Rinaldi, B., Cowling, B.S., Ferry, A., Klaholz, B., Payrastre, B., Laporte, J., Friant, S., 2012. Phosphatase-dead myotubularin ameliorates X-linked centronuclear myopathy phenotypes in mice. PLoS Genet 8(10), e1002965.

Antonsson, B.E., 1994. Purification and characterization of phosphatidylinositol synthase from human placenta. Biochem J 297 (Pt 3), 517-522.

Audhya, A., Foti, M., Emr, S.D., 2000. Distinct roles for the yeast phosphatidylinositol 4-kinases, Stt4p and Pik1p, in secretion, cell growth, and organelle membrane dynamics. Mol Biol Cell 11(8), 2673-2689.

Azzedine, H., Bolino, A., Taieb, T., Birouk, N., Di Duca, M., Bouhouche, A., Benamou, S., Mrabet, A., Hammadouche, T., Chkili, T., Gouider, R., Ravazzolo, R., Brice, A., Laporte, J., LeGuern, E., 2003. Mutations in MTMR13, a New Pseudophosphatase Homologue of MTMR2 and Sbf1, in Two Families with an Autosomal Recessive Demyelinating Form of Charcot-Marie-Tooth Disease Associated with Early-Onset Glaucoma. Am. J. Hum. Genet. 72(5), 1141-1153.

Barr, F.A., 2013. Review series: Rab GTPases and membrane identity: causal or inconsequential? J. Cell Biol. 202(2), 191-199.

Barth, P.G., Dubowitz, V., 1998. X-linked myotubular myopathy - a long-term follow-up study. . Eur.J.Paed.Neurol. 1, 49-56.

Beggs, A.H., Bohm, J., Snead, E., Kozlowski, M., Maurer, M., Minor, K., Childers, M.K., Taylor, S.M., Hitte, C., Mickelson, J.R., Guo, L.T., Mizisin, A.P., Buj-Bello, A., Tiret, L., Laporte, J., Shelton, G.D., 2010. MTM1 mutation associated with X-linked myotubular myopathy in Labrador Retrievers. Proc. Natl. Acad. Sci. U. S. A. 107(33), 14697-14702.

Begley, M.J., Dixon, J.E., 2005. The structure and regulation of myotubularin phosphatases. Curr. Opin. Struct. Biol. 15(6), 614-620.

Begley, M.J., Taylor, G.S., Brock, M.A., Ghosh, P., Woods, V.L., Dixon, J.E., 2006. Molecular basis for substrate recognition by MTMR2, a myotubularin family phosphoinositide phosphatase. Proc. Natl. Acad. Sci. U. S. A. 103(4), 927-932.

Begley, M.J., Taylor, G.S., Kim, S.A., Veine, D.M., Dixon, J.E., Stuckey, J.A., 2003. Crystal structure of a phosphoinositide phosphatase, MTMR2: insights into myotubular myopathy and Charcot-Marie-Tooth syndrome. Mol. Cell 12(6), 1391-1402.

Berger, P., Bonneick, S., Willi, S., Wymann, M., Suter, U., 2002. Loss of phosphatase activity in myotubularin-related protein 2 is associated with Charcot-Marie-Tooth disease type 4B1. Hum. Mol. Genet. 11(13), 1569-1579.

Berger, P., Niemann, A., Suter, U., 2006. Schwann cells and the pathogenesis of inherited motor and sensory neuropathies (Charcot-Marie-Tooth disease). Glia 54(4), 243-257.

Berger, P., Schaffitzel, C., Berger, I., Ban, N., Suter, U., 2003. Membrane association of myotubularin-related protein 2 is mediated by a pleckstrin homology-GRAM domain and a coiled-coil dimerization module. Proc. Natl. Acad. Sci. U. S. A. 100(21), 12177-12182.

Berggard, T., Arrigoni, G., Olsson, O., Fex, M., Linse, S., James, P., 2006. 140 mouse brain proteins identified by Ca2+-calmodulin affinity chromatography and tandem mass spectrometry. J. Proteome Res. 5(3), 669-687.

Bertazzi, D.L., De Craene, J.O., Bar, S., Sanjuan-Vazquez, M., Raess, M.A., Friant, S., 2015. [Phosphoinositides: lipidic essential actors in the intracellular traffic]. Biologie aujourd'hui 209(1), 97-109.

Biancalana, V., Caron, O., Gallati, S., Baas, F., Kress, W., Novelli, G., D'Apice, M.R., Lagier-Tourenne, C., Buj-Bello, A., Romero, N.B., Mandel, J.L., 2003. Characterisation of mutations in 77 patients with X-linked myotubular myopathy, including a family with a very mild phenotype. Hum. Genet. 112(2), 135-142.

Biancalana, V., Scheidecker, S., Miguet, M., Laquerriere, A., Romero, N.B., Stojkovic, T., Abath Neto, O., Mercier, S., Voermans, N., Tanner, L., Rogers, C., Ollagnon-Roman, E., Roper, H., Boutte, C., Ben-Shachar, S., Lornage, X., Vasli, N., Schaefer, E., Laforet, P., Pouget, J., Moerman, A., Pasquier, L., Marcorelle, P., Magot, A., Kusters, B., Streichenberger, N., Tranchant, C., Dondaine, N., Schneider, R., Gasnier, C., Calmels, N., Kremer, V., Nguyen, K., Perrier, J., Kamsteeg, E.J., Carlier, P., Carlier, R.Y., Thompson, J., Boland, A., Deleuze, J.F., Fardeau, M., Zanoteli, E., Eymard, B., Laporte, J., 2017. Affected female carriers of MTM1 mutations display a wide spectrum of clinical and pathological involvement: delineating diagnostic clues. Acta Neuropathol.

Bitoun, M., Maugenre, S., Jeannet, P.Y., Lacene, E., Ferrer, X., Laforet, P., Martin, J.J., Laporte, J., Lochmuller, H., Beggs, A.H., Fardeau, M., Eymard, B., Romero, N.B., Guicheney, P., 2005. Mutations in dynamin 2 cause dominant centronuclear myopathy. Nat. Genet. 37(11), 1207-1209.

Blondeau, F., Laporte, J., Bodin, S., Superti-Furga, G., Payrastre, B., Mandel, J.L., 2000. Myotubularin, a phosphatase deficient in myotubular myopathy, acts on phosphatidylinositol 3-kinase and phosphatidylinositol 3-phosphate pathway. Hum. Mol. Genet. 9(15), 2223-2229.

Boal, F., Mansour, R., Gayral, M., Saland, E., Chicanne, G., Xuereb, J.M., Marcellin, M., Burlet-Schiltz, O., Sansonetti, P.J., Payrastre, B., Tronchere, H., 2015. TOM1 is a PI5P effector involved in the regulation of endosomal maturation. J. Cell Sci. 128(4), 815-827.

Bolino, A., Bolis, A., Previtali, S.C., Dina, G., Bussini, S., Dati, G., Amadio, S., Del Carro, U., Mruk, D.D., Feltri, M.L., Cheng, C.Y., Quattrini, A., Wrabetz, L., 2004. Disruption of Mtmr2

produces CMT4B1-like neuropathy with myelin outfolding and impaired spermatogenesis. J. Cell Biol. 167(4), 711-721.

Bolino, A., Lonie, L.J., Zimmer, M., Boerkoel, C.F., Takashima, H., Monaco, A.P., Lupski, J.R., 2001. Denaturing high-performance liquid chromatography of the myotubularin-related 2 gene (MTMR2) in unrelated patients with Charcot-Marie-Tooth disease suggests a low frequency of mutation in inherited neuropathy. Neurogenetics 3(2), 107-109.

Bolino, A., Marigo, V., Ferrera, F., Loader, J., Romio, L., Leoni, A., Di Duca, M., Cinti, R., Cecchi, C., Feltri, M.L., Wrabetz, L., Ravazzolo, R., Monaco, A.P., 2002. Molecular characterization and expression analysis of Mtmr2, mouse homologue of MTMR2, the Myotubularin-related 2 gene, mutated in CMT4B. Gene 283(1-2), 17-26.

Bolino, A., Muglia, M., Conforti, F.L., LeGuern, E., Salih, M.A., Georgiou, D.M., Christodoulou, K., Hausmanowa-Petrusewicz, I., Mandich, P., Schenone, A., Gambardella, A., Bono, F., Quattrone, A., Devoto, M., Monaco, A.P., 2000. Charcot-Marie-Tooth type 4B is caused by mutations in the gene encoding myotubularin-related protein-2. Nat. Genet. 25(1), 17-19.

Bolis, A., Coviello, S., Bussini, S., Dina, G., Pardini, C., Previtali, S.C., Malaguti, M., Morana, P., Del Carro, U., Feltri, M.L., Quattrini, A., Wrabetz, L., Bolino, A., 2005. Loss of Mtmr2 phosphatase in Schwann cells but not in motor neurons causes Charcot-Marie-Tooth type 4B1 neuropathy with myelin outfoldings. J. Neurosci. 25(37), 8567-8577.

Bolis, A., Coviello, S., Visigalli, I., Taveggia, C., Bachi, A., Chishti, A.H., Hanada, T., Quattrini, A., Previtali, S.C., Biffi, A., Bolino, A., 2009. Dlg1, Sec8, and Mtmr2 regulate membrane homeostasis in Schwann cell myelination. J. Neurosci. 29(27), 8858-8870.

Bonangelino, C.J., Nau, J.J., Duex, J.E., Brinkman, M., Wurmser, A.E., Gary, J.D., Emr, S.D., Weisman, L.S., 2002. Osmotic stress-induced increase of phosphatidylinositol 3,5-bisphosphate requires Vac14p, an activator of the lipid kinase Fab1p. J. Cell Biol. 156(6), 1015-1028.

Bong, S.M., Son, K.B., Yang, S.W., Park, J.W., Cho, J.W., Kim, K.T., Kim, H., Kim, S.J., Kim, Y.J., Lee, B.I., 2016. Crystal Structure of Human Myotubularin-Related Protein 1 Provides Insight into the Structural Basis of Substrate Specificity. PloS one 11(3), e0152611.

Bonneick, S., Boentert, M., Berger, P., Atanasoski, S., Mantei, N., Wessig, C., Toyka, K.V., Young, P., Suter, U., 2005. An animal model for Charcot-Marie-Tooth disease type 4B1. Hum. Mol. Genet. 14(23), 3685-3695.

Bremmer-Bout, M., Aartsma-Rus, A., de Meijer, E.J., Kaman, W.E., Janson, A.A., Vossen, R.H., van Ommen, G.J., den Dunnen, J.T., van Deutekom, J.C., 2004. Targeted exon skipping in transgenic hDMD mice: A model for direct preclinical screening of human-specific antisense oligonucleotides. Molecular therapy : the journal of the American Society of Gene Therapy 10(2), 232-240.

Buj-Bello, A., Fougerousse, F., Schwab, Y., Messaddeq, N., Spehner, D., Pierson, C.R., Durand, M., Kretz, C., Danos, O., Douar, A.M., Beggs, A.H., Schultz, P., Montus, M., Denefle, P., Mandel, J.L., 2008. AAV-mediated intramuscular delivery of myotubularin corrects the myotubular myopathy phenotype in targeted murine muscle and suggests a function in plasma membrane homeostasis. Hum. Mol. Genet. 17(14), 2132-2143.

Buj-Bello, A., Furling, D., Tronchere, H., Laporte, J., Lerouge, T., Butler-Browne, G.S., Mandel, J.L., 2002a. Muscle-specific alternative splicing of myotubularin-related 1 gene is impaired in DM1 muscle cells. Hum. Mol. Genet. 11(19), 2297-2307.

Buj-Bello, A., Laugel, V., Messaddeq, N., Zahreddine, H., Laporte, J., Pellissier, J.F., Mandel, J.L., 2002b. The lipid phosphatase myotubularin is essential for skeletal muscle maintenance but not for myogenesis in mice. Proc. Natl. Acad. Sci. U. S. A. 99(23), 15060-15065.

Bulley, S.J., Clarke, J.H., Droubi, A., Giudici, M.L., Irvine, R.F., 2015. Exploring phosphatidylinositol 5-phosphate 4-kinase function. Advances in biological regulation 57, 193-202.

Byrne, L.J., O'Callaghan, K.J., Tuite, M.F., 2005. Heterologous gene expression in yeast. Methods Mol. Biol. 308, 51-64.

Calkhoven, C.F., Bouwman, P.R., Snippe, L., Ab, G., 1994. Translation start site multiplicity of the CCAAT/enhancer binding protein alpha mRNA is dictated by a small 5' open reading frame. Nucleic Acids Res. 22(25), 5540-5547.

Cao, C., Backer, J.M., Laporte, J., Bedrick, E.J., Wandinger-Ness, A., 2008. Sequential actions of myotubularin lipid phosphatases regulate endosomal PI(3)P and growth factor receptor trafficking. Mol. Biol. Cell 19(8), 3334-3346.

Cao, C., Laporte, J., Backer, J.M., Wandinger-Ness, A., Stein, M.P., 2007. Myotubularin lipid phosphatase binds the hVPS15/hVPS34 lipid kinase complex on endosomes. Traffic 8(8), 1052-1067.

Ceyhan-Birsoy, O., Agrawal, P.B., Hidalgo, C., Schmitz-Abe, K., DeChene, E.T., Swanson, L.C., Soemedi, R., Vasli, N., Iannaccone, S.T., Shieh, P.B., Shur, N., Dennison, J.M., Lawlor, M.W., Laporte, J., Markianos, K., Fairbrother, W.G., Granzier, H., Beggs, A.H., 2013. Recessive truncating titin gene, TTN, mutations presenting as centronuclear myopathy. Neurology 81(14), 1205-1214.

Childers, M.K., Joubert, R., Poulard, K., Moal, C., Grange, R.W., Doering, J.A., Lawlor, M.W., Rider, B.E., Jamet, T., Daniele, N., Martin, S., Riviere, C., Soker, T., Hammer, C., Van Wittenberghe, L., Lockard, M., Guan, X., Goddard, M., Mitchell, E., Barber, J., Williams, J.K., Mack, D.L., Furth, M.E., Vignaud, A., Masurier, C., Mavilio, F., Moullier, P., Beggs, A.H., Buj-Bello, A., 2014. Gene therapy prolongs survival and restores function in murine and canine models of myotubular myopathy. Sci Transl Med 6(220), 220ra210.

Choudhury, P., Srivastava, S., Li, Z., Ko, K., Albaqumi, M., Narayan, K., Coetzee, W.A., Lemmon, M.A., Skolnik, E.Y., 2006. Specificity of the myotubularin family of phosphatidylinositol-3-phosphatase is determined by the PH/GRAM domain. J. Biol. Chem. 281(42), 31762-31769.

Chow, C.Y., Landers, J.E., Bergren, S.K., Sapp, P.C., Grant, A.E., Jones, J.M., Everett, L., Lenk, G.M., McKenna-Yasek, D.M., Weisman, L.S., Figlewicz, D., Brown, R.H., Meisler, M.H., 2009. Deleterious variants of FIG4, a phosphoinositide phosphatase, in patients with ALS. Am J Hum Genet 84(1), 85-88.

Chow, C.Y., Zhang, Y., Dowling, J.J., Jin, N., Adamska, M., Shiga, K., Szigeti, K., Shy, M.E., Li, J., Zhang, X., Lupski, J.R., Weisman, L.S., Meisler, M.H., 2007. Mutation of FIG4 causes neurodegeneration in the pale tremor mouse and patients with CMT4J. Nature 448(7149), 68-72.

Coers, C., Telerman-Toppet, N., Gerard, J.M., Szliwowski, H., Bethlem, J., van Wijngaarden, G.K., 1976. Changes in motor innervation and histochemical pattern of muscle fibers in some congenital myopathies. Neurology 26(11), 1046-1053.

Cooke, F.T., Dove, S.K., McEwen, R.K., Painter, G., Holmes, A.B., Hall, M.N., Michell, R.H., Parker, P.J., 1998. The stress-activated phosphatidylinositol 3-phosphate 5-kinase Fab1p is essential for vacuole function in S. cerevisiae. Curr. Biol. 8(22), 1219-1222.

Cowling, B.S., Chevremont, T., Prokic, I., Kretz, C., Ferry, A., Coirault, C., Koutsopoulos, O., Laugel, V., Romero, N.B., Laporte, J., 2014. Reducing dynamin 2 expression rescues X-linked centronuclear myopathy. J Clin Invest 124(3), 1350-1363.

Cui, X., De Vivo, I., Slany, R., Miyamoto, A., Firestein, R., Cleary, M.L., 1998. Association of SET domain and myotubularin-related proteins modulates growth control. Nat. Genet. 18(4), 331-337.

Das, S., Dowling, J., Pierson, C.R., 1993. X-Linked Centronuclear Myopathy, in: Pagon, R.A., Adam, M.P., Ardinger, H.H., Wallace, S.E., Amemiya, A., Bean, L.J.H., Bird, T.D., Ledbetter, N., Mefford, H.C., Smith, R.J.H., Stephens, K. (Eds.), GeneReviews(R). Seattle (WA).

De Craene, J.O., Bertazzi, D.L., Bar, S., Friant, S., 2017. Phosphoinositides, Major Actors in Membrane Trafficking and Lipid Signaling Pathways. International journal of molecular sciences 18(3).

de Gouyon, B.M., Zhao, W., Laporte, J., Mandel, J.L., Metzenberg, A., Herman, G.E., 1997. Characterization of mutations in the myotubularin gene in twenty six patients with X-linked myotubular myopathy. Hum. Mol. Genet. 6(9), 1499-1504.

De Matteis, M., Godi, A., Corda, D., 2002. Phosphoinositides and the golgi complex. Curr Opin Cell Biol 14(4), 434-447.

Di Paolo, G., De Camilli, P., 2006. Phosphoinositides in cell regulation and membrane dynamics. Nature 443(7112), 651-657.

Doerks, T., Strauss, M., Brendel, M., Bork, P., 2000. GRAM, a novel domain in glucosyltransferases, myotubularins and other putative membrane-associated proteins. Trends Biochem. Sci. 25(10), 483-485.

Dove, S.K., Cooke, F.T., Douglas, M.R., Sayers, L.G., Parker, P.J., Michell, R.H., 1997. Osmotic stress activates phosphatidylinositol-3,5-bisphosphate synthesis. Nature 390(6656), 187-192.

Dowling, J.J., Joubert, R., Low, S.E., Durban, A.N., Messaddeq, N., Li, X., Dulin-Smith, A.N., Snyder, A.D., Marshall, M.L., Marshall, J.T., Beggs, A.H., Buj-Bello, A., Pierson, C.R., 2012. Myotubular myopathy and the neuromuscular junction: a novel therapeutic approach from mouse models. Dis Model Mech 5(6), 852-859.

Dowling, J.J., Vreede, A.P., Low, S.E., Gibbs, E.M., Kuwada, J.Y., Bonnemann, C.G., Feldman, E.L., 2009. Loss of myotubularin function results in T-tubule disorganization in zebrafish and human myotubular myopathy. PLoS Genet 5(2), e1000372.

Duex, J.E., Nau, J.J., Kauffman, E.J., Weisman, L.S., 2006a. Phosphoinositide 5-phosphatase Fig 4p is required for both acute rise and subsequent fall in stress-induced phosphatidylinositol 3,5-bisphosphate levels. Eukaryot. Cell 5(4), 723-731.

Duex, J.E., Tang, F., Weisman, L.S., 2006b. The Vac14p-Fig4p complex acts independently of Vac7p and couples PI3,5P2 synthesis and turnover. J. Cell Biol. 172(5), 693-704.

Dupin, I., Sakamoto, Y., Etienne-Manneville, S., 2011. Cytoplasmic intermediate filaments mediate actin-driven positioning of the nucleus. J. Cell Sci. 124(Pt 6), 865-872.

Efe, J.A., Botelho, R.J., Emr, S.D., 2007. Atg18 regulates organelle morphology and Fab1 kinase activity independent of its membrane recruitment by phosphatidylinositol 3,5-bisphosphate. Mol Biol Cell 18(11), 4232-4244.

Eugster, A., Pecheur, E.I., Michel, F., Winsor, B., Letourneur, F., Friant, S., 2004. Ent5p is required with Ent3p and Vps27p for ubiquitin-dependent protein sorting into the multivesicular body. Mol Biol Cell 15(7), 3031-3041.

Fabre, S., Reynaud, C., Jalinot, P., 2000. Identification of functional PDZ domain binding sites in several human proteins. Mol. Biol. Rep. 27(4), 217-224.

Fetalvero, K.M., Yu, Y., Goetschkes, M., Liang, G., Valdez, R.A., Gould, T., Triantafellow, E., Bergling, S., Loureiro, J., Eash, J., Lin, V., Porter, J.A., Finan, P.M., Walsh, K., Yang, Y.,

Mao, X., Murphy, L.O., 2013. Defective autophagy and mTORC1 signaling in myotubularin null mice. Mol. Cell. Biol. 33(1), 98-110.

Fidzianska, A., Warlo, I., Goebel, H.H., 1994. Neonatal centronuclear myopathy with N-CAM decorated myotubes. Neuropediatrics 25(3), 158-161.

Firestein, R., Cui, X., Huie, P., Cleary, M.L., 2000. Set domain-dependent regulation of transcriptional silencing and growth control by SUV39H1, a mammalian ortholog of Drosophila Su(var)3-9. Mol. Cell. Biol. 20(13), 4900-4909.

Firestein, R., Nagy, P.L., Daly, M., Huie, P., Conti, M., Cleary, M.L., 2002. Male infertility, impaired spermatogenesis, and azoospermia in mice deficient for the pseudophosphatase Sbf1. J Clin Invest 109(9), 1165-1172.

Franklin, N.E., Bonham, C.A., Xhabija, B., Vacratsis, P.O., 2013. Differential phosphorylation of the phosphoinositide 3-phosphatase MTMR2 regulates its association with early endosomal subtypes. J. Cell Sci. 126(Pt 6), 1333-1344.

Franklin, N.E., Taylor, G.S., Vacratsis, P.O., 2011. Endosomal targeting of the phosphoinositide 3-phosphatase MTMR2 is regulated by an N-terminal phosphorylation site. J. Biol. Chem. 286(18), 15841-15853.

Friant, S., Pecheur, E.I., Eugster, A., Michel, F., Lefkir, Y., Nourrisson, D., Letourneur, F., 2003. Ent3p Is a PtdIns(3,5)P2 effector required for protein sorting to the multivesicular body. Dev Cell 5(3), 499-511.

Gary, J.D., Sato, T.K., Stefan, C.J., Bonangelino, C.J., Weisman, L.S., Emr, S.D., 2002. Regulation of Fab1 phosphatidylinositol 3-phosphate 5-kinase pathway by Vac7 protein and Fig4, a polyphosphoinositide phosphatase family member. Mol. Biol. Cell 13(4), 1238-1251.

Gayathri, N., Das, S., Vasanth, A., Devi, M.G., Ramamohan, Y., Santosh, V., Yasha, T.C., Shankar, S.K., 2000. Centronuclear myopathy--morphological relation to developing human skeletal muscle: a clinicopathological evaluation. Neurology India 48(1), 19-28.

Gillooly, D.J., Morrow, I.C., Lindsay, M., Gould, R., Bryant, N.J., Gaullier, J.M., Parton, R.G., Stenmark, H., 2000. Localization of phosphatidylinositol 3-phosphate in yeast and mammalian cells. Embo J 19(17), 4577-4588.

Giudici, M.L., Clarke, J.H., Irvine, R.F., 2016. Phosphatidylinositol 5-phosphate 4-kinase gamma (PI5P4Kgamma), a lipid signalling enigma. Advances in biological regulation 61, 47-50.

Goldfarb, L.G., Park, K.Y., Cervenakova, L., Gorokhova, S., Lee, H.S., Vasconcelos, O., Nagle, J.W., Semino-Mora, C., Sivakumar, K., Dalakas, M.C., 1998. Missense mutations in desmin associated with familial cardiac and skeletal myopathy. Nat. Genet. 19(4), 402-403.

Gozani, O., Karuman, P., Jones, D.R., Ivanov, D., Cha, J., Lugovskoy, A.A., Baird, C.L., Zhu, H., Field, S.J., Lessnick, S.L., Villasenor, J., Mehrotra, B., Chen, J., Rao, V.R., Brugge, J.S., Ferguson, C.G., Payrastre, B., Myszka, D.G., Cantley, L.C., Wagner, G., Divecha, N., Prestwich, G.D., Yuan, J., 2003a. The PHD Finger of the Chromatin-Associated Protein ING2 Functions as a Nuclear Phosphoinositide Receptor. Cell 114, 99-111.

Gozani, O., Karuman, P., Jones, D.R., Ivanov, D., Cha, J., Lugovskoy, A.A., Baird, C.L., Zhu, H., Field, S.J., Lessnick, S.L., Villasenor, J., Mehrotra, B., Chen, J., Rao, V.R., Brugge, J.S., Ferguson, C.G., Payrastre, B., Myszka, D.G., Cantley, L.C., Wagner, G., Divecha, N., Prestwich, G.D., Yuan, J., 2003b. The PHD finger of the chromatin-associated protein ING2 functions as a nuclear phosphoinositide receptor. Cell 114(1), 99-111.

Grogan, P.M., Tanner, S.M., Orstavik, K.H., Knudsen, G.P., Saperstein, D.S., Vogel, H., Barohn, R.J., Herbelin, L.L., McVey, A.L., Katz, J.S., 2005. Myopathy with skeletal asymmetry and hemidiaphragm elevation is caused by myotubularin mutations. Neurology 64(9), 1638-1640.

Gruenberg, J., Stenmark, H., 2004. The biogenesis of multivesicular endosomes. Nat. Rev. Mol. Cell Biol. 5(4), 317-323.

GTEx_consortium, 2015. Human genomics. The Genotype-Tissue Expression (GTEx) pilot analysis: multitissue gene regulation in humans. Science 348(6235), 648-660.

Guittard, G., Gerard, A., Dupuis-Coronas, S., Tronchere, H., Mortier, E., Favre, C., Olive, D., Zimmermann, P., Payrastre, B., Nunes, J.A., 2009. Cutting edge: Dok-1 and Dok-2 adaptor molecules are regulated by phosphatidylinositol 5-phosphate production in T cells. J. Immunol. 182(7), 3974-3978.

Guo, S., Stolz, L.E., Lemrow, S.M., York, J.D., 1999. SAC1-like domains of yeast SAC1, INP52, and INP53 and of human synaptojanin encode polyphosphoinositide phosphatases. J. Biol. Chem. 274(19), 12990-12995.

Gupta, V.A., Hnia, K., Smith, L.L., Gundry, S.R., McIntire, J.E., Shimazu, J., Bass, J.R., Talbot, E.A., Amoasii, L., Goldman, N.E., Laporte, J., Beggs, A.H., 2013. Loss of catalytically inactive lipid phosphatase myotubularin-related protein 12 impairs myotubularin stability and promotes centronuclear myopathy in zebrafish. PLoS Genet 9(6), e1003583.

Hammans, S.R., Robinson, D.O., Moutou, C., Kennedy, C.R., Dennis, N.R., Hughes, P.J., Ellison, D.W., 2000. A clinical and genetic study of a manifesting heterozygote with X-linked myotubular myopathy. Neuromuscular disorders : NMD 10(2), 133-137.

Heckmatt, J.Z., Sewry, C.A., Hodes, D., Dubowitz, V., 1985. Congenital centronuclear (myotubular) myopathy: a clinical, pathological and genetic study in eight children. Brain 108, 941-964.

Helliwell, T.R., Ellis, I.H., Appleton, R.E., 1998. Myotubular myopathy: morphological, immunohistochemical and clinical variation. Neuromuscular disorders : NMD 8(3-4), 152-161.

Henderson, M., De Waele, L., Hudson, J., Eagle, M., Sewry, C., Marsh, J., Charlton, R., He, L., Blakely, E.L., Horrocks, I., Stewart, W., Taylor, R.W., Longman, C., Bushby, K., Barresi, R., 2013. Recessive desmin-null muscular dystrophy with central nuclei and mitochondrial abnormalities. Acta Neuropathol. 125(6), 917-919.

Henne, W.M., Buchkovich, N.J., Emr, S.D., 2011. The ESCRT pathway. Dev Cell 21(1), 77-91.

Herman, G.E., Finegold, M., Zhao, W., de Gouyon, B., Metzenberg, A., 1999. Medical complications in long-term survivors with X-linked myotubular myopathy. J. Pediatr. 134(2), 206-214.

Herman, G.E., Kopacz, K., Zhao, W., Mills, P.L., Metzenberg, A., Das, S., 2002. Characterization of mutations in fifty North American patients with X- linked myotubular myopathy. Hum. Mutat. 19(2), 114-121.

Herman, P.K., Emr, S.D., 1990. Characterization of VPS34, a gene required for vacuolar protein sorting and vacuole segregation in Saccharomyces cerevisiae. Mol. Cell. Biol. 10(12), 6742-6754.

Hnia, K., Tronchere, H., Tomczak, K.K., Amoasii, L., Schultz, P., Beggs, A.H., Payrastre, B., Mandel, J.L., Laporte, J., 2011. Myotubularin controls desmin intermediate filament architecture and mitochondrial dynamics in human and mouse skeletal muscle. J Clin Invest 121(1), 70-85.

Hoffjan, S., Thiels, C., Vorgerd, M., Neuen-Jacob, E., Epplen, J.T., Kress, W., 2006. Extreme phenotypic variability in a German family with X-linked myotubular myopathy associated with E404K mutation in MTM1. Neuromuscular disorders : NMD 16(11), 749-753.

Holz, C., Prinz, B., Bolotina, N., Sievert, V., Bussow, K., Simon, B., Stahl, U., Lang, C., 2003. Establishing the yeast Saccharomyces cerevisiae as a system for expression of human proteins on a proteome-scale. J. Struct. Funct. Genomics 4(2-3), 97-108.

Hotta, K., Kitamoto, T., Kitamoto, A., Mizusawa, S., Matsuo, T., Nakata, Y., Kamohara, S., Miyatake, N., Kotani, K., Komatsu, R., Itoh, N., Mineo, I., Wada, J., Yoneda, M., Nakajima, A., Funahashi, T., Miyazaki, S., Tokunaga, K., Masuzaki, H., Ueno, T., Hamaguchi, K., Tanaka, K., Yamada, K., Hanafusa, T., Oikawa, S., Yoshimatsu, H., Sakata, T., Matsuzawa, Y., Nakao, K., Sekine, A., 2011. Association of variations in the FTO, SCG3 and MTMR9 genes with metabolic syndrome in a Japanese population. J. Hum. Genet. 56(9), 647-651.

Houlden, H., King, R.H., Wood, N.W., Thomas, P.K., Reilly, M.M., 2001. Mutations in the 5' region of the myotubularin-related protein 2 (MTMR2) gene in autosomal recessive hereditary neuropathy with focally folded myelin. Brain 124(Pt 5), 907-915.

Hu, J., Prinz, W.A., Rapoport, T.A., 2011. Weaving the Web of ER Tubules. Cell 147(6), 1226-1231.

Huttlin, E.L., Jedrychowski, M.P., Elias, J.E., Goswami, T., Rad, R., Beausoleil, S.A., Villen, J., Haas, W., Sowa, M.E., Gygi, S.P., 2010. A tissue-specific atlas of mouse protein phosphorylation and expression. Cell 143(7), 1174-1189.

Ikonomov, O.C., Sbrissa, D., Delvecchio, K., Xie, Y., Jin, J.P., Rappolee, D., Shisheva, A., 2011. The phosphoinositide kinase PIKfyve is vital in early embryonic development: preimplantation lethality of PIKfyve-/- embryos but normality of PIKfyve+/- mice. J Biol Chem 286(15), 13404-13413.

Ikonomov, O.C., Sbrissa, D., Fligger, J., Delvecchio, K., Shisheva, A., 2010. ArPIKfyve regulates Sac3 protein abundance and turnover: disruption of the mechanism by Sac3I41T mutation causing Charcot-Marie-Tooth 4J disorder. J Biol Chem 285(35), 26760-26764.

Itoh, T., Takenawa, T., 2002. Phosphoinositide-binding domains: Functional units for temporal and spatial regulation of intracellular signalling. Cell. Signal. 14(9), 733-743.

Janota, C.S., Calero-Cuenca, F.J., Costa, J., Gomes, E.R., 2017. SnapShot: Nucleo-cytoskeletal Interactions. Cell 169(5), 970-970 e971.

Jean, S., Cox, S., Schmidt, E.J., Robinson, F.L., Kiger, A., 2012. Sbf/MTMR13 coordinates PI(3)P and Rab21 regulation in endocytic control of cellular remodeling. Mol. Biol. Cell 23(14), 2723-2740.

Jin, N., Chow, C.Y., Liu, L., Zolov, S.N., Bronson, R., Davisson, M., Petersen, J.L., Zhang, Y., Park, S., Duex, J.E., Goldowitz, D., Meisler, M.H., Weisman, L.S., 2008. VAC14 nucleates a protein complex essential for the acute interconversion of PI3P and PI(3,5)P(2) in yeast and mouse. EMBO J 27(24), 3221-3234.

Joubert, O., Nehme, R., Bidet, M., Mus-Veteau, I., 2010. Heterologous expression of human membrane receptors in the yeast Saccharomyces cerevisiae. Methods Mol. Biol. 601, 87-103.

Jungbluth, H., Sewry, C.A., Buj-Bello, A., Kristiansen, M., Orstavik, K.H., Kelsey, A., Manzur, A.Y., Mercuri, E., Wallgren-Pettersson, C., Muntoni, F., 2003. Early and severe presentation of X-linked myotubular myopathy in a girl with skewed X-inactivation. Neuromuscular disorders : NMD 13(1), 55-59.

Jungbluth, H., Wallgren-Pettersson, C., Laporte, J., 2008. Centronuclear (myotubular) myopathy. Orphanet J Rare Dis 3, 26.

Kachroo, A.H., Laurent, J.M., Yellman, C.M., Meyer, A.G., Wilke, C.O., Marcotte, E.M., 2015. Evolution. Systematic humanization of yeast genes reveals conserved functions and genetic modularity. Science 348(6237), 921-925.

Katzmann, D.J., Stefan, C.J., Babst, M., Emr, S.D., 2003. Vps27 recruits ESCRT machinery to endosomes during MVB sorting. J. Cell Biol. 162(3), 413-423.

Ketel, K., Krauss, M., Nicot, A.S., Puchkov, D., Wieffer, M., Muller, R., Subramanian, D., Schultz, C., Laporte, J., Haucke, V., 2016. A phosphoinositide conversion mechanism for exit from endosomes. Nature 529(7586), 408-412.

Keune, W.J., Jones, D.R., Divecha, N., 2013. PtdIns5P and Pin1 in oxidative stress signaling. Advances in biological regulation 53(2), 179-189.

Kihara, A., Noda, T., Ishihara, N., Ohsumi, Y., 2001. Two distinct Vps34 phosphatidylinositol 3-kinase complexes function in autophagy and carboxypeptidase Y sorting in Saccharomyces cerevisiae. J. Cell Biol. 152(3), 519-530.

Kim, S.A., Taylor, G.S., Torgersen, K.M., Dixon, J.E., 2002. Myotubularin and MTMR2, phosphatidylinositol 3-phosphatases mutated in myotubular myopathy and type 4B Charcot-Marie-Tooth disease. J. Biol. Chem. 277(6), 4526-4531.

Kim, S.A., Vacratsis, P.O., Firestein, R., Cleary, M.L., Dixon, J.E., 2003. Regulation of myotubularin-related (MTMR)2 phosphatidylinositol phosphatase by MTMR5, a catalytically inactive phosphatase. Proc. Natl. Acad. Sci. U. S. A. 100(8), 4492-4497.

Kornberg, R.D., McConnell, H.M., 1971. Lateral diffusion of phospholipids in a vesicle membrane. Proc Natl Acad Sci U S A 68(10), 2564-2568.

Kozak, M., 1995. Adherence to the first-AUG rule when a second AUG codon follows closely upon the first. Proc. Natl. Acad. Sci. U. S. A. 92(7), 2662-2666.

Kristiansen, M., Knudsen, G.P., Tanner, S.M., McEntagart, M., Jungbluth, H., Muntoni, F., Sewry, C., Gallati, S., Orstavik, K.H., Wallgren-Pettersson, C., 2003. X-inactivation patterns in carriers of X-linked myotubular myopathy. Neuromuscular disorders : NMD 13(6), 468-471.

Kutchukian, C., Lo Scrudato, M., Tourneur, Y., Poulard, K., Vignaud, A., Berthier, C., Allard, B., Lawlor, M.W., Buj-Bello, A., Jacquemond, V., 2016. Phosphatidylinositol 3-kinase inhibition restores Ca2+ release defects and prolongs survival in myotubularin-deficient mice. Proc. Natl. Acad. Sci. U. S. A. 113(50), 14432-14437.

Laporte, J., Bedez, F., Bolino, A., Mandel, J.L., 2003. Myotubularins, a large disease-associated family of cooperating catalytically active and inactive phosphoinositides phosphatases. Hum. Mol. Genet. 12 Spec No 2, R285-292.

Laporte, J., Biancalana, V., Tanner, S.M., Kress, W., Schneider, V., Wallgren-Pettersson, C., Herger, F., Buj-Bello, A., Blondeau, F., Liechti-Gallati, S., Mandel, J.L., 2000. MTM1 mutations in X-linked myotubular myopathy. Hum. Mutat. 15(5), 393-409.

Laporte, J., Blondeau, F., Buj-Bello, A., Tentler, D., Kretz, C., Dahl, N., Mandel, J.L., 1998. Characterization of the myotubularin dual specificity phosphatase gene family from yeast to human. Hum. Mol. Genet. 7(11), 1703-1712.

Laporte, J., Hu, L.J., Kretz, C., Mandel, J.L., Kioschis, P., Coy, J.F., Klauck, S.M., Poustka, A., Dahl, N., 1996. A gene mutated in X-linked myotubular myopathy defines a new putative tyrosine phosphatase family conserved in yeast. Nat. Genet. 13(2), 175-182.

Laporte, J., Kress, W., Mandel, J.L., 2001. Diagnosis of X-linked myotubular myopathy by detection of myotubularin. Ann. Neurol. 50(1), 42-46.

Lawlor, M.W., Armstrong, D., Viola, M.G., Widrick, J.J., Meng, H., Grange, R.W., Childers, M.K., Hsu, C.P., O'Callaghan, M., Pierson, C.R., Buj-Bello, A., Beggs, A.H., 2013. Enzyme replacement therapy rescues weakness and improves muscle pathology in mice with X-linked myotubular myopathy. Hum. Mol. Genet. 22(8), 1525-1538.

Lawlor, M.W., Beggs, A.H., Buj-Bello, A., Childers, M.K., Dowling, J.J., James, E.S., Meng, H., Moore, S.A., Prasad, S., Schoser, B., Sewry, C.A., 2016. Skeletal Muscle Pathology in X-Linked Myotubular Myopathy: Review With Cross-Species Comparisons. J. Neuropathol. Exp. Neurol. 75(2), 102-110.

Lawlor, M.W., Viola, M.G., Meng, H., Edelstein, R.V., Liu, F., Yan, K., Luna, E.J., Lerch-Gaggl, A., Hoffmann, R.G., Pierson, C.R., Buj-Bello, A., Lachey, J.L., Pearsall, S., Yang, L., Hillard, C.J., Beggs, A.H., 2014. Differential muscle hypertrophy is associated with satellite cell numbers and Akt pathway activation following activin type IIB receptor inhibition in Mtm1 p.R69C mice. Am. J. Pathol. 184(6), 1831-1842.

Lecompte, O., Poch, O., Laporte, J., 2008. PtdIns5P regulation through evolution: roles in membrane trafficking? Trends Biochem. Sci. 33(10), 453-460.

Lemmon, M.A., 2003. Phosphoinositide recognition domains. Traffic 4(4), 201-213.

Lenk, G.M., Szymanska, K., Debska-Vielhaber, G., Rydzanicz, M., Walczak, A., Bekiesinska-Figatowska, M., Vielhaber, S., Hallmann, K., Stawinski, P., Buehring, S., Hsu, D.A., Kunz, W.S., Meisler, M.H., Ploski, R., 2016. Biallelic Mutations of VAC14 in Pediatric-Onset Neurological Disease. Am J Hum Genet 99(1), 188-194.

Li, X., Tran, K.M., Aziz, K.E., Sorokin, A.V., Chen, J., Wang, W., 2016. Defining the Protein-Protein Interaction Network of the Human Protein Tyrosine Phosphatase Family. Mol. Cell. Proteomics 15(9), 3030-3044.

Lim, H.J., Joo, S., Oh, S.H., Jackson, J.D., Eckman, D.M., Bledsoe, T.M., Pierson, C.R., Childers, M.K., Atala, A., Yoo, J.J., 2015. Syngeneic Myoblast Transplantation Improves Muscle Function in a Murine Model of X-Linked Myotubular Myopathy. Cell Transplant. 24(9), 1887-1900.

Lin, A., Krockmalnic, G., Penman, S., 1990. Imaging cytoskeleton--mitochondrial membrane attachments by embedment-free electron microscopy of saponin-extracted cells. Proc. Natl. Acad. Sci. U. S. A. 87(21), 8565-8569.

Liu, Y., Bankaitis, V.A., 2010. Phosphoinositide phosphatases in cell biology and disease. Prog Lipid Res 49(3), 201-217.

Lorenzo, O., Urbe, S., Clague, M.J., 2006. Systematic analysis of myotubularins: heteromeric interactions, subcellular localisation and endosome related functions. J. Cell Sci. 119(Pt 14), 2953-2959.

Love, D.R., Hill, D.F., Dickson, G., Spurr, N.K., Byth, B.C., Marsden, R.F., Walsh, F.S., Edwards, Y.H., Davies, K.E., 1989. An autosomal transcript in skeletal muscle with homology to dystrophin. Nature 339(6219), 55-58.

Mack, D.L., Poulard, K., Goddard, M.A., Latournerie, V., Snyder, J.M., Grange, R.W., Elverman, M.R., Denard, J., Veron, P., Buscara, L., Le Bec, C., Hogrel, J.Y., Brezovec, A.G., Meng, H., Yang, L., Liu, F., O'Callaghan, M., Gopal, N., Kelly, V.E., Smith, B.K., Strande, J.L., Mavilio, F., Beggs, A.H., Mingozzi, F., Lawlor, M.W., Buj-Bello, A., Childers, M.K., 2017. Systemic AAV8-Mediated Gene Therapy Drives Whole-Body Correction of Myotubular Myopathy in Dogs. Molecular therapy : the journal of the American Society of Gene Therapy 25(4), 839-854.

Marcus, A.J., Ullman, H.L., Safier, L.B., 1969. Lipid composition of subcellular particles of human blood platelets. J Lipid Res 10(1), 108-114.

McEntagart, M., Parsons, G., Buj-Bello, A., Biancalana, V., Fenton, I., Little, M., Krawczak, M., Thomas, N., Herman, G., Clarke, A., Wallgren-Pettersson, C., 2002. Genotype-phenotype correlations in X-linked myotubular myopathy. Neuromuscular disorders : NMD 12(10), 939-946.

Mersiyanova, I.V., Perepelov, A.V., Polyakov, A.V., Sitnikov, V.F., Dadali, E.L., Oparin, R.B., Petrin, A.N., Evgrafov, O.V., 2000. A new variant of Charcot-Marie-Tooth disease type 2 is probably the result of a mutation in the neurofilament-light gene. Am. J. Hum. Genet. 67(1), 37-46.

Mizuno-Yamasaki, E., Medkova, M., Coleman, J., Novick, P., 2010. Phosphatidylinositol 4-phosphate controls both membrane recruitment and a regulatory switch of the Rab GEF Sec2p. Dev Cell 18(5), 828-840.

Mochizuki, Y., Majerus, P.W., 2003. Characterization of myotubularin-related protein 7 and its binding partner, myotubularin-related protein 9. Proc. Natl. Acad. Sci. U.S.A. 100(17), 9768-9773.

Mochizuki, Y., Ohashi, R., Kawamura, T., Iwanari, H., Kodama, T., Naito, M., Hamakubo, T., 2013. Phosphatidylinositol 3-phosphatase myotubularin-related protein 6 (MTMR6) is regulated by small GTPase Rab1B in the early secretory and autophagic pathways. J. Biol. Chem. 288(2), 1009-1021.

Nakano, M., Fukuda, M., Kudo, T., Matsuzaki, N., Azuma, T., Sekine, K., Endo, H., Handa, T., 2009a. Flip-flop of phospholipids in vesicles: kinetic analysis with time-resolved small-angle neutron scattering. J Phys Chem B 113(19), 6745-6748.

Nakano, M., Fukuda, M., Kudo, T., Miyazaki, M., Wada, Y., Matsuzaki, N., Endo, H., Handa, T., 2009b. Static and dynamic properties of phospholipid bilayer nanodiscs. J Am Chem Soc 131(23), 8308-8312.

Nakhro, K., Park, J.M., Hong, Y.B., Park, J.H., Nam, S.H., Yoon, B.R., Yoo, J.H., Koo, H., Jung, S.C., Kim, H.L., Kim, J.Y., Choi, K.G., Choi, B.O., Chung, K.W., 2013. SET binding factor 1 (SBF1) mutation causes Charcot-Marie-Tooth disease type 4B3. Neurology 81(2), 165-173.

Nandurkar, H.H., Caldwell, K.K., Whisstock, J.C., Layton, M.J., Gaudet, E.A., Norris, F.A., Majerus, P.W., Mitchell, C.A., 2001. Characterization of an adapter subunit to a phosphatidylinositol (3)P 3- phosphatase: identification of a myotubularin-related protein lacking catalytic activity. Proc. Natl. Acad. Sci. U. S. A. 98(17), 9499-9504.

Nandurkar, H.H., Huysmans, R., 2002. The myotubularin family: novel phosphoinositide regulators. IUBMB Life 53(1), 37-43.

Nandurkar, H.H., Layton, M., Laporte, J., Selan, C., Corcoran, L., Caldwell, K.K., Mochizuki, Y., Majerus, P.W., Mitchell, C.A., 2003. Identification of myotubularin as the lipid phosphatase catalytic subunit associated with the 3-phosphatase adapter protein, 3-PAP. Proc. Natl. Acad. Sci. U. S. A. 100(15), 8660-8665.

Nicot, A.S., Laporte, J., 2008. Endosomal phosphoinositides and human diseases. Traffic 9(8), 1240-1249.

Nicot, A.S., Toussaint, A., Tosch, V., Kretz, C., Wallgren-Pettersson, C., Iwarsson, E., Kingston, H., Garnier, J.M., Biancalana, V., Oldfors, A., Mandel, J.L., Laporte, J., 2007. Mutations in amphiphysin 2 (BIN1) disrupt interaction with dynamin 2 and cause autosomal recessive centronuclear myopathy. Nat. Genet. 39(9), 1134-1139.

Niebuhr, K., Giuriato, S., Pedron, T., Philpott, D.J., Gaits, F., Sable, J., Sheetz, M.P., Parsot, C., Sansonetti, P.J., Payrastre, B., 2002. Conversion of PtdIns(4,5)P(2) into PtdIns(5)P by the S.flexneri effector IpgD reorganizes host cell morphology. Embo J 21(19), 5069-5078.

Nikawa, J., Yamashita, S., 1984. Molecular cloning of the gene encoding CDPdiacylglycerol-inositol 3-phosphatidyl transferase in Saccharomyces cerevisiae. Eur J Biochem 143(2), 251-256.

Nishino, I., Minami, N., Kobayashi, O., Ikezawa, M., Goto, Y., Arahata, K., Nonaka, I., 1998. MTM1 gene mutations in Japanese patients with the severe infantile form of myotubular myopathy. Neuromuscul.Disord. 8, 453-458.

Odorizzi, G., Babst, M., Emr, S.D., 1998. Fab1p PtdIns(3)P 5-kinase function essential for protein sorting in the multivesicular body. Cell 95(6), 847-858.

Oldfors, A., Kyllerman, M., Wahlstrom, J., Darnfors, C., Henriksson, K.G., 1989. X-linked myotubular myopathy: clinical and pathological findings in a family. Clin.Genet. 36, 5-14.

Oppelt, A., Lobert, V.H., Haglund, K., Mackey, A.M., Rameh, L.E., Liestol, K., Schink, K.O., Pedersen, N.M., Wenzel, E.M., Haugsten, E.M., Brech, A., Rusten, T.E., Stenmark, H., Wesche, J., 2013. Production of phosphatidylinositol 5-phosphate via PIKfyve and MTMR3 regulates cell migration. EMBO Rep 14(1), 57-64.

Panaretou, C., Domin, J., Cockcroft, S., Waterfield, M.D., 1997. Characterization of p150, an adaptor protein for the human phosphatidylinositol (PtdIns) 3-kinase. Substrate presentation by phosphatidylinositol transfer protein to the p150.Ptdins 3-kinase complex. J Biol Chem 272(4), 2477-2485.

Parrish, W.R., Stefan, C.J., Emr, S.D., 2004. Essential role for the myotubularin-related phosphatase Ymr1p and the synaptojanin-like phosphatases Sjl2p and Sjl3p in regulation of phosphatidylinositol 3-phosphate in yeast. Mol Biol Cell 15(8), 3567-3579.

Parrish, W.R., Stefan, C.J., Emr, S.D., 2004. Essential role for the myotubularin-related phosphatase Ymr1p and the synaptojanin-like phosphatases Sjl2p and Sjl3p in regulation of phosphatidylinositol 3-phosphate in yeast. Mol. Biol. Cell 15(8), 3567-3579.

Payrastre, B., Missy, K., Giuriato, S., Bodin, S., Plantavid, M., Gratacap, M., 2001. Phosphoinositides: key players in cell signalling, in time and space. Cell. Signal. 13(6), 377-387.

Penisson-Besnier, I., Biancalana, V., Reynier, P., Cossee, M., Dubas, F., 2007. Diagnosis of myotubular myopathy in the oldest known manifesting female carrier: a clinical and genetic study. Neuromuscular disorders : NMD 17(2), 180-185.

Pierson, C.R., Agrawal, P.B., Blasko, J., Beggs, A.H., 2007. Myofiber size correlates with MTM1 mutation type and outcome in X-linked myotubular myopathy. Neuromuscular disorders : NMD 17(7), 562-568.

Pierson, C.R., Dulin-Smith, A.N., Durban, A.N., Marshall, M.L., Marshall, J.T., Snyder, A.D., Naiyer, N., Gladman, J.T., Chandler, D.S., Lawlor, M.W., Buj-Bello, A., Dowling, J.J., Beggs, A.H., 2012. Modeling the human MTM1 p.R69C mutation in murine Mtm1 results in exon 4 skipping and a less severe myotubular myopathy phenotype. Hum. Mol. Genet. 21(4), 811-825.

Plant, P.J., Correa, J., Goldenberg, N., Bain, J., Batt, J., 2009. The inositol phosphatase MTMR4 is a novel target of the ubiquitin ligase Nedd4. Biochem. J. 419(1), 57-63.

Previtali, S.C., Zerega, B., Sherman, D.L., Brophy, P.J., Dina, G., King, R.H.M., Salih, M.M., Feltri, L., Quattrini, A., Ravazzolo, R., Wrabetz, L., Monaco, A.P., Bolino, A., 2003. Myotubularin-related 2 protein phosphatase and neurofilament light chain protein, both mutated in CMT neuropathies, interact in peripheral nerve. Hum. Mol. Genet. 12(14), 1713-1723.

Quattrone, A., Gambardella, A., Bono, F., Aguglia, U., Bolino, A., Bruni, A.C., Montesi, M.P., Oliveri, R.L., Sabatelli, M., Tamburrini, O., Valentino, P., Van Broeckhoven, C., Zappia, M., 1996. Autosomal recessive hereditary motor and sensory neuropathy with focally folded myelin sheaths: clinical, electrophysiologic, and genetic aspects of a large family. Neurology 46(5), 1318-1324.

Raess, M.A., Friant, S., Cowling, B.S., Laporte, J., 2017. WANTED - Dead or alive: Myotubularins, a large disease-associated protein family. Advances in biological regulation 63, 49-58.

Ralston, E., Lu, Z., Biscocho, N., Soumaka, E., Mavroidis, M., Prats, C., Lomo, T., Capetanaki, Y., Ploug, T., 2006. Blood vessels and desmin control the positioning of nuclei in skeletal muscle fibers. J. Cell. Physiol. 209(3), 874-882.

Rameh, L.E., Tolias, K.F., Duckworth, B.C., Cantley, L.C., 1997. A new pathway for synthesis of phosphatidylinositol-4,5-bisphosphate. Nature 390(6656), 192-196.

Ramel, D., Lagarrigue, F., Pons, V., Mounier, J., Dupuis-Coronas, S., Chicanne, G., Sansonetti, P.J., Gaits-Iacovoni, F., Tronchere, H., Payrastre, B., 2011. Shigella flexneri infection generates the lipid PI5P to alter endocytosis and prevent termination of EGFR signaling. Sci Signal 4(191), ra61.

Robinson, F.L., Dixon, J.E., 2005. The phosphoinositide-3-phosphatase MTMR2 associates with MTMR13, a membrane-associated pseudophosphatase also mutated in type 4B Charcot-Marie-Tooth disease. J. Biol. Chem. 280(36), 31699-31707.

Robinson, F.L., Dixon, J.E., 2006. Myotubularin phosphatases: policing 3-phosphoinositides. Trends Cell Biol. 16(8), 403-412.

Roman, W., Martins, J.P., Carvalho, F.A., Voituriez, R., Abella, J.V.G., Santos, N.C., Cadot, B., Way, M., Gomes, E.R., 2017. Myofibril contraction and crosslinking drive nuclear movement to the periphery of skeletal muscle. Nat. Cell Biol.

Romero, N.B., 2010. Centronuclear myopathies: a widening concept. Neuromuscular disorders : NMD 20(4), 223-228.

Royer, B., Hnia, K., Gavriilidis, C., Tronchere, H., Tosch, V., Laporte, J., 2013. The myotubularin-amphiphysin 2 complex in membrane tubulation and centronuclear myopathies. EMBO Rep. 14(10), 907-915.

Rual, J.F., Venkatesan, K., Hao, T., Hirozane-Kishikawa, T., Dricot, A., Li, N., Berriz, G.F., Gibbons, F.D., Dreze, M., Ayivi-Guedehoussou, N., Klitgord, N., Simon, C., Boxem, M., Milstein, S., Rosenberg, J., Goldberg, D.S., Zhang, L.V., Wong, S.L., Franklin, G., Li, S., Albala, J.S., Lim, J., Fraughton, C., Llamosas, E., Cevik, S., Bex, C., Lamesch, P., Sikorski, R.S., Vandenhaute, J., Zoghbi, H.Y., Smolyar, A., Bosak, S., Sequerra, R., Doucette-Stamm, L., Cusick, M.E., Hill, D.E., Roth, F.P., Vidal, M., 2005. Towards a proteome-scale map of the human protein-protein interaction network. Nature 437(7062), 1173-1178.

Sabha, N., Volpatti, J.R., Gonorazky, H., Reifler, A., Davidson, A.E., Li, X., Eltayeb, N.M., Dall'Armi, C., Di Paolo, G., Brooks, S.V., Buj-Bello, A., Feldman, E.L., Dowling, J.J., 2016. PIK3C2B inhibition improves function and prolongs survival in myotubular myopathy animal models. J Clin Invest 126(9), 3613-3625.

Sanchez-Juan, P., Bishop, M.T., Aulchenko, Y.S., Brandel, J.P., Rivadeneira, F., Struchalin, M., Lambert, J.C., Amouyel, P., Combarros, O., Sainz, J., Carracedo, A., Uitterlinden, A.G., Hofman, A., Zerr, I., Kretzschmar, H.A., Laplanche, J.L., Knight, R.S., Will, R.G., van Duijn, C.M., 2012. Genome-wide study links MTMR7 gene to variant Creutzfeldt-Jakob risk. Neurobiol. Aging 33(7), 1487 e1421-1488.

Saporta, A.S., Sottile, S.L., Miller, L.J., Feely, S.M., Siskind, C.E., Shy, M.E., 2011. Charcot-Marie-Tooth disease subtypes and genetic testing strategies. Ann. Neurol. 69(1), 22-33.

Sarnat, H.B., Roth, S.I., Jimenez, J.F., 1981. Neonatal myotubular myopathy: neuropathy and failure of postnatal maturation of fetal muscle. Can.J.Neurol.Sci. 8, 313-320.

Sbrissa, D., Ikonomov, O.C., Deeb, R., Shisheva, A., 2002. Phosphatidylinositol 5-phosphate biosynthesis is linked to PIKfyve and is involved in osmotic response pathway in mammalian cells. J. Biol. Chem. 277(49), 47276-47284.

Schaletzky, J., Dove, S.K., Short, B., Lorenzo, O., Clague, M.J., Barr, F.A., 2003. Phosphatidylinositol-5-phosphate activation and conserved substrate specificity of the myotubularin phosphatidylinositol 3-phosphatases. Curr. Biol. 13(6), 504-509.

Schara, U., Kress, W., Tucke, J., Mortier, W., 2003. X-linked myotubular myopathy in a female infant caused by a new MTM1 gene mutation. Neurology 60(8), 1363-1365.

Schu, P.V., Takegawa, K., Fry, M.J., Stack, J.H., Waterfield, M.D., Emr, S.D., 1993. Phosphatidylinositol 3-kinase encoded by yeast VPS34 gene essential for protein sorting. Science 260(5104), 88-91.

Senderek, J., Bergmann, C., Weber, S., Ketelsen, U.P., Schorle, H., Rudnik-Schoneborn, S., Buttner, R., Buchheim, E., Zerres, K., 2003. Mutation of the SBF2 gene, encoding a novel member of the myotubularin family, in Charcot-Marie-Tooth neuropathy type 4B2/11p15. Hum. Mol. Genet. 12(3), 349-356.

Shelton, G.D., Rider, B.E., Child, G., Tzannes, S., Guo, L.T., Moghadaszadeh, B., Troiano, E.C., Haase, B., Wade, C.M., Beggs, A.H., 2015. X-linked myotubular myopathy in Rottweiler dogs is caused by a missense mutation in Exon 11 of the MTM1 gene. Skeletal muscle 5(1), 1.

Shisheva, A., 2008. PIKfyve: Partners, significance, debates and paradoxes. Cell Biol. Int. 32(6), 591-604.

Silver, M.M., Gilbert, J.J., Stewart, S., Brabyn, D., Jung, J., 1986. Morphologic and morphometric analysis of muscle in X-linked myotubular myopathy. Hum.Pathol. 17, 1167-1178.

Slessareva, J.E., Routt, S.M., Temple, B., Bankaitis, V.A., Dohlman, H.G., 2006. Activation of the phosphatidylinositol 3-kinase Vps34 by a G protein alpha subunit at the endosome. Cell 126(1), 191-203.

Song, H.O., Lee, J., Ji, Y.J., Dwivedi, M., Cho, J.H., Park, B.J., Ahnn, J., 2010. Calcineurin regulates coelomocyte endocytosis via DYN-1 and CUP-4 in Caenorhabditis elegans. Mol. Cells 30(3), 255-262.

Spector, A.A., Yorek, M.A., 1985. Membrane lipid composition and cellular function. J. Lipid Res. 26(9), 1015-1035.

Spiegelhalter, C., Laporte, J.F., Schwab, Y., 2014. Correlative light and electron microscopy: from live cell dynamic to 3D ultrastructure. Methods Mol. Biol. 1117, 485-501.

Spiro, A.J., Shy, G.M., Gonatas, N.K., 1966. Myotubular myopathy. Persistence of fetal muscle in an adolescent boy. Arch. Neurol. 14(1), 1-14.

Srivastava, S., Li, Z., Lin, L., Liu, G., Ko, K., Coetzee, W.A., Skolnik, E.Y., 2005. The phosphatidylinositol 3-phosphate phosphatase myotubularin- related protein 6 (MTMR6) is a negative regulator of the Ca2+-activated K+ channel KCa3.1. Mol. Cell. Biol. 25(9), 3630-3638.

Staiano, L., De Leo, M.G., Persico, M., De Matteis, M.A., 2015. Mendelian disorders of PI metabolizing enzymes. Biochim. Biophys. Acta 1851(6), 867-881.

Sutton, I.J., Winer, J.B., Norman, A.N., Liechti-Gallati, S., MacDonald, F., 2001. Limb girdle and facial weakness in female carriers of X-linked myotubular myopathy mutations. Neurology 57(5), 900-902.

Tanner, S.M., Orstavik, K.H., Kristiansen, M., Lev, D., Lerman-Sagie, T., Sadeh, M., Liechti-Gallati, S., 1999a. Skewed X-inactivation in a manifesting carrier of X-linked myotubular myopathy and in her non-manifesting carrier mother. Hum. Genet. 104(3), 249-253.

Tanner, S.M., Schneider, V., Thomas, N.S., Clarke, A., Lazarou, L., Liechti-Gallati, S., 1999b. Characterization of 34 novel and six known MTM1 gene mutations in 47 unrelated X-linked myotubular myopathy patients. Neuromuscular disorders : NMD 9(1), 41-49.

Tasfaout, H., Buono, S., Guo, S., Kretz, C., Messaddeq, N., Booten, S., Greenlee, S., Monia, B.P., Cowling, B.S., Laporte, J., 2017. Antisense oligonucleotide-mediated Dnm2 knockdown prevents and reverts myotubular myopathy in mice. Nature communications 8, 15661.

Taylor, G.S., Maehama, T., Dixon, J.E., 2000. Inaugural article: myotubularin, a protein tyrosine phosphatase mutated in myotubular myopathy, dephosphorylates the lipid second messenger, phosphatidylinositol 3-phosphate. Proc. Natl. Acad. Sci. U. S. A. 97(16), 8910-8915.

Thomas, N.S., Williams, H., Cole, G., Roberts, K., Clarke, A., Liechti-Gallati, S., Braga, S., Gerber, A., Meier, C., Moser, H., et al, 1990. X linked neonatal centronuclear/myotubular myopathy: evidence for linkage to Xq28 DNA marker loci. J.Med.Genet. 27, 284-287.

Tinsley, J.M., Fairclough, R.J., Storer, R., Wilkes, F.J., Potter, A.C., Squire, S.E., Powell, D.S., Cozzoli, A., Capogrosso, R.F., Lambert, A., Wilson, F.X., Wren, S.P., De Luca, A., Davies, K.E., 2011. Daily treatment with SMTC1100, a novel small molecule utrophin upregulator, dramatically reduces the dystrophic symptoms in the mdx mouse. PloS one 6(5), e19189.

Tosch, V., Rohde, H.M., Tronchere, H., Zanoteli, E., Monroy, N., Kretz, C., Dondaine, N., Payrastre, B., Mandel, J.L., Laporte, J., 2006. A novel PtdIns3P and PtdIns(3,5)P2 phosphatase with an inactivating variant in centronuclear myopathy. Hum. Mol. Genet. 15(21), 3098-3106.

Toussaint, A., Cowling, B.S., Hnia, K., Mohr, M., Oldfors, A., Schwab, Y., Yis, U., Maisonobe, T., Stojkovic, T., Wallgren-Pettersson, C., Laugel, V., Echaniz-Laguna, A., Mandel, J.L., Nishino, I., Laporte, J., 2011. Defects in amphiphysin 2 (BIN1) and triads in several forms of centronuclear myopathies. Acta Neuropathol. 121(2), 253-266.

Trevelyan, W.E., 1966. Preparation of phosphatidyl inositol from baker's yeast. J Lipid Res 7(3), 445-447.

Tronchere, H., Laporte, J., Pendaries, C., Chaussade, C., Liaubet, L., Pirola, L., Mandel, J.L., Payrastre, B., 2004. Production of phosphatidylinositol 5-phosphate by the phosphoinositide 3-phosphatase myotubularin in mammalian cells. J. Biol. Chem. 279(8), 7304-7312.

Tsai, T.C., Horinouchi, H., Noguchi, S., Minami, N., Murayama, K., Hayashi, Y.K., Nonaka, I., Nishino, I., 2005. Characterization of MTM1 mutations in 31 Japanese families with myotubular myopathy, including a patient carrying 240 kb deletion in Xq28 without male hypogenitalism. Neuromuscular disorders : NMD 15, 245-252.

Tsujita, K., Itoh, T., Ijuin, T., Yamamoto, A., Shisheva, A., Laporte, J., Takenawa, T., 2004. Myotubularin regulates the function of the late endosome through the gram domain-phosphatidylinositol 3,5-bisphosphate interaction. J. Biol. Chem. 279(14), 13817-13824.

Vaccari, I., Dina, G., Tronchere, H., Kaufman, E., Chicanne, G., Cerri, F., Wrabetz, L., Payrastre, B., Quattrini, A., Weisman, L.S., Meisler, M.H., Bolino, A., 2011. Genetic Interaction between MTMR2 and FIG4 Phospholipid Phosphatases Involved in Charcot-Marie-Tooth Neuropathies. PLoS Genet 7(10), e1002319.

Van Wijngaarden, G.K., Fleury, P., Bethlem, J., Hugo Meijer, A.E.F., 1969. Familial myotubular myopathy. Neurology 19, 901-908.

van Wijngaarden, G.K., Fleury, P., Bethlem, J., Meijer, A.E., 1969. Familial "myotubular" myopathy. Neurology 19(9), 901-908.

Vanhaesebroeck, B., Guillermet-Guibert, J., Graupera, M., Bilanges, B., 2010. The emerging mechanisms of isoform-specific PI3K signalling. Nat. Rev. Mol. Cell Biol. 11(5), 329-341.

Vanhaesebroeck, B., Leevers, S.J., Ahmadi, K., Timms, J., Katso, R., Driscoll, P.C., Woscholski, R., Parker, P.J., Waterfield, M.D., 2001. Synthesis and function of 3-phosphorylated inositol lipids. Annu Rev Biochem 70, 535-602.

Velichkova, M., Juan, J., Kadandale, P., Jean, S., Ribeiro, I., Raman, V., Stefan, C., Kiger, A.A., 2010. Drosophila Mtm and class II PI3K coregulate a PI(3)P pool with cortical and endolysosomal functions. J. Cell Biol. 190(3), 407-425.

Viaud, J., Lagarrigue, F., Ramel, D., Allart, S., Chicanne, G., Ceccato, L., Courilleau, D., Xuereb, J.M., Pertz, O., Payrastre, B., Gaits-Iacovoni, F., 2014. Phosphatidylinositol 5-phosphate regulates invasion through binding and activation of Tiam1. Nature communications 5, 4080.

Vicinanza, M., Korolchuk, V.I., Ashkenazi, A., Puri, C., Menzies, F.M., Clarke, J.H., Rubinsztein, D.C., 2015. PI(5)P regulates autophagosome biogenesis. Mol. Cell 57(2), 219-234.

Villen, J., Beausoleil, S.A., Gerber, S.A., Gygi, S.P., 2007. Large-scale phosphorylation analysis of mouse liver. Proc. Natl. Acad. Sci. U. S. A. 104(5), 1488-1493.

Walker, D.M., Urbe, S., Dove, S.K., Tenza, D., Raposo, G., Clague, M.J., 2001. Characterization of MTMR3. an inositol lipid 3-phosphatase with novel substrate specificity. Curr. Biol. 11(20), 1600-1605.

Weidner, P., Sohn, M., Gutting, T., Friedrich, T., Gaiser, T., Magdeburg, J., Kienle, P., Ruh, H., Hopf, C., Behrens, H.M., Rocken, C., Hanoch, T., Seger, R., Ebert, M.P., Burgermeister, E., 2016. Myotubularin-related protein 7 inhibits insulin signaling in colorectal cancer. Oncotarget.

Wilmshurst, J.M., Lillis, S., Zhou, H., Pillay, K., Henderson, H., Kress, W., Muller, C.R., Ndondo, A., Cloke, V., Cullup, T., Bertini, E., Boennemann, C., Straub, V., Quinlivan, R., Dowling, J.J., Al-Sarraj, S., Treves, S., Abbs, S., Manzur, A.Y., Sewry, C.A., Muntoni, F., Jungbluth, H., 2010. RYR1 mutations are a common cause of congenital myopathies with central nuclei. Ann. Neurol. 68(5), 717-726.

Xhabija, B., Taylor, G.S., Fujibayashi, A., Sekiguchi, K., Vacratsis, P.O., 2011. Receptor mediated endocytosis 8 is a novel PI(3)P binding protein regulated by myotubularin-related 2. FEBS Lett. 585(12), 1722-1728.

Yamamoto, A., DeWald, D.B., Boronenkov, I.V., Anderson, R.A., Emr, S.D., Koshland, D., 1995. Novel PI(4)P 5-kinase homologue, Fab1p, essential for normal vacuole function and morphology in yeast. Mol. Biol. Cell 6(5), 525-539.

Yoshimura, S., Gerondopoulos, A., Linford, A., Rigden, D.J., Barr, F.A., 2010. Family-wide characterization of the DENN domain Rab GDP-GTP exchange factors. J. Cell Biol. 191(2), 367-381.

Yu, J., He, X., Chen, Y.G., Hao, Y., Yang, S., Wang, L., Pan, L., Tang, H., 2013. Myotubularin-related protein 4 (MTMR4) attenuates BMP/Dpp signaling by dephosphorylation of Smad proteins. J. Biol. Chem. 288(1), 79-88.

Yu, S., Manson, J., White, S., Bourne, A., Waddy, H., Davis, M., Haan, E., 2003. X-linked myotubular myopathy in a family with three adult survivors. Clin. Genet. 64(2), 148-152.

Zanoteli, E., Oliveira, A.S.B., Schmidt, B., Gabbai, A.A., 1998. Centronuclear myopathy: clinical aspects of ten Brazilian patients with childhood onset. J Neurol Sciences 158, 76-82.

Zhang, J., Wong, C.H., Xia, W., Mruk, D.D., Lee, N.P., Lee, W.M., Cheng, C.Y., 2005. Regulation of Sertoli-germ cell adherens junction dynamics via changes in protein-protein interactions of the N-cadherin-beta-catenin protein complex which are possibly mediated by c-Src and

myotubularin-related protein 2: an in vivo study using an androgen suppression model. Endocrinology 146(3), 1268-1284.

Zhang, Z.Y., Maclean, D., McNamara, D.J., Sawyer, T.K., Dixon, J.E., 1994. Protein tyrosine phosphatase substrate specificity: size and phosphotyrosine positioning requirements in peptide substrates. Biochemistry 33(8), 2285-2290.

Zinser, E., Sperka-Gottlieb, C.D., Fasch, E.V., Kohlwein, S.D., Paltauf, F., Daum, G., 1991. Phospholipid synthesis and lipid composition of subcellular membranes in the unicellular eukaryote Saccharomyces cerevisiae. J Bacteriol 173(6), 2026-2034.

Zou, W., Lu, Q., Zhao, D., Li, W., Mapes, J., Xie, Y., Wang, X., 2009. Caenorhabditis elegans myotubularin MTM-1 negatively regulates the engulfment of apoptotic cells. PLoS Genet 5(10), e1000679.

Appendix

Appendix 1:

WANTED - Dead or alive: Myotubularins, a large disease-associated protein family.

Raess *et al.* 2017

Advances in Biological Regulation

Advances in Biological Regulation 63 (2017) 49–58

Contents lists available at ScienceDirect

Advances in Biological Regulation

journal homepage: www.elsevier.com/locate/jbior

WANTED – Dead or alive: Myotubularins, a large disease-associated protein family

Matthieu A. Raess [a, b, c, d, e], Sylvie Friant [e], Belinda S. Cowling [a, b, c, d], Jocelyn Laporte [a, b, c, d, *]

[a] Institut de Génétique et de Biologie Moléculaire et Cellulaire (IGBMC), 1 Rue Laurent Fries, BP10142, 67404 Illkirch, France
[b] INSERM U964, 67404 Illkirch, France
[c] CNRS, UMR7104, 67404 Illkirch, France
[d] Fédération de Médecine Translationnelle de Strasbourg (FMTS), Université de Strasbourg, 67404 Illkirch, France
[e] Department of Molecular and Cellular Genetics, UMR7156, Université de Strasbourg and CNRS, 21 Rue Descartes, 67084 Strasbourg, France

ARTICLE INFO

Article history:
Received 30 August 2016
Received in revised form 13 September 2016
Accepted 13 September 2016
Available online 15 September 2016

Keywords:
Congenital myopathy
Neuropathy
GTEx database
Sbf1
Myotubular myopathy
Myotubularin

ABSTRACT

Myotubularins define a large family of proteins conserved through evolution. Several members are mutated in different neuromuscular diseases including centronuclear myopathies and Charcot-Marie-Tooth (CMT) neuropathies, or are linked to a predisposition to obesity and cancer. While some members have phosphatase activity against the 3-phosphate of phosphoinositides, regulating the phosphorylation status of PtdIns3*P* and PtdIns(3,5)P_2 implicated in membrane trafficking and autophagy, and producing PtdIns5*P*, others lack key residues in the catalytic site and are classified as dead-phosphatases. However, these dead phosphatases regulate phosphoinositide-dependent cellular pathways by binding to catalytically active myotubularins. Here we review previous studies on the molecular regulation and physiological roles of myotubularins. We also used the recent myotubularins three-dimensional structures to underline key residues that are mutated in neuromuscular diseases and required for enzymatic activity. In addition, through database mining and analysis, expression profile and specific isoforms of the different myotubularins are described in depth, as well as a revisited protein interaction network. Comparison of the interactome and expression data for each myotubularin highlights specific protein complexes and tissues where myotubularins should have a key regulatory role.

Contents

Abbreviations: MTM, Myotubularins; PPIn, phosphoinositides; PtdIns, phosphatidylinositol; CNM, centronuclear myopathy; CMT, Charcot-Marie-Tooth neuropathy; PH-GRAM, Pleckstrin Homology, Glucosyltransferase, Rab-like GTPase Activator and Myotubularins; FYVE, Fab1-YOTB-Vac1-EEA1; NFL, neurofilament light chain.

* Corresponding author. Institut de Génétique et de Biologie Moléculaire et Cellulaire (IGBMC), 1 Rue Laurent Fries, BP10142, 67404 Illkirch, France.
E-mail addresses: raess@igbmc.fr (M.A. Raess), s.friant@unistra.fr (S. Friant), belinda@igbmc.fr (B.S. Cowling), jocelyn@igbmc.fr (J. Laporte).

http://dx.doi.org/10.1016/j.jbior.2016.09.001
2212-4926/

1. Introduction

Myotubularins constitute a large disease-associated family highly conserved through evolution with similarities to phosphatases. In humans there are 14 clear paralogs of myotubularins: the first identified was MTM1 followed by 13 myotubularin-related proteins MTMR1 to MTMR13 (Laporte et al., 1996, 2003; Robinson and Dixon, 2006). Among them, 8 proteins are active phosphatases while 6 are catalytically dead, with a functional cooperation between members of these two classes (Kim et al., 2003; Nandurkar et al., 2003). In addition MTMR14 protein (also named hJUMPY) has been described (Tosch et al., 2006), however phylogenetic studies and protein domain composition suggested it defines a close but distinct protein family, and therefore this protein will not be discussed further in this review. Additional pseudogenes related to myotubularins also exist (Alonso et al., 2004).

Although active myotubularins have been tentatively classified as Protein Tyrosine Phosphatases (PTP) based on the presence of a $C(X)_5R$ motif, they are specific phosphoinositides (PPIn) 3-phosphatases that dephosphorylate the phosphatidylinositol-3-monophosphate (PtdIns3*P*) and PtdIns(3,5)P_2 into PtdIns and PtdIns5*P*, respectively (Blondeau et al., 2000; Taylor et al., 2000; Tronchere et al., 2004; Walker et al., 2001). Conversely, dead myotubularins share a similar organization in domains but lack the phosphatase activity (Cui et al., 1998; Nandurkar et al., 2001). PPIn are lipid second messengers implicated in a wide range of cellular processes from cell growth and survival to cytoskeleton dynamics (Di Paolo and De Camilli, 2006; Staiano et al., 2015). More specifically, PtdIns3*P* and PtdIns(3,5)P_2 regulate membrane trafficking at the endosomal level and autophagy, which are the most studied and characterized functions of myotubularins (Nicot and Laporte, 2008; Robinson and Dixon, 2006). PtdIns5*P* is implicated in several cellular processes including oxidative stress signaling, growth factor signaling and transcriptional regulation (Bulley et al., 2015; Giudici et al., 2016; Gozani et al., 2003; Keune et al., 2013; Ramel et al., 2011).

Myotubularins have been found in almost all eukaryotes from yeast to mammals, with few exceptions, such as *P. falciparum* (Lecompte et al., 2008). Orthologs for the 14 human myotubularins are found in chordates, except in rodents where MTMR8 is absent at least in mice and rats. A co-evolution has been observed between active and dead myotubularins, as well as between active myotubularins and antagonist kinases (Lecompte et al., 2008); for example MTM1 with the class-III PtdIns 3-kinase VPS34 (PIK3C3) and its regulator VPS15 (PIK3R4). Why have so many myotubularins been duplicated and conserved? Indeed, the presence of 14 similar proteins in humans could lead to functional redundancy, however this high evolutionary pressure suggests that each myotubularin has one or several specific function(s). This specificity could be related to tissue expression or splice isoforms, or particular protein-protein interactions. This specific point will be developed in this review.

To date, mutations were found in 3 myotubularin genes in monogenic human diseases. *MTM1* is mutated in X-linked centronuclear myopathy (XLCNM, OMIM: 310400) also called myotubular myopathy, characterized by hypotonia at birth, a very severe and generalized muscle weakness, external ophthalmoplegia and respiratory distress (Jungbluth et al., 2008; Laporte et al., 1996). Two other myotubularins, *MTMR2* (encoding active phosphatase) and *MTMR13/SBF2* (dead phosphatase), are mutated in Charcot-Marie-Tooth neuropathy type 4B1 (4B1, OMIM: 601382) and 4B2 (CMT4B2, OMIM: 604563), respectively (Azzedine et al., 2003; Bolino et al., 2000; Senderek et al., 2003). CMT4B1 and 2 are two distinct but close forms of autosomal recessive demyelinating neuropathy affecting peripheral nerves and leading to pronounced muscular atrophy and weakness of distal limbs. In addition, several myotubularins are linked to multifactorial diseases as colorectal, gastric and lung cancers (MTMR3 and 7) (Hu et al., 2011; Song et al., 2010; Weidner et al., 2016), obesity (MTMR9) (Hotta et al., 2011) and Creutzfeldt–Jakob disease (MTMR7) (Sanchez-Juan et al., 2012). The fact that ubiquitously expressed myotubularins are implicated in different tissue-specific diseases again indicates that the apparent biochemical redundancy is in fact hiding tissue-specific functions.

This review focuses on recent advances concerning 3 main aspects of the myotubularin family: gene expression, protein interactions and protein structure. Through database mining and analysis, the interaction network of myotubularins is revisited and integrated, and their expression profiles and specific isoforms are described.

2. Myotubularins: protein domains and interactions

Myotubularins are multidomain proteins that share the same central core composed of the PH-GRAM (Pleckstrin Homology - Glucosyltransferase, Rab-like GTPase Activator and Myotubularins) domain that could bind to PPIn or proteins and the phosphatase-like domain (Fig. 1A) (Begley et al., 2003; Choudhury et al., 2006; Doerks et al., 2000; Tsujita et al., 2004). In the 8 active myotubularins (MTM1, MTMR1-4 and 6–8), the catalytic domain contains the consensus $C(X)_5R$ signature motif (Alonso et al., 2004; Zhang et al., 1994). In the 6 phosphatase dead myotubularins (MTMR9-12, MTMR5/Sbf1 and MTMR13/Sbf2), the absence of enzymatic activity is due to the substitution of catalytically essential residues such as the cysteine in the consensus motif (Cui et al., 1998; Nandurkar et al., 2003).

Myotubularins can have several other functional domains: the PDZ binding site (MTM1, MTMR1 and 2) mediates protein-protein interactions, the PH (Pleckstrin homology) (MTMR5 and 13) and FYVE (Fab1-YOTB-Vac1-EEA1) (MTMR3 and 4) domains can bind PPIn (Itoh and Takenawa, 2002), and the DENN domain (MTMR5 and 13) is involved in small Rab GTPase regulation (Fabre et al., 2000; Jean et al., 2012; Yoshimura et al., 2010). By combining domain organization and phylogenetics, 6 different subgroups are highlighted, each containing exclusively active or dead members (Fig. 1B). In addition, all myotubularins except MTMR10 contain a coiled-coil (CC) domain that is critical for their homodimerization and/or heterodimerization (Berger et al., 2006; Lorenzo et al., 2006). Dimerization also appears to depend on the PH-GRAM domain (Berger et al., 2006).

Indeed, all myotubularins except MTMR11 have been shown to interact either with themselves or with other myotubularins (Fig. 1C) (Berger et al., 2006; Gupta et al., 2013; Kim et al., 2003; Lorenzo et al., 2006; Mochizuki and Majerus, 2003; Nandurkar et al., 2003; Schaletzky et al., 2003; Zou et al., 2009). Within the 14 members, 9 have been reported to form homodimers; this could enhance the membrane targeting by coupling two PH-GRAM domains (Berger et al., 2003). At least for MTM1, homo-oligomerization controls its allosteric activity, and *in vitro* MTM1 incubated with its substrate PtdIns3*P* forms a heptamer in the presence of PtdIns5*P* (Schaletzky et al., 2003). One of the most notable characteristics of this family is that most heterodimers are formed by a coupling between active and dead phosphatases. For example, MTMR2 forms heterodimers with its dead homologs MTMR5/Sbf1, MTMR10, MTMR12 and MTMR13/Sbf2. The fact that mutations in MTMR13 lead to a similar neuropathy (CMT4B) as defects in MTMR2 confirms the physiological importance of dead phosphatases and heterodimers. MTMR9 interacts with 3 different active myotubularins of the same phylogenic subgroup (MTMR6, 7 and 8)

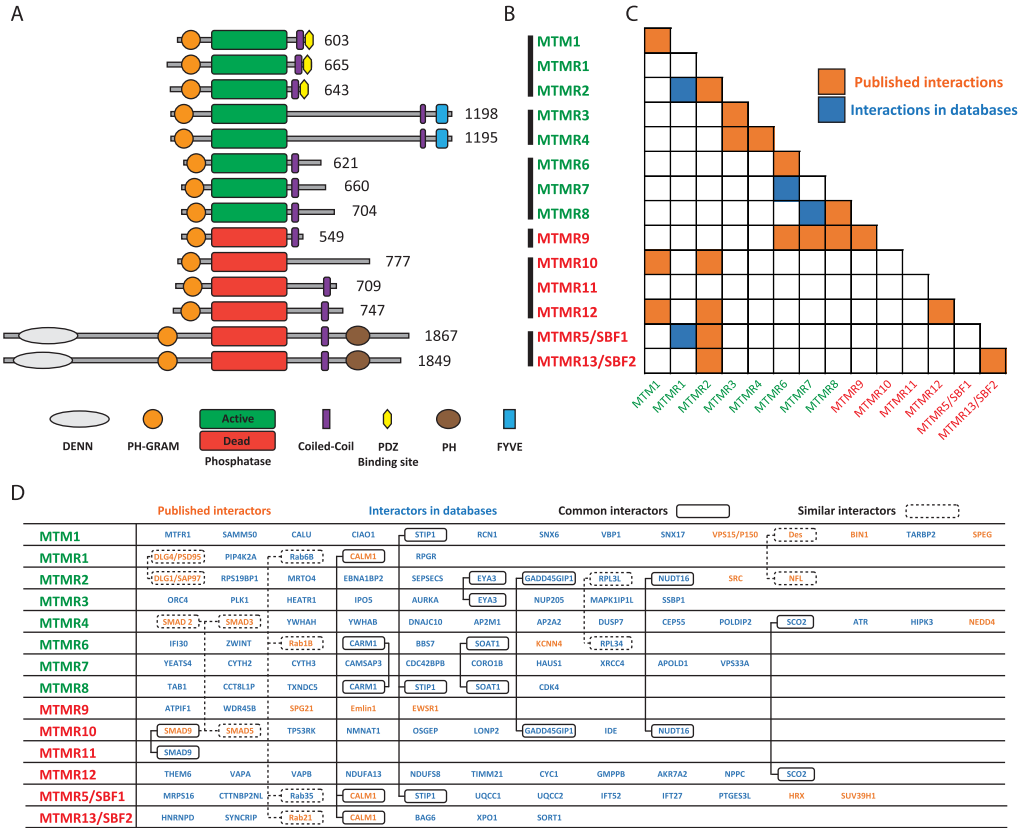

Fig. 1. Human myotubularins: domain organization and interactome. A. Scaled representation of the protein domains of human myotubularins. All myotubularins share the PH-GRAM and phosphatase (active or dead) domains. For each myotubularin, amino acid length of the most described protein isoform is indicated. **B**. Classification of myotubularins into 6 subgroups based on protein organization and phylogenetics (indicated by the vertical bars on the left). Active myotubularins are represented in green and dead myotubularins in red. **C**. Known protein interactions within the myotubularin family. Published interactions are in orange while interactions found in databases (Biogrid - the biogrid.org) are in blue. **D**. List of known interactors for each myotubularin. Published interactors are represented in orange while interactors found in databases with a minimum MUSEscore of 0,95 (Biogrid and Li et al., 2016) are in blue. Common interactors and interactors of the same protein family are surrounded and related together by a continuous and stippled line, respectively. Similar interactors found for a specific myotubularin are not surrounded.

and increases their enzymatic activity (Mochizuki and Majerus, 2003). In the same way, MTMR5 increases the enzymatic activity of MTMR2 and both are related to male infertility due to impaired spermatogenesis (Bolino et al., 2004; Firestein et al., 2002; Kim et al., 2003). In some heterodimers, such as MTM1-MTMR12, MTMR2-MTMR5 and MTMR2-MTMR13, the dead myotubularin may regulate the cellular localization of the active member (Gupta et al., 2013; Kim et al., 2003; Nandurkar et al., 2003). Dead myotubularins appear early in evolution and are conserved in many species (Laporte et al., 2003; Lecompte et al., 2008). Altogether, this suggests (1) a co-evolution between active and dead myotubularins and (2) that myotubularins rely on oligomerization for their function since very early in the evolution. Heterodimers can also be formed between two active members of the same phylogenic subgroup, as for MTMR1-MTMR2, MTMR3-MTMR4, MTMR6-MTMR7 and MTMR7-MTMR8 (Fig. 1C).

Numerous interactors have been identified for each myotubularin (Fig. 1D) (Biogrid - thebiogrid.org and Intact - http://www.ebi.ac.uk/intact/) (Agrawal et al., 2014; Berggard et al., 2006; Cao et al., 2007; Cui et al., 1998; Fabre et al., 2000; Firestein et al., 2000; Jean et al., 2012; Li et al., 2016; Plant et al., 2009; Royer et al., 2013; Rual et al., 2005; Srivastava et al., 2005; Yu et al., 2013; Zhang et al., 2005). Some myotubularins share common interactors or interactors from the same protein family. For example, MTMR6 and MTMR8 both interact with SOAT1, a protein localized in the endoplasmic reticulum, which is also the presumed localization of these myotubularins. MTM1 interacts with desmin and MTMR2 with neurofilament light chain (NFL), that are two intermediate filament proteins specifically found in muscles and neurons, respectively (Hnia et al., 2011; Previtali et al., 2003). This is consistent with mutations in MTM1 and desmin leading to myopathies and mutations in MTMR2 and NFL leading to CMT neuropathies (Goldfarb et al., 1998; Mersiyanova et al., 2000). Another well-represented group of interactors is the Rab family: MTMR1-RAB6B, MTMR6-RAB1B, MTMR5-RAB35 and MTMR13-RAB21 (Jean et al., 2012; Mochizuki et al., 2013). Rabs constitute a very large GTPase family regulating many steps of membrane trafficking, one of the main cellular functions in which myotubularins are implicated (Barr, 2013). Of note, myotubularins implicated in 3 heterodimers share common or similar interactors: MTMR1-MTMR2, MTMR1-MTMR5 and MTMR2-MTMR10. For example, MTMR1 and MTMR5 heterodimerize and interact with different Rab GTPases (Fig. 1D).

3. Myotubularins: tissue expression

To investigate how myotubularin genes are expressed in human tissues, we mined the Genotype-Tissue Expression (GTEx) database, which has been built by systematic RNA-sequencing using samples of 51 different tissues from hundreds of donors and 2 transformed cell types in culture. Fig. 2 shows for each gene the relative expression in all tested tissues, and highlights in which tissue a specific myotubularin is the most/less expressed. This is not absolute expression, therefore a gene cannot be directly compared to another for the same tissue. A dendrogram was generated using the Pearson correlation coefficient to highlight hierarchical clustering of myotubularins sharing similar profiles of expression. Whilst this is one of many possible dendrograms and thus it has to be interpreted cautiously, two main groups of myotubularins can be distinguished based on expression profiles: MTMR1-3-8-11-12-13 (upper branch, Fig. 2), and the others (lower branch). Discriminant tissues between the two groups are brain (almost all regions), skin, vagina and prostate. This does not seem to be directly related to phylogenetic classification, to active/dead and active/active heterodimers or to myotubularins sharing common interactors. However, some links can be made. For example, MTMR7 and MTMR9 that form an active/dead heterodimer have the closest expression profiles and are both strongly expressed in brain tissues. A similar link applies to MTM1, MTMR2 and MTMR10, which have correlated expression patterns: they form two active/dead heterodimers MTM1/MTMR10 and MTMR2/MTMR10, and MTMR2 and MTMR10 have common interactors (Fig. 1C and D) (Lorenzo et al., 2006).

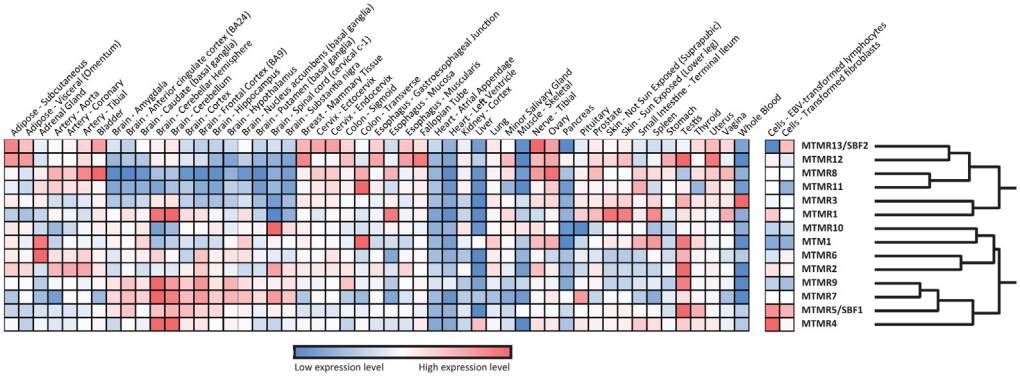

Fig. 2. Myotubularins tissue expression. Heatmap of myotubularin genes relative expression within 51 different tissues underlining in which tissue a specific myotubularin is the most/least expressed (left panel), and absolute expression in 2 cell types. Expression levels have been obtained by mining the GTEx database (www.gtexportal.org/home/). Dendrogram highlighting the hierachical clustering of myotubularins (right panel), using the Pearson correlation coefficient and average linkage.

Concerning myotubularins related to monogenic diseases, while MTM1 has a low expression level in striated muscles compared to other tissues such as nerves, colon or testis, mutations in the *MTM1* gene lead to a severe myopathy. Thus, the MTM1 tissue-specific function could be explained by interactions with partners that are only expressed in muscle, such as desmin (Hnia et al., 2011). On the contrary, MTMR2 and MTMR13 are highly expressed in nerves, which is consistent with the neuropathies observed due to mutations in these genes. In addition, MTMR2 binds the neuronal intermediate filament NFL (Previtali et al., 2003), highlighting a potential molecular basis common to different CMT neuropathy forms. A link can be observed between MTMR2 and MTMR5, known to form heterodimers; they both have a high relative expression level in testis, and defects of these genes lead to male infertility by impaired spermatogenesis (Bolino et al., 2004; Firestein et al., 2002), therefore adding weight to the physiological significance of this data.

Myotubularins expression levels have also been measured in two cell types, lymphocytes and fibroblasts, that are easily derived from human cells. These cells could allow diagnosis at the protein level or be dedifferentiated into induced pluripotent stem (IPS) cells that could be reprogrammed into specific cell types, allowing study of the pathocellular mechanisms. This time, absolute expression levels of all myotubularins are compared (Fig. 2). Some myotubularins, such as MTMR5 or MTMR2, are well expressed in both lymphocytes and fibroblasts, whereas for other myotubularins fibroblasts show a higher expression level, as for MTMR13 for which study in these cell types might be more adapted. Therefore, interpreting this data can be useful in deciding which cell lines should be used for research and diagnostic purposes.

4. Myotubularin: mRNA isoforms

The study of gene expression does not take splicing events into account. Indeed, a specific gene is often spliced into several mRNA isoforms that could be translated into different protein isoforms. In this review, we use the term “isoform” to define a variant of the same protein or mRNA, and “homologs” for different genes. Fig. 3 summarizes the myotubularin mRNA isoforms expression within all tissues present in the GTEx database. Only significantly expressed mRNA isoforms have been represented, and color-coded based on their predicted protein product: the main protein isoform from the literature, longer/shorter protein isoforms, or non-coding mRNA isoforms. For each mRNA isoform, the expression level is indicated as a percentage of total gene expression.

Interestingly, the main mRNA isoform studied in the literature is not always the most expressed (MTM1, MTMR3, MTMR10, MTMR11 and MTMR12). For MTMR10, the most expressed isoform encodes only the PH-GRAM; it raises the possibility that this protein isoform exerts a dominant negative effect on oligomerization of myotubularins or on cellular functions. MTMR2 has 4 well expressed mRNA isoforms: one translated into the main 643 amino acids (aa) protein isoform and the three others translated into a 571 aa protein isoform lacking the N-terminal extremity before the PH-GRAM (Bolino et al., 2001). The latter is present in all tissues except brain, and may have a specific function. In addition, some isoforms are tissue-specific, as for MTM1 with 2 isoforms only expressed in skeletal muscle. Corresponding peptides lack a part of the PH-GRAM domain and could support a muscle-specific function altered in the MTM1-related myopathy. In total, 10 myotubularins express mRNA isoforms leading to shorter proteins and MTMR1 displays an isoform predicted to encode a longer protein. These differences can affect various protein domains as the FYVE domain for MTMR3 and MTMR4 or the DENN domain for MTMR5, and thus could highly impact on protein conformation or protein-protein/protein-lipid interactions.

For MTM1, MTMR11 and MTMR13, the prevailing mRNA isoforms are non-coding, or the corresponding peptides have not been identified yet, questioning the function of such isoforms. Finally, some isoforms described in the literature are not represented here because they were absent in the GTEx database. This is the case for various MTMR1 mRNA isoforms that are known to be well expressed in some tissues (Buj-Bello et al., 2002).

In the future, it would be important to characterize the cellular activity of these tissue-specific isoforms, in order to get insight into their physiological relevance.

5. Myotubularins: protein structure

Between 2003 and 2016, the crystal structures of 4 active myotubularins have been determined: MTMR1 (PDB: 5C16), MTMR2 (1LW3, 1ZVR, 1M7R and 1ZSQ), MTMR6 (2YFO) and MTMR8 (4YZI) (Begley et al., 2003, 2006; Bong et al., 2016). A crystal structure of mouse MTMR5 has also be resolved, but only contains the C-terminal PH domain (1V5U). No major differences have been described between the 4 structures, except for the orientation of the MTMR6 PH-GRAM domain; this could impact MTMR6 oligomerization properties (Bong et al., 2016). From a 3D point of view, myotubularins are globular proteins with two main parts: the PH-GRAM domain and the catalytic domain, connected by a linker (Fig. 4A) (Begley et al., 2003). N-terminal extremities, coiled-coil domains and PDZ binding sites are absent of these structures, presumably because they are too flexible or cleaved by proteolysis. In addition, the cysteine residue of the catalytic $C(X)_5R$ motif has been mutated into a serine for crystallization, except for MTMR6.

The PH-GRAM domain consists in 7 β-strands and 1 α-helix. The main characteristic of the catalytic domain is the substrate binding pocket that is significantly deeper and wider than that of classical tyrosine phosphatases, explaining the unique specificity of myotubularins for membrane-embedded PPIn substrates (Fig. 4A) (Begley et al., 2003). Indeed, active myotubularins specifically hydrolyze the D-3 position of PtdIns3*P* and PtdIns(3,5)P_2, two PPIn with large phosphorylated inositol headgroups that perfectly fit in the catalytic pocket. The D-3 phosphate is then trapped by its interaction with the main chain of 6 residues from the $C(X)_5R$ motif loop (on MTMR2 sequence: Cys417, Ser418, Gly420, Trp421, Asp422 and Arg423) (Fig. 4B).

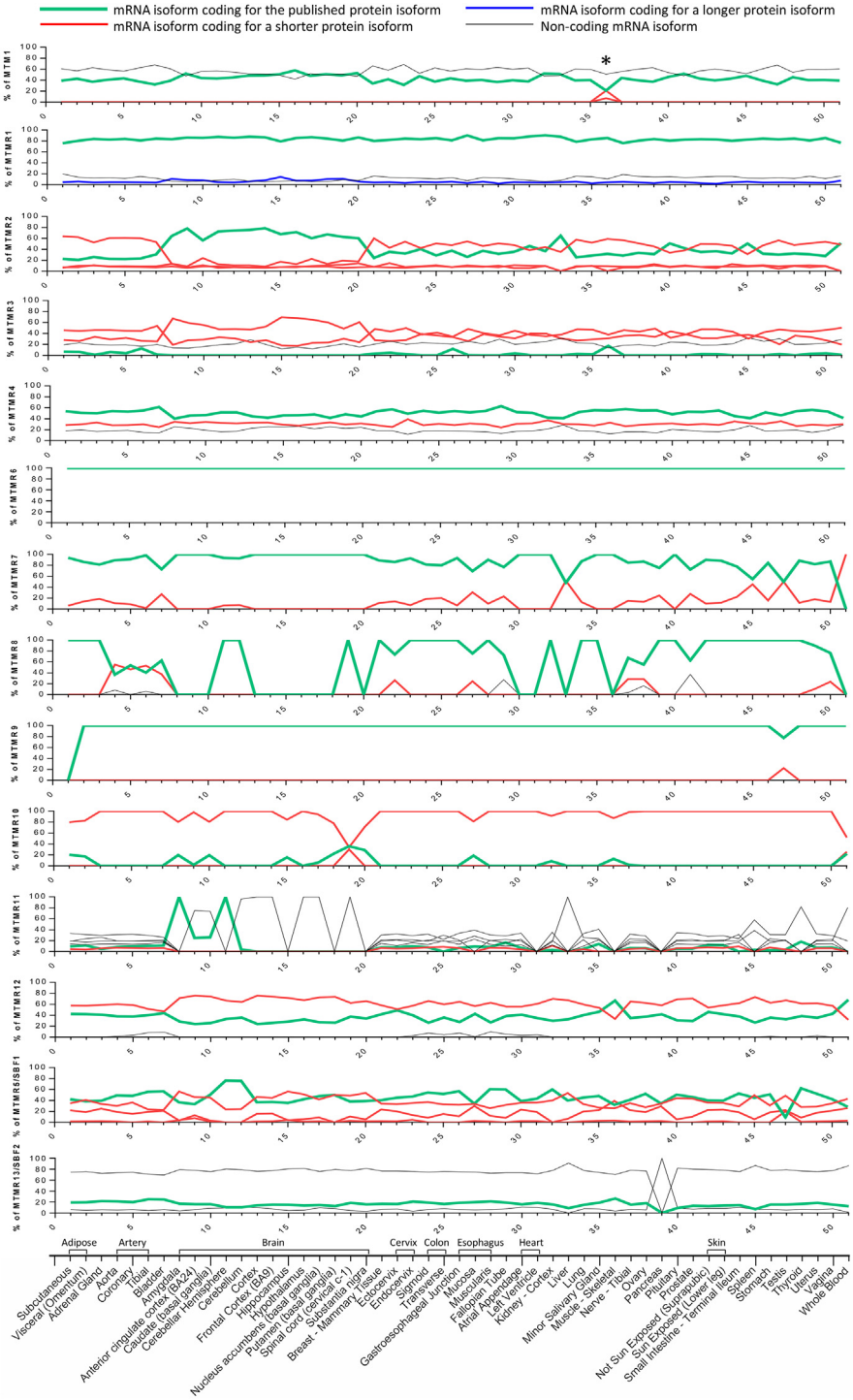

Fig. 3. Myotubularin mRNA isoforms. For each myotubularin indicated on the left, the most expressed isoforms present in the GTEx database are represented as a percentage of total gene expression. Only the most expressed isoforms are shown. The mRNA isoforms coding for the main published protein isoforms are indicated in green, shorter isoforms in red and longer isoforms in blue. Several non-coding isoforms indicated in black have been found well expressed, for which no corresponding peptides have been described yet. The star indicates specific MTM1 mRNA isoforms in skeletal muscle, the tissue affected in MTM1-related myopathy. For several myotubularins as MTMR3, MTMR10 and MTMR12, and to a less extend MTMR2, the main expressed isoforms are different than the published isoforms used for functional characterization of the related proteins; for MTMR11 and MTMR13 the main expressed isoforms are predicted non-coding.

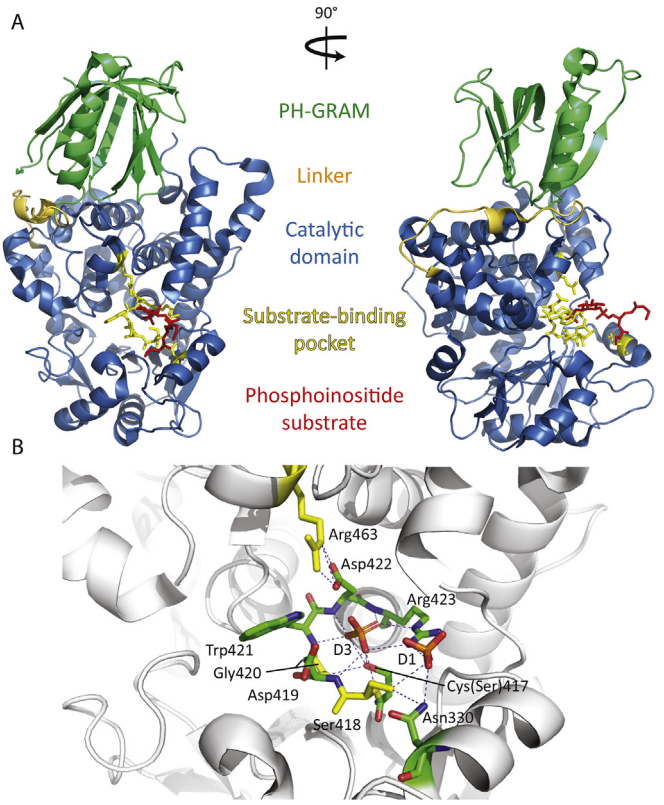

Fig. 4. The myotubularins protein structure. A. Overall view of the myotubularin structure. The crystal structure of MTMR2 (PDB:1ZSQ) is used as a model, with a front view and a view rotated at 90°. Domain names and the phosphoinositide substrate (here PtdIns3*P*) are indicated on the two representations. **B**. Zoom on the substrate-binding pocket. Residues forming the $C(X)_5R$ loop and other important residues are represented using stick models. Residues affected by missense mutations in MTM1-linked centronuclear myopathy are colored in yellow. No missense mutations have been found in *MTMR2* or *MTMR13* genes in the catalytic pocket. The cysteine residue of the $C(X)_5R$ motif is mutated to serine in the structure for crystallization purposes. Hydrogen bonds between the two phosphate groups in position D1 and D3 of PtdIns3*P*/PtdIns(3,5)P_2 and surrounding residues of the active site are represented by stippled lines.

Concerning the catalytic activity, the nucleophile Cys417 residue attacks the phosphorous atom in position D-3 of the PPIn substrate, forming a phosphoenzyme intermediate, then the aspartic acid (Asp422 in MTMR2) donates a proton to the released dephosphorylated substrate, before hydrolysis yielding free enzyme and inorganic phosphate (Begley and Dixon, 2005; Begley et al., 2006; Nandurkar and Huysmans, 2002). Myotubularins are different from classical PTPs because the catalytic aspartate residue lies directly in the catalytic $C(X)_5R$ loop and not in a WPD-loop. The D-1 phosphate of the PPIn interacts with the side chain of two residues from the $C(X)_5R$ motif (on MTMR2 sequence: Ser418 and Arg423), but also with Asn330, which is conserved in all active myotubularins suggesting an important role in PPIn substrate binding. Some other residues help to maintain the three-dimensional structure of this catalytic pocket, like Arg463 (on MTMR2) that is also conserved in all myotubularins. A phosphate in position D-4 would generate a steric clash with several residues of the catalytic pocket, excluding PtdIns(3,4)P_2 and PtdIns(3,4,5)P_3 from potential substrates.

Another consideration for myotubularin substrate specificity is that active myotubularins are electrostatically polarized proteins, with one strongly electropositive side containing the catalytic site (Begley et al., 2006). This would create electrostatic interactions between the positively charged face of myotubularins and the negatively charged membranes containing PPIn, contributing to substrate-binding affinity. This electropositive patch around the catalytic pocket seems to be specific for active myotubularins, while several dead myotubularins have an electronegative surface, suggesting a poor affinity toward lipid membranes. Furthermore, active myotubularins could bind either membranes or dead-phosphatase homologs through the same interface.

The three-dimensional structure can also be very useful to understand the effect of disease-associated mutations and thereby to evaluate the importance of mutated residues for the function or the stability of the protein. The majority of MTM1, MTMR2 and MTMR13 missense mutations affect residues in the hydrophobic core structure of the PH-GRAM and catalytic domains, and replace native amino acids by bulkier residues, or decrease van der Waals contacts or alter internal hydrogen bonds, consequently disrupting the protein core structure. In addition, two clusters of solvent-accessible

missense mutations at the surface of the MTM1 protein can be observed: the Pro179-Asn180-Arg184 cluster and the Asp431-Asp433 cluster (numbered in MTM1 sequence) that could be potential binding sites for interactors (Begley et al., 2003). In the active site, the Ser376, Gly378 and Arg421 (numbered Ser418, Gly420 and Arg463 in MTMR2 structure in Fig. 4B) are frequent sites of mutations found in MTM1: the Ser376 and Gly378 directly bind the D-3 phosphate of the PPIn and the Arg421 is a key factor to maintain the position of the catalytic loop. Thus, mutations of these residues would directly prevent any catalytic activity.

6. Conclusion

Myotubularins define a large and highly conserved family of proteins with some noteworthy characteristics. They are classified in the Protein Tyrosine Phosphatases (PTP) family but have a specific phosphatase activity against phosphoinositides. One other feature is the presence of catalytically active and dead phosphatases, where dead myotubularins regulate their active homologs. Although they are ubiquitously expressed, three myotubularin genes – *MTM1*, *MTMR2* and *MTMR13* – are mutated in tissue-specific neuromuscular diseases, suggesting tissue-specific splice isoforms or specific protein-protein or protein-lipid interactions.

Future experiments will be needed to address this tissue specificity. While the function of myotubularins and PPIn substrates and products was well studied in cell systems, their physiological role *in vivo* is still barely understood. Another key issue is the pathological mechanism(s) associated to myotubularin-related diseases. Data showed that MTM1-related myopathy or phenotypes can be rescued in mice and drosophilia by inhibition or muscle-specific ablation of the class II PtdIns 3-kinase, pointing to the importance of PPIn regulation by myotubularin (Sabha et al., 2016; Velichkova et al., 2010). However, the same mouse disease model can also be rescued by expressing a phosphatase inactive MTM1 protein, supporting that PPIn-unrelated functions of myotubularin are implicated in this pathology (Amoasii et al., 2012). Due to the importance of myotubularins and PPIn pathways in metabolism and cellular integrity, it is expected that their dysregulation in more common diseases will be highlighted in the future.

Acknowledgements

We thank lab members for fruitful discussions, and R Schneider for help with data mining.

This work was funded by the CNRS, Université de Strasbourg (S Friant), the Agence Nationale de la Recherche (ANR-13-BSV2-0004 to J Laporte and S Friant) and by the Association Française contre les Myopathies AFM-Téléthon (AFM-SB/CP/2013-0133/16551 to S Friant and PhD fellowship to MA Raess). BS Cowling and J Laporte are supported by Inserm.

References

Agrawal, P.B., Pierson, C.R., Joshi, M., Liu, X., Ravenscroft, G., Moghadaszadeh, B., Talabere, T., Viola, M., Swanson, L.C., Haliloglu, G., Talim, B., Yau, K.S., Allcock, R.J., Laing, N.G., Perrella, M.A., Beggs, A.H., 2014. SPEG interacts with myotubularin, and its deficiency causes centronuclear myopathy with dilated cardiomyopathy. Am. J. Hum. Genet. 95 (2), 218–226.

Alonso, A., Sasin, J., Bottini, N., Friedberg, I., Friedberg, I., Osterman, A., Godzik, A., Hunter, T., Dixon, J.E., Mustelin, T., 2004. Protein tyrosine phosphatases in the human genome. Cell 117 (6), 699–711.

Amoasii, L., Bertazzi, D.L., Tronchere, H., Hnia, K., Chicanne, G., Rinaldi, B., Cowling, B.S., Ferry, A., Klaholz, B., Payrastre, B., Laporte, J., Friant, S., 2012. Phosphatase-dead myotubularin ameliorates X-linked centronuclear myopathy phenotypes in mice. PLoS Genet. 8 (10), e1002965.

Azzedine, H., Bolino, A., Taieb, T., Birouk, N., Di Duca, M., Bouhouche, A., Benamou, S., Mrabet, A., Hammadouche, T., Chkili, T., Gouider, R., Ravazzolo, R., Brice, A., Laporte, J., LeGuern, E., 2003. Mutations in MTMR13, a new pseudophosphatase homologue of MTMR2 and Sbf1, in two families with an autosomal recessive demyelinating form of charcot-marie-tooth disease associated with early-onset glaucoma. Am. J. Hum. Genet. 72 (5), 1141–1153.

Barr, F.A., 2013. Review series: Rab GTPases and membrane identity: causal or inconsequential? J. Cell Biol. 202 (2), 191–199.

Begley, M.J., Dixon, J.E., 2005. The structure and regulation of myotubularin phosphatases. Curr. Opin. Struct. Biol. 15 (6), 614–620.

Begley, M.J., Taylor, G.S., Brock, M.A., Ghosh, P., Woods, V.L., Dixon, J.E., 2006. Molecular basis for substrate recognition by MTMR2, a myotubularin family phosphoinositide phosphatase. Proc. Natl. Acad. Sci. U. S. A. 103 (4), 927–932.

Begley, M.J., Taylor, G.S., Kim, S.A., Veine, D.M., Dixon, J.E., Stuckey, J.A., 2003. Crystal structure of a phosphoinositide phosphatase, MTMR2: insights into myotubular myopathy and Charcot-Marie-Tooth syndrome. Mol. Cell 12 (6), 1391–1402.

Berger, P., Niemann, A., Suter, U., 2006. Schwann cells and the pathogenesis of inherited motor and sensory neuropathies (Charcot-Marie-Tooth disease). Glia 54 (4), 243–257.

Berger, P., Schaffitzel, C., Berger, I., Ban, N., Suter, U., 2003. Membrane association of myotubularin-related protein 2 is mediated by a pleckstrin homology-GRAM domain and a coiled-coil dimerization module. Proc. Natl. Acad. Sci. U. S. A. 100 (21), 12177–12182.

Berggard, T., Arrigoni, G., Olsson, O., Fex, M., Linse, S., James, P., 2006. 140 mouse brain proteins identified by Ca2+-calmodulin affinity chromatography and tandem mass spectrometry. J. Proteome Res. 5 (3), 669–687.

Blondeau, F., Laporte, J., Bodin, S., Superti-Furga, G., Payrastre, B., Mandel, J.L., 2000. Myotubularin, a phosphatase deficient in myotubular myopathy, acts on phosphatidylinositol 3-kinase and phosphatidylinositol 3-phosphate pathway. Hum. Mol. Genet. 9 (15), 2223–2229.

Bolino, A., Bolis, A., Previtali, S.C., Dina, G., Bussini, S., Dati, G., Amadio, S., Del Carro, U., Mruk, D.D., Feltri, M.L., Cheng, C.Y., Quattrini, A., Wrabetz, L., 2004. Disruption of Mtmr2 produces CMT4B1-like neuropathy with myelin outfolding and impaired spermatogenesis. J. Cell Biol. 167 (4), 711–721.

Bolino, A., Lonie, L.J., Zimmer, M., Boerkoel, C.F., Takashima, H., Monaco, A.P., Lupski, J.R., 2001. Denaturing high-performance liquid chromatography of the myotubularin-related 2 gene (MTMR2) in unrelated patients with Charcot-Marie-Tooth disease suggests a low frequency of mutation in inherited neuropathy. Neurogenetics 3 (2), 107–109.

Bolino, A., Muglia, M., Conforti, F.L., LeGuern, E., Salih, M.A., Georgiou, D.M., Christodoulou, K., Hausmanowa-Petrusewicz, I., Mandich, P., Schenone, A., Gambardella, A., Bono, F., Quattrone, A., Devoto, M., Monaco, A.P., 2000. Charcot-Marie-Tooth type 4B is caused by mutations in the gene encoding myotubularin-related protein-2. Nat. Genet. 25 (1), 17–19.

Bong, S.M., Son, K.B., Yang, S.W., Park, J.W., Cho, J.W., Kim, K.T., Kim, H., Kim, S.J., Kim, Y.J., Lee, B.I., 2016. Crystal structure of human myotubularin-related protein 1 provides insight into the structural basis of substrate specificity. PLoS One 11 (3), e0152611.

Buj-Bello, A., Furling, D., Tronchere, H., Laporte, J., Lerouge, T., Butler-Browne, G.S., Mandel, J.L., 2002. Muscle-specific alternative splicing of myotubularin-related 1 gene is impaired in DM1 muscle cells. Hum. Mol. Genet. 11 (19), 2297–2307.
Bulley, S.J., Clarke, J.H., Droubi, A., Giudici, M.L., Irvine, R.F., 2015. Exploring phosphatidylinositol 5-phosphate 4-kinase function. Adv. Biol. Regul. 57, 193–202.
Cao, C., Laporte, J., Backer, J.M., Wandinger-Ness, A., Stein, M.P., 2007. Myotubularin lipid phosphatase binds the hVPS15/hVPS34 lipid kinase complex on endosomes. Traffic 8 (8), 1052–1067.
Choudhury, P., Srivastava, S., Li, Z., Ko, K., Albaqumi, M., Narayan, K., Coetzee, W.A., Lemmon, M.A., Skolnik, E.Y., 2006. Specificity of the myotubularin family of phosphatidylinositol-3-phosphatase is determined by the PH/GRAM domain. J. Biol. Chem. 281 (42), 31762–31769.
Cui, X., De Vivo, I., Slany, R., Miyamoto, A., Firestein, R., Cleary, M.L., 1998. Association of SET domain and myotubularin-related proteins modulates growth control. Nat. Genet. 18 (4), 331–337.
Di Paolo, G., De Camilli, P., 2006. Phosphoinositides in cell regulation and membrane dynamics. Nature 443 (7112), 651–657.
Doerks, T., Strauss, M., Brendel, M., Bork, P., 2000. GRAM, a novel domain in glucosyltransferases, myotubularins and other putative membrane-associated proteins. Trends Biochem. Sci. 25 (10), 483–485.
Fabre, S., Reynaud, C., Jalinot, P., 2000. Identification of functional PDZ domain binding sites in several human proteins. Mol. Biol. Rep. 27 (4), 217–224.
Firestein, R., Cui, X., Huie, P., Cleary, M.L., 2000. Set domain-dependent regulation of transcriptional silencing and growth control by SUV39H1, a mammalian ortholog of Drosophila Su(var)3-9. Mol. Cell Biol. 20 (13), 4900–4909.
Firestein, R., Nagy, P.L., Daly, M., Huie, P., Conti, M., Cleary, M.L., 2002. Male infertility, impaired spermatogenesis, and azoospermia in mice deficient for the pseudophosphatase Sbf1. J. Clin. Invest. 109 (9), 1165–1172.
Giudici, M.L., Clarke, J.H., Irvine, R.F., 2016. Phosphatidylinositol 5-phosphate 4-kinase gamma (PI5P4Kgamma), a lipid signalling enigma. Adv. Biol. Regul. 61, 47–50.
Goldfarb, L.G., Park, K.Y., Cervenakova, L., Gorokhova, S., Lee, H.S., Vasconcelos, O., Nagle, J.W., Semino-Mora, C., Sivakumar, K., Dalakas, M.C., 1998. Missense mutations in desmin associated with familial cardiac and skeletal myopathy. Nat. Genet. 19 (4), 402–403.
Gozani, O., Karuman, P., Jones, D.R., Ivanov, D., Cha, J., Lugovskoy, A.A., Baird, C.L., Zhu, H., Field, S.J., Lessnick, S.L., Villasenor, J., Mehrotra, B., Chen, J., Rao, V.R. , Brugge, J.S., Ferguson, C.G., Payrastre, B., Myszka, D.G., Cantley, L.C., Wagner, G., Divecha, N., Prestwich, G.D., Yuan, J., 2003. The PHD finger of the chromatin-associated protein ING2 functions as a nuclear phosphoinositide receptor. Cell 114, 99–111.
Gupta, V.A., Hnia, K., Smith, L.L., Gundry, S.R., McIntire, J.E., Shimazu, J., Bass, J.R., Talbot, E.A., Amoasii, L., Goldman, N.E., Laporte, J., Beggs, A.H., 2013. Loss of catalytically inactive lipid phosphatase myotubularin-related protein 12 impairs myotubularin stability and promotes centronuclear myopathy in zebrafish. PLoS Genet. 9 (6), e1003583.
Hnia, K., Tronchere, H., Tomczak, K.K., Amoasii, L., Schultz, P., Beggs, A.H., Payrastre, B., Mandel, J.L., Laporte, J., 2011. Myotubularin controls desmin intermediate filament architecture and mitochondrial dynamics in human and mouse skeletal muscle. J. Clin. Invest. 121 (1), 70–85.
Hotta, K., Kitamoto, T., Kitamoto, A., Mizusawa, S., Matsuo, T., Nakata, Y., Kamohara, S., Miyatake, N., Kotani, K., Komatsu, R., Itoh, N., Mineo, I., Wada, J., Yoneda, M., Nakajima, A., Funahashi, T., Miyazaki, S., Tokunaga, K., Masuzaki, H., Ueno, T., Hamaguchi, K., Tanaka, K., Yamada, K., Hanafusa, T., Oikawa, S., Yoshimatsu, H., Sakata, T., Matsuzawa, Y., Nakao, K., Sekine, A., 2011. Association of variations in the FTO, SCG3 and MTMR9 genes with metabolic syndrome in a Japanese population. J. Hum. Genet. 56 (9), 647–651.
Hu, J., Prinz, W.A., Rapoport, T.A., 2011. Weaving the web of ER tubules. Cell 147 (6), 1226–1231.
Itoh, T., Takenawa, T., 2002. Phosphoinositide-binding domains: functional units for temporal and spatial regulation of intracellular signalling. Cell. Signal. 14 (9), 733–743.
Jean, S., Cox, S., Schmidt, E.J., Robinson, F.L., Kiger, A., 2012. Sbf/MTMR13 coordinates PI(3)P and Rab21 regulation in endocytic control of cellular remodeling. Mol. Biol. Cell 23 (14), 2723–2740.
Jungbluth, H., Wallgren-Pettersson, C., Laporte, J., 2008. Centronuclear (myotubular) myopathy. Orphanet J. Rare Dis. 3, 26.
Keune, W.J., Jones, D.R., Divecha, N., 2013. PtdIns5P and Pin1 in oxidative stress signaling. Adv. Biol. Regul. 53 (2), 179–189.
Kim, S.A., Vacratsis, P.O., Firestein, R., Cleary, M.L., Dixon, J.E., 2003. Regulation of myotubularin-related (MTMR)2 phosphatidylinositol phosphatase by MTMR5, a catalytically inactive phosphatase. Proc. Natl. Acad. Sci. U. S. A. 100 (8), 4492–4497.
Laporte, J., Bedez, F., Bolino, A., Mandel, J.L., 2003. Myotubularins, a large disease-associated family of cooperating catalytically active and inactive phosphoinositides phosphatases. Hum. Mol. Genet. 12 (Spec No 2), R285–R292.
Laporte, J., Hu, L.J., Kretz, C., Mandel, J.L., Kioschis, P., Coy, J.F., Klauck, S.M., Poustka, A., Dahl, N., 1996. A gene mutated in X-linked myotubular myopathy defines a new putative tyrosine phosphatase family conserved in yeast. Nat. Genet. 13 (2), 175–182.
Lecompte, O., Poch, O., Laporte, J., 2008. PtdIns5P regulation through evolution: roles in membrane trafficking? Trends Biochem. Sci. 33 (10), 453–460.
Li, X., Tran, K.M., Aziz, K.E., Sorokin, A.V., Chen, J., Wang, W., 2016. Defining the protein-protein interaction network of the human protein tyrosine phosphatase family. Mol. Cell Proteomics 15 (9), 3030–3044.
Lorenzo, O., Urbe, S., Clague, M.J., 2006. Systematic analysis of myotubularins: heteromeric interactions, subcellular localisation and endosome related functions. J. Cell Sci. 119 (Pt 14), 2953–2959.
Mersiyanova, I.V., Perepelov, A.V., Polyakov, A.V., Sitnikov, V.F., Dadali, E.L., Oparin, R.B., Petrin, A.N., Evgrafov, O.V., 2000. A new variant of Charcot-Marie-Tooth disease type 2 is probably the result of a mutation in the neurofilament-light gene. Am. J. Hum. Genet. 67 (1), 37–46.
Mochizuki, Y., Majerus, P.W., 2003. Characterization of myotubularin-related protein 7 and its binding partner, myotubularin-related protein 9. Proc. Natl. Acad. Sci. U. S. A. 100 (17), 9768–9773.
Mochizuki, Y., Ohashi, R., Kawamura, T., Iwanari, H., Kodama, T., Naito, M., Hamakubo, T., 2013. Phosphatidylinositol 3-phosphatase myotubularin-related protein 6 (MTMR6) is regulated by small GTPase Rab1B in the early secretory and autophagic pathways. J. Biol. Chem. 288 (2), 1009–1021.
Nandurkar, H.H., Caldwell, K.K., Whisstock, J.C., Layton, M.J., Gaudet, E.A., Norris, F.A., Majerus, P.W., Mitchell, C.A., 2001. Characterization of an adapter subunit to a phosphatidylinositol (3)P 3- phosphatase: identification of a myotubularin-related protein lacking catalytic activity. Proc. Natl. Acad. Sci. U. S. A. 98 (17), 9499–9504.
Nandurkar, H.H., Huysmans, R., 2002. The myotubularin family: novel phosphoinositide regulators. IUBMB Life 53 (1), 37–43.
Nandurkar, H.H., Layton, M., Laporte, J., Selan, C., Corcoran, L., Caldwell, K.K., Mochizuki, Y., Majerus, P.W., Mitchell, C.A., 2003. Identification of myotubularin as the lipid phosphatase catalytic subunit associated with the 3-phosphatase adapter protein, 3-PAP. Proc. Natl. Acad. Sci. U. S. A. 100 (15), 8660–8665.
Nicot, A.S., Laporte, J., 2008. Endosomal phosphoinositides and human diseases. Traffic 9 (8), 1240–1249.
Plant, P.J., Correa, J., Goldenberg, N., Bain, J., Batt, J., 2009. The inositol phosphatase MTMR4 is a novel target of the ubiquitin ligase Nedd4. Biochem. J. 419 (1), 57–63.
Previtali, S.C., Zerega, B., Sherman, D.L., Brophy, P.J., Dina, G., King, R.H.M., Salih, M.M., Feltri, L., Quattrini, A., Ravazzolo, R., Wrabetz, L., Monaco, A.P., Bolino, A., 2003. Myotubularin-related 2 protein phosphatase and neurofilament light chain protein, both mutated in CMT neuropathies, interact in peripheral nerve. Hum. Mol. Genet. 12 (14), 1713–1723.
Ramel, D., Lagarrigue, F., Pons, V., Mounier, J., Dupuis-Coronas, S., Chicanne, G., Sansonetti, P.J., Gaits-Iacovoni, F., Tronchere, H., Payrastre, B., 2011. Shigella flexneri infection generates the lipid PI5P to alter endocytosis and prevent termination of EGFR signaling. Sci. Signal 4 (191), ra61.
Robinson, F.L., Dixon, J.E., 2006. Myotubularin phosphatases: policing 3-phosphoinositides. Trends Cell Biol. 16 (8), 403–412.
Royer, B., Hnia, K., Gavriilidis, C., Tronchere, H., Tosch, V., Laporte, J., 2013. The myotubularin-amphiphysin 2 complex in membrane tubulation and centronuclear myopathies. EMBO Rep. 14 (10), 907–915.
Rual, J.F., Venkatesan, K., Hao, T., Hirozane-Kishikawa, T., Dricot, A., Li, N., Berriz, G.F., Gibbons, F.D., Dreze, M., Ayivi-Guedehoussou, N., Klitgord, N., Simon, C., Boxem, M., Milstein, S., Rosenberg, J., Goldberg, D.S., Zhang, L.V., Wong, S.L., Franklin, G., Li, S., Albala, J.S., Lim, J., Fraughton, C., Llamosas, E., Cevik, S., Bex, C., Lamesch, P., Sikorski, R.S., Vandenhaute, J., Zoghbi, H.Y., Smolyar, A., Bosak, S., Sequerra, R., Doucette-Stamm, L., Cusick, M.E., Hill, D.E., Roth, F.P., Vidal, M., 2005. Towards a proteome-scale map of the human protein-protein interaction network. Nature 437 (7062), 1173–1178.

Sabha, N., Volpatti, J.R., Gonorazky, H., Reifler, A., Davidson, A.E., Li, X., Eltayeb, N.M., Dall'Armi, C., Di Paolo, G., Brooks, S.V., Buj-Bello, A., Feldman, E.L., Dowling, J.J., 2016. PIK3C2B inhibition improves function and prolongs survival in myotubular myopathy animal models. J. Clin. Invest. 126 (9), 3613–3625.

Sanchez-Juan, P., Bishop, M.T., Aulchenko, Y.S., Brandel, J.P., Rivadeneira, F., Struchalin, M., Lambert, J.C., Amouyel, P., Combarros, O., Sainz, J., Carracedo, A., Uitterlinden, A.G., Hofman, A., Zerr, I., Kretzschmar, H.A., Laplanche, J.L., Knight, R.S., Will, R.G., van Duijn, C.M., 2012. Genome-wide study links MTMR7 gene to variant Creutzfeldt-Jakob risk. Neurobiol. Aging 33 (7), 1487 e1421–1488.

Schaletzky, J., Dove, S.K., Short, B., Lorenzo, O., Clague, M.J., Barr, F.A., 2003. Phosphatidylinositol-5-phosphate activation and conserved substrate specificity of the myotubularin phosphatidylinositol 3-phosphatases. Curr. Biol. 13 (6), 504–509.

Senderek, J., Bergmann, C., Weber, S., Ketelsen, U.P., Schorle, H., Rudnik-Schoneborn, S., Buttner, R., Buchheim, E., Zerres, K., 2003. Mutation of the SBF2 gene, encoding a novel member of the myotubularin family, in Charcot-Marie-Tooth neuropathy type 4B2/11p15. Hum. Mol. Genet. 12 (3), 349–356.

Song, H.O., Lee, J., Ji, Y.J., Dwivedi, M., Cho, J.H., Park, B.J., Ahnn, J., 2010. Calcineurin regulates coelomocyte endocytosis via DYN-1 and CUP-4 in Caenorhabditis elegans. Mol. Cells 30 (3), 255–262.

Srivastava, S., Li, Z., Lin, L., Liu, G., Ko, K., Coetzee, W.A., Skolnik, E.Y., 2005. The phosphatidylinositol 3-phosphate phosphatase myotubularin- related protein 6 (MTMR6) is a negative regulator of the Ca2+-activated K+ channel KCa3.1. Mol. Cell Biol. 25 (9), 3630–3638.

Staiano, L., De Leo, M.G., Persico, M., De Matteis, M.A., 2015. Mendelian disorders of PI metabolizing enzymes. Biochim. Biophys. Acta 1851 (6), 867–881.

Taylor, G.S., Maehama, T., Dixon, J.E., 2000. Inaugural article: myotubularin, a protein tyrosine phosphatase mutated in myotubular myopathy, dephosphorylates the lipid second messenger, phosphatidylinositol 3-phosphate. Proc. Natl. Acad. Sci. U. S. A. 97 (16), 8910–8915.

Tosch, V., Rohde, H.M., Tronchere, H., Zanoteli, E., Monroy, N., Kretz, C., Dondaine, N., Payrastre, B., Mandel, J.L., Laporte, J., 2006. A novel PtdIns3P and PtdIns(3,5)P2 phosphatase with an inactivating variant in centronuclear myopathy. Hum. Mol. Genet. 15 (21), 3098–3106.

Tronchere, H., Laporte, J., Pendaries, C., Chaussade, C., Liaubet, L., Pirola, L., Mandel, J.L., Payrastre, B., 2004. Production of phosphatidylinositol 5-phosphate by the phosphoinositide 3-phosphatase myotubularin in mammalian cells. J. Biol. Chem. 279 (8), 7304–7312.

Tsujita, K., Itoh, T., Ijuin, T., Yamamoto, A., Shisheva, A., Laporte, J., Takenawa, T., 2004. Myotubularin regulates the function of the late endosome through the gram domain-phosphatidylinositol 3,5-bisphosphate interaction. J. Biol. Chem. 279 (14), 13817–13824.

Velichkova, M., Juan, J., Kadandale, P., Jean, S., Ribeiro, I., Raman, V., Stefan, C., Kiger, A.A., 2010. Drosophila Mtm and class II PI3K coregulate a PI(3)P pool with cortical and endolysosomal functions. J. Cell Biol. 190 (3), 407–425.

Walker, D.M., Urbe, S., Dove, S.K., Tenza, D., Raposo, G., Clague, M.J., 2001. Characterization of MTMR3. an inositol lipid 3-phosphatase with novel substrate specificity. Curr. Biol. 11 (20), 1600–1605.

Weidner, P., Sohn, M., Gutting, T., Friedrich, T., Gaiser, T., Magdeburg, J., Kienle, P., Ruh, H., Hopf, C., Behrens, H.M., Rocken, C., Hanoch, T., Seger, R., Ebert, M.P., Burgermeister, E., 2016. Myotubularin-related protein 7 inhibits insulin signaling in colorectal cancer. Oncotarget 7 (31), 50490–50506.

Yoshimura, S., Gerondopoulos, A., Linford, A., Rigden, D.J., Barr, F.A., 2010. Family-wide characterization of the DENN domain Rab GDP-GTP exchange factors. J. Cell Biol. 191 (2), 367–381.

Yu, J., He, X., Chen, Y.G., Hao, Y., Yang, S., Wang, L., Pan, L., Tang, H., 2013. Myotubularin-related protein 4 (MTMR4) attenuates BMP/Dpp signaling by dephosphorylation of Smad proteins. J. Biol. Chem. 288 (1), 79–88.

Zhang, J., Wong, C.H., Xia, W., Mruk, D.D., Lee, N.P., Lee, W.M., Cheng, C.Y., 2005. Regulation of Sertoli-germ cell adherens junction dynamics via changes in protein-protein interactions of the N-cadherin-beta-catenin protein complex which are possibly mediated by c-Src and myotubularin-related protein 2: an in vivo study using an androgen suppression model. Endocrinology 146 (3), 1268–1284.

Zhang, Z.Y., Maclean, D., McNamara, D.J., Sawyer, T.K., Dixon, J.E., 1994. Protein tyrosine phosphatase substrate specificity: size and phosphotyrosine positioning requirements in peptide substrates. Biochemistry 33 (8), 2285–2290.

Zou, W., Lu, Q., Zhao, D., Li, W., Mapes, J., Xie, Y., Wang, X., 2009. Caenorhabditis elegans myotubularin MTM-1 negatively regulates the engulfment of apoptotic cells. PLoS Genet. 5 (10), e1000679.

Appendix 2:

Phosphoinositides: lipidic essential actors in the intracellular traffic.

Bertazzi *et al.* 2015

Biologie Aujourd'hui

Biologie Aujourd'hui, 209 (1), 97-109 (2015)

DOI: 10.1051/jbio/2015006

Les phosphoinositides, des lipides acteurs essentiels du trafic intracellulaire

Dimitri L. Bertazzi, Johan-Owen De Craene, Séverine Bär, Myriam Sanjuan-Vazquez, Matthieu A. Raess et Sylvie Friant

Département de Génétique Moléculaire et Cellulaire, UMR 7156, Université de Strasbourg et CNRS, 67084 Strasbourg, France

Auteur correspondant : Sylvie Friant, s.friant@unistra.fr

Reçu le 19 novembre 2014

Résumé – Les phosphoinositides sont des lipides impliqués dans le transport vésiculaire des protéines entre les différents compartiments. Ils agissent par le recrutement et/ou l'activation de protéines effectrices et sont de ce fait impliqués dans la régulation de différentes fonctions cellulaires telles que le bourgeonnement vésiculaire, la fusion ou la dynamique des membranes et du cytosquelette. Bien que présents en faible concentration dans les membranes, leur rôle est indispensable à la survie des cellules et doit être régulé avec précision. Le contrôle de leur fonction se fait par la phosphorylation/déphosphorylation des positions D3, D4 et/ou D5 de leur anneau inositol par des kinases et phosphatases spécifiques des différentes membranes intracellulaires. Ces enzymes sont en partie conservées entre la levure et l'Homme et leur perte de fonction peut entraîner des maladies génétiques graves comme les myopathies.

Mots clés : Lipides / trafic intracellulaire / phosphoinositide / phosphatase / kinase

Abstract – Phosphoinositides: lipidic essential actors in the intracellular traffic.

Phosphoinositides (PPIn) are lipids involved in the vesicular transport of proteins between the different intracellular compartments. They act by recruiting and/or activating effector proteins and are thus involved in crucial cellular functions including vesicle budding, fusion and dynamics of membranes and regulation of the cytoskeleton. Although they are present in low concentrations in membranes, their activity is essential for cell survival and needs to be tightly controlled. Therefore, phosphatases and kinases specific of the various cellular membranes can phosphorylate/dephosphorylate their inositol ring on the positions D3, D4 and/or D5. The differential phosphorylation determines the intracellular localisation and the activity of the PPIn. Indeed, non-phosphorylated phosphatidylinositol (PtdIns) is the basic component of the PPIn and can be found in all eukaryotic cells at the cytoplasmic face of the ER, the Golgi, mitochondria and microsomes. It can get phosphorylated on position D4 to obtain PtdIns4*P*, a PPIn enriched in the Golgi compartment and involved in the maintenance of this organelle as well as anterograde and retrograde transport to and from the Golgi. PtdIns phosphorylation on position D3 results in PtdIns3*P* that is required for endosomal transport and multivesicular body (MVB) formation and sorting. These monophosphorylated PtdIns can be further phosphorylated to produce bisphophorylated PtdIns. Thus, PtdIns(4,5)P_2, mainly produced by PtdIns4*P* phosphorylation, is enriched in the plasma membrane and involved in the regulation of actin cytoskeleton and endocytosis. PtdIns(3,5)P_2, mainly produced by PtdIns3*P* phosphorylation, is enriched in late endosomes, MVBs and the lysosome/vacuole and plays a role in endosome to vacuole transport. PtdIns(3,4)P_2 is absent in yeast, cells and mainly produced by PtdIns4*P* phosphorylation in human cells; PtdIns(3,4)P_2 is localised in the plasma membrane and plays an important role as a second messenger by recruiting specific

Article publié par EDP Sciences

protein kinases (Akt and PDK1). Finally the triple phosphorylated PPIn, PtdIns(3,4,5)P_3 also absent in yeast, is produced by the phosphorylation of PtdIns(3,4)P_2 and localized at the plasma membrane of human cells where it binds proteins via their PH domain. Interaction partners include members of the Arf (ADP-ribosylation factors) family, PDK1 (Phosphoinositide Dependent Kinase 1) and Akt. Therefore this last PPIn is essential for the control of cell proliferation and its deregulation leads to the development of numerous cancers. In conclusion, the regulation of PPIn phosphorylation/dephosphorylation is complex and needs to be very precisely regulated. Indeed phosphatases and kinases allow the maintenance of the equilibrium between the different forms. PPIn play a crucial role in numerous cellular functions and a loss in their synthesis or regulation results in severe genetic diseases.

Key words: Lipids / intracellular trafficking / phosphoinositides / phosphatase / kinase

Abréviations

ENTH	*Epsin N-Terminal Homology*
ESCRT	*Endosomal Sorting Complex Required for Transport*
FYVE	Fab1, YGL023, Vps27, EEA1
MVB	*MultiVesicular Body*
Osh1	*Oxysterol binding protein homologue 1*
PC	PhosphatidylCholine,
PE	PhosphatidylEthanolamine
PH	*Pleckstrin Homology*
PHD	*Plant HomeoDomain finger*
PIKfyve	PtdIns3P 5-Kinase (humaine)
Pis1	PtdIns synthase 1
PPIn	PolyPhosphoInositides
PS	PhosphatidylSérine,
PtdIns	PhosphatidylInositol
PtdIns3P	PhosphatidylInositol 3-phosphate
PtdIns(3,4)P_2	PhosphatidylInositol 3, 4-bisphosphate
PtdIns(3,4,5)P_3	PhosphatidylInositol 3, 4,5-trisphosphate
PTEN	*Phosphatase and TENsin homolog*
SM	SphingoMyéline
Vps34	*Vacuolar Protein Sorting 34*

1 Le métabolisme des phosphoinositides membranaires

1.1 Les lipides, constituants majoritaires des membranes

Les membranes ne sont pas des structures figées mais dynamiques dont les propriétés physico-chimiques font partie des facteurs ayant permis l'apparition de la vie. En effet, l'environnement, au sens large, est caractérisé par des variations de température, d'humidité, de pH, d'ensoleillement, de pression osmotique ou de source d'énergie, autant de facteurs auxquels tout organisme vivant doit s'adapter afin de conserver un équilibre interne. C'est pour gagner en stabilité face à toutes ces fluctuations incontrôlables que la cellule s'est organisée de façon à limiter les variations intracellulaires. La membrane plasmique est le premier rempart permettant de séparer le milieu extérieur du cytoplasme. Sa composition lui assure une protection mécanique et un contrôle des échanges avec l'extérieur grâce à une perméabilité très sélective.

La membrane plasmique s'organise en deux feuillets de phospholipides, la bicouche, dans laquelle s'enchâssent les macromolécules protéiques, stérols et glycolipides. Les phospholipides qui constituent cette bicouche sont amphiphiles avec un groupe hydrophile (tête) lié à un groupe hydrophobe (queue). Au sein de la bicouche, les groupes hydrophobes se font face, générant un espace hydrophobe entre les deux feuillets membranaires. Cette propriété est très importante pour l'ancrage dans la membrane de molécules lipidiques (stérols ou céramides), de protéines transmembranaires ou de protéines ayant une ancre lipidique. La composition en lipides des membranes varie selon les organismes (eucaryotes ou procaryotes), les types cellulaires (au sein des tissus d'un même organisme pluricellulaire), le type de membrane (plasmique, réticulum endoplasmique, endosomes, appareil de Golgi, mitochondries et autres compartiments intracellulaires) et même l'état de la cellule (au repos ou en réponse à un stress/stimulus) (Spector & Yorek, 1985 ; Zinser *et al.*, 1991).

Les membranes sont composées principalement de cinq phospholipides : la phosphatidylcholine (PC), la phosphatidyléthanolamine (PE), la phosphatidylsérine (PS), le phosphatidylinositol (PtdIns) et la sphingomyéline (SM). Les stérols, bien que présents dans les membranes cellulaires, ne forment pas la membrane par eux-mêmes mais modulent sa

fluidité, essentielle pour la diffusion latérale des molécules dans la bicouche. Le double feuillet lipidique des membranes présente également une distribution asymétrique des phospholipides entre les feuillets interne et externe, qui résulte en partie de la diffusion verticale entre les deux feuillets par *flip-flop*, un mécanisme peu efficace.

Si la membrane plasmique joue un rôle essentiel de barrière sélective, on retrouve dans les cellules eucaryotes d'autres structures membranaires intracellulaires telles que les organites et les vésicules de transport. L'organisation de ces membranes ainsi que leur composition diffèrent selon la nature du compartiment. En effet, le réticulum endoplasmique, l'appareil de Golgi, les lysosomes (la vacuole chez les levures), les endosomes et les vésicules de transport sont entourés d'une seule bicouche lipidique. L'espace à l'intérieur de ces compartiments intracellulaires est nommé lumen ou lumière. En revanche, le noyau, les mitochondries, les chloroplastes des végétaux chlorophylliens et les vésicules autophagiques sont délimités par une double bicouche lipidique. Chacun de ces compartiments intracellulaires s'acquitte de fonctions bien précises nécessaires à la vie de la cellule (Spector & Yorek, 1985). Cette dernière doit donc chorégraphier le transport vésiculaire de protéines de manière spatiotemporelle entre ces différents compartiments. Il est par conséquent indispensable pour la cellule de discriminer un compartiment intracellulaire d'un autre. Ceci passe par l'attribution d'une identité propre à chacun des organites allant même jusqu'à distinguer les faces « *cis* » des faces « *trans* » de l'appareil de Golgi. Ces « cartes d'identité » propres à chaque compartiment intracellulaire sont essentiellement définies par les molécules tapissant le feuillet cytoplasmique des membranes. Parmi ces molécules, les lipides membranaires, et plus particulièrement les phosphoinositides jouent un rôle majeur dans la régulation spatiotemporelle de différents processus cellulaires tels que la dynamique du cytosquelette, le trafic membranaire, la prolifération et la survie cellulaire.

1.2 Les phosphoinositides, des médiateurs lipides

Les polyphosphoinositides (PPIn) sont des constituants mineurs des membranes cellulaires, représentant moins de 10 % des phospholipides cellulaires (Payrastre *et al.*, 2001). Les PPIn sont composés d'une molécule de glycérol estérifiée en position SN1 et SN2 par deux chaînes d'acides gras et reliée en position SN3 à un anneau inositol par l'intermédiaire d'un groupement phosphate (Payrastre *et al.*, 2001). Chez l'Homme, les acides gras les plus courants dans le PtdIns sont l'acide stéarique (18:0) en position SN1 et l'acide arachidonique (20:4) en SN2 (Marcus *et al.*, 1969). Chez la levure *Saccharomyces cerevisiae*, la nature des acides gras est légèrement différente ; on retrouve ainsi une majorité d'acide oléique (18:1), d'acide palmitoléique (16:1) et d'acide palmitique (16:0) (Trevelyan, 1966). Etant donné que les diverses espèces de PPIn dérivent du PtdIns, on estime que leurs compositions en acides gras sont les mêmes que celles du PtdIns.

L'anneau inositol des PPIn est un polyol de cyclohexane dont les position D3, D4 et D5 sont phosphorylables, générant potentiellement sept PPIn différents (figure 1) : le phosphatidylinositol 3-phosphate (PtdIns3P), le PtdIns4P, le PtdIns5P, le PtdIns 3,4-bisphosphate (PtdIns(3,4)P_2), le PtdIns(3,5)P_2, le PtdIns(4,5)P_2 et le PtdIns 3,4,5-trisphosphate (PtdIns(3,4,5)P_3). Malgré leur faible concentration dans les membranes, les PPIn jouent un rôle essentiel dans le recrutement et/ou l'activation de protéines effectrices. De plus, leur présence dans une membrane donnée et leurs niveaux varient grâce aux lipides kinases et phosphatases spécifiques des différentes membranes, permettant ainsi la régulation spatiotemporelle de divers événements tels que le bourgeonnement, la fusion ou la dynamique des membranes (Payrastre *et al.*, 2001).

1.3 Le phosphatidylinositol PtdIns, précurseur des phosphoinositides

Le PtdIns, point de départ du métabolisme des PPIn, est un phospholipide ubiquitaire dans les cellules eucaryotes mais dont la proportion varie selon le type de membrane. En effet, les PPIn sont tous métabolisés directement ou séquentiellement à partir du PtdIns (figure 1). Chez la levure *S. cerevisiae*, le PtdIns est synthétisé par la PtdIns synthase 1 (Pis1) au niveau de la face cytoplasmique de la membrane du réticulum endoplasmique, de l'appareil de Golgi, des mitochondries et des microsomes (Nikawa & Yamashita, 1984). Chez l'Homme, cette synthèse est catalysée par l'homologue de Pis1, la PtdIns Synthase qui présente une distribution similaire à celle de Pis1 chez la levure (Antonsson, 1994).

Le PtdIns est également recyclé par la conversion du PtdIns3P, du PtdIns4P et du PtdIns5P en PtdIns par l'action de lipides phosphatases (figure 1). Chez l'Homme, les myotubularines (MTM1, MTMR1-4,6,7) sont des 3-phosphatases déphosphorylant spécifiquement la position D3 et réalisant, entre autres, la conversion du PtdIns3P en PtdIns (Laporte *et al.*, 2003). Les autres phosphatases sont moins spécifiques car elles sont capables de déphosphoryler le PtdIns3P en PtdIns, comme la PPIn phosphatase SAC1, qui déphosphoryle également le PtdIns4P et probablement le PtdIns5P en PtdIns (Liu & Bankaitis, 2010). La levure *S. cerevisiae* présente également une phosphatase spécifique de la

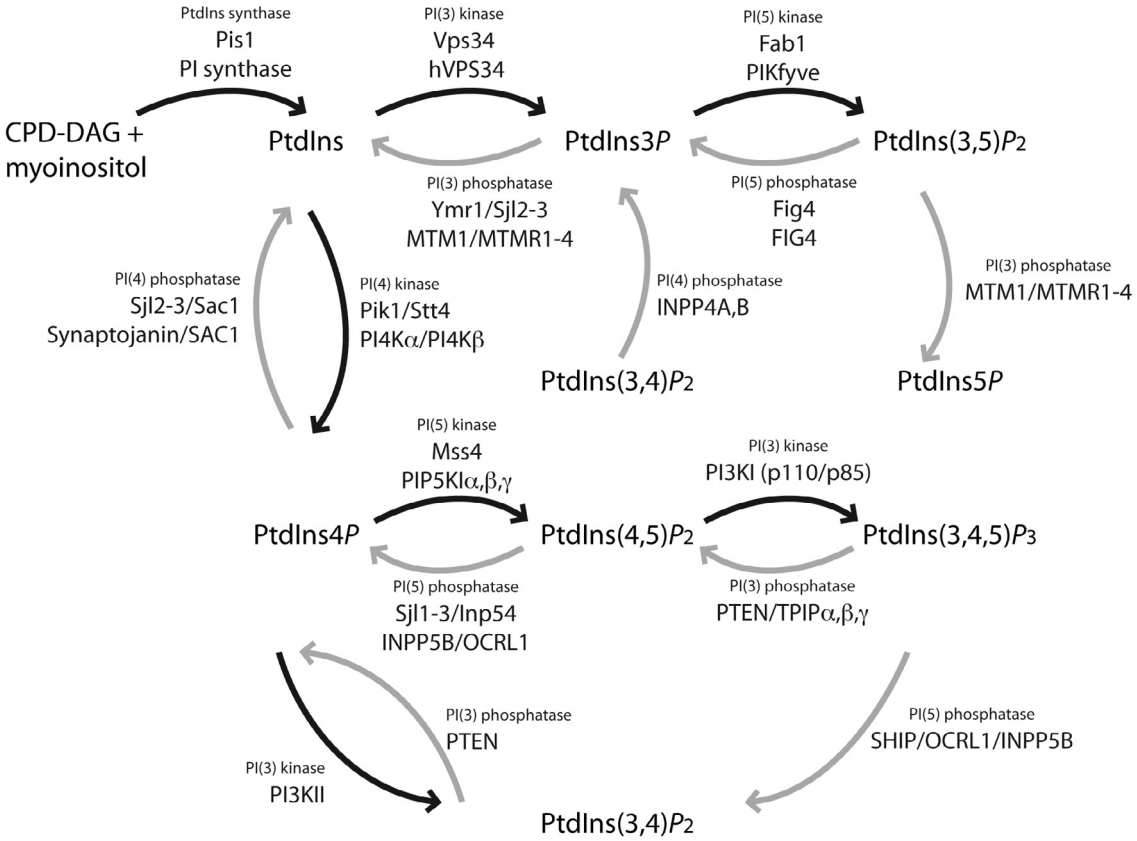

Fig. 1. Synthèse des phosphoinositides chez la levure *S.cerevisiae* et chez l'Homme avec les enzymes impliquées. Les réactions de phosphorylation sont représentées par des flèches noires et celles de déphosphorylation par des flèches grises. Le nom des enzymes de levure (quand elles existent) est indiqué en haut et leur homologue chez l'Homme est noté en-dessous.

position D3 avec son unique homologue de myotubularine Ymr1. Cette activité sur le PtdIns3*P* est partagée avec des phosphatases plus générales que sont les *Synaptojanin-like protein* 1 et 2 (Sjl2 et Sjl3) et Sac1, aussi capables de convertir le PtdIns4*P* en PtdIns (Parrish *et al.*, 2004).

2 Le PtdIns4*P*, un effecteur clé du trafic au niveau de l'appareil de Golgi

2.1 Synthèse du PtdIns4*P*

Le PtdIns4*P* représente environ 30 % des PPIn totaux chez la levure, et approximativement 45 % chez l'Homme (Payrastre *et al.*, 2001). Il est enrichi au niveau de l'appareil de Golgi où il est majoritairement généré par phosphorylation du PtdIns par des PI 4-kinases (De Matteis *et al.*, 2002). Il peut aussi résulter de la déphosphorylation du PtdIns(4,5)P_2 et du PtdIns(3,4)P_2 par des PI 5-phosphatases et des PI 3-phosphatases, respectivement (figure 1). Chez *S. cerevisiae*, les PI 4-kinases Pik1 et Stt4 réalisent la conversion du PtdIns en PtdIns4*P* au niveau de l'appareil de Golgi et de la membrane plasmique, respectivement (Audhya *et al.*, 2000). La déphosphorylation du PtdIns(4,5)P_2 en PtdIns4*P* est orchestrée par les 5-phosphatases Inp51/Sjl1, Inp52/Sjl2, Inp53/Sjl3 et Inp54 (figure 1) (Liu & Bankaitis, 2010). Chez l'Homme, les PPIn 4-kinases PI4Kα et PI4Kβ synthétisent le PtdIns4*P* à partir du précurseur PtdIns. Par ailleurs, le PtdIns4*P*peut être synthétisé à partir du PtdIns(3,4)P_2 par la 3-phosphatase PTEN ou à partir du PtdIns(4,5)P_2 par les 5-phosphatases OCRL1 (*Occulo-cerebro-renal syndrome protein 1*), INPP5B (Inositol Polyphosphate Phosphatase 5B) et les synaptojanines 1 et 2 (figure 1) (Liu & Bankaitis, 2010). Des mutations dans *OCRL1* sont à l'origine du syndrome occulo-cérébro-rénal de Lowe.

2.2 Rôle physiologique du PtdIns4*P*

Le PtdIns4*P* a pendant longtemps été considéré comme un simple précurseur d'autres PPIn. Chez

la levure, le PtdIns4*P* est présent dans deux compartiments distincts : la membrane plasmique et le réseau *trans*-golgien (Audhya *et al.*, 2000). L'appareil de Golgi constitue un carrefour central dans le trafic membranaire, où les protéines et les membranes de divers compartiments intracellulaires s'échangent, nécessitant donc la régulation spatio-temporelle très précise de ces processus. Le PtdIns4*P* serait impliqué dans le maintien de l'identité de l'appareil de Golgi, afin de préserver son rôle dans le trafic intracellulaire. Ainsi, chez la levure, le PtdIns4*P* a été montré comme ayant une fonction dans le transport de protéines : le transport antérograde à partir du réseau *trans*-golgien et le transport rétrograde vers l'appareil de Golgi (Audhya *et al.*, 2000). De plus, chez la levure le PtdIns4*P* est important pour la formation des vésicules de sécrétion allant du Golgi vers la membrane plasmique (Mizuno-Yamasaki *et al.*, 2010). De nombreuses protéines interagissant avec le PtdIns4*P* ont été identifiées et sont localisées à l'appareil de Golgi (Lemmon, 2003). Par exemple, la protéine de levure Osh1 (*Oxysterol binding protein homologue*), requise pour le transport des stérols, est localisée à l'appareil de Golgi *via* son domaine PH (*Pleckstrin Homology*) qui lie le PtdIns4*P* (Levine & Munro, 2002).

L'homologue humain de Osh1, la protéine OSBP (*OxySterol Binding Protein*), également impliquée dans le transport intracellulaire des stérols, se localise au niveau du Golgi grâce à l'interaction entre son domaine PH et le PtdIns4*P* (Levine & Munro, 2002). Cependant, si cette interaction est essentielle à la localisation de OSBP, elle n'est pas suffisante puisqu'elle nécessite également l'interaction avec une GTPase golgienne (*ADP-Ribosylation Factor* ou ARF) (Levine & Munro, 2002). Deux autres protéines, FAPP1 et FAPP2 (*Four-Phosphate-Adaptor Protéine 1 et 2*) qui régulent le trafic membranaire golgien, sont également en complexe avec ARF et interagissent avec le PtdIns4*P* *via* leur domaine PH (Lemmon, 2003). Cette interaction protéine-lipide jouerait un rôle dans le transport vésiculaire antérograde du Golgi vers la membrane plasmique en contrôlant la production de vésicules bourgeonnant depuis l'appareil de Golgi (Godi *et al.*, 2004).

3 Le PtdIns3*P*, un lipide essentiel au trafic membranaire au niveau des endosomes

3.1 Synthèse du PtdIns3*P*

Le PtdIns3*P* représente environ 30 % des PPIn totaux de levure et est présent en quantité équivalente aux PtdIns4*P*. Par ailleurs chez l'Homme, il représente moins de 15 % des PPIn mono-phosphorylés et est largement minoritaire par rapport au PtdIns4*P* (Payrastre *et al.*, 2001). Le PtdIns3*P* est produit par phosphorylation du PtdIns en position D3 de l'inositol ou par déphosphorylation du PtdIns(3,4)P_2 ou du PtdIns(3,5)P_2 (figure 1).

Chez la levure *S. cerevisiae,* une seule enzyme catalyse spécifiquement et uniquement la phosphorylation du PtdIns en PtdIns3*P*, la lipide kinase Vps34 (*Vacuolar Protein Sorting 34*) (Herman & Emr, 1990 ; Schu *et al.*, 1993). L'activité de Vps34 est régulée par la protéine kinase Vps15 et est indispensable à la formation du MVB (*MultiVesicular Body* ou corps multivésiculaire). De façon intéressante, il a été montré que la régulation positive de Vps34 par Vps15 est stimulée par l'interaction directe entre les sept répétitions WD (Trp-Asp) situées dans la région C-terminale de cette dernière et la sous-unité Gα de la protéine Gpa1. Le domaine C-terminal de Vps15 se comporterait ainsi comme la sous-unité β de la protéine G. Ainsi, il y aurait un couplage entre la signalisation médiée par les protéines G au niveau de la membrane plasmique et le tri des récepteurs de cette signalisation au niveau des endosomes. De plus, l'interaction du complexe Vps34-Vps15 avec Gpa1 stimule la production de PtdIns3*P* aux endosomes (Slessareva *et al.*, 2006).

Le génome humain code pour huit lipide-kinases capables de produire du PtdIns3*P* et regroupées en trois classes, selon leurs spécificités de substrat et leur homologie (Vanhaesebroeck *et al.*, 2001) :

- Deux phosphoinositides 3-kinases de classe I (PI3K I) qui phosphorylent surtout le PtdIns(4,5)P_2 en PtdIns(3,4,5)P_3.
- Trois phosphoinositides 3-kinases de classe II (PI3K II) qui phosphorylent surtout le PtdIns4*P* en PtdIns(3,4)P_2.
- La phosphoinositide 3-kinase de classe III, qui est l'homologue de la protéine de levure Vps34. Tout comme Vps34, la PI3K III humaine est spécifique du PtdIns et est par conséquent probablement à l'origine de l'essentiel du PtdIns3*P* cellulaire. La sous-unité régulatrice de hVps34 est la protéine p150, l'homologue de Vps15 de levure (Panaretou *et al.*, 1997). Une étude phylogénétique a mis en évidence la coévolution de l'unique PI3K III et de sa sous-unité régulatrice Vps15 chez la plupart des eucaryotes, de la levure à l'Homme en passant par les amibes et les parasites (Lecompte *et al.*, 2008).

Chez la levure, le PtdIns3*P* est également synthétisé par les lipides phosphatases Fig4 (*Factor Induced Gene 4*, également appelée Sac3), Sjl2/Inp52, Sjl3/Inp53 et Sac1. Elles possèdent toutes un domaine SAC catalytique permettant de déphosphoryler différents PPIn dont le PtdIns(3,5)P_2 en PtdIns3*P* (Liu & Bankaitis, 2010). Fig4 est la seule PtdIns 5-phosphatase spécifique du PtdIns(3,5)P_2

(Gary *et al.*, 2002). L'homologue humain FIG4/SAC3 remplit des fonctions cellulaires similaires à Fig4. Des mutations dans le gène humain *FIG4* sont à l'origine du syndrome de Charcot-Marie-Tooth type 4J, une maladie neuromusculaire de forme récessive qui se traduit par une démyélinisation des axones (Liu & Bankaitis, 2010). Avec *MTMR2*, *FIG4* est donc le deuxième gène codant pour une lipide phosphatase impliquée dans une maladie neuromusculaire.

3.2 Rôle physiologique du PtdIns3*P*

Dans les cellules de levure et de mammifères, le PtdIns3*P* est enrichi au niveau de la membrane des endosomes précoces et à la membrane des vésicules internes des endosomes tardifs (ou corps multivésiculaires, ou MVB) (Gillooly *et al.*, 2000). Au niveau des endosomes précoces, il joue un rôle central dans le recrutement de protéines effectrices telles que la protéine de levure Vps27 ou son homologue humaine Hrs (*Hepatocyte growth factor*-R*egulated tyrosine kinase Substrate*), deux protéines du complexe ESCRT-0 (*Endosomal Sorting Complex Required for Transport*) impliquées dans le tri endosomal des protéines et la formation du MVB (Henne *et al.*, 2011). Ces deux protéines comportent un domaine FYVE (Fab1, YGL023, Vps27, et EEA1) liant le PtdIns3*P* endosomal et un motif de recrutement du complexe ESCRT-1 (Gruenberg & Stenmark, 2004). Ceci permet de recruter les deux autres complexes ESCRT-2 et 3 dont l'action concertée permet l'internalisation des protéines membranaires dans les vésicules internes du MVB (Henne *et al.*, 2011). Cette internalisation est indispensable à l'arrêt des cascades de signalisation médiées par des récepteurs transmembranaires et à l'adressage de protéines membranaires à la vacuole/lysosome.

La protéine adaptatrice humaine EEA1 (*Early Endosomal Antigen 1*) se lie également au PtdIns3*P* avec une forte affinité *via* son domaine FYVE et régule les processus de fusion membranaire entre endosomes en recrutant la GTPase Rab5 aux endosomes (Gruenberg & Stenmark, 2004).

De même, la PtdIns3*P* 5-kinase Fab1 (*S. cerevisiae*) ou PIKfyve (humaine), qui catalyse la phosphorylation du PtdIns3*P* en PtdIns(3,5)P_2, se fixe au PtdIns3*P* *via* son domaine FYVE (Payrastre *et al.*, 2001). Ainsi, un des rôles physiologiques du PtdIns3*P* est de servir de précurseur à la synthèse du PtdIns(3,5)P_2.

Chez la levure *S. cerevisiae*, la délétion du gène *VPS34* n'est pas létale mais elle entraîne une croissance très lente et une forte diminution de la résistance à de nombreux facteurs (température, pH, éthanol, hygromycine B, stress hyperosmotique, caféine ou rapamycine). La levure *vps34Δ* présente également d'importants défauts de trafic membranaire qui se traduisent par une morphologie et un transport vacuolaire anormaux, l'excrétion de la carboxypeptidase Y (CPY) et un défaut d'autophagie (Kihara *et al.*, 2001). Un des rôles essentiels de cette lipide kinase de levure est donc d'assurer l'intégrité du tri des protéines à destination de la vacuole en produisant du PtdIns3*P*, lequel permettra le recrutement de protéines effectrices du trafic (Henne *et al.*, 2011).

4 Le PtdIns5*P*, un phosphoinositide méconnu

4.1 Synthèse du PtdIns5*P*

Le PtdIns5*P* est le PPIn mono-phosphate identifié le plus récemment (Rameh *et al.*, 1997). Il est longtemps resté méconnu en raison de sa faible concentration basale dans les cellules de mammifères, mais également des difficultés liées aux techniques permettant de le séparer du PtdIns4*P*. En effet, en conditions basales dans les cellules de mammifères, le PtdIns5*P* représente moins de 10 % des PPIn monophosphates (Payrastre *et al.*, 2001).

Par ailleurs, aucune étude n'a mis en évidence la présence de PtdIns5*P* dans une souche sauvage de levure *S. cerevisiae*. En effet, Ymr1, l'unique représentante des myotubularines dans la levure, est dépourvue d'activité 3-phosphatase à l'encontre du PtdIns(3,5)P_2 (Taylor *et al.*, 2000 ; Parrish *et al.*, 2004).

Chez l'humain, le PtdIns5*P* est produit par la lipide kinase PIKfyve directement à partir du PtdIns (figure 1). *In vivo,* la surexpression de PIKfyve induit une augmentation de PtdIns5*P*, tandis que des souris hétérozygotes PIKfyve +/*null* présentent des niveaux réduits de PtdIns5*P* en comparaison avec les souris témoins, sans pour autant que cela affecte la viabilité des souris mutantes (Ikonomov *et al.*, 2011).

Du côté des lipides phosphatases, on retrouve les membres de la famille des myotubularines (MTM1, MTMR1-4,6,7) qui possèdent une activité 3-phosphatase à l'encontre du PtdIns(3,5)P_2, et génèrent ainsi du PtdIns5*P* (figure 1) (Laporte *et al.*, 2003).

4.2 Rôle physiologique du PtdIns5*P*

Le rôle du PtdIns5*P* dans les cellules de mammifères est encore relativement mal compris. Une fraction du PtdIns5*P* a été détectée au niveau du noyau et serait impliquée dans la réponse au stress, notamment en modulant l'activité du régulateur transcriptionnel

ING2. ING2 est en outre la première protéine identifiée comme ayant un domaine de liaison spécifique au PtdIns5P, nommé PHD (*Plant HomeoDomain finger*), un domaine en doigt de zinc (Gozani *et al.*, 2003).

5 Le PtdIns(4,5)P_2, un phosphoinositide impliqué dans l'endocytose

5.1 Synthèse du PtdIns(4,5)P_2

Chez la levure, le PtdIns(4,5)P_2 est présent en quantité équivalente au PtdIns4P, soit approximativement 30 % des PPIn totaux et plus de 90 % des différents PPIn bis-phosphorylés. Chez l'Homme, il représente environ 45 % des PPIn totaux et plus de 90 % des différents PPIn bis-phosphorylés. Le PtdIns(4,5)P_2 est donc un PPIn majoritaire (Di Paolo & De Camilli, 2006).

Le PtdIns(4,5)P_2 est synthétisé par la PPIn 5-kinase Mss4 chez la levure (figure 1) et il est présent essentiellement à la membrane plasmique (figure 2) (Desrivières *et al.*, 1998).

Chez l'Homme, plusieurs PPIn-kinases à l'origine du PtdIns(4,5)P_2 ont été identifiées : les PIP5K de type I α, β et γ sont localisées à la membrane plasmique et convertissent le PtdIns4P en PtdIns(4,5)P_2 (Ishihara *et al.*, 1998) ; tandis que les PIP4K de type II sont situées au niveau de l'appareil de Golgi et convertissent le PtdIns5P en PtdIns(4,5)P_2 (Bunce *et al.*, 2008 ; Clarke *et al.*, 2008). Contrairement à la levure, les mammifères synthétisent également du PtdIns(3,4,5)P_3 qui peut servir de substrat à des PPIn 3-phosphatases telles que PTEN (*Phosphatase and TENsin homolog*), TPIPα, β et γ pour produire du PtdIns(4,5)P_2 (figure 1) (Liu & Bankaitis, 2010).

5.2 Rôle physiologique du PtdIns(4,5)P_2

Chez *S. cerevisiae* et dans les cellules humaines, le PtdIns(4,5)P_2 est majoritairement présent dans le feuillet cytoplasmique de la membrane plasmique (figure 2), où il agit comme un régulateur majeur du cytosquelette d'actine et de l'endocytose. Chez *S. cerevisiae*, Mss4 agit en combinaison avec la PtdIns 4-kinase Stt4 à la membrane plasmique pour générer le PtdIns(4,5)P_2 à partir de PtdIns. Ce PPIn est essentiel pour l'activation de la cascade de signalisation des MAP kinases médiée par Rho1/Pkc1. En effet, la localisation correcte de Rom2, la GEF (*GTP Exchange Factor*) de la GTPase Rho1, dépend directement de l'interaction entre son domaine PH et le PtdIns(4,5)P_2 membranaire (Audhya & Emr, 2002). L'organisation du cytosquelette d'actine dépend en grande partie de cette voie de signalisation (Desrivières *et al.*, 1998). L'activité de Mss4 et la synthèse de PtdIns(4,5)P_2 remplissent également une fonction essentielle dans l'endocytose qui dépend de l'actine chez la levure (Sun *et al.*, 2007). En effet, les protéines effectrices de l'endocytose comme les domaines ENTH (*Epsin N-Terminal Homology*), ANTH (*AP-180 N-Terminal Homology*) ou PH (*Pleckstrin Homology*) possèdent un domaine de liaison au PtdIns(4,5)P_2 (Itoh & Takenawa, 2002 ; De Craene *et al.*, 2012).

Chez l'Homme, le PtdIns(4,5)P_2 joue un rôle majeur dans la régulation de différentes voies de signalisation, notamment en raison des variations rapides auxquelles il peut être soumis par le jeu des kinases et phosphatases à PPIn (figure 1). À l'instar de celui de la levure, le PtdIns(4,5)P_2 remplit chez l'homme une fonction importante dans la régulation du cytosquelette d'actine. En effet, plusieurs études ont révélé des interactions entre le PtdIns(4,5)P_2 et des protéines régulatrices de la polymérisation de l'actine. Dans les cellules de mammifères, le PtdIns(4,5)P_2 est principalement requis au niveau de la membrane plasmique pour l'endocytose médiée par la clathrine (figure 2) (Di Paolo & De Camilli, 2006). Il sert alors de signal de recrutement à de nombreuses protéines effectrices de l'étape d'internalisation de l'endocytose, *via* un domaine protéique (ENTH, ANTH, PH) liant spécifiquement le PtdIns(4,5)P_2 (Itoh & Takenawa, 2002 ; Di Paolo & De Camilli, 2006 ; De Craene *et al.*, 2012). Ainsi, le domaine ENTH de l'Epsine1 lie le PtdIns(4,5)P_2, et cette interaction induit un réarrangement structural de l'extrémité N-terminale en une hélice-α qui va pénétrer dans la bicouche lipidique et générer la courbure membranaire nécessaire à la formation de la vésicule d'endocytose (Ford *et al.*, 2001).

6 Le PtdIns(3,5)P_2, un phosphoinositide régulant le trafic endosome-lysosome

6.1 Synthèse du PtdIns(3,5)P_2

Le PtdIns(3,5)P_2 est également un PPIn peu abondant puisqu'il représente moins de 5 % des PPIn totaux chez l'Homme et chez *S. cerevisiae ;* il est enrichi au niveau des endosomes tardifs, du MVB et du lysosome/vacuole (figure 2) (Di Paolo & De Camilli, 2006).

La levure *S. cerevisiae* synthétise séquentiellement le PtdIns(3,5)P_2, d'abord sous l'action de la PtdIns 3-kinase Vps34 qui génère le PtdIns3P, puis par phosphorylation du PtdIns3P en PtdIns(3,5)P_2 par la PtdIns3P 5-kinase Fab1 (figure 1). Chez la levure, un stress hyperosmotique stimule très fortement la

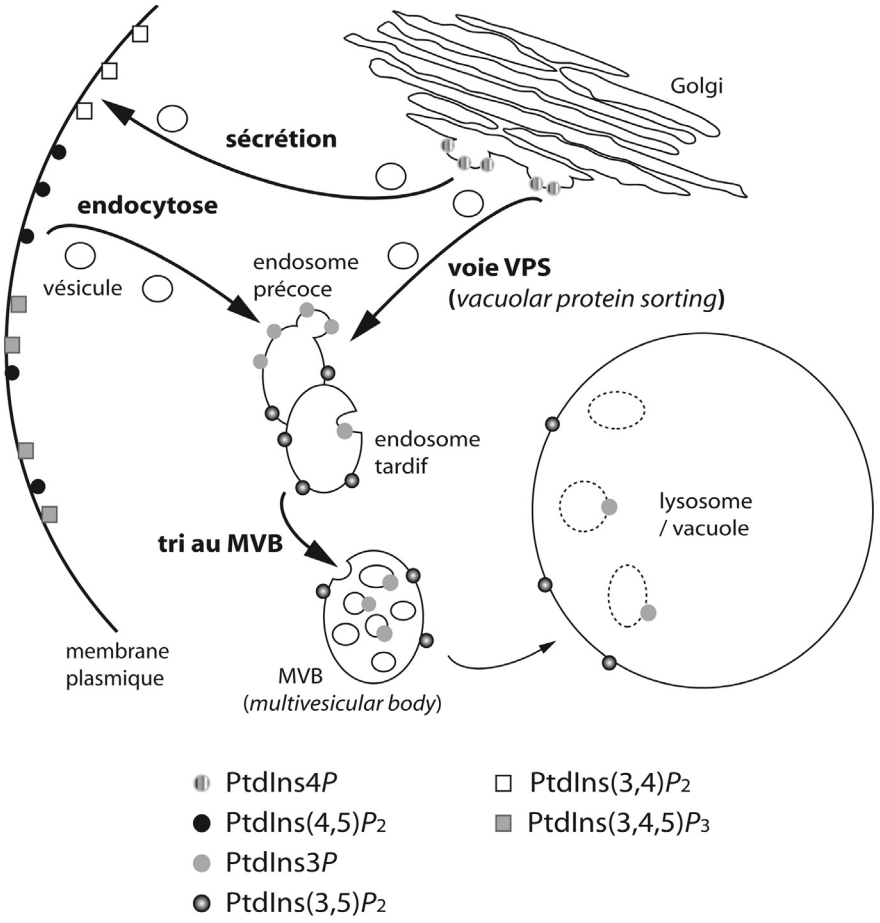

Fig. 2. Localisation intracellulaire des différents phosphoinositides et voies du trafic membranaire. Les différents phosphoinositides (PPIn) sont spécifiquement enrichis dans des membranes définies. Ils sont représentés par des symboles : en rond les PPIn impliqués dans le trafic intracellulaire avec les étapes qu'ils régulent ; en carré les PPIn impliqués dans la signalisation cellulaire, ces deux types de PPIn sont absents chez la levure.

synthèse du PtdIns(3,5)P_2 qui voit son taux intracellulaire augmenter de 20 fois (Dove *et al.*, 1997). La synthèse du PtdIns(3,5)P_2 est régulée par les protéines vacuolaires membranaires Vac7 et Vac14 (Bonangelino *et al.*, 2002). En effet, dans des mutants affectés dans les gènes *FAB1*, *VAC7* ou *VAC14,* le PtdIns(3,5)P_2 n'est pas détectable, et ce indépendamment des conditions osmotiques (Bonangelino *et al.*, 2002). Si Vac7 et Vac14 sont indispensables à la synthèse de PtdIns(3,5)P_2, elles n'interagissent pas puisque Vac7 est l'activateur majeur de Fab1 lors d'un choc hyperosmotique, alors que Vac14 agit dans le cadre d'un complexe avec la lipide phosphatase Fig4 pour réguler le renouvellement du PtdIns(3,5)P_2 (Duex *et al.*, 2006b). Ceci est très surprenant car la stimulation de la synthèse du PtdIns(3,5)P_2 en réponse au stress osmotique est dépendante de réactions antagonistes de phosphorylation du PtdIns(3)P en PtdIns(3,5)P_2 et de la déphosphorylation de celui-ci en PtdIns3P dans un cycle futile (Duex *et al.*, 2006a). Il existe donc une interdépendance essentielle entre la lipide kinase et la phosphatase pour réguler le taux de PtdIns(3,5)P_2 mais également pour activer la production de PtdIns(3,5)P_2 en réponse à un stimulus.

Chez l'Homme, la voie de synthèse du PtdIns(3,5)P_2 est similaire à celle de la levure et c'est PIKfyve, l'unique homologue de Fab1, qui est à l'origine du PtdIns(3,5)P_2 (figure 1) (Shisheva, 2008). A ce jour, aucune PPIn 4-phosphatase hydrolysant le PtdIns(3,4,5)P_3 n'a pu être mise en évidence. Par conséquent, il semblerait que l'unique voie de synthèse du PtdIns(3,5)P_2 passe par la phosphorylation du PtdIns3P (figure 1). De plus, la régulation de la synthèse du PtdIns(3,5)P_2 est conservée chez l'Homme, en effet PIKfyve interagit avec de multiples partenaires jouant un rôle dans l'homéostasie du PtdIns(3,5)P_2 (Shisheva, 2008). Par exemple, PIKfyve interagit avec son enzyme antagoniste Sac3/Fig4

déphosphorylant spécifiquement le PtdIns(3,5)P_2 en PtdIns3P. Cette interaction indirecte se fait par le biais de la protéine adaptatrice ArPIKfyve/Vac14 qui stabilise le complexe et stimule l'activité de PIKfyve (Ikonomov *et al.*, 2010).

Une étude plus récente démontre clairement l'homologie dans la voie de synthèse du PtdIns(3,5)P_2 entre la levure et les mammifères (Jin *et al.*, 2008). En effet, que ce soit chez la levure ou la souris, la protéine Vac14 joue un rôle de plate-forme pour la régulation de la synthèse du PtdIns(3,5)P_2, en interagissant directement avec Fab1/PIKfyve, Fig4/Sac3 et Vac7 qui sont les effecteurs de cette voie de synthèse. Ainsi Vac7, Fab1 et Fig4 pourront entrer en contact par l'intermédiaire de leur liaison à différentes régions de Vac14 (Jin *et al.*, 2008).

6.2 Rôle physiologique du PtdIns(3,5)P_2

Différentes études ont montré le rôle du PtdIns(3,5)P_2 dans la régulation du trafic entre les endosomes et la vacuole (l'équivalent du lysosome chez la levure) (figure 2).

Chez *S. cerevisiae*, les cellules *fab1Δ* présentent un défaut de croissance à 23 °C, ne sont pas viables à 37 °C et montrent un défaut d'acidification de la vacuole. Elles montrent aussi d'importants défauts d'homéostasie vacuolaire avec un compartiment vacuolaire anormalement élargi, occupant jusqu'à 80 % du volume de la cellule. Cet encombrement lié à la taille de la vacuole peut également causer une distribution incorrecte des chromosomes lors de la division cellulaire (Yamamoto *et al.*, 1995). La présence de Vac7 et de Vac14, qui régulent la synthèse du PtdIns(3,5)P_2 par Fab1, est requise pour permettre le maintien de la morphologie vacuolaire ainsi que pour la transmission correcte de la vacuole de la cellule mère à la cellule fille (Bonangelino *et al.*, 2002).

Le PtdIns(3,5)P_2 joue un rôle essentiel dans le tri des protéines membranaires au niveau des endosomes tardifs/MVB (Odorizzi *et al.*, 1998). Les protéines membranaires à destination de la vacuole sont marquées par de l'ubiquitine au niveau des endosomes. Ces cargos ubiquitinés sont reconnus successivement par les complexes ESCRT-0 à -2 pour leur internalisation dans les vésicules internes de l'endosome afin de former le MVB, dont la fusion avec la vacuole aboutit au largage des vésicules dans la lumière de la vacuole (Gruenberg & Stenmark, 2004). Au niveau des endosomes, les epsines de levure Ent3 et Ent5 interagissent avec le PtdIns(3,5)P_2 grâce à leur domaine ENTH, et elles sont indispensables pour le tri des cargos au MVB (Friant *et al.*, 2003 ; Eugster *et al.*, 2004). La protéine liant le plus spécifiquement et avec le plus d'affinité le PtdIns(3,5)P_2 est à l'heure actuelle la protéine de levure Svp1/Atg18, qui joue un rôle dans l'autophagie chez la levure. De manière intéressante, Svp1/Atg18 régule aussi l'activité de Fab1, en se liant également à la protéine régulatrice Vac7 (elle-même recrutée par la protéine plate-forme Vac14). Ainsi, Svp1/Atg18 agirait comme un senseur du taux de PtdIns(3,5)P_2 en permettant la régulation de sa synthèse *via* un rétrocontrôle impliquant Vac7 et Vac14 (Efe *et al.*, 2007).

Chez la souris, le mutant PIKfyve$^{KO/KO}$ meurt très tôt au cours du développement embryonnaire (Ikonomov *et al.*, 2011), ce qui témoigne de l'importance fondamentale de ce lipide membranaire dans les processus cellulaires. Fab1 et PIKfyve possèdent toutes les deux un domaine FYVE capable de lier le PtdIns3P. Cette interaction avec le PtdIns3P va entraîner leur recrutement aux endosomes, où le PtdIns3P est enrichi, et permettre la synthèse du PtdIns(3,5)P_2 (figure 2) (Sbrissa *et al.*, 2002). PIKfyve a été décrite comme ayant un rôle dans divers processus tels que le tri endosomal des protéines, l'homéostasie vacuolaire/lysosomale ou la régulation de voies de signalisation (Payrastre *et al.*, 2001).

7 Le PtdIns(3,4)P_2, un second messager lipidique

7.1 Synthèse du PtdIns(3,4)P_2

Chez la levure *S. cerevisiae*, aucune étude n'a pu mettre en évidence la présence du PtdIns(3,4)P_2. Chez l'Homme, le PtdIns(3,4)P_2 est essentiellement localisé à la membrane plasmique (figure 2) et compte pour moins de 10 % des PPIn totaux en condition basale. Cependant, ces niveaux peuvent transitoirement augmenter en réponse à une stimulation par des facteurs de croissance ou des cytokines (Payrastre *et al.*, 2001). Le PtdIns(3,4)P_2 est obtenu majoritairement par la phosphorylation du PtdIns4P en PtdIns(3,4)P_2 par les PI3K II (figure 1). La déphosphorylation du PtdIns(3,4,5)P_3 en PtdIns(3,4)P_2 peut être réalisée par les PPIn 5-phosphatases SHIP1/INPP5D, SHIP2/INPPL1, OCRL1, INPP5B ainsi que par les Synaptojanines 1 et 2 (figure 1) (Liu & Bankaitis, 2010).

7.2 Rôle physiologique du PtdIns(3,4)P_2

Plusieurs études suggèrent que le PtdIns(3,4)P_2 fonctionne comme un second messager. En effet, il est par exemple capable de recruter les protéine-kinases Akt et PDK1 *via* leurs domaines PH. Le lien entre le PtdIns(3,4)P_2 et la voie de signalisation PI3K/Akt suggère que ce PPIn pourrait être impliqué dans un grand nombre de processus biologiques comme le contrôle du cycle cellulaire, la survie, l'angiogenèse, la

prolifération ou le métabolisme du glucose. L'équilibre entre le PtdIns(3,4)P_2 et le PtdIns(3,4,5)P_3 par le jeu des lipides kinases et phosphatases (figure 1) pourrait donc jouer un rôle essentiel dans la régulation des voies de signalisation en aval de Akt (Hers *et al.*, 2011). Malgré les nombreuses études sur ce PPIn, sa fonction à la membrane plasmique est peu documentée, en effet la plupart des études se focalisent sur le PtdIns(3,4,5)P_3.

Parmi les différents domaines protéiques, seuls les domaines PH de la protéine TAPP1 (*tandem PH domain containing protein 1*) interagissent spécifiquement avec le PtdIns(3,4)P_2. La protéine TAPP1 régule l'organisation du cytosquelette d'actine. Une étude suggère que la liaison de TAPP1 au PtdIns(3,4)P_2 favoriserait le recrutement à la membrane plasmique de PTPL1 (*Protein Tyrosine Phosphatase Like protein 1*, ou FAP-1), une tyrosine phosphatase ubiquitaire impliquée dans la survie cellulaire (Kimber *et al.*, 2003).

8 Le PtdIns(3,4,5)P_3, un effecteur clé de la voie de signalisation PI3K/Akt

8.1 Synthèse du PtdIns(3,4,5)P_3

La levure *S. cerevisiae* ne présente pas de taux détectable de PtdIns(3,4,5)P_3 et celui-ci est donc considéré comme absent de cet organisme. Chez l'Homme, le PtdIns(3,4,5)P_3 représente moins de 5 % des PPIn totaux et il est quasiment indétectable dans des cellules quiescentes. Ses niveaux intracellulaires peuvent cependant augmenter de façon rapide et transitoire, jusqu'à 100 fois en réponse à un agoniste (Milne *et al.*, 2005). Le PtdIns(3,4,5)P_3 est essentiellement synthétisé à la membrane plasmique (figure 2) par les PPIn 3-kinases de classe I à partir du PtdIns(4,5)P_2 (figure 1), mais il n'est pas exclu que des pools minoritaires de PtdIns(3,4,5)P_3 puissent exister à la membrane de compartiments intracellulaires en réponse à un agoniste (Payrastre *et al.*, 2001).

La synthèse du PtdIns(3,4,5)P_3 est finement régulée, étant donné que cette molécule signal est au centre de nombreuses voies de signalisation. Parmi les régulateurs du taux intracellulaire de PtdIns(3,4,5)P_3, on retrouve la phosphatase PTEN qui catalyse la déphosphorylation en position 3 du PtdIns(3,4,5)P_3 pour produire du PtdIns(4,5)P_2. PTEN a été caractérisée comme un suppresseur de tumeur et des mutations dans PTEN sont impliquées dans de nombreux cancers (Liu & Bankaitis, 2010). Le rôle principal de PTEN est de réguler le cycle cellulaire et l'apoptose *via* son activité phosphatase requise pour la régulation de la voie de signalisation dépendant de la kinase Akt.

8.2 Rôle physiologique du PtdIns(3,4,5)P_3

Bien qu'il soit présent à de très faibles taux, le PtdIns(3,4,5)P_3 est sans doute le PPIn dont le rôle est le mieux caractérisé. En effet, ses effecteurs impliqués dans différentes voies de signalisation le lient *via* leurs domaines PH, et sa dérégulation entraîne le développement de nombreux cancers. Parmi les effecteurs, il y a des facteurs d'échange de petites protéines G de la famille Arf (*ADP-ribosylation factors*). D'autres effecteurs sont les sérine-thréonine kinases PDK1 (*Phosphoinositide Dependent Kinase 1*) et Akt ainsi que la phospholipase Cγ (PLCγ) qui font ainsi le lien entre ce PPIn et le contrôle de fonctions cellulaires telles que la prolifération et la survie cellulaire, la dynamique du cytosquelette, la mobilité, le trafic membranaire et l'apoptose (Lemmon, 2003).

Un des rôles les plus étudiés du PtdIns(3,4,5)P_3 est celui de régulateur de la kinase Akt qui lie ce PPIn *via* son domaine PH. Akt joue un rôle très important car d'une part elle va permettre l'activation de la PI3K I et la synthèse du PtdIns(3,4,5)P_3, et d'autre part sa liaison au PtdIns(3,4,5)P_3 *via* son domaine PH va lui permettre d'être ancrée à la membrane plasmique, où elle sera phosphorylée et activée par la protéine kinase PDK1 (Hers *et al.*, 2011). Chez les mammifères, il existe trois isoformes d'Akt nommées Akt1, Akt2 et Akt3 qui sont activées par des facteurs de croissance ou d'autres stimuli extracellulaires, ainsi que par des mutations oncogéniques dans différents régulateurs d'Akt (Ras, les sous-unités p110 et p85 de la PI3K I et PTEN). En effet, le domaine PH d'Akt lie aussi le PtdIns(3,4)P_2 qui est produit par PTEN à partir du PtdIns(3,4,5)P_3 (figure 1) (Hers *et al.*, 2011). La voie de signalisation PtdIns(3,4,5)P_3/PtdIns(3,4)P_2/Akt est impliquée dans la régulation de nombreuses fonctions biologiques dont la prolifération cellulaire, la survie et le métabolisme. La dérégulation d'Akt aboutit à des cancers, des diabètes et des maladies cardiovasculaires et neurologiques. Il est donc très important de trouver des inhibiteurs agissant sur Akt pour traiter ces pathologies. Ainsi, parmi les inhibiteurs couramment utilisés en thérapie, beaucoup agissent sur la liaison entre les PPIn et le domaine PH d'Akt (Hers *et al.*, 2011).

Conclusion

Les phosphoinositides sont des molécules lipidiques qui coordonnent le trafic intracellulaire. Les différentes formes phosphorylées des PPIn sont contrôlées par un jeu de kinases et de phosphatases en réponse à des stimuli. Les sept PPIn sont présents en quantité variable dans les cellules et certaines espèces sont enrichies dans des compartiments intracellulaires bien précis. Les PPIn sont tous virtuellement inter-convertibles

sous réserve que l'organisme possède le jeu d'enzymes appropriées. Ainsi, le PtdIns5P, le PtdIns(3,4)P_2 et le PtdIns(3,4,5)P_3, présents chez les mammifères, n'ont pu être mis en évidence dans la levure *S. cerevisiae*. Les PPIn jouent un rôle essentiel dans l'identité des membranes intracellulaires. De plus, des changements locaux dans les niveaux de PPIn permettent une régulation spatiotemporelle de divers événements tels que le bourgeonnement vésiculaire, la fusion membranaire ou la dynamique du trafic intracellulaire. Du fait de leur faible abondance, moins de 10 % des phospholipides cellulaires, les PPIn peuvent être soumis localement à des variations très fortes dans leur concentration ; c'est plus particulièrement le cas pour le PtdIns(3,4,5)P_3 en réponse à une stimulation cellulaire chez les mammifères et le PtdIns(3,5)P_2 en réponse à un choc osmotique chez la levure. Ainsi de nombreuses études se sont penchées sur le métabolisme des PPIn, leurs localisations et leurs rôles intracellulaires. En effet, malgré leur faible proportion, ils jouent un rôle essentiel dans le recrutement et/ou l'activation de protéines effectrices et interviennent dans la régulation de différentes fonctions cellulaires.

Remerciements. Ce travail a bénéficié du soutien du CNRS (ATIP-CNRS 05-00932 et ATIP-Plus 2008-3098 à S.F.), de la Fondation pour la Recherche Médicale (FRM INE20051105238 et FRM-Comité Alsace 2006CX67-1 à S.F. et bourse post-doctorale FRM à J-O.D.C.), de l'Agence Nationale de la Recherche (ANR-07-BLAN-0065 et ANR-13-BSV2-0004 à S.F.), de l'Association Française contre les Myopathies (AFM-SB/CP/2013-0133/16551 à S.F. et financement de thèse à D.L.B et M.R.) et du programme IDEX de l'Université de Strasbourg (financement de thèse à M.S-V.). Nous remercions aussi nos collaborateurs Bernard Payrastre (I2MC, Toulouse), Jocelyn Laporte et Jean-Louis Mandel (IGBMC, Illkirch) pour leur aide précieuse, et Bruno Goud (Institut Curie, Paris) pour son soutien sans faille.

Références

Antonsson, B.E. (1994). Purification and characterization of phosphatidylinositol synthase from human placenta. *Biochem J,* 297, 517-522.

Audhya, A., and Emr, S.D. (2002). Stt4 PI 4-kinase localizes to the plasma membrane and functions in the Pkc1-mediated MAP kinase cascade. *Dev Cell,* 2, 593-605.

Audhya, A., Foti, M., and Emr, S.D. (2000). Distinct roles for the yeast phosphatidylinositol 4-kinases, Stt4p and Pik1p, in secretion, cell growth, and organelle membrane dynamics. *Mol Biol Cell*, 11, 2673-2689.

Bonangelino, C.J., Nau, J.J., Duex, J.E., Brinkman, M., Wurmser, A.E., Gary, J.D., Emr, S.D., and Weisman, L.S. (2002). Osmotic stress-induced increase of phosphatidylinositol 3,5-bisphosphate requires Vac14p, an activator of the lipid kinase Fab1p. *J Cell Biol*, 156, 1015-1028.

Bunce, M.W., Boronenkov, I.V., and Anderson, R.A. (2008). Coordinated activation of the nuclear ubiquitin ligase Cul3-SPOP by the generation of phosphatidylinositol 5-phosphate. *J Biol Chem*, 283, 8678-8686.

Clarke, J.H., Emson, P.C., and Irvine, R.F. (2008). Localization of phosphatidylinositol phosphate kinase IIgamma in kidney to a membrane trafficking compartment within specialized cells of the nephron. *Am J Physiol Renal Physiol*, 295, F1422-1430.

De Craene, J.O., Ripp, R., Lecompte, O., Thompson, J.D., Poch, O., and Friant, S. (2012). Evolutionary analysis of the ENTH/ANTH/VHS protein superfamily reveals a coevolution between membrane trafficking and metabolism. *BMC Genomics*, 13, 297.

De Matteis, M., Godi, A., and Corda, D. (2002). Phosphoinositides and the Golgi complex. *Curr Opin Cell Biol*, 14, 434-447.

Desrivières, S., Cooke, F.T., Parker, P.J., and Hall, M.N. (1998). MSS4, a phosphatidylinositol-4-phosphate 5-kinase required for organization of the actin cytoskeleton in *Saccharomyces cerevisiae*. *J Biol Chem*, 273, 15787-15793.

Di Paolo, G., and De Camilli, P. (2006). Phosphoinositides in cell regulation and membrane dynamics. *Nature*, 443, 651-657.

Dove, S.K., Cooke, F.T., Douglas, M.R., Sayers, L.G., Parker, P.J., and Michell, R.H. (1997). Osmotic stress activates phosphatidylinositol-3,5-bisphosphate synthesis. *Nature,* 390, 187-192.

Duex, J.E., Nau, J.J., Kauffman, E.J., and Weisman, L.S. (2006a). Phosphoinositide 5-phosphatase Fig 4p is required for both acute rise and subsequent fall in stress-induced phosphatidylinositol 3,5-bisphosphate levels. *Eukaryot Cell*, 5, 723-731.

Duex, J.E., Tang, F., and Weisman, L.S. (2006b). The Vac14p-Fig4p complex acts independently of Vac7p and couples PI3,5P2 synthesis and turnover. *J Cell Biol,* 172, 693-704.

Efe, J.A., Botelho, R.J., and Emr, S.D. (2007). Atg18 regulates organelle morphology and Fab1 kinase activity independent of its membrane recruitment by phosphatidylinositol 3,5-bisphosphate. *Mol Biol Cell*, 18, 4232-4244.

Eugster, A., Pécheur, E.I., Michel, F., Winsor, B., Letourneur, F., and Friant, S. (2004). Ent5p is required with Ent3p and Vps27p for ubiquitin-dependent protein sorting into the multivesicular body. *Mol Biol Cell,* 15, 3031-3041.

Ford, M.G., Pearse, B.M., Higgins, M.K., Vallis, Y., Owen, D.J., Gibson, A., Hopkins, C.R., Evans, P.R., and McMahon, H.T. (2001). Simultaneous binding of PtdIns(4,5)P2 and clathrin by AP180 in the nucleation of clathrin lattices on membranes. *Science*, 291, 1051-1055.

Friant, S., Pécheur, E.I., Eugster, A., Michel, F., Lefkir, Y., Nourrisson, D., and Letourneur, F. (2003). Ent3p

Is a PtdIns(3,5)P2 effector required for protein sorting to the multivesicular body. *Dev Cell*, 5, 499-511.

Gary, J.D., Sato, T.K., Stefan, C.J., Bonangelino, C.J., Weisman, L.S., and Emr, S.D. (2002). Regulation of Fab1 phosphatidylinositol 3-phosphate 5-kinase pathway by Vac7 protein and Fig4, a polyphosphoinositide phosphatase family member. *Mol Biol Cell,* 13, 1238-1251.

Gillooly, D.J., Morrow, I.C., Lindsay, M., Gould, R., Bryant, N.J., Gaullier, J.M., Parton, R.G., and Stenmark, H. (2000). Localization of phosphatidylinositol 3-phosphate in yeast and mammalian cells. *EMBO J,* 19, 4577-4588.

Godi, A., Di Campli, A., Konstantakopoulos, A., Di Tullio, G., Alessi, D.R., Kular, G.S., Daniele, T., Marra, P., Lucocq, J.M., and De Matteis, M.A. (2004). FAPPs control Golgi-to-cell-surface membrane traffic by binding to ARF and PtdIns(4)P. *Nat Cell Biol*, 6, 393-404.

Gozani, O., Karuman, P., Jones, D.R., Ivanov, D., Cha, J., Lugovskoy, A.A., Baird, C.L., Zhu, H., Field, S.J., Lessnick, S.L., Villasenor J., Mehrotra B., Chen J., Rao V.R., Brugge J.S., Ferguson C.G., Payrastre B., Myszka D.G., Cantley L.C., Wagner G., Divecha N., Prestwich GD., and Yuan J. (2003). The PHD finger of the chromatin-associated protein ING2 functions as a nuclear phosphoinositide receptor. *Cell* , 114, 99-111.

Gruenberg, J., and Stenmark, H. (2004). The biogenesis of multivesicular endosomes. *Nat Rev Mol Cell Biol*, 5, 317-323.

Henne, W.M., Buchkovich, N.J., and Emr, S.D. (2011). The ESCRT pathway. *Dev Cell*, 21, 77-91.

Herman, P.K., and Emr, S.D. (1990). Characterization of VPS34, a gene required for vacuolar protein sorting and vacuole segregation in *Saccharomyces cerevisiae. Mol Cell Biol,* 10, 6742-6754.

Hers, I., Vincent, E.E., and Tavare, J.M. (2011). Akt signalling in health and disease. *Cell Signal,* 23, 1515-1527.

Ikonomov, O.C., Sbrissa, D., Delvecchio, K., Xie, Y., Jin, J.P., Rappolee, D., and Shisheva, A. (2011). The phosphoinositide kinase PIKfyve is vital in early embryonic development: preimplantation lethality of PIKfyve-/- embryos but normality of PIKfyve+/- mice. *J Biol Chem,* 286, 13404-13413.

Ikonomov, O.C., Sbrissa, D., Fligger, J., Delvecchio, K., and Shisheva, A. (2010). ArPIKfyve regulates Sac3 protein abundance and turnover: disruption of the mechanism by Sac3I41T mutation causing Charcot-Marie-Tooth 4J disorder. *J Biol Chem*, 285, 26760-26764.

Ishihara, H., Shibasaki, Y., Kizuki, N., Wada, T., Yazaki, Y., Asano, T., and Oka, Y. (1998). Type I phosphatidylinositol-4-phosphate 5-kinases. Cloning of the third isoform and deletion/substitution analysis of members of this novel lipid kinase family. *J Biol Chem,* 273, 8741-8748.

Itoh, T., and Takenawa, T. (2002). Phosphoinositide-binding domains: Functional units for temporal and spatial regulation of intracellular signalling. *Cell Signal*, 14, 733-743.

Jin, N., Chow, C.Y., Liu, L., Zolov, S.N., Bronson, R., Davisson, M., Petersen, J.L., Zhang, Y., Park, S., Duex, J.E., Goldowitz D., Meisler M.H., and Weisman L.S. (2008). VAC14 nucleates a protein complex essential for the acute interconversion of PI3P and PI(3,5)P(2) in yeast and mouse. *EMBO J*, 27, 3221-3234.

Kihara, A., Noda, T., Ishihara, N., and Ohsumi, Y. (2001). Two distinct Vps34 phosphatidylinositol 3-kinase complexes function in autophagy and carboxypeptidase Y sorting in *Saccharomyces cerevisiae. J Cell Biol*, 152, 519-530.

Kimber, W.A., Deak, M., Prescott, A.R., and Alessi, D.R. (2003). Interaction of the protein tyrosine phosphatase PTPL1 with the PtdIns(3,4)P2-binding adaptor protein TAPP1. *Biochem J,* 376, 525-535.

Laporte, J., Bedez, F., Bolino, A., and Mandel, J.L. (2003). Myotubularins, a large disease-associated family of cooperating catalytically active and inactive phosphoinositides phosphatases. *Hum Mol Genet,* 12 Spec No 2, R285-292.

Lecompte, O., Poch, O., and Laporte, J. (2008). PtdIns5P regulation through evolution: roles in membrane trafficking? *Trends Biochem Sci*, 33, 453-460.

Lemmon, M.A. (2003). Phosphoinositide recognition domains. *Traffic,* 4, 201-213.

Levine, T.P., and Munro, S. (2002). Targeting of Golgi-specific pleckstrin homology domains involves both PtdIns 4-kinase-dependent and -independent components. *Curr Biol*, 12, 695-704.

Liu, Y., and Bankaitis, V.A. (2010). Phosphoinositide phosphatases in cell biology and disease. *Prog Lipid Res*, 49, 201-217.

Marcus, A.J., Ullman, H.L., and Safier, L.B. (1969). Lipid composition of subcellular particles of human blood platelets. *J Lipid Res*, 10, 108-114.

Milne, S.B., Ivanova, P.T., DeCamp, D., Hsueh, R.C., and Brown, H.A. (2005). A targeted mass spectrometric analysis of phosphatidylinositol phosphate species. *J Lipid Res,* 46, 1796-1802.

Mizuno-Yamasaki, E., Medkova, M., Coleman, J., and Novick, P. (2010). Phosphatidylinositol 4-phosphate controls both membrane recruitment and a regulatory switch of the Rab GEF Sec2p. *Dev Cell*, 18, 828-840.

Nikawa, J., and Yamashita, S. (1984). Molecular cloning of the gene encoding CDPdiacylglycerol-inositol 3-phosphatidyl transferase in *Saccharomyces cerevisiae. Eur J Biochem*, 143, 251-256.

Odorizzi, G., Babst, M., and Emr, S.D. (1998). Fab1p PtdIns(3)P 5-kinase function essential for protein sorting in the multivesicular body. *Cell*, 95, 847-858.

Panaretou, C., Domin, J., Cockcroft, S., and Waterfield, M.D. (1997). Characterization of p150, an adaptor protein for the human phosphatidylinositol (PtdIns) 3-kinase. Substrate presentation by phosphatidylinositol transfer protein to the p150.Ptdins 3-kinase complex. *J Biol Chem*, 272, 2477-2485.

Parrish, W.R., Stefan, C.J., and Emr, S.D. (2004). Essential role for the myotubularin-related phosphatase Ymr1p and the synaptojanin-like phosphatases Sjl2p and Sjl3p in regulation of phosphatidylinositol 3-phosphate in yeast. *Mol Biol Cell*, 15, 3567-3579.

Payrastre, B., Missy, K., Giuriato, S., Bodin, S., Plantavid, M., and Gratacap, M. (2001). Phosphoinositides: key players in cell signalling, in time and space. *Cell Signal,* 13, 377-387.

Rameh, L.E., Tolias, K.F., Duckworth, B.C., and Cantley, L.C. (1997). A new pathway for synthesis of phosphatidylinositol-4,5-bisphosphate. *Nature,* 390, 192-196.

Sbrissa, D., Ikonomov, O.C., Deeb, R., and Shisheva, A. (2002). Phosphatidylinositol 5-phosphate biosynthesis is linked to PIKfyve and is involved in osmotic response pathway in mammalian cells. *J Biol Chem*, 277, 47276-47284.

Schu, P.V., Takegawa, K., Fry, M.J., Stack, J.H., Waterfield, M.D., and Emr, S.D. (1993). Phosphatidylinositol 3-kinase encoded by yeast VPS34 gene essential for protein sorting. *Science*, 260, 88-91.

Shisheva, A. (2008). PIKfyve: Partners, significance, debates and paradoxes. *Cell Biol Int,* 32, 591-604.

Slessareva, J.E., Routt, S.M., Temple, B., Bankaitis, V.A., and Dohlman, H.G. (2006). Activation of the phosphatidylinositol 3-kinase Vps34 by a G protein alpha subunit at the endosome. *Cell*, 126, 191-203.

Spector, A.A., and Yorek, M.A. (1985). Membrane lipid composition and cellular function. *J Lipid Res*, 26, 1015-1035.

Sun, Y., Carroll, S., Kaksonen, M., Toshima, J.Y., and Drubin, D.G. (2007). PtdIns(4,5)P2 turnover is required for multiple stages during clathrin- and actin-dependent endocytic internalization. *J Cell Biol*, 177, 355-367.

Taylor, G.S., Maehama, T., and Dixon, J.E. (2000). Inaugural article: myotubularin, a protein tyrosine phosphatase mutated in myotubular myopathy, dephosphorylates the lipid second messenger, phosphatidylinositol 3-phosphate. *Proc Natl Acad Sci USA*, 97, 8910-8915.

Trevelyan, W.E. (1966). Preparation of phosphatidyl inositol from baker's yeast. *J Lipid Res*, 7, 445-447.

Vanhaesebroeck, B., Leevers, S.J., Ahmadi, K., Timms, J., Katso, R., Driscoll, P.C., Woscholski, R., Parker, P.J., and Waterfield, M.D. (2001). Synthesis and function of 3-phosphorylated inositol lipids. *Annu Rev Biochem*, 70, 535-602.

Yamamoto, A., DeWald, D.B., Boronenkov, I.V., Anderson, R.A., Emr, S.D., and Koshland, D. (1995). Novel PI(4)P 5-kinase homologue, Fab1p, essential for normal vacuole function and morphology in yeast. *Mol Biol Cell*, 6, 525-539.

Zinser, E., Sperka-Gottlieb, C.D., Fasch, E.V., Kohlwein, S.D., Paltauf, F., and Daum, G. (1991). Phospholipid synthesis and lipid composition of subcellular membranes in the unicellular eukaryote *Saccharomyces cerevisiae*. *J Bacteriol*, 173, 2026-2034.

Appendix 3:

Expression of the neuropathy-associated MTMR2 gene rescues MTM1-associated myopathy.

Raess *et al.* 2017

Human Molecular Genetics

Expression of the neuropathy-associated MTMR2 gene rescues MTM1-associated myopathy

Matthieu A Raess[1,2,3,4,5], Belinda S Cowling[1,2,3,4], Dimitri L Bertazzi[5], Christine Kretz[1,2,3,4], Bruno Rinaldi[5], Jean-Marie Xuereb[6], Pascal Kessler[1,2,3,4], Norma B Romero[8,9,10], Bernard Payrastre[6,7], Sylvie Friant[5]*, Jocelyn Laporte[1,2,3,4]*

1 Department of Translational Medicine, Institut de Génétique et de Biologie Moléculaire et Cellulaire (IGBMC), 1 Rue Laurent Fries, BP10142, 67404 Illkirch, France

2 INSERM U964, 67404 Illkirch, France

3 CNRS, UMR7104, 67404 Illkirch, France

4 Fédération de Médecine Translationnelle de Strasbourg (FMTS), Université de Strasbourg, 67404 Illkirch, France

5 Université de Strasbourg, CNRS, GMGM UMR7156, F-67000 Strasbourg, France

6 INSERM U1048 and Université Toulouse 3, Institut des Maladies Métaboliques et Cardiovasculaires (I2MC), 31432 Toulouse, France

7 CHU de Toulouse, Laboratoire d'Hématologie, 31059 Toulouse, France

8 Sorbonne Universities, Pierre and Marie Curie University, National Institute of Health and Medical Research, National Center for Scientific Research, Center for Research in Myology, Pitié-Salpêtrière Hospital, 75013 Paris, France

9 Unit of Neuromuscular Morphology, Institute of Myology, Pitié-Salpêtrière Hospital, 75013 Paris, France

10 Reference Center for Neuromuscular Pathology Paris-East, Institute of Myology, Pitié-Salpêtrière Hospital, Public Hospital Network of Paris, 75013 Paris, France.

* Equal contributors

Correspondence to

Jocelyn Laporte

IGBMC

1 rue Laurent Fries, BP10142

67404 Illkirch, France

E-mail: jocelyn@igbmc.fr

Phone: (+33) 388 65 34 12

Abstract

Myotubularins are active or dead phosphoinositides phosphatases defining a large protein family conserved through evolution and implicated in different neuromuscular diseases. Loss-of-function mutations in myotubularin (MTM1) cause the severe congenital myopathy called myotubular myopathy (or X-linked centronuclear myopathy) while mutations in the myotubularin-related protein MTMR2 cause a recessive Charcot-Marie-Tooth peripheral neuropathy (CMT4B1). Here we aimed to determine the functional specificity and redundancy of MTM1 and MTMR2, and to assess their abilities to compensate for a potential therapeutic strategy. Using molecular investigations and heterologous expression of human myotubularins in yeast cells and in *Mtm1* knockout mice, we characterized several naturally occurring MTMR2 isoforms with different activities. We identified the N-terminal domain as responsible for functional differences between MTM1 and MTMR2. An N-terminal extension observed in MTMR2 is absent in MTM1, and only the short MTMR2 isoform lacking this N-terminal extension behaved similarly as MTM1 in yeast and mice. Moreover, adeno-associated virus (AAV)-mediated exogenous expression of several MTMR2 isoforms ameliorates the myopathic phenotype due to MTM1 loss, with increased muscle force, reduced myofiber atrophy, and reduction of the intracellular disorganization hallmarks associated to myotubular myopathy. Noteworthy, the short MTMR2 isoform provided a better rescue when compared to the long MTMR2 isoform. In conclusion, these results point to the molecular basis for myotubularins functional specificity. They also provide the proof-of-concept that expression of the neuropathy-associated *MTMR2* gene improves the MTM1-associated myopathy, thus identifying MTMR2 as a novel therapeutic target for myotubular myopathy.

Introduction

Myotubularin (MTM1) and myotubularin-related proteins (MTMR) define a conserved protein family implicated in different neuromuscular diseases (1). They have been classified in the phosphatase super-family. In humans, eight myotubularins share the C(X)5R motif found in tyrosine and dual-specificity phosphatases and display enzymatic activity, while the six others lack this motif and are named dead-phosphatases. Unexpectedly, it was found that enzymatically active myotubularins do not act on proteins but dephosphorylate phosphoinositides (PPIn), lipids concentrated in specific membrane sub-domains (2, 3). PPIn are lipid second messengers implicated in a wide range of cellular processes including signaling and intracellular organization (4). Myotubularins are PPIn 3-phosphatases that dephosphorylate the phosphatidylinositol 3-phosphate (PtdIns3*P*) and the phosphatidylinositol 3,5-bisphosphate (PtdIns(3,5)P_2), leading to the production of PtdIns5*P* (2, 3, 5-7). PtdIns5*P* is implicated in transcriptional regulation and growth factor signaling, while PtdIns3*P* and PtdIns(3,5)P_2 regulate membrane trafficking and autophagy. PtdIns3*P* is produced through the phosphorylation of PtdIns by class II and III PtdIns 3-kinases and PtdIns(3,5)P_2 is obtained mainly from the phosphorylation of PtdIns3*P* by PIKfyve (8, 9). They recruit proteins to specific endosomal pools or to particular endoplasmic reticulum sites where autophagosomes are formed. For example, the FYVE (Fab1-YOTB-Vac1-EEA1) domain of EEA1 binds specifically PtdIns3*P* concentrated on early endosomes to regulate endosomal fusion and cargo delivery (9). Dead myotubularins oligomerize with and regulate the enzymatic activity and/or subcellular localization of their active homologs (10-12). In addition to the active or dead phosphatase domain, myotubularins share a PH-GRAM (Pleckstrin Homology, Glucosyltransferase, Rab-like GTPase Activator and Myotubularin) domain that bind to PPIn or proteins, and a coiled-coil domain implicated in their oligomerization (1).

There are 14 myotubularins in human and one active myotubularin in yeast *Saccharomyces cerevisiae* (1, 13). The yeast myotubularin Ymr1 regulates vacuole protein sorting and its absence induces vacuolar fragmentation (14). Expression of human myotubularin MTM1 in yeast leads to the enlargement of the vacuole as a consequence of its phosphatase activity and PtdIns3*P* decrease (2, 15). In human, mutations in MTM1 cause the severe congenital myopathy called myotubular myopathy (or X-linked centronuclear myopathy; OMIM 310400) (16), while mutations in either the active MTMR2 or the dead-phosphatase MTMR13 cause Charcot-Marie-Tooth (CMT) peripheral neuropathies (CMT4B1, OMIM 601382 and CMT4B2, OMIM 604563 respectively)(17-19). In addition, putative mutations in MTMR5 (Sbf1) were linked to CMT4B3 (OMIM 615284) and axonal neuropathy (20-22). Thus, lack of one myotubularin is not fully compensated by its homologs, while they are ubiquitously expressed. Moreover, the related diseases affect different tissues. Of note, MTM1 and MTMR2 are part of the same evolutionary sub-group based on their sequence (13). Thus, this suggests uncharacterized tissue-specific functions potentially reflecting different protein isoforms having specific activities or interactors. Here, we show that there are two protein isoforms of MTMR2 and we studied their *in vivo* functions in yeast and in mice. We report that only the short MTMR2 isoform complements the yeast *ymr1Δ* mutant phenotypes at a similar level as MTM1. Moreover, both MTMR2 isoforms ameliorated the myopathy phenotypes displayed by *Mtm1* knockout (KO) mice, and specifically the short MTMR2 isoform produced a better disease rescue.

Results

MTMR2 splicing variants are differentially expressed and encode for long and short protein isoforms

Mutations in the *MTMR2* gene are responsible for Charcot-Marie-Tooth neuropathy (CMT4B1) whereas mutations in MTM1 lead to X-linked centronuclear myopathy (XLCNM), suggesting that these two ubiquitously expressed myotubularins have distinct functions. Most tissues contain more than a single isoform, thus their localization and extent of expression could help explain their different functions. In order to investigate MTMR2 function, we first defined its tissue expression and isoforms. In mice, four *MTMR2* mRNA isoforms (V1 to V4) have been previously reported in peripheral nerves, potentially coding for 2 protein isoforms (Supplementary material Fig. S1A-B) (23). Variants V2 to V4 differ from variant V1 by the inclusion of alternative exons 1a and/or 2a leading to a premature stop codon and unmasking an alternative start site in exon 3. Variant V1 encodes a 643 amino acids protein that we named MTMR2-L (long) while the other isoforms code for a 571 aa protein named MTMR2-S (short) that was previously detected in various cell lines (23). The two protein isoforms differ only in their translation start sites; MTMR2-S starts right before the PH-GRAM domain while the MTMR2-L has an extended N-terminal sequence without known homology to any protein domain and that was not visible in the crystal structure (Fig. 1C; Supplementary material, Fig. S1B) (24, 25). The expression level of these isoforms was first investigated in human through mining the GTEx expression database encompassing data on 51 human tissues (26). Variant V1 is the major *MTMR2* RNA in brain, liver and spleen while variant V2 is predominant in the other tissues. The different variants were only poorly expressed in skeletal muscle (Fig. 1A). In mouse, RT-PCR and Sanger sequencing confirmed the existence of the four *MTMR2* mRNA variants (V1 to V4) in tibialis anterior (TA) skeletal muscle of wild type (WT) and *Mtm1* KO mice and in the liver (Supplementary material Fig.

S1C-1D), suggesting that both MTMR2-L and MTMR2-S proteins are present in skeletal muscle.

Short but not long MTMR2 isoform displays an MTM1-like activity in yeast cells

To compare the cellular function of MTM1, MTMR2-L and MTMR2-S proteins *in vivo*, we used heterologous expression of these human myotubularins in yeast cells. Yeast is a good model to study phosphoinositide-dependent membrane trafficking as it is conserved from yeast to higher eukaryotes (27). In yeast cells, vacuole volume, morphology, acidity and membrane potential are controlled by PtdIns(3,5)P_2 that is produced through the phosphorylation of PtdIns3*P* by Fab1/PIKfyve kinase. In *fab1Δ* mutant cells, the vacuole is very large and unilobed due to low levels of PtdIns(3,5)P_2 (15, 28, 29). On the contrary, *ymr1Δ* cells lacking the unique yeast myotubularin have fragmented vacuoles due to excess of PtdIns(3,5)P_2 and/or PtdIns3*P* (14), and this phenotype is complemented by the expression of the human MTM1 that induces a large vacuole phenotype (15). To determine MTM1, MTMR2-L and MTMR2-S intracellular localization, we overexpressed GFP-tagged fusions in *ymr1Δ* cells. MTM1-GFP and MTMR2-S-GFP proteins were concentrated to a membrane punctate structure adjacent to the vacuole (also positive for the FM4-64 lipid dye), while MTMR2-L-GFP was mainly in the cytoplasm (Fig. 2C). We next assessed the vacuolar morphology upon overexpression of either GFP-tagged or untagged human myotubularins in *ymr1Δ* cells by staining the vacuolar membrane with the lipophilic dye FM4-64 (Fig. 2B-C). To detect MTMR2 isoforms, a mouse monoclonal antibody was raised against recombinant full length human MTMR2-L. This antibody was validated on the transformed yeast protein extracts, and specifically recognized MTMR2-L and MTMR2-S (Fig. 2A). Vacuoles were significantly enlarged upon expression of MTM1 or MTMR2-S in *ymr1Δ* cells while they remained fragmented with MTMR2-L. MTM1 and MTMR2-S are inducing a large vacuolar morphology mimicking a *fab1Δ* phenotype due to the high expression levels of these

phosphatases (overexpression plasmid). These results show that only the membrane localized myotubularin constructs rescued the vacuole morphology defects of *ymr1Δ* cells. Since the vacuolar morphology reflects the PtdIns(3,5)P_2 level and as PtdIns(3,5)P_2 is not abundant enough to be detected in normal growth conditions (29), we quantified by mass assay the level of PtdIns5*P*, the lipid produced by myotubularin phosphatase activity from PtdIns(3,5)P_2 (Fig. 2F). PtdIns5*P* level was increased by MTM1 and MTMR2-S overexpression in *ymr1Δ* cells, while MTMR2-L had no effect. We also quantified the PtdIns3*P* myotubularin substrate level, by counting the punctate structures that were positive for DsRED-FYVE, a reporter for PtdIns3*P*-enriched membranes (27) (Fig. 2D-E). Overexpression of MTM1 and MTMR2-S significantly reduced PtdIns3*P* level while MTMR2-L had no effect. However, previous data showed MTMR2-L had a strong phosphatase activity *in vitro* (5, 7), suggesting that the cytoplasmic localization of this isoform in yeast cells does not allow PPIn substrate dephosphorylation. In conclusion, only MTMR2-S has a similar phosphatase activity and localization as MTM1 in yeast cells, while MTMR2-L behaves differently.

Exogenous expression of MTMR2 short isoform in the *Mtm1* KO mice rescues muscle weight and force similarly to MTM1 expression.

To assess whether in mammals MTMR2-S is also functionally closer to MTM1 compared to MTMR2-L, we overexpressed MTM1, MTMR2-L and MTMR2-S in the *Mtm1* KO mouse and analyzed different myopathy-like phenotypes. The different myotubularins were expressed from Adeno-associated virus AAV2/1 under the control of the CMV promoter and the recombinant virions were injected into the TA muscles of 2-3 week old *Mtm1* KO mice. The *Mtm1* KO mice develop a progressive muscle atrophy and weakness starting at 2-3 weeks and leading to death by 8 weeks, the TA muscle being the most affected muscle detected in

this model (30, 31). We have previously shown that AAV-mediated expression of MTM1 for 4 weeks in the TA muscle, corrects the myopathy phenotype in *Mtm1* KO mice (15). Therefore to determine the impact of introducing MTMR2-L and MTMR2-S into *Mtm1* KO mice, we followed our previously described protocol for AAV injections (15), using MTM1 as a positive control for the rescue, and empty AAV2/1 as a disease control in the contralateral muscle. The MTM1, MTMR2-L and MTMR2-S human myotubularins were expressed in injected TA, as revealed from anti-MTM1 and anti-MTMR2 western-blot analyzes (Fig. 3A). Endogenous MTMR2 proteins were not detected in muscle injected with empty AAV, most likely due to the low level of endogenous expression (Fig. 3A).

Four weeks after AAV injection, the TA muscle weight of the *Mtm1* KO mice was decreased by 2.5 fold compared to WT mice, both injected with empty AAV control. MTM1 or MTMR2-S expression in *Mtm1* KO mice increased muscle mass significantly compared to the empty AAV control (1.5 fold), contrary to MTMR2-L (Fig. 3B). To address a potential hypertrophic effect of human MTM1 or MTMR2 constructs in wild type (WT) mice, TA muscle weight of injected WT mice was quantified (Supplementary material, Fig. S2). No muscle mass increased was noted with any myotubularins indicating that the amelioration observed in the *Mtm1* KO mice was not due to a hypertrophic effect but to a functional rescue.

The *Mtm1* KO mice displayed very weak muscle force compared to WT mice, and all myotubularin constructs including MTMR2-L improved the TA specific muscle force (Fig. 3C). Noteworthy, a similar rescue was observed for MTM1 and MTMR2-S, significantly above that observed for MTMR2-L injected muscles. These results show that both MTMR2-L and MTMR2-S isoforms improve the muscle weakness due to loss of MTM1, and MTMR2-S expression induces a rescue akin to that observed by MTM1 gene replacement.

The MTMR2 isoforms rescue the histopathological hallmarks of the *Mtm1* KO mouse.

In the *Mtm1 KO* mice, TA injections of AAV2/1 carrying MTM1, MTMR2-L or MTMR2-S increased muscle mass (except for MTMR2-L) and force (Fig. 3). To analyze the rescue at the histological level, fiber size and nuclei localization were determined (Fig. 4). HE (hematoxylin-eosin) staining revealed increased fiber size in AAV-MTM1 and AAV-MTMR2-S than in *Mtm1* KO muscle treated with empty AAV or MTMR2-L (Fig. 4A), even though we observed spatial heterogeneity in the muscle, with some regions still displaying smaller atrophic fibers. Morphometric analysis revealed that among the different myotubularins tested, MTM1 induced a clear shift toward larger fiber diameters compared to MTMR2 constructs and empty AAV (Fig. 4C). A very significant difference ($P<0.0001$) was observed between AAV-MTM1 (mean 58.4%) and AAV-MTMR2-L (mean 26.2%) in the percentage of muscle fibers having an area above 800 μm^2, and the difference was less significant ($P=0.033$) between MTM1 and MTMR2-S (39.8%) (Fig. 4D). Since nuclei are abnormally located within muscle fibers in *Mtm1* KO mice, we analyzed the distribution of nuclei. Injection of MTM1, MTMR2-S or MTMR2-L into the TA muscle of *Mtm1* KO increased significantly the percentage of well-positioned peripheral nuclei compared with contralateral control muscles injected with empty AAV (Fig. 4E). The succinate dehydrogenase (SDH) staining shows accumulation at the periphery and center in the *Mtm1* KO fibers (15), while it is greatly ameliorated upon expression of the different myotubularin constructs (Fig. 4B). These results show that both MTMR2 isoforms were able to ameliorate the histopathological hallmarks of the MTM1 myopathy, where MTMR2-S was more effective.

MTMR2 isoforms rescue *Mtm1* KO muscle disorganization and normalize PtdIns3*P* levels.

Patients with myotubular myopathy and the *Mtm1* KO mice display an intracellular disorganization of their muscle fibers at the ultrastructural level (30, 32). To determine the organization of the contractile apparatus and triads, the ultrastructure of the different injected TA muscles was assessed by electron microscopy. As previously published, we observed Z-line and mitochondria misalignment, thinner sarcomeres and lack of well-organized triads in the *Mtm1* KO muscle injected with empty AAV (15) (Fig. 5A). Expression of MTM1 and both MTMR2 isoforms improved these different phenotypes, with the observation of well-organized triads with two sarcoplasmic reticulum cisternae associated with a central transverse-tubule (T-tubule) in muscles injected with MTM1, MTMR2-L or MTMR2-S (Fig. 5A). Moreover, AAV-mediated expression of MTM1, MTMR2-L and MTMR2-S increased the number of triads per sarcomere back to almost WT levels, with a better effect for MTMR2-S compared to MTMR2-L (Fig. 5B).

In yeast, only MTMR2-S but not MTMR2-L regulated the PtdIns3*P* myotubularin substrate level, as well as the one of PtdIns(3,5)P_2 as assessed by vacuolar morphology (Fig. 2B). To determine whether the rescuing capacity of MTMR2 in mice was linked to its enzymatic activity, we quantified the intracellular levels of PtdIns3*P* in the AAV empty, MTM1, MTMR2-L and MTMR2-S injected TA muscles of *Mtm1* KO mice (Fig. 6A). PtdIns3*P* level was 2.3 fold higher in empty AAV injected *Mtm1* KO muscle than in WT muscle, reflecting the impact of the loss of MTM1 on its PtdIns3*P* lipid substrate. Upon expression of MTM1, the PtdIns3*P* level decreased to wild type levels, reflecting the *in vivo* phosphatase activity of MTM1. Both MTMR2 isoforms induced a decrease in PtdIns3*P* level when expressed in the *Mtm1* KO mice, however only the short MTMR2-S isoform normalized PtdIns3*P* to wild type levels. These results show that MTMR2 displays an *in vivo* enzymatic activity in muscle.

Moreover, the MTMR2 catalytic activity correlates with the rescue observed by exogenous expression in the *Mtm1* KO myopathic mice.

Taken together, the results in *Mtm1* KO mice expressing MTM1 or MTMR2 isoforms show that the different phenotypes associated to the myopathy including reduced muscle force, myofiber atrophy, nuclei mispositioning, sarcomere and triad disorganization and increased PtdIns3*P* levels, were ameliorated compared to the control muscle injected with empty AAV (Table 1). Noteworthy, as observed in yeast studies, the shorter isoform MTMR2-S provided a better rescue than MTMR2-L, and was often comparable to MTM1.

Expression of the MTMR2 short isoform is reduced in the *Mtm1* KO mice muscles

Based on the GTEx expression database, the different MTMR2 mRNA variants (V1 to V4) producing these two MTMR2 protein isoforms are expressed in different tissues, with a low expression level in the skeletal muscle (Fig. 1). However, despite their strong rescue properties upon overexpression in TA muscles of *Mtm1* KO mice (Fig. 3-5, 6A; Table 1), endogenous expression of MTMR2 variants does not compensate for the loss of MTM1 function in the myopathy patients. To help understand the difference in rescue observed between the MTMR2-L and -S isoforms, we quantified mRNA levels of the different MTMR2 variants (V1 to V4) in TA muscles of *Mtm*1 KO compared to wild type (WT) mice (Fig. 6B). The results show that MTMR2 mRNA total level was decreased in *Mtm1* KO muscles by 2 fold. This was mainly due to a strong decrease in the V2 and V3 transcripts encoding the MTMR2-S isoform, while the level of the V1 transcript coding for MTMR2-L remained statistically unchanged between *Mtm1* KO and WT mice. Note that these decrease were not observed in Supplementary Fig. S1D since it presents a conventional RT-PCR that does not allow quantification. A similar downregulation of V2 and V3 transcripts encoding the MTMR2-S isoform was observed in XLCNM patient muscles (Fig. 6C). These data

suggest that the lack of compensation of MTM1 loss by endogenous MTMR2 is linked to the low expression level of MTMR2 associated to MTMR2-S decreased level in skeletal muscles. Alternatively, this could be linked to the low level of MTMR2 proteins in the muscle.

Discussion

Here we aimed to determine functional specificities and redundancies of MTM1 and MTMR2 myotubularins belonging to the same family of proteins, but whose mutations result in different diseases affecting different tissues, a myopathy and a neuropathy, respectively. We also tested their abilities to compensate for each other as a potential novel therapeutic strategy. Using molecular investigations and overexpression of these human myotubularins in yeast cells and in the skeletal muscle of the *Mtm1* KO myopathic mice, we characterized two MTMR2 isoforms with different catalytic activities linked to their ability to access their PPIn substrates. Moreover, we showed that overexpression of MTMR2 rescues the myopathy due to MTM1 loss and that compared to MTMR2-L, the short MTMR2-S isoform displayed a better PtdIns3*P* phosphatase activity in yeast and in mice, correlating with better rescuing properties in myotubularin-depleted *ymr1Δ* yeast cells and in *Mtm1* KO mice. The fact that MTMR2-L partially improved the phenotypes of *Mtm1* KO mice despite performing poorly in yeast assays could be due to a lack of regulatory proteins in the yeast heterologous system.

MTMR2 isoforms and functions

There are four naturally occurring MTMR2 mRNA variants in human and mice encoding two protein isoforms (MTMR2-L and -S), differing by a 72 aa extension at the N-terminal. MTMR2-S displayed a higher phosphatase activity than MTMR2-L *in vivo* in yeast and mouse, suggesting the N-terminal is important for the regulation of MTMR2 function. The phosphorylation of the serine 58, within this N-terminal extension, was shown to be important for MTMR2 endosomal membrane localization and catalytic function (33, 34). Indeed, the

MTMR2-S58A phosphorylation-deficient mutant was localized to membrane structures and was active towards PtdIns3*P*, contrary to the phosphomimetic mutant MTMR2-S58E (33, 34). Here, we show that the MTMR2-S protein lacking the N-terminal sequence encompassing the S58 phosphorylated residue is concentrated to membranes when expressed in yeast (Fig. 2B) and is more active towards PtdIns3*P* compared to MTMR2-L in yeast (Fig. 2D) and in murine muscles (Fig. 6A). The N-terminal extension of MTMR2 was not resolved in the crystallographic structure, supporting the hypothesis that it can adopt different conformations and might regulate MTMR2 functions (24, 25). These results show that there are two forms of MTMR2, MTMR2-S mainly membrane localized and with high phosphatase activity *in vivo* and MTMR2-L whose membrane localization is dependent on phosphorylation at the S58 residue. Interestingly, in brain expression is biased towards the *MTMR2* V1 variant coding for MTMR2-L (Fig. 1). The S58 phosphorylation is mediated by Erk2 kinase whose expression in brain is precisely higher than in other tissues, correlating with MTMR2-L expression (GTEx database).

Functional redundancy and compensation within myotubularins

There are 14 myotubularins mostly ubiquitously expressed in human tissues, but the loss of MTM1 leads specifically to a severe congenital myopathy. This reveals that *MTM1* homologs, notably the closer *MTMR2* homolog, do not compensate for the lack of MTM1 in the skeletal muscles when expressed at endogenous levels. We provide evidence that MTMR2-S is downregulated in the skeletal muscles of the myopathic *Mtm1* KO mice. Moreover, compared to brain and other tissues, the expression of MTMR2 transcripts is low in skeletal muscles. Altogether this suggests that this low expression of MTMR2 in muscle exacerbated by its downregulation in the myopathy mouse model and in XLCNM patient muscles is the basis for the lack of compensation. Indeed, the MTMR2-S improves better both functional and structural myopathic phenotypes and is more significantly downregulated than MTMR2-L in

the myopathic muscles. This reveals that the molecular basis for the functional difference between MTM1 and MTMR2 resides in the N-terminal extension upstream the PH-GRAM domain, with the MTMR2-S lacking this extension displaying similar *in vivo* functions as MTM1 in yeast and in mice. Removal of this N-terminal extension in the native MTMR2-L isoform converts MTMR2 activity into an MTM1-like activity.

The ability of MTMR2-S to rescue myopathic phenotypes in *Mtm1* KO mice after muscle expression could be due to the observed normalization of PtdIns3*P* levels. A previous study in the drosophila mutant of the *MTM1* ortholog (*mtm*) showed that impairment of class II PtdIns 3-kinase prevents the phenotypes and death of the *mtm* mutant (35). More recently, two studies proposed that normalization of PtdIns3*P* levels through downregulation of class II PtdIns 3-kinase PIK3C2B or broad inhibition of PtdIns 3-kinase activity and thus PtdIns3*P* production by wortmannin, rescues the muscle phenotypes of *Mtm1* KO mice (36, 37). Other therapeutic proof-of-concepts have been reported that do not target PPIn normalization, such as downregulation/normalization of *DNM2* (31), expression of catalytic dead MTM1-C375S (15) or inhibition of autophagy (38). Thus, it is also possible that the exogenously expressed MTMR2-L or MTMR2-S act in a PPIn-independent way to improve the *Mtm1* KO phenotypes. Of note, the MTM1-C375S dead-phosphatase mutant does not improve the triad shape that is well rescued upon expression of active MTM1 or MTMR2-S, supporting an important role of PPIn at the triad.

MTMR2 as a novel therapeutic target for myotubular myopathy

Here we provide the proof-of-concept that MTMR2 could be used as a therapeutic target. Intramuscular AAV transduction of human MTMR2 into *Mtm1* KO mice greatly improved the phenotypes, supporting the rescue is cell autonomous in muscle. While this actual protocol aimed to investigate the cell autonomous compensation by MTMR2 through intramuscular injection, it was not possible to determine the extent of the rescue and the long-term potential

of MTMR2-mediated rescue as *Mtm1* KO mice die at around 2 months most probably from respiratory failure and feeding defect. Complementation of myotubular myopathy by recombinant MTM1 or MTM1 re-expressed from injected AAVs were previously proposed as potential therapies (39, 40). Expression of MTMR2 in muscle could be an attractive alternative that may not elicit immune response against the transgene, as the majority of patients with myotubular myopathy have a strong decrease or a total loss of MTM1 (41, 42). Our data support that MTMR2-S isoform has a better rescuing ability than the main described MTMR2-L isoform and is a naturally occurring variant, including in muscle. Since MTMR2-S transcripts are decreased in the *Mtm1* KO muscles, a potential strategy will be to promote their expression by modulation of *MTMR2* alternative splicing or exogenous expression. Alternatively, since MTMR2 ameliorates the myopathy due to the lack of MTM1, it would be interesting to test whether MTM1 delivery may be a therapeutic option for CMT4B caused by MTMR2 mutations.

Materials and methods

Ethic statement

Mice were humanely killed by cervical dislocation after injection of pentobarbital, according to national and European legislations on animal experimentation.

Sample collection was performed with written informed consent from the patients or parents according to the declaration of Helsinki. The 3 XLCNM patients had the following mutations in *MTM1*:

Plasmids and constructs

The human *MTM1* (1812 bp, 603 aa) and *MTMR2-L* (1932 bp, 643 aa) ORFs were cloned into the pDONR207 plasmid (Invitrogen, Carlsbad, CA) to generate entry clones (pSF108 and pSF98 respectively). The pDONR207-MTMR2-S (1716 bp, 571 aa, pSF101) has been

obtained by site-directed mutagenesis on *MTMR2-L* into the pSF98 vector, to delete the 216 first nucleotides corresponding to the 72 first amino acids. Gateway system (Invitrogen, Carlsbad, CA) was used to clone the different myotubularin constructs into yeast destination expression vectors pAG424GPD-ccdB-EGFP (43) and pVV200 (44) obtained from the European Saccharomyces cerevisiae Archive for Functional Analysis EUROSCARF, or into a pAAV-MCS vector (CMV promoter). All constructs were verified by sequencing. The pCS211 DsRED-FYVE plasmid was previously described (27).

Antibodies

Primary antibodies used were rabbit polyclonal anti-MTM1 (2827), mouse monoclonal anti-MTMR2 (4G3), mouse monoclonal anti-phosphoglycerate Kinase 1 (PGK1, Invitrogen) and mouse monoclonal anti-glyceraldehyde-3-phosphate dehydrogenase (anti-GAPDH, Chemicon by Merk Millipore, Darmstadt , Germany). Anti-MTM1 and anti-MTMR2 antibodies were made onsite at the antibodies facility of the Institut de Génétique et Biologie Moléculaire et Cellulaire (IGBMC). Anti-MTMR2 antibodies were raised against full length human MTMR2 and validated in this study using transfected COS-7 cells. Secondary antibodies against mouse and rabbit IgG, conjugated with horseradish peroxidase (HRP) were obtained from Jackson ImmunoResearch Laboratories (West Grove, PA).

In vivo models

The S. cerevisiae *ymr1Δ* (MATα, ura3-52, leu2-3,112, his3-Δ200, trp1-Δ901, lys2-801, suc2-Δ9 ymr1::HIS3) (14) and WT (MATα, his3Δ1, leu2Δ0, lys2Δ0, ura3Δ0) strains were grown at 30°C in rich medium (YPD): 1% yeast extract, 2% peptone, 2% glucose or synthetic drop-out medium (SC): 0.67% yeast nitrogen base without amino acids, 2% glucose and the appropriate amino acids mixture to ensure plasmid maintenance. We did not use the *ymr1Δ* (MATα, his3Δ1, leu2Δ0, lys2Δ0, ura3Δ0, ymr1::KanMX) in the BY4742 background from

the yeast systematic deletion collection, because it does not have the *ymr1Δ* phenotype described by Scott D Emr's laboratory (14).

In this study we used wild-type and *Mtm1* KO 129 PAS mice. The *Mtm1* KO mice are characterized by a progressive muscle atrophy and weakness starting at 2-3 weeks and leading to death by 8 weeks (30). Animals were housed in a temperature-controlled room (19–22°C) with a 12:12-h light/dark cycle.

Bioinformatics analysis

Expression levels of *MTMR2* mRNA isoforms was obtained by mining the Genotype-Tissue Expression (GTEx, www.gtexportal.org/home/) database, which has been built by systematic RNA-sequencing using samples of 51 different tissues from hundreds of donors and two transformed cell types in culture. We then used this data to calculate the relative expression of *MTMR2* mRNA isoforms in the 20 most relevant tissues, and to create a heat map underlining in which tissue a specific isoform is the most/least expressed.

Alignment of the N-terminal part of MTM1, MTMR2-L and MTMR2-S was done using Jalview (www.jalview.org/) and aligning amino acids were identified by Clustalx color coding.

Expression analysis

Total RNA was purified from tibialis anterior (TA) muscle and liver of 7 week-old wild-type and *Mtm1* KO mice, or from muscle biopsies of XLCNM patients and controls, using trizol reagent (Invitrogen, Carlsbad, CA) according to the manufacturer's instructions. cDNAs were synthesized from 500 ng of total RNA using Superscript II reverse transcriptase (Invitrogen) and random hexamers.

PCR amplification of 1/10 diluted cDNA from TA muscle and liver was performed using a forward primer from the 5'-UTR of *MTMR2*: 5'-AGCGGCCTCCAGTTTCTCGCGC-3' and

a reverse primer from exon 3: 5'-TCTCTCCTGGAAGCAGGGCTGGTTCC-3', for 35 cycles of amplification at 72°C (and 65°C as melting temperature) and 30 min of final extension at 72°C, as previously described (23). The products were analyzed on a 2% agarose gel, each band has been purified using Nucleospin Gel and PCR cleanup kit (Macherey-Nagel, Düren, Germany), then cloned into a pJet2.1 vector using the CloneJet PCR cloning kit (ThermoFisher Scientific, Waltham, MA), and sequenced by Sanger.

Quantitative PCR amplification of 1/10 diluted cDNAs from mouse TA muscles or human muscle biopsies was performed on Light-Cycler 480 II instrument (Roche, Basel, Swiss) using 53°C as melting temperature. Specific sets of primers were used for each mouse *MTMR2* isoform: forward 5'-GACTCACTGTCCAGTGCTTC-3' and reverse 5'-CCTCCCTCAGGACCCTCA-3' for mouse V1, forward 5'-GACTCACTGTCCAGTGCTTC-3' and reverse 5'-CAGCTGGGCACTCCCTCA-3' for mouse V2, forward 5'-AAGATAAAACATCTCAAAAATTATAATTGCTTC-3' and reverse 5'-CAGCTGGGCACTCCCTCA-3' for mouse V3, forward 5'-AAGATAAAACATCTCAAAAATTATAATTGCTTC-3' and reverse 5'-GACTCACTGTCCAGTGCTTC-3' for mouse V4. Another set of primers (forward 5'-TCCTGTGTCTAATGGCTTGC-3' and reverse 5'-AACCAAGAGGGCAGGATATG-3') amplifying a sequence common to all mouse isoforms has been used to quantify total mouse MTMR2. Other specific sets of primers were used for each human *MTMR2* isoform: forward 5'-ACTCCTTGTCCAGTGCCTC-3' and reverse 5'-GACTCCCTCAGGACCCTC-3' for human V1, forward 5'-AAGATAAAACATCTCAAAAATTATAATTGCCTC-3' and reverse 5'-GACTCCCTCAGGACCCTC-3' for human V2, forward 5'-AAGATAAAACATCTCAAAAATTATAATTGCCTC-3' and reverse 5'-GAGCGAGACTCCCTCCTC-3' for human V3, forward 5'-AAGATAAAACATCTCAAAAATTATAATTGCCTC-3' and reverse 5'-

CTGGACTGCATGGGCCTC-3' for human V4. Another set of primers (forward 5'-TTTCCTGTCTCTAATAACCTGCC-3' and reverse 5'-CCAGGAGGGCAGGGTATG-3') amplifying a sequence common to all human isoforms has been used to quantify total human MTMR2. For all qPCR, the *HPRT* gene expression was used as control because of the non-variation in its expression between control and XLCNM muscles.

Western blot

Total proteins were extracted from yeast cells (OD_{600nm}=0.5-0.9, minimum 3 clones per construct) by TCA precipitation and NaOH lysis (45), and from TA muscles (minimum 10 muscles per construct) by homogenization in RIPA buffer using a tissue homogenizer (Omni TH, Kennesaw, GA). Protein lysates were analyzed by SDS-PAGE and Western blotting on nitrocellulose membrane. Proteins were detected using primary antibody (anti-MTM1 1/500, anti-MTMR2 1/1000, anti-PGK1 1/1000 and anti-GAPDH 1/1000) followed by incubation with the secondary antibody coupled to HRP, and extensive washing. Membranes were revealed by ECL chemiluminescent reaction kit (Supersignal west pico kit, ThermoFisher Scientific, Waltham, MA).

Yeast phenotyping

ymr1Δ yeast cells were transformed using the LiAc-PEG method (46) by yeast expression plasmids pAG424GPD-ccdB-EGFP (2µ, GFP tag at C-ter) or pVV200 (2µ, no tag) containing *MTM1*, *MTMR2-L* or *MTMR2-S* cDNA. Yeast cells transformed by empty plasmids were used as controls.

For vacuole staining, 1 OD_{600nm} unit of cells was harvested by a 500xg centrifugation for 1 min, incubated in 50 µl YPD medium with 2 µl FM4-64 (200 µM, Invitrogen) for 15 min at 30°C, prior washing with 900 µl YPD and chasing by incubation at 30°C for 10 min followed by a second wash in SC complete medium, the stained living yeast cells were observed by

fluorescent microscopy. Between 100 and 600 cells per clone (three different clones per construct) were counted and classified into two categories: large or medium unilobar vacuole, and small or fragmented vacuole.

For PtdIns*3P* quantification, yeast cells were co-transformed by a pVV200 plasmid (empty or containing *MTM1*, *MTMR2-L* or *MTMR2-S* cDNA) and the pCS211 plasmid expressing the DsRED-FYVE reporter for PtdIns3*P*-enriched membrane structures (27). After fluorescence microscopy, the number of dots per cell was quantified on minimum 100 cells per clone (2 different clones per construct).

For PtdIns5*P* quantification, yeast *ymr1Δ* cells producing the different MTM1 and MTMR2 constructs were grown to exponential phase. Lipid extraction was done as described in Hama *et al.* on 200 OD_{600nm} units of cells (47). Quantification of the PtdIns(5)P level was performed as described by Morris et al. (48) and the results were normalized based on the total lipid concentration.

All fluorescence microscopy observations were done with 100X/1.45 oil objective (Zeiss) on a fluorescence Axio Observer D1 microscope (Zeiss) using GPF or DsRED filter and DIC optics. Images were captured with a CoolSnap HQ2 photometrix camera (Roper Scientific) and treated by ImageJ (Rasband W.S., ImageJ, U. S. National Institutes of Health, Bethesda, Maryland, USA, http://imagej.nih.gov/ij/).

PtdIns3*P* quantification by ELISA in muscle extracts

PtdIns3*P* Mass ELISAs were performed on lipid extracts from whole tibialis anterior (TA) muscle preparations according to the manufacturer's recommendations and using the PtdIns3*P* Mass ELISA kit (Echelon Biosciences, Salt Lake City, UT). TA muscles from 7 week-old wild-type of *Mtm1* KO mice were weighed, grinded into a powder using a mortar and pestle under liquid nitrogen and then incubated in ice cold 5% TCA to extract lipids. Extracted lipids were resuspended in PBS-T with 3% protein stabilizer and then spotted on PtdIns3*P* Mass

ELISA plates in duplicates. PtdIns3*P* levels were detected by measuring absorbance at 450 nm on a plate reader. Specific amounts were determined by comparison of values to a standard curve generated with known amounts of PtdIns3*P*.

AAV production

rAAV2/1 vectors were generated by a triple transfection of AAV-293 cell line with pAAV2-insert containing the insert under the control of the CMV promoter and flanked by serotype-2 inverted terminal repeats, pXR1 containing *rep* and *cap* genes of AAV serotype-1, and pHelper encoding the adenovirus helper functions. Viral vectors were purified and quantified by real time PCR using a plasmid standard pAAV-eGFP. Titers are expressed as viral genomes per ml (vg/ml) and rAAV titers used here were $5\text{-}7.10^{11}$ vg/ml.

AAV transduction of tibialis anterior muscles of wild-type and *Mtm1* KO mice

Two- to 3-week-old wild-type or *Mtm1* KO male 129PAS mice were anesthetized by intraperitoneal injection of 5 ml/g of ketamine (20 mg/mL; Virbac, Carros, France) and xylazine (0.4%, Rompun; Bayer, Wuppertal, Germany). Tibialis anterior (TA) muscles were injected with 20 ml of AAV2/1 preparations or sterile AAV2/1 empty vector. Four weeks later, mice were anesthetized and the TA muscle was either functionally analyzed (as described below), or directly dissected and frozen in nitrogen-cooled isopentane for histology, or fixed for electron microscopy (as described below).

Functional analysis of the muscle

Muscle force measurements were evaluated by measuring *in situ* muscle contraction in response to nerve and muscle stimulation, as described previously (31). Animals were anesthetized by intraperitoneal injection of pentobarbital sodium (50 mg per kg). The distal tendon of the TA was detached and tied with a silk ligature to an isometric transducer (Harvard Bioscience, Holliston, MA). The sciatic nerve was distally stimulated, response to

tetanic stimulation (pulse frequency of 50 to 143 Hz) was recorded, and absolute maximal force was determined. After contractile measurements, the animals were sacrificed by cervical dislocation. To determine specific maximal force, TA muscles were dissected and weighed.

Histology

Transverse cryosections (9 µm) of mouse TA skeletal muscles were stained with hematoxylin and eosin (HE) or Succinate dehydrogenase (SDH) and viewed with a NanoZoomer 2.0HT slide scanner (Hamamatsu, Hamamatsu city, Japan). Fiber area was analyzed on HE sections, using the RoiManager plugin of ImageJ image analysis software. The percentage of peripheral nuclei was counted using the cell counter plugin of ImageJ image analysis software.

Electron microscopy

TA muscles of anesthetized mice were fixed with 4% PFA and 2.5% glutaraldehyde in 0.1 M phosphate buffer (pH 7.2) and processed as described (49). Ratio of triads/sarcomere was calculated by dividing number of triad structure identified by the total number of sarcomere present on the section (2 mice per genotype, minimum 10 fibers analyzed per mice, minimum 20 triads per fiber).

Statistical analysis

Data are mean ± s.e.m. or ± SD as noted in the figure legend. Statistical analysis was performed using 1-way ANOVA followed by Tukey's multiple comparisons test for all data except for the expression analysis (Fig. 6B-C) where an unpaired 2-tailed Student's *t* test was performed. A *P* value less than 0.05 was considered significant.

Author contribution

J.L., S.F. and B.C. provided direction for the project, conceived and designed the experiments; D.L.B. and M.R. performed yeast experiments and data analyses; J.M.X. and

B.P. performed the PI5P mass assay on total lipid extracts from yeast; B.R. and D.L.B. constructed the yeast expression plasmids; M.R. constructed the AAV plasmids; M.R. and B.C. designed and performed the mice experiments and data analyses; M.R. performed the experiment on human biopsies; N.R. provided the human muscle biopsies; C.K. maintained the mouse lines and did the genotyping; P.K. conceived an ImageJ macro to analyze the nuclei positioning; M.R., J.L., S.F and B.C. analyzed the data and wrote the manuscript.

Acknowledgements

We thank Raphael Schneider, Hichem Tasfaout, Pascale Koebel, Nadia Messadeq, Josiane Hergueux, Coralie Spiegelhalter, Bruno Rinaldi for excellent technical assistance. We thank Scott D. Emr (Cornell University, USA) and Christopher J. Stefan (University College London, UK) for sharing yeast strains and plasmids. We thank V. Laugel (Strasbourg hospital, France) for sharing an XLCNM patient muscle biopsy. We thank the very helpful platforms of the IGBMC: the imaging center, the antibodies facility, the animal house, the cell culture facility, and the molecular biology facility.

This work was supported by the Centre National de la Recherche Scientifique (CNRS); the Institut National de la Santé et de la Recherche Médicale (INSERM); Université de Strasbourg; the Agence Nationale de la Recherche

No competing interest declared.

References

1 Raess, M.A., Friant, S., Cowling, B.S. and Laporte, J. (2017) WANTED - Dead or alive: Myotubularins, a large disease-associated protein family. *Advances in biological regulation*, **63**, 49-58.

2 Blondeau, F., Laporte, J., Bodin, S., Superti-Furga, G., Payrastre, B. and Mandel, J.L. (2000) Myotubularin, a phosphatase deficient in myotubular myopathy, acts on phosphatidylinositol 3-kinase and phosphatidylinositol 3-phosphate pathway. *Hum. Mol. Genet.*, **9**, 2223-2229.

3 Taylor, G.S., Maehama, T. and Dixon, J.E. (2000) Inaugural article: myotubularin, a protein tyrosine phosphatase mutated in myotubular myopathy, dephosphorylates the lipid second messenger, phosphatidylinositol 3-phosphate. *Proc. Natl. Acad. Sci. U. S. A.*, **97**, 8910-8915.
4 Vicinanza, M., D'Angelo, G., Di Campli, A. and De Matteis, M.A. (2008) Function and dysfunction of the PI system in membrane trafficking. *EMBO J*, **27**, 2457-2470.
5 Tronchere, H., Laporte, J., Pendaries, C., Chaussade, C., Liaubet, L., Pirola, L., Mandel, J.L. and Payrastre, B. (2004) Production of phosphatidylinositol 5-phosphate by the phosphoinositide 3-phosphatase myotubularin in mammalian cells. *J. Biol. Chem.*, **279**, 7304-7312.
6 Walker, D.M., Urbe, S., Dove, S.K., Tenza, D., Raposo, G. and Clague, M.J. (2001) Characterization of MTMR3. an inositol lipid 3-phosphatase with novel substrate specificity. *Curr. Biol.*, **11**, 1600-1605.
7 Berger, P., Bonneick, S., Willi, S., Wymann, M. and Suter, U. (2002) Loss of phosphatase activity in myotubularin-related protein 2 is associated with Charcot-Marie-Tooth disease type 4B1. *Hum. Mol. Genet.*, **11**, 1569-1579.
8 Jin, N., Lang, M.J. and Weisman, L.S. (2016) Phosphatidylinositol 3,5-bisphosphate: regulation of cellular events in space and time. *Biochem. Soc. Trans.*, **44**, 177-184.
9 Schink, K.O., Raiborg, C. and Stenmark, H. (2013) Phosphatidylinositol 3-phosphate, a lipid that regulates membrane dynamics, protein sorting and cell signalling. *BioEssays*, **35**, 900-912.
10 Berger, P., Berger, I., Schaffitzel, C., Tersar, K., Volkmer, B. and Suter, U. (2006) Multi-level regulation of myotubularin-related protein-2 phosphatase activity by myotubularin-related protein-13/set-binding factor-2. *Hum. Mol. Genet.*, **15**, 569-579.
11 Kim, S.A., Vacratsis, P.O., Firestein, R., Cleary, M.L. and Dixon, J.E. (2003) Regulation of myotubularin-related (MTMR)2 phosphatidylinositol phosphatase by MTMR5, a catalytically inactive phosphatase. *Proc. Natl. Acad. Sci. U. S. A.*, **100**, 4492-4497.
12 Nandurkar, H.H., Layton, M., Laporte, J., Selan, C., Corcoran, L., Caldwell, K.K., Mochizuki, Y., Majerus, P.W. and Mitchell, C.A. (2003) Identification of myotubularin as the lipid phosphatase catalytic subunit associated with the 3-phosphatase adapter protein, 3-PAP. *Proc. Natl. Acad. Sci. U. S. A.*, **100**, 8660-8665.
13 Lecompte, O., Poch, O. and Laporte, J. (2008) PtdIns5P regulation through evolution: roles in membrane trafficking? *Trends Biochem. Sci.*, **33**, 453-460.
14 Parrish, W.R., Stefan, C.J. and Emr, S.D. (2004) Essential role for the myotubularin-related phosphatase Ymr1p and the synaptojanin-like phosphatases Sjl2p and Sjl3p in regulation of phosphatidylinositol 3-phosphate in yeast. *Mol. Biol. Cell*, **15**, 3567-3579.
15 Amoasii, L., Bertazzi, D.L., Tronchere, H., Hnia, K., Chicanne, G., Rinaldi, B., Cowling, B.S., Ferry, A., Klaholz, B., Payrastre, B. *et al.* (2012) Phosphatase-dead myotubularin ameliorates X-linked centronuclear myopathy phenotypes in mice. *PLoS Genet*, **8**, e1002965.
16 Laporte, J., Hu, L.J., Kretz, C., Mandel, J.L., Kioschis, P., Coy, J.F., Klauck, S.M., Poustka, A. and Dahl, N. (1996) A gene mutated in X-linked myotubular myopathy defines a new putative tyrosine phosphatase family conserved in yeast. *Nat. Genet.*, **13**, 175-182.
17 Bolino, A., Muglia, M., Conforti, F.L., LeGuern, E., Salih, M.A., Georgiou, D.M., Christodoulou, K., Hausmanowa-Petrusewicz, I., Mandich, P., Schenone, A. *et al.* (2000) Charcot-Marie-Tooth type 4B is caused by mutations in the gene encoding myotubularin-related protein-2. *Nat. Genet.*, **25**, 17-19.
18 Senderek, J., Bergmann, C., Weber, S., Ketelsen, U.P., Schorle, H., Rudnik-Schoneborn, S., Buttner, R., Buchheim, E. and Zerres, K. (2003) Mutation of the SBF2 gene, encoding a novel member of the myotubularin family, in Charcot-Marie-Tooth neuropathy type 4B2/11p15. *Hum. Mol. Genet.*, **12**, 349-356.
19 Azzedine, H., Bolino, A., Taieb, T., Birouk, N., Di Duca, M., Bouhouche, A., Benamou, S., Mrabet, A., Hammadouche, T., Chkili, T. *et al.* (2003) Mutations in MTMR13, a New Pseudophosphatase Homologue of MTMR2 and Sbf1, in Two Families with an Autosomal Recessive Demyelinating Form of Charcot-Marie-Tooth Disease Associated with Early-Onset Glaucoma. *Am. J. Hum. Genet.*, **72**, 1141-1153.

20 Alazami, A.M., Alzahrani, F., Bohlega, S. and Alkuraya, F.S. (2014) SET binding factor 1 (SBF1) mutation causes Charcot-Marie-tooth disease type 4B3. *Neurology*, **82**, 1665-1666.
21 Manole, A., Horga, A., Gamez, J., Raguer, N., Salvado, M., San Millan, B., Navarro, C., Pittmann, A., Reilly, M.M. and Houlden, H. (2017) SBF1 mutations associated with autosomal recessive axonal neuropathy with cranial nerve involvement. *Neurogenetics*, **18**, 63-67.
22 Nakhro, K., Park, J.M., Hong, Y.B., Park, J.H., Nam, S.H., Yoon, B.R., Yoo, J.H., Koo, H., Jung, S.C., Kim, H.L. *et al.* (2013) SET binding factor 1 (SBF1) mutation causes Charcot-Marie-Tooth disease type 4B3. *Neurology*, **81**, 165-173.
23 Bolino, A., Marigo, V., Ferrera, F., Loader, J., Romio, L., Leoni, A., Di Duca, M., Cinti, R., Cecchi, C., Feltri, M.L. *et al.* (2002) Molecular characterization and expression analysis of Mtmr2, mouse homologue of MTMR2, the Myotubularin-related 2 gene, mutated in CMT4B. *Gene*, **283**, 17-26.
24 Begley, M.J., Taylor, G.S., Brock, M.A., Ghosh, P., Woods, V.L. and Dixon, J.E. (2006) Molecular basis for substrate recognition by MTMR2, a myotubularin family phosphoinositide phosphatase. *Proc. Natl. Acad. Sci. U. S. A.*, **103**, 927-932.
25 Begley, M.J., Taylor, G.S., Kim, S.A., Veine, D.M., Dixon, J.E. and Stuckey, J.A. (2003) Crystal structure of a phosphoinositide phosphatase, MTMR2: insights into myotubular myopathy and Charcot-Marie-Tooth syndrome. *Mol. Cell*, **12**, 1391-1402.
26 GTEx_consortium. (2015) Human genomics. The Genotype-Tissue Expression (GTEx) pilot analysis: multitissue gene regulation in humans. *Science*, **348**, 648-660.
27 Katzmann, D.J., Stefan, C.J., Babst, M. and Emr, S.D. (2003) Vps27 recruits ESCRT machinery to endosomes during MVB sorting. *J. Cell Biol.*, **162**, 413-423.
28 Cooke, F.T., Dove, S.K., McEwen, R.K., Painter, G., Holmes, A.B., Hall, M.N., Michell, R.H. and Parker, P.J. (1998) The stress-activated phosphatidylinositol 3-phosphate 5-kinase Fab1p is essential for vacuole function in S. cerevisiae. *Curr. Biol.*, **8**, 1219-1222.
29 Dove, S.K., Cooke, F.T., Douglas, M.R., Sayers, L.G., Parker, P.J. and Michell, R.H. (1997) Osmotic stress activates phosphatidylinositol-3,5-bisphosphate synthesis. *Nature*, **390**, 187-192.
30 Buj-Bello, A., Laugel, V., Messaddeq, N., Zahreddine, H., Laporte, J., Pellissier, J.F. and Mandel, J.L. (2002) The lipid phosphatase myotubularin is essential for skeletal muscle maintenance but not for myogenesis in mice. *Proc. Natl. Acad. Sci. U. S. A.*, **99**, 15060-15065.
31 Cowling, B.S., Chevremont, T., Prokic, I., Kretz, C., Ferry, A., Coirault, C., Koutsopoulos, O., Laugel, V., Romero, N.B. and Laporte, J. (2014) Reducing dynamin 2 expression rescues X-linked centronuclear myopathy. *J Clin Invest*, **124**, 1350-1363.
32 Spiro, A.J., Shy, G.M. and Gonatas, N.K. (1966) Myotubular myopathy. Persistence of fetal muscle in an adolescent boy. *Arch. Neurol.*, **14**, 1-14.
33 Franklin, N.E., Bonham, C.A., Xhabija, B. and Vacratsis, P.O. (2013) Differential phosphorylation of the phosphoinositide 3-phosphatase MTMR2 regulates its association with early endosomal subtypes. *J. Cell Sci.*, **126**, 1333-1344.
34 Franklin, N.E., Taylor, G.S. and Vacratsis, P.O. (2011) Endosomal targeting of the phosphoinositide 3-phosphatase MTMR2 is regulated by an N-terminal phosphorylation site. *J. Biol. Chem.*, **286**, 15841-15853.
35 Velichkova, M., Juan, J., Kadandale, P., Jean, S., Ribeiro, I., Raman, V., Stefan, C. and Kiger, A.A. (2010) Drosophila Mtm and class II PI3K coregulate a PI(3)P pool with cortical and endolysosomal functions. *J. Cell Biol.*, **190**, 407-425.
36 Kutchukian, C., Lo Scrudato, M., Tourneur, Y., Poulard, K., Vignaud, A., Berthier, C., Allard, B., Lawlor, M.W., Buj-Bello, A. and Jacquemond, V. (2016) Phosphatidylinositol 3-kinase inhibition restores Ca2+ release defects and prolongs survival in myotubularin-deficient mice. *Proc. Natl. Acad. Sci. U. S. A.*, **113**, 14432-14437.
37 Sabha, N., Volpatti, J.R., Gonorazky, H., Reifler, A., Davidson, A.E., Li, X., Eltayeb, N.M., Dall'Armi, C., Di Paolo, G., Brooks, S.V. *et al.* (2016) PIK3C2B inhibition improves function and prolongs survival in myotubular myopathy animal models. *J Clin Invest*, **126**, 3613-3625.

38 Fetalvero, K.M., Yu, Y., Goetschkes, M., Liang, G., Valdez, R.A., Gould, T., Triantafellow, E., Bergling, S., Loureiro, J., Eash, J. *et al.* (2013) Defective autophagy and mTORC1 signaling in myotubularin null mice. *Mol. Cell. Biol.*, **33**, 98-110.
39 Childers, M.K., Joubert, R., Poulard, K., Moal, C., Grange, R.W., Doering, J.A., Lawlor, M.W., Rider, B.E., Jamet, T., Daniele, N. *et al.* (2014) Gene therapy prolongs survival and restores function in murine and canine models of myotubular myopathy. *Sci Transl Med*, **6**, 220ra210.
40 Lawlor, M.W., Armstrong, D., Viola, M.G., Widrick, J.J., Meng, H., Grange, R.W., Childers, M.K., Hsu, C.P., O'Callaghan, M., Pierson, C.R. *et al.* (2013) Enzyme replacement therapy rescues weakness and improves muscle pathology in mice with X-linked myotubular myopathy. *Hum. Mol. Genet.*, **22**, 1525-1538.
41 Laporte, J., Biancalana, V., Tanner, S.M., Kress, W., Schneider, V., Wallgren-Pettersson, C., Herger, F., Buj-Bello, A., Blondeau, F., Liechti-Gallati, S. *et al.* (2000) MTM1 mutations in X-linked myotubular myopathy. *Hum. Mutat.*, **15**, 393-409.
42 Laporte, J., Kress, W. and Mandel, J.L. (2001) Diagnosis of X-linked myotubular myopathy by detection of myotubularin. *Ann. Neurol.*, **50**, 42-46.
43 Alberti, S., Gitler, A.D. and Lindquist, S. (2007) A suite of Gateway cloning vectors for high-throughput genetic analysis in Saccharomyces cerevisiae. *Yeast*, **24**, 913-919.
44 Van Mullem, V., Wery, M., De Bolle, X. and Vandenhaute, J. (2003) Construction of a set of Saccharomyces cerevisiae vectors designed for recombinational cloning. *Yeast*, **20**, 739-746.
45 Volland, C., Urban-Grimal, D., Geraud, G. and Haguenauer-Tsapis, R. (1994) Endocytosis and degradation of the yeast uracil permease under adverse conditions. *J. Biol. Chem.*, **269**, 9833-9841.
46 Gietz, D., St Jean, A., Woods, R.A. and Schiestl, R.H. (1992) Improved method for high efficiency transformation of intact yeast cells. *Nucleic Acids Res.*, **20**, 1425.
47 Hama, H., Takemoto, J.Y. and DeWald, D.B. (2000) Analysis of phosphoinositides in protein trafficking. *Methods*, **20**, 465-473.
48 Morris, J.B., Hinchliffe, K.A., Ciruela, A., Letcher, A.J. and Irvine, R.F. (2000) Thrombin stimulation of platelets causes an increase in phosphatidylinositol 5-phosphate revealed by mass assay. *FEBS Lett.*, **475**, 57-60.
49 Cowling, B.S., Toussaint, A., Amoasii, L., Koebel, P., Ferry, A., Davignon, L., Nishino, I., Mandel, J.L. and Laporte, J. (2011) Increased expression of wild-type or a centronuclear myopathy mutant of dynamin 2 in skeletal muscle of adult mice leads to structural defects and muscle weakness. *Am. J. Pathol.*, **178**, 2224-2235.

Figure legends

Figure 1: MTMR2 splicing isoforms are differentially expressed and encode for long and short protein isoforms. (**A**) Comparative expression of MTMR2 mRNA isoforms V1 to V4 in 20 human tissues from GTEx database mining (top). Human MTMR2 V2 isoform contains additional exons 1a and 2a compared to V1, V3 contains exon 1a and V4 contains exons 1a and 2b. Tissue expression of each isoform independently (bottom). (**B**) Protein domains MTMR2-L encoded by V1 mRNA isoform, and MTMR2-S encoded by the other isoforms, compared to MTM1.

Figure 2: Short but not long MTMR2 isoform displays an MTM1-like activity. Exogenous expression of human MTM1 and MTMR2 long and short isoforms using the high copy number plasmid 2µ in *ymr1Δ* yeast cells. (**A**) Detection of exogenously expressed human myotubularins by western blot using anti-MTM1 or anti-MTMR2 antibodies, in two independents blots with the same samples. Wild-type (WT) and *ymr1Δ* yeast strains with empty vectors are used as controls. Pgk1p is used as a loading control. This blot is representative of at least 3 independent experiments. (**B**) Quantification of vacuolar morphology in yeast cells over-expressing untagged myotubularins. Three clones analyzed per constructs; the number of cells counted per clone is indicated above. Data represent means ± s.e.m. ****p<0.0001, ns not significant (ANOVA test). (**C**) Localization of GFP-tagged human myotubularins. Vacuole morphology is assessed by the lipophilic dye FM4-64 and Nomarski differential contrast. *ymr1Δ* yeast cells and MTMR2-L expressing cells display a fragmented vacuole while MTM1 and MTMR2-S over-expressing cells have a large vacuole. **(D)** FYVE punctuated localization in yeast clones expressing untagged myotubularins and DsRED-tagged FYVE domain that specifically binds PtdIns3*P*. (**E**) PtdIns3*P* quantification by counting the number of FYVE-positive dots per cell, as represented in (D). . PtdIns3*P* is

decreased upon MTM1 and MTMR2-S expression but not with MTMR2-L. Data represent means ± s.e.m. *p<0.05, **p<0.01 (ANOVA test). **(F)** PtdIns5*P* quantification by mass assay on total lipid extract from yeast cells over-expressing untagged myotubularins. Three clones analyzed per constructs. Data represent means ± s.e.m. *p<0.05 (ANOVA test).

Figure 3: The MTMR2 short isoform rescues muscle weight and force similarly as MTM1 in the *Mtm1* KO myopathic mouse. TA muscles from 2-3 week-old *Mtm1* KO mice were injected with AAV2/1 expressing myotubularins and analyzed 4 weeks later. (**A**) Detection of exogenously expressed human myotubularins by western blot using anti-MTM1 or anti-MTMR2 antibodies; GAPDH is used as a loading control. Unspecific bands are indicated by a star. This blot is representative for each construct, and at least 10 muscles per construct were analyzed. (**B**) Ratio of muscle weight of TA expressing human myotubularins compared to the contralateral leg injected with empty AAV. MTMR2-S improved muscle mass similarly as MTM1 while MTMR2-L had no effect. A value of 1 was set for the *Mtm1* KO mice injected with empty AAV. n>10. Data represent means ± s.e.m. ****p<0.0001, ns not significant (ANOVA test). (**C**) Specific maximal force of TA muscle (absolute values). Both MTMR2 isoforms improved muscle force. n>7. Data represent means ± s.e.m. **p<0.01, ****p<0.0001, ns not significant (ANOVA test).

Figure 4: Both long and short MTMR2 isoforms improve the histological hallmarks of the *Mtm1* KO mouse. TA muscles from *Mtm1* KO mice were injected with AAV2/1 expressing myotubularins 2-3 week-old and analyzed 4 weeks later. (**A**) Hematoxylin-eosin staining of TA muscle sections. Scale bar 100 µm. **(B)** Succinate dehydrogenase (SDH) staining of TA muscle sections. Scale bar 100 µm. (**C**) Quantification of fiber area. Fiber size is grouped into 200 μm^2 intervals and represented as a percentage of total fibers in each group. n>1000 for 8 mice. (**D**) Percentage of fibers above 800 μm^2. n>8. Data represent

means ± s.e.m. *p<0.05, ***p<0.001, ****p<0.0001 (ANOVA test). The value for WT is statistically different from all *Mtm1* KO injected groups. (**E**) Nuclei positioning in TA muscle. Percentage of well-positioned peripheral nuclei. n>6 animals. Data represent means ± s.e.m. ***p<0.001, ****p<0.0001 (ANOVA test). The value for WT is statistically different from all *Mtm1* KO injected groups.

Figure 5: MTMR2 isoforms rescue the muscle ultrastructure and triad morphology of the *Mtm1* KO muscles. TA muscles from *Mtm1* KO mice were injected with AAV2/1 expressing myotubularins. (**A**) Electron microscopy pictures displaying sarcomere, mitochondria and triad organization. Scale bar 1 µm. Representative triads are displayed in the zoom square. (**B**) Quantification of the number of well-organized triads per sarcomere. n>20 images for 2 mice each. All muscles expressing myotubularins quantify differently than the *Mtm1* KO. Data represent means ± s.e.m. *p<0.05, ****p<0.0001 (ANOVA test).

Figure 6: The MTMR2-S short isoform is reduced in the *Mtm1* KO mouse and its overexpression normalizes PtdIns3*P* level. (**A**) Quantification of PtdIns3*P* level by competitive ELISA in TA muscles from *Mtm1* KO mice expressing different myotubularins and in WT muscles. n>3 mice. Data represent means ± s.e.m. *p<0.05, **p<0.01, ***p<0.001 (ANOVA test). PtdIns3*P* levels in *Mtm1* KO muscles expressing the different myotubularins are not statistically different from the WT controls. (**B**) Quantification by qRT-PCR of MTMR2 isoforms (V1 to V4) in the TA muscle of *Mtm1* KO mice compared to WT mice. n>6. Each isoform is presented as an independent ratio, with a value of 1 set for expression in WT mice. Data represent means ± s.d. **p<0.01, ***p<0.001, ****p<0.0001, ns not significant (Student's t-test). **(C)** Quantification by qRT-PCR of MTMR2 isoforms (V1 to V4) in muscles of MTM1 patients compared to controls. N=3. Each isoform is presented as an

independent ratio, with a value of 1 set for expression in control patients. Data represent means ± s.d. The *P* value is indicated for each isoform (Student's t-test).

Table 1: Rescuing effects of MTM1 and MTMR2 isoforms on several hallmarks of myotubular myopathy.

	Mtm1 KO + empty AAV	*Mtm1* KO + MTM1	*Mtm1* KO + MTMR2-L	*Mtm1* KO + MTMR2-S	WT + empty AAV
Muscle weight	-	++	-	++	+++
Muscle force	-	++	+	++	+++
Fiber size	-	++	+	+	+++
Nuclei positioning	-	++	++	++	+++
Number of well-organized triads/sarcomere	-	++	+	++	+++
PtdIns*3P* level	-	+++	++	+++	+++

"+,++,+++": increasing rescuing ability of myotubularins, ranging from "-": no rescue to "+++": WT phenotype

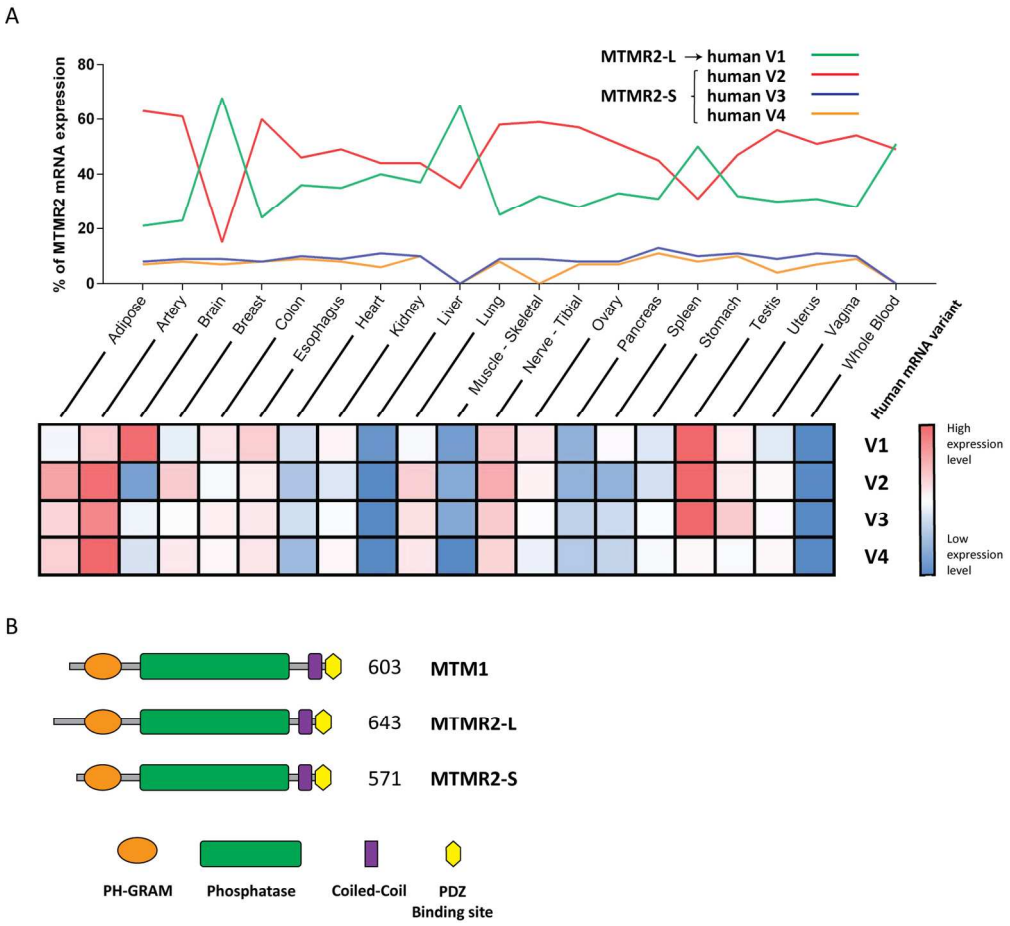

Figure 1

151x139mm (300 x 300 DPI)

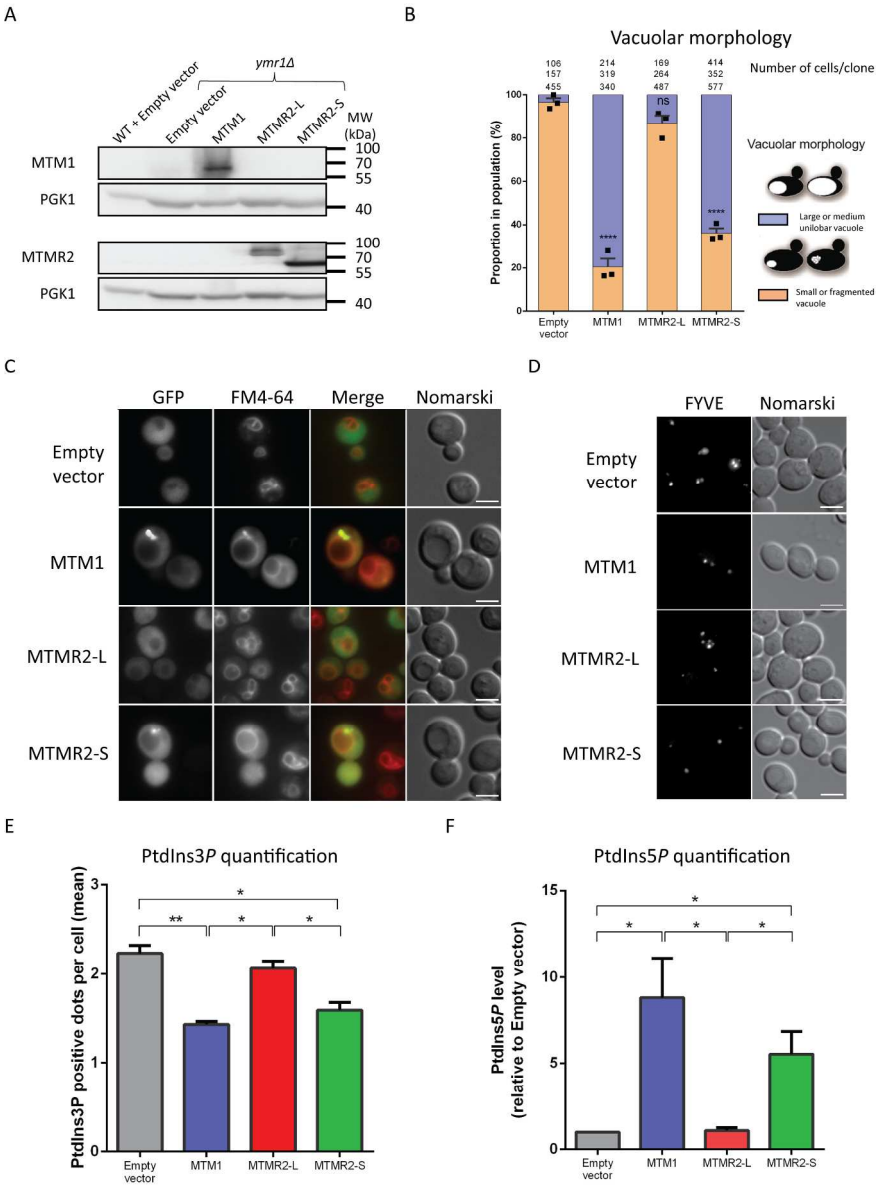

Figure 2

197x271mm (300 x 300 DPI)

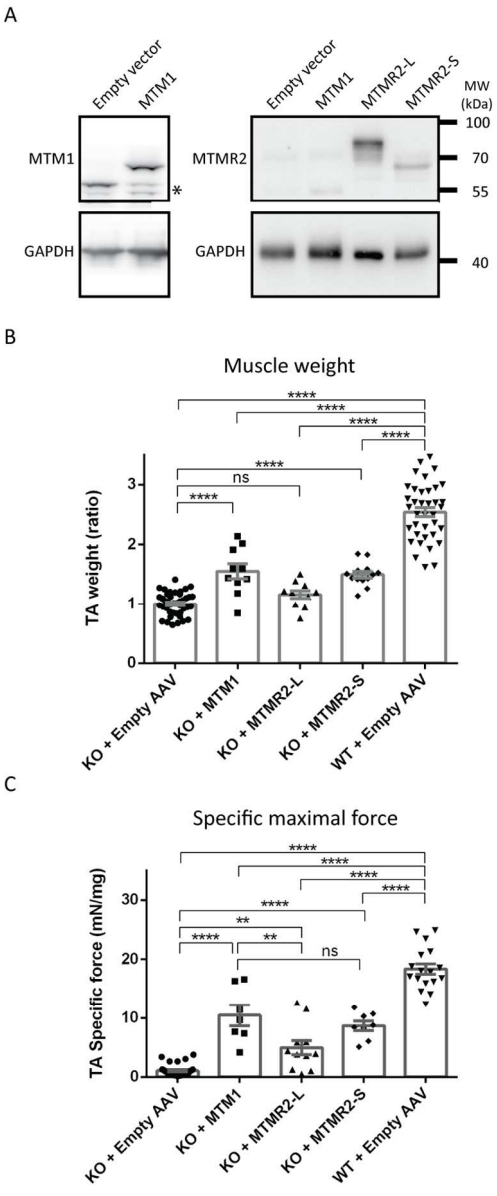

Figure 3

66x161mm (300 x 300 DPI)

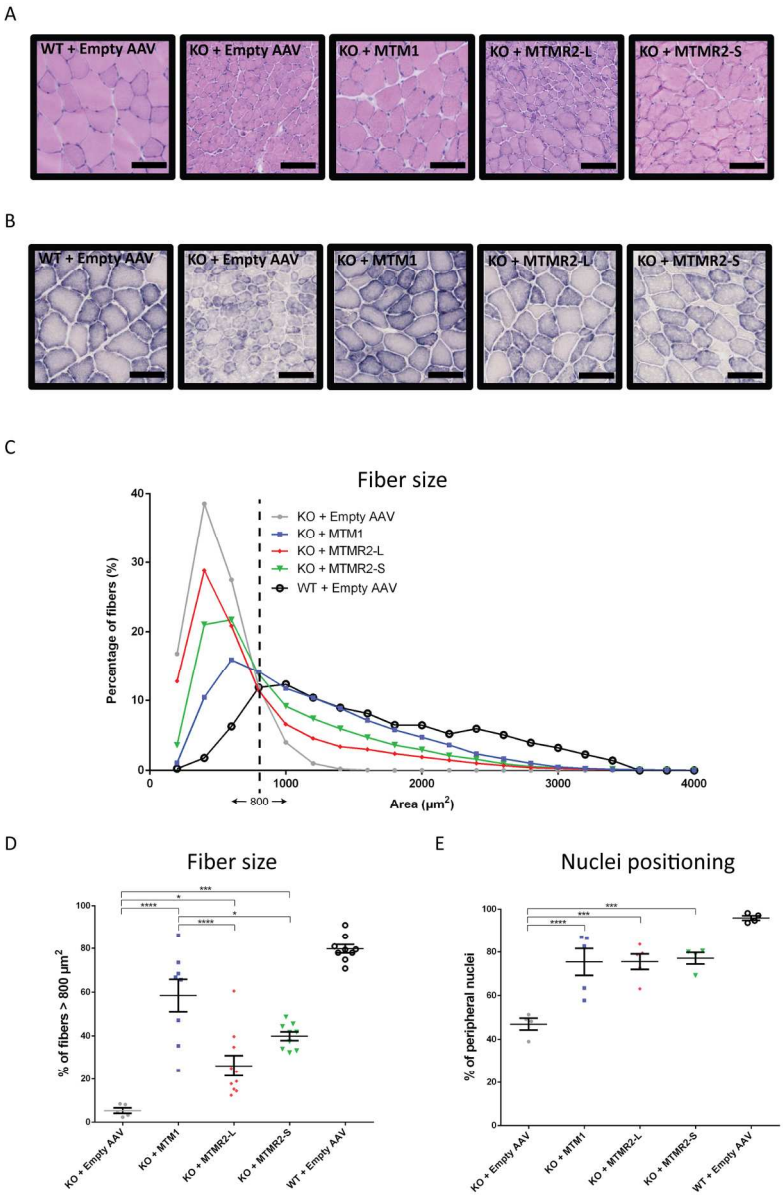

Figure 4

134x206mm (300 x 300 DPI)

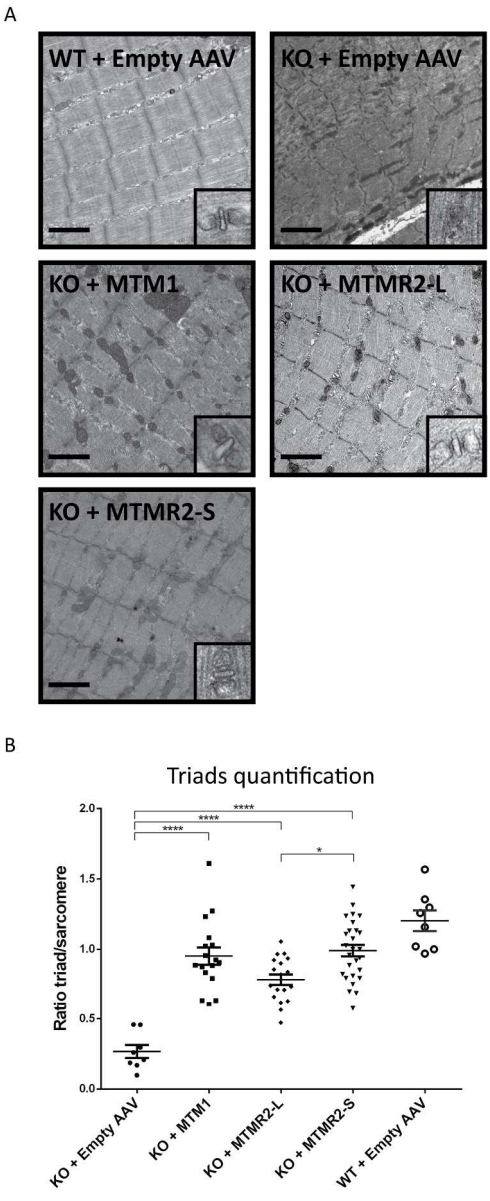

Figure 5

108x268mm (300 x 300 DPI)

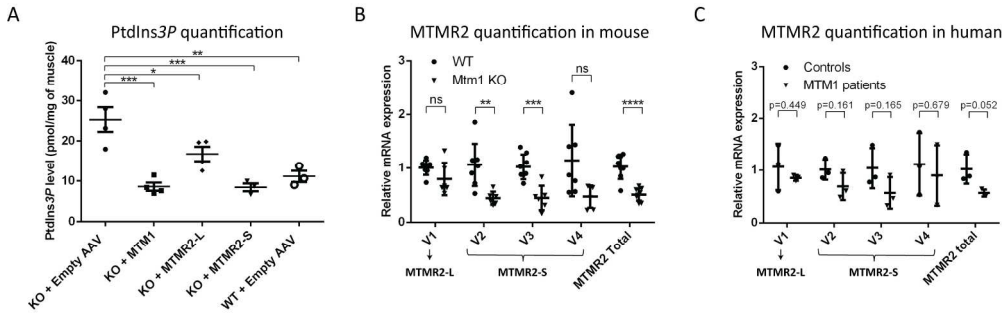

Figure 6

198x63mm (300 x 300 DPI)

Supplementary material

A

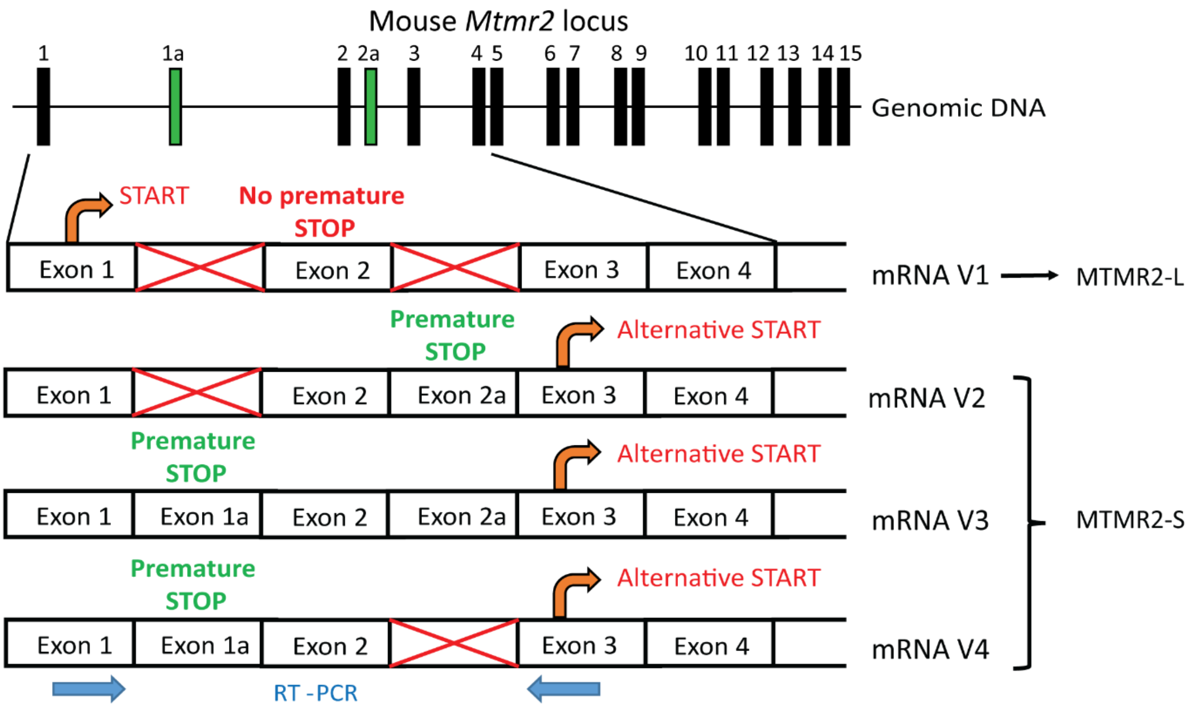

B

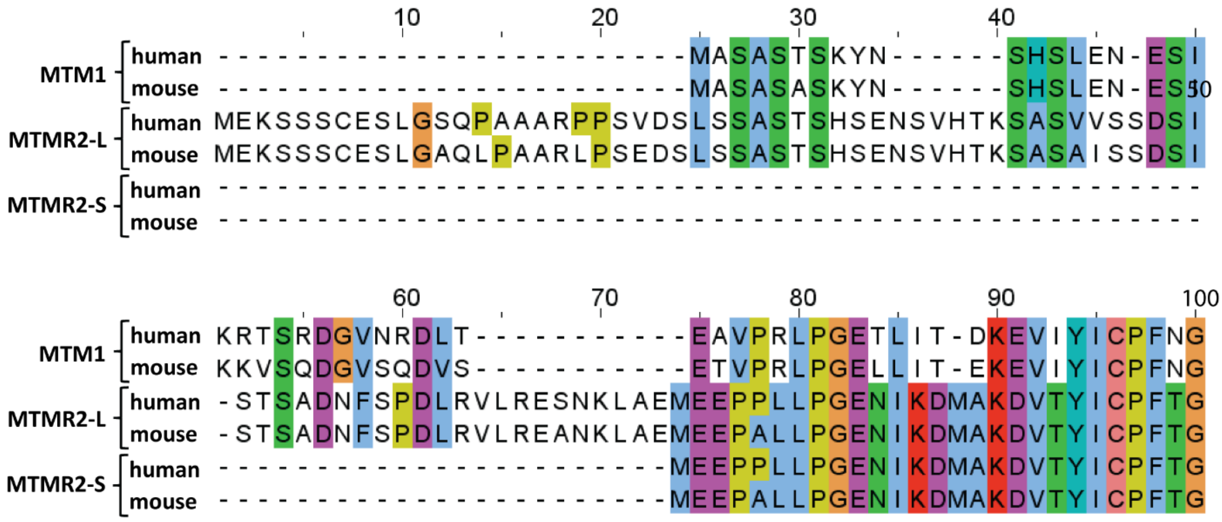

C

<u>Sequence of exon 1a:</u>

TTAATGTGTTAAGAACCATTGACATTTGAAGATCATCAGAAGTGAAGATAAAACATCTCAAAAATTATAAT

<u>Sequence of exon 2a:</u>

GAGTGCCCAGCTGCTTGGGTTTTAGTTGATGCCAGACATAGTCAAGTTGACAGCCAAGATTAGCCATCAC
ACCAGTGTTCTATCCTGTTGAATCCAATTCTATAG

D

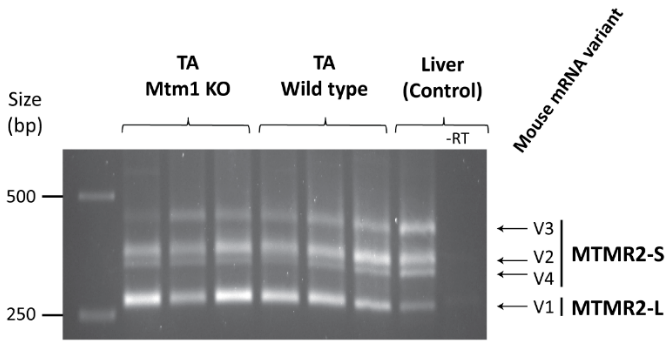

Supplementary Figure S1: MTMR2 mRNA and protein isoforms in human and mouse. (**A**) Genomic structure and mRNA isoforms of MTMR2 in mouse. Inclusion of any combination of the alternative exons 1a or 2a brings a premature stop codon and unmasks an alternative start site in exon 3. Murine MTMR2 V1 encodes for the MTMR2-L while isoforms V2 to V4 encode for MTMR2-S. (**B**) Protein alignment of the N-terminal region of human and mouse MTM1, MTMR2-L and MTMR2-S. The PH-GRAM domain starts at position 75. (**C**) Sequence of mouse alternative exons 1a and 2a from sequencing of RT-PCR products from muscle. (**D**) PCR between exons 1 and 3 of MTMR2 on cDNA from TA muscles isolated from WT and *Mtm1* KO mice and from WT liver. The 4 mRNA variants are detected.

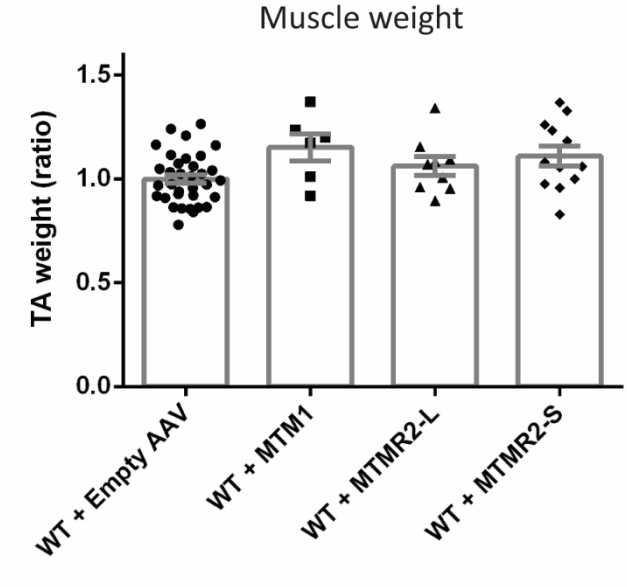

Supplementary Figure S2: Expression of MTMR2 isoforms does not induce muscle hypertrophy in WT mice. TA muscles from WT mice were injected with AAV2/1 expressing myotubularins at 3 week-old and analyzed 4 weeks later. Ratio of muscle weight of TA expressing human myotubularins compared to the contralateral leg injected with empty AAV. A value of 1 is set for the WT TA muscle weight. n>5. Data represent means ± s.e.m. No significant differences (ANOVA test).

Matthieu RAESS

Deciphering the functional and molecular differences between MTM1 and MTMR2 to better understand two neuromuscular diseases.

Résumé

MTM1 et MTMR2 sont 2 phosphatases de phosphoinositides appartenant à la famille des myotubularines, conservée pendant l'évolution. Bien qu'étant très similaires, des mutations dans MTM1 entraînent la sévère myopathie XLCNM alors que les mutations dans MTMR2 entraînent la neuropathie CMT4B. On ne comprend pas encore les bases moléculaires de cette spécificité de tissu, et il n'existe aucun traitement spécifique pour ces maladies.

J'ai tout d'abord caractérisé l'activité des 2 isoformes endogènes de MTMR2, nommés MTMR2-L et MTMR2-S. J'ai démontré que la différence fonctionnelle entre MTM1 et MTMR2 s'explique principalement par l'extension N-terminale de MTMR2, et que l'isoforme MTMR2-S dépourvu de cette extension entraîne les mêmes phénotypes que MTM1. Ensuite, grâce à l'injection d'AAV dans les souris *Mtm1* KO, j'ai démontré que l'expression exogène des isoformes de MTMR2, et surtout de MTMR2-S, améliore grandement l'atrophie musculaire, la force musculaire et les marqueurs histologiques de ces souris myopathiques.

Ces résultats révèlent une première base moléculaire expliquant les spécificités fonctionnelles de MTM1 et MTMR2, et montrent que MTMR2 est une cible thérapeutique potentielle pour la myopathie XLCNM.

Mots-clés : myopathie centronucléaire liée à l'X, myotubularine, phosphoinositides, thérapie génique.

Abstract

MTM1 and MTMR2 are 2 phosphatases of phosphoinositides that belong to the myotubularin family conserved through evolution. Despite their high level of similarity, mutations in MTM1 lead to the severe XLCNM myopathy while mutations in MTMR2 lead to the CMT4B neuropathy. The molecular bases for the surprising tissue-specific functions of these ubiquitously expressed proteins was unclear. Moreover, there is no specific therapy for these diseases.

I first characterized the activity of the two naturally occurring isoforms of MTMR2, that we named MTMR2-L (long) and MTMR2-S (short). I found that the **functional differences between MTM1 and MTMR2 reside** mostly **in the N-terminal extension** of MTMR2-L, and that the endogenous MTMR2-S isoform lacking this N-terminal extension behaves similarly as MTM1. Then, using the myopathic *Mtm1* KO mouse and AAV-mediated expression, I showed that exogenous expression of **MTMR2 isoforms, and specifically of MTMR2-S, strongly improved the** muscle atrophy, muscle force and the histological hallmarks of the myopathic mice.

These data reveal a first molecular basis for the functional specificities of MTM1 and MTMR2, and **highlight MTMR2 as a therapeutic target for XLCNM myopathy.**

Key words: X-linked centronuclear myopathy, myotubularin, phosphoinositides, gene therapy.